VOLUME 115 NUMBER 1

THE ASTROPHYSICAL JOURNAL

AN INTERNATIONAL REVIEW OF SPECTROSCOPY AND ASTRONOMICAL PHYSICS

JANUARY 1952

THE UNIVERSITY OF CHICAGO PRESS
CHICAGO, ILLINOIS, U.S.A.

January 1952 Vol. 115, No. 1

THE ASTROPHYSICAL JOURNAL

AN INTERNATIONAL REVIEW OF SPECTROSCOPY AND ASTRONOMICAL PHYSICS

Published in Collaboration with the American Astronomical Society

---

The Astrophysical Journal is published bimonthly by the University of Chicago at the University of Chicago Press, 5750 Ellis Avenue, Chicago 37, Illinois, during July, September, November, January, March, and May. ¶Two volumes are published per year, one beginning with the January issue and the other beginning with the July issue. The subscription price is $6.00 per volume or $12.00 per year; the price of single copies is $3.00. (Orders for service of less than a volume will be charged at the single copy rate.) ¶Postage is prepaid by the publishers on all orders from the United States and its possessions. No extra charge is made for postage to countries in the Pan American Postal Union. ¶Postage is charged extra as follows: for Canada, 20 cents per volume, 40 cents per year (total $6.20 per volume, $12.40 per year); on single copies 5 cents (total $3.05); for all other countries in the Postal Union, 50 cents per volume, $1.00 per year (total $6.50 per volume, $13.00 per year), on single copies 10 cents (total $3.10). ¶Subscriptions are payable in advance. Please make all remittances payable to The University of Chicago Press, in United States currency or its equivalent by postal or express money orders or bank drafts.

The following is an authorized agent:

For the British Empire, except North America and Australasia: The Cambridge University Press, Bentley House, 200 Euston Road, London, N.W. 1, England. Prices of yearly subscriptions and of single copies may be had on application.

Claims for missing numbers should be made within the month following the regular month of publication. The publishers expect to supply missing numbers free only when losses have been sustained in transit, and when the reserve stock will permit.

Business correspondence should be addressed to The University of Chicago Press, Chicago 37, Illinois.

Communications for the editors and manuscripts should be addressed to: W. W. Morgan, Editor of THE ASTROPHYSICAL JOURNAL, Yerkes Observatory, Williams Bay, Wisconsin.

Line drawings and photographs should be made by the author, and all marginal notes such as co-ordinates, wave lengths, etc., should be included in the cuts. It will not be possible to set up such material in type.

One copy of the corrected galley proof should be returned as soon as possible to the editor, Yerkes Observatory, Williams Bay, Wisconsin. Authors should take notice that the manuscript will not be sent to them with the proof.

The cable address is "Observatory, Williamsbay, Wisconsin."

The articles in this journal are indexed in the *International Index to Periodicals*, New York, N.Y.

Applications for permission to quote from this journal should be addressed to The University of Chicago Press, and will be freely granted.

Microfilms of complete journal volumes are available to regular subscribers only and may be obtained at the end of the year. Orders and inquiries should be addressed to University Microfilms, 313 North First Street, Ann Arbor, Michigan.

Notice to subscribers: If you change your address, please notify us and your local postmaster immediately.

Entered as second-class matter, July 31, 1940, at the Post-Office at Chicago, Ill., under the Act of March 3, 1879.
Acceptance for mailing at special rate of postage provided for in United States Postal Act of October 3, 1917, Section 1103, amended February 28, 1925.

[PRINTED IN U.S.A.]

THE ASTROPHYSICAL JOURNAL

AN INTERNATIONAL REVIEW OF SPECTROSCOPY AND ASTRONOMICAL PHYSICS

VOLUME 115 JANUARY 1952 NUMBER 1

DEVELOPMENTS IN THE PRACTICAL USE OF PHOTOCELLS FOR MEASURING FAINT LIGHT*

GERALD E. KRON
Lick Observatory, University of California
Received July 5, 1951

ABSTRACT

Infrared-sensitive emission photocells do not operate with high efficiency in an electronic tube amplifier unless a grid resistor of at least 2.5×10^{13} ohms is used or unless the gas-multiplying factor of the cell can be made large without sacrificing stability. A method for practicable use of grid resistors at least as high as 5.0×10^{13} ohms is given. In addition, a method is given for making photocells operate stably with high gas multiplication. The material in this paper may be used as the basis for design of an astronomical photoelectric photometer for use in spectral regions, including the near infrared. The photometer will have satisfactory linearity over large brightness ratios, and it will perform on faint light as efficiently and as usefully for astronomical purposes, as an equivalent system using a multiplier phototube.

INTRODUCTION

This paper describes the development work undertaken at the Lick Observatory to improve existing methods of using photoelectric cells for the measurement of faint infrared light. The work was started early in 1947, and it reached the state described in this paper by late 1949.[1]

The success of the multiplier phototube for the measurement of faint blue and visual light may raise the question of why further effort should be expended on phototube development. The 1P21 multiplier, while not the ideal detector for astronomical purposes because of its spectral response, is nevertheless the best photoelectric device now available for the measurement of faint light in the shorter-wave-length regions of the spectrum. One would expect that employment of an infrared-sensitive surface in a multiplier phototube similar in other respects to the 1P21 would achieve a simple and effective means of measuring faint infrared light and thus would do away entirely with the use of diode emission-type photocells as radiation detectors. As a matter of fact, the first developmental multiplier phototubes, made by V. K. Zworykin, were infrared-sensitive, and by 1940 two types of infrared multipliers were available. These multipliers are no longer on the market, but recently the Radio Corporation of America made available for testing an infrared-sensitive version of the 1P21, designated "type C-7050." The results of our

* *Contributions from Lick Observatory*, Ser. II, No. 38.

[1] The work was supported by ONR Contract.

trial of a single sample of the C-7050 have been published in detail elsewhere;[2] hence a brief description of the results is all that need be given here. This multiplier was tested on starlight in both the unrefrigerated and the refrigerated condition. Its signal-to-noise ratio (hereafter called "S/N") was inferior to that of a typical unrefrigerated photocell by a factor of 2000 when the multiplier was unrefrigerated, and by a factor of 40 when the multiplier was refrigerated with dry ice. This result came from operation of the photocell under conditions represented by the relatively imperfect state of our development in 1948.

Recently, H. L. Johnson[3] has employed the C-7050 refrigerated with liquid air. When so refrigerated, the operating potential of the multiplier may be made very high, and the multiplication per stage may be brought to values comparable with that of the 1P21. Johnson found that certain selected samples of the C-7050 then became sufficiently sensitive to be useful for astronomical purposes. Unfortunately, the high cost of the C-7050 and its present unavailability make its use impractical for astronomical purposes. Until this condition is changed by some manufacturer, the best way to measure faint infrared light is with a photocell operated under appropriate conditions.

The technique that made possible employment of the infrared-sensitive photoemissive cell for faint light was developed by J. S. Hall,[4] who found that by refrigerating the photocell he could reduce by a very large factor the thermionic dark current that had made these photocells impractical for faint light. Refrigeration was most conveniently done by surrounding the photocell with solid carbon dioxide. Hall demonstrated the effectiveness of his method by making numerous measurements of the distribution of stellar radiation; he employed a Western Electric type D-97087 caesium-oxide-on-silver (*CsO-Ag*) photocell used with an electrometer for measuring the electrical output. Later, Stebbins and Whitford adopted the refrigeration method and the D-97087 cell, but employed the cell with Whitford's thermionic amplifier.[5] The instrument thus constituted has been used by Stebbins and Whitford in their six-color photometry of stars and nebulae.

ELEMENTARY DEVELOPMENT

The first modifications of the foregoing methods that were made at the Lick Observatory resulted principally from the use of improved component parts available partly as a result of war developments. In 1946 we adopted the subminiature Victoreen type 5800 electrometer tube (formerly the VX-41 and VX-41A) in place of the bulky tubes formerly used. We also surveyed promising photocells available on the market and adopted the Continental Electric type CE-25A/B with base removed.[6] For the grid resistor, across which the electrical signal from the photocell appears, we adopted Victoreen resistors, which are available in values up to 10^{14} ohms. These resistors are compact and have good mechanical properties, and specimens with good electrical properties can be found by selection.

The small size of the new parts invited placing them close together and refrigerating all of them (photocell, electrometer tube, and grid resistor) instead of segregating the photocell for refrigeration by itself. In this way the temperature of the grid resistor was reduced from 300° to 194° K, resulting in a reduction in the resistor thermal noise by a factor of 1.25. In addition, the residual grid current of the 5800 tube was found to have diminished to such an extent that it was removed from consideration as an important source of noise in the input circuit.

The small size of the new components resulted, furthermore, in a decrease in the capacity of the input circuit. In many respects this capacity is the most important characteristic of the circuit. If it could be reduced to 0.1×10^{-12} farads, very high-valued

[2] *Harvard Circ.*, No. 451, p. 37, 1949.

[3] Private communication.

[4] *Ap. J.*, **79**, 145, 1934.

[5] *Ap. J.*, **76**, 213, 1932.

[6] *Pub. A.S.P.*, **58**, 241, 1946; **59**, 173, 1947.

grid resistors could be employed directly without prohibitively slow response, the usual advantages of high signal voltages would result, and the use of photocells at high efficiency would follow directly. A photometer built with the large components available ten years ago has an input capacity of about 20×10^{-12} farads for the usual plate amplification connection of the tube. The new parts, under similar operating conditions, have an input capacity of only 8.8×10^{-12} farads. If the amplifier is operated as a cathode-follower, the effective input capacity drops to 6.6×10^{-12} farads, and if all shielding, plus the photocell cathode, is returned to the tube cathode instead of to ground (see circuit diagram, Fig. 1), the effective input capacity is only 5.1×10^{-12} farads.[7] The reduction in capacity achieved by circuit connection is an apparent one caused by partial direct-capacity feedback from the cathode return; but electrically the effect is real, and it results in a genuine improvement of the input characteristics. For the standard time-constant (product of resistance by capacity) of 1.5 seconds to be employed throughout

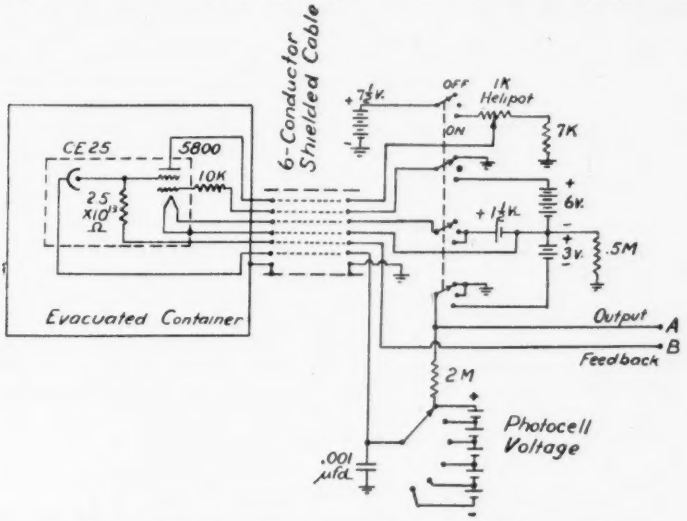

FIG. 1.—Diagram of circuit immediately associated with photocell

this paper, the grid resistor may be 2.9×10^{11} ohms, without employing devices any more complicated than small parts and a cathode-follower connection. A resistance of about one-fourth this amount would have to be used with a photometer having an input capacity of 20×10^{-12} farads. If the thermal noise of the input resistor is the chief source of noise in the circuit under consideration, then the reduction in input capacity by a factor of 4 will, by itself, cause an increase in S/N by a factor of 2. A conservative estimate of the increase in S/N caused by all these improvements is by a factor of 2.5, or by 1 stellar mag.

Calculations of theoretical input noise levels can be made from the known constants of the input circuit by means of formulae available in many places in the literature.[8] Let us suppose that we have an input resistor of 3×10^{11} ohms and the standard time-constant

[7] The quoted values for input capacity were measured in the laboratory by using a rate-of-charge method with a grid resistor of 10^{13} ohms.

[8] See, e.g., p. 437 of Strong's *Procedures in Experimental Physics* (New York: Prentice-Hall, Inc., 1938). Here the author, Whitford, has given formulae in a form convenient for one working with d.c. circuits and long time-constants.

of 1.5 seconds, which will allow a measurement in the convenient interval of 10 seconds. The two important sources of noise in the input circuit will be the thermal noise of the grid resistor and the shot component of the photocell dark current, if we assume a negligible contribution from the shot component of the grid current. The dark current of a refrigerated CE-25 operating at low voltage is about 10^{-16} amperes for a good cell; and a current of this amount will have a shot-noise component of 0.6×10^{-6} r.m.s. volts across the resistor. The thermal noise of the grid resistor, on the other hand, is 23×10^{-6} r.m.s. volts, a factor thirty-nine times greater than the noise contributed by the photocell. The chief reason for the success of the multiplier lies in its ability to amplify greatly before the introduction of a resistor into the circuit, thereby removing the thermal noise of the resistor from consideration as an important factor. If the resistor is removed entirely, the observer will be forced to work with a rate-of-charge method, with its inherent serious practical disadvantages over the constant-deflection method.

To a limited extent, amplification within a photocell can be accomplished by filling the photocell with an inert gas under low pressure. The gas molecules are ionized by electronic bombardment, and the resultant secondary electrons are collected, along with the primary electrons, by the anode. The maximum gas multiplication that may be used to advantage in *CsO-Ag* photocells at room temperature is 8–12, whereas at 194° K this value may be made as high as 20–25. Higher values of gas multiplication result in damage to the cathode of the photocell and in high noise levels, because of bombardment of the cathode by gas ions.[9] Clearly, however, if the gas multiplication could be somewhat higher than 39, sufficient amplification would be available to make the photocell-noise level appreciably greater than the resistor thermal-noise level, and the photocell would then be operating under conditions near perfection. It is a fact, furthermore, that increase of the grid resistor will cause the signal to increase directly in proportion, but it will cause the resistor thermal noise to increase only as the square root. Therefore, if means can be found to increase the grid resistor without prohibitive increase in the time-constant, we shall have available another method for decreasing the disparity between the noise level of the photocell and that of the grid resistor. The remainder of this paper will be devoted to a description of operational methods for accomplishing an increase of the grid resistor to values as high as 5×10^{13} ohms and of a method for constructing gas-filled photocells so they may be used at high multiplying factors.

INCREASE OF GRID RESISTANCE

There are at least two practicable methods for artificially modifying the characteristics of the input circuit of a photocell-amplifier assembly so that the grid resistor may be increased by a large factor without sacrificing other desirable properties of the circuit. Both methods involve the use of electrical feedback, and either will permit increase of the grid resistor by a factor of more than 100 without increase in the effective time-constant. If the grid resistor were the sole source of noise in the circuit, the factor-of-100 increase in resistance would result in an increase in S/N by a factor of 10.

The first of the two methods is based upon the principle of capacity neutralization; that is to say, direct feedback is employed in such a way, and to such a degree, as to turn part of the input capacity of the photometer circuit into an artificial negative capacity,[10] which will neutralize part of the remaining positive capacity and effectively reduce the input capacity by a factor limited only by the stability of the feedback amplifier. Techni-

[9] H. L. Johnson has pointed out that a photocell operating at a gas-multiplying factor of about 20 or more shows a decrease in S/N for moderately faint light, although it operates well on very faint light and on comparitively bright light. My experience supports this observation, but there seems to be no apparent explanation for the phenomenon. The effect is not large, and it disappears for gas-multiplying factors under 15.

[10] This is simply an extension of the principle employed when the cathode-follower circuit was adopted.

cal aspects of this circuit, as well as a practicable design, have already been published.[11] A theoretical discussion also has been published by H. L. Johnson.[12]

A photometer operating on the direct-feedback principle was used at the Lick Observatory for routine photoelectric photometry for about a year. It was found that the method could be employed with grid resistors at least as high as 1×10^{13} ohms, with good circuit stability and with good results when used for the photometry of variable stars. The circuit was found impracticable for use in determining magnitudes, however, owing to a limited range of linear operation. The input grid of electrometer tubes will give appreciable nonlinear operation if used with signals much over 1 volt. Inasmuch as the minimum useful signal of an operational photometer is about 5 millivolts, it is clear that the allowable range is only by a factor of 200. The voltage range (equivalent to light-range) can be extended by control of the gas multiplication of the photocell. Such a practice, however, may result in a small change in the color sensitivity of the cell, and, moreover, the wait for recovery of the cell after a voltage change is time-consuming. The signal range can also be extended by employing two grid resistors of different values and a switching arrangement so that either resistor may be used. In practice it was found that a change in grid resistor required a compensating change in feedback value. This procedure was so time-consuming that the operational efficiency on magnitude work was seriously impaired and the method was judged to be impracticable, except for variable-star photometry.

The second means to be considered for increasing the grid resistor of a photometer depends upon the use of inverse feedback, injected via the grid resistor. This type of circuit also has been treated theoretically by H. L. Johnson.[13] When development of the inverse-feedback photometer was under way, this type of circuit was found to be relatively sensitive to noise instability in the feedback amplifier. Because the amplifier was required to be of relatively high gain (about 100, compared with 3–4 for the direct-feedback circuit), the problem of noise reduction turned out to be a serious one, and most of the developmental work was devoted to a solution of this problem. Simple, conventional, direct-coupled amplifiers were found to be too noisy for use, probably because of the phenomenon of cathode fluctuation noise. The so-called "contact-modulated" amplifier[14] is less affected by tube noise than a conventional direct-coupled amplifier, and it has been found satisfactory for the feedback amplifier in the application considered here. The contact-modulated amplifier performs best when operated from a low-impedance source, such as a thermocouple. In the present application, the contact-modulated amplifier does not perform so well as when operated from a low-impedance source. However, continuous operation with an equivalent noise, referred to the input grid, of 0.5 microvolts peak-to-peak is possible, and this value is sufficiently low for satisfactory performance.

PRACTICAL CIRCUIT

Figure 2 is a circuit diagram of a practical contact-modulated, direct-coupled amplifier. The input from the 5800 stage (terminal *A*) is grounded by one pair of points of a vibratory "chopper" at a rate of 60 times per second; thus if a voltage exists at *A*, the chopper will turn it into a pulsating square-wave voltage. This pulsating voltage may now be amplified by an a.c. amplifier, consisting in this case of two stages of triode amplification. The output from the a.c. amplifier is a 60 c.p.s. alternating voltage with sufficient harmonics to approximate a square wave. The second pair of contacts in the same chopper then grounds the output of the a.c. amplifier through a condenser. The effect is

[11] *Pub. A.S.P.*, **59**, 190, 1947; *Electronics*, August, 1948.

[12] *Ap. J.*, **107**, 34, 1948; *Lick Obs. Contr.*, Ser. II, No. 21.

[13] *Pub. A.S.P.*, **60**, 303, 1948.

[14] R. Gunn, *Rev. Sci. Instr.*, **9**, 267, 1938; Liston, Quinn, Sargeant, and Scott, *Rev. Sci. Instr.*, **17**, 194, 1946.

to restore the amplified voltage to its original pulsating condition, which is changed back to simple d.c. voltage by means of resistance-capacity smoothing circuits. The band width of the amplifier is limited on the high-frequency side by a shunt capacity to ground from the plate of the first triode, and on the low-frequency side by the interstage coupling network.

The amplifier of Figure 2 is designed so that the d.c. output is opposite in phase to the d.c. input. Therefore, if the output is coupled to the input, an inverse-feedback condition will exist. When the 5800 stage is added according to the terminal coding in Figures 1 and 2, the assembly becomes an inverse-feedback, direct-coupled amplifier having an internal loop gain of from 50 to 100 (depending upon the gain potentiometer setting) with 100 per cent feedback. The apparent voltage gain from the photocell to the output will be close to unity. The good effects of the inverse-feedback amplifier are twofold: the effective time-

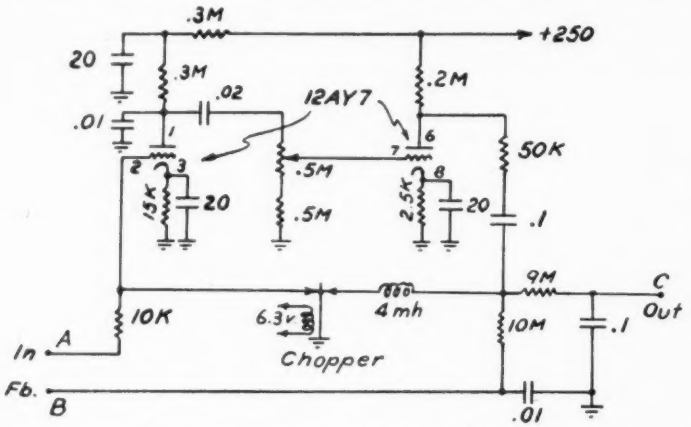

FIG. 2.—Diagram of feedback amplifier. The terminal coding indicates connections to the circuit of Figure 1. The output may be connected to a galvanometer or to the amplifier of Figure 3 if the self-recording feature is desired.

constant of the input circuit will be decreased by a factor approximately equal to the loop gain, and the over-all linearity of the circuit for large signals will be improved. The circuit here described will operate over an output range up to 25 volts without showing an appreciable error caused by nonlinearity.

Experimental work with the inverse-feedback amplifier has shown that the Victoreen grid resistors can be a source of difficulty sufficiently acute to make operation of the amplifier impossible. We noted that some circuits would respond very slowly to light, whereas others would respond unreasonably fast, all things being equal except identity of the parts constituting the amplifiers. Very fast response was sometimes accompanied by a strong tendency for the amplifier to "overshoot," a condition that suggests incipient oscillation. It was found that the circuit element responsible for this unconventional behavior was the input resistor and that the trouble could be cured permanently for a given amplifier by selection of a grid resistor having suitable characteristics. Practically all resistors of 1×10^{13} ohms were found to be useful, about 50 per cent of 2.5×10^{13} ohm resistors were good, while only about one in three of value 5×10^{13} ohms could be used.[15]

[15] H. L. Johnson (n. 12) has studied the behavior of high-value Victoreen resistors. He finds that "fast" resistors behave electrically as if they were connected in series with a very high inductance. The phenomenon of the "slow" resistor is similar to the behavior to be expected from a pure ohmic resistor with a parallel capacitance. It may be presumed that both phenomena are caused by a transient non-

In Figure 2 an interstage gain control is provided, to allow some adjustment of the effective indication time of the circuit. A range of from 10 to 20 seconds is provided by the control for an input resistor of 5×10^{13} ohms. The 4 millihenry choke in the output-point circuit of the chopper decreases sparking of these points to a negligible value. We use the Brown Converter as a chopper. The points must be adjusted to be "make-before-break"; that is to say, during no part of their operating cycle must the input and output circuits of the contact-modulated amplifier be simultaneously ungrounded.

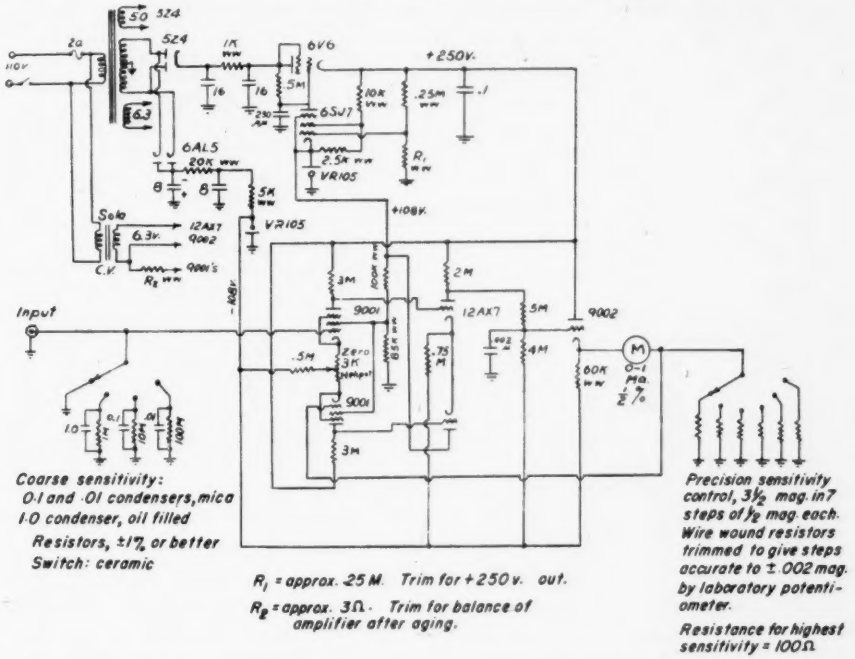

FIG. 3.—Diagram of an amplifier suitable for driving an Esterline-Angus or a Brown recorder from the circuits of Figures 1 and 2. The power supply of this amplifier may be bled for power to run the feedback amplifier of Figure 2.

The amplifier of Figure 2 is highly sensitive to hum potentials arising from stray pick-up. A hum frequency will appear at the output of the amplifier as a d.c. voltage; thus any *variation* in the hum, caused, for example, by variations in the line voltage, will appear as noise in the d.c. output. If the effective hum level referred to the first grid is 10 microvolts and the line voltage varies by 10 per cent, an output noise of 1 microvolt will result. This is the maximum tolerable noise level. The amplifier must be built with unusual attention to hum reduction, particularly if the power supply is built into a common chassis. The best way to reduce hum is to build the amplifier with a separate power supply. Figure 3 shows a d.c. power amplifier useful for coupling the feedback amplifier to a meter; the amplifier also contains a power supply that may be bled for power to run the chopper amplifier in a separate chassis.

ohmic behavior of the resistor during a voltage change. The transient effect is neither caused, nor influenced, by refrigeration. It may be possible to compensate the effect by means of modification of the external circuit, but we have found no practicable way of making a suitable modification.

Figure 4 shows the parts for a complete photocell feedback photometer, which consists of the receiver, the complete amplifier, and the recorder. All components, with the exception of the 5800 stage, are operated from the 120-volt line. The amplifier contains all the circuit elements of Figures 1, 2, and 3, with the exception of the parts contained in the receiver. The amplifier carries on its front panel all the controls, and it may be employed with a multiplier as well as with the photocell, with the addition of a voltage supply to furnish the dynode potentials to the multiplier. Figure 5 shows the interior of the refrigerated photocell receiver. The compact mounting of the small parts can be seen; the external cubical case is made of balsa wood for thermal insulation. The dry ice is pulverized thoroughly and packed into this wooden case. The electrical connections are introduced into the evacuated receiver by means of the base connections of a standard metal vacuum tube that has had its envelope and all internal structure removed.

The circuits of Figures 1, 2, and 3 constitute the electrical parts for a photoelectric photometer that can be used with negligible systematic instrumental error for making magnitude comparisons over large ranges in intensity. The output of the circuit of Figure 2 (terminal *C*) may be followed by a 10/1 attenuator, simply by providing a switch to add a 1-megohm resistor to ground. If these circuits are employed with a meter having a long scale, the total range in light-intensity that can be measured with satisfactory precision is 1000 to 1, or 7.5 mag. An effective means of increasing the range is to place a fine screen over the objective of the telescope. The photometer described here has been employed in a program to determine red magnitudes,[16] and further information on characteristics of the photometer as a whole is given in that report.

RADIO INTERFERENCE

The circuits of Figures 1 and 2 are sensitive to interference from strong radio fields, such as those emanating from near-by broadcasting stations. Long-wave interference can be eliminated by simple by-passing of the leads of the receiver where they enter the evacuated tank. Small by-pass condensers for this purpose may be seen in Figure 5. Intense high-frequency fields, such as those from powerful FM or television transmitters, are much more difficult to cope with, and they require the use of specialized shielding and by-passing. Each radio-interference problem is a special case and must be dealt with by applying appropriate methods. The principal reason for mentioning radio interference here is to help trace the source of an otherwise unexplainable high noise level in a given photometer installation.

EFFECTS OF REFRIGERATION ON CIRCUIT COMPONENTS

a) *Resistors.*—Victoreen resistors have a negative temperature coefficient, and it is reasonable to expect that their values will increase considerably when their temperature is greatly reduced. We have observed an increase of 19 per cent over the room-temperature value when refrigerated with dry ice and a 290 per cent increase when refrigerated with liquid nitrogen. The noise level of the resistors decreases with refrigeration with dry ice; experiments to determine noise level with liquid nitrogen refrigeration are complicated by the large change in resistance and its accompanying change in time-constant, and these experiments are incomplete. Our experiments were made with about ten resistors, all of which have been temperature-cycled many times, and we have noted no other effects of refrigeration on the resistors.

b) *The 5800 tube.*—This tube at room temperature is remarkable for its low value of cathode fluctuation noise. At reduced temperatures, however, there may be a large increase in this form of noise, which may be returned to the small value for the tube at normal temperature by increasing the filament current, which can conveniently be done by operating the filament directly from a dry cell without a series resistor. Refrigeration

[16] Kron and Smith, *Ap. J.*, **113**, 324, 1951; *Lick Obs. Contr.*, Ser. II, No. 34.

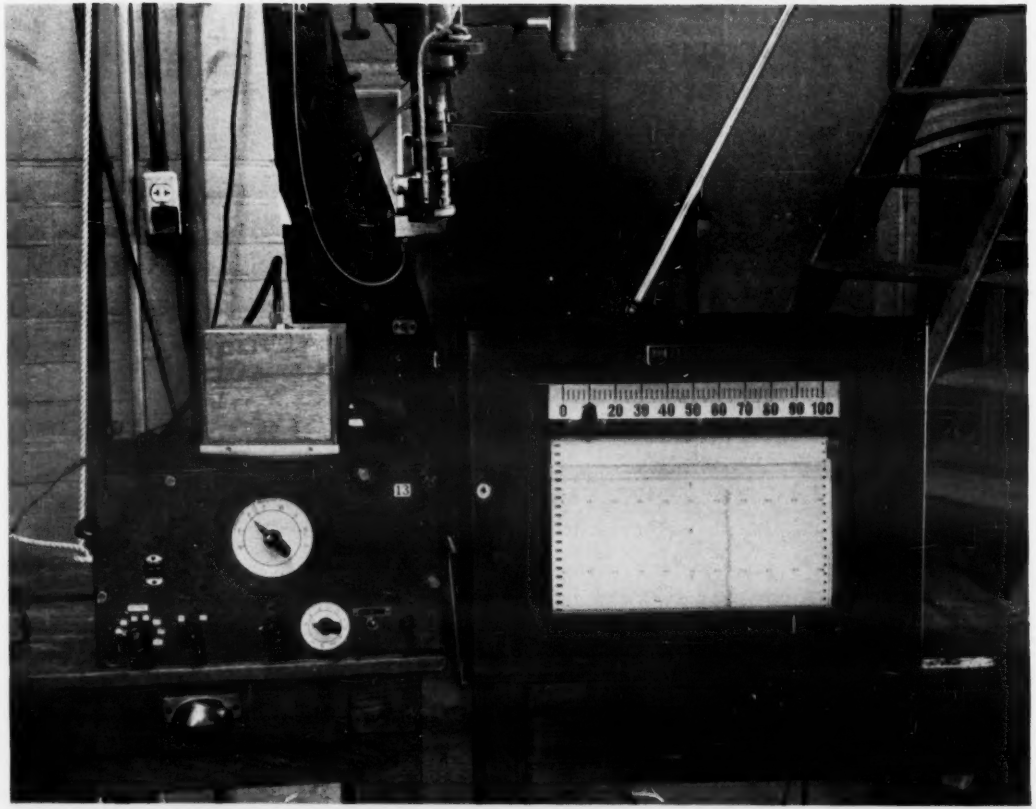

FIG. 4.—Complete photometric equipment in the dome of the 12-inch refractor. The photocell light-receiver may be seen on top of the amplifier. The amplifier contains all circuit elements shown in Figures 1, 2, and 3.

FIG. 5.—The light-receiver, showing interior construction. Photocell and 5800 tube are inclosed in the central structure, which forms the inner shield. The grid resistor is visible, as well as small by-pass condensers for reducing radio interference.

with dry ice and liquid nitrogen causes a small decrease in plate current and a considerable decrease in the shot noise of the grid current, which suggests that the grid current may be reduced by the refrigeration. In other respects the 5800 tube seems to be unaffected by refrigeration.

c) The photocell.—When a gas-filled photocell is refrigerated, the dark current diminishes, and the cell may be operated at increased gas multiplication by raising the cell voltage. The dark current of a photocell has two components—that portion of the current caused by simple leakage conduction and that portion caused by thermal emission of the cathode material. The conduction current is nearly proportional to the applied voltage, and it is practically independent of the cell temperature. The emission current, on the other hand, is approximately an exponential function of applied voltage, and it is strongly affected by ambient temperature. These differences between the properties of the two components of dark current may be used, if one desires, as part of a thorough investigation of the properties of a given cell, to measure each component by itself.

At room temperature the emission current of the average CE-25 photocell is wholly dominant, whereas at the temperature of dry ice the conduction current may dominate. At the temperature of liquid nitrogen the emission current becomes practically zero, and the conduction current is wholly dominant. Most CE-25 photocells show such a small emission dark current at the temperature of dry ice or lower that reliable measurements cannot conveniently be made with the photometer itself. Noise-level measurements indicate that the dark current of a good CE-25 refrigerated with dry ice and polarized with 16 volts (too low for appreciable gas multiplication) is less than 10^{-16} amperes, but probably greater than 2×10^{-17} amperes. The conduction current under the same conditions is about 10^{-16} amperes or less. The dark resistivity, exclusive of conductivity effects caused by the emission, is therefore about 1.6×10^{17} ohms, for a good tube. A gas-multiplying factor of 2–4 will bring the shot noise from the emission current into equality with the shot noise of the conduction current. Cooling with liquid nitrogen gives no important further decreases in total dark current. The conduction component of the dark current stays about the same, and it conceals the large decrease in the emission current, which becomes too small to be detected.

The maximum gas-multiplying factor at which a CE-25 may be operated at room temperature without disproportionate increase in dark-noise level depends upon the cell, but it is about 6–10, which is a factor that is reached with about 90 volts on the cell. At the temperature of dry ice the gas multiplication may be raised to 15–25, depending upon the cell, at cell voltages from about 130 to 150. At the temperature of liquid nitrogen the one cell tried could be operated at a gas-multiplying factor of over 50 without excessive dark noise. It is apparent that further improvement in S/N should result from refrigeration with liquid nitrogen, but so far our experience is too meager to be certain of an improvement in practice.

Within the rather considerable errors of observation, the quantum efficiency of a photosurface remains independent of temperature. In our experience refrigeration has caused no damage to photocells.

Figure 6 shows some noise records of a photocell photometer operating at a voltage sensitivity of 1 millivolt per scale unit, with an effective time-constant of 1.5 seconds and with a grid resistor of 2.5×10^{13} ohms. Record *A* shows the noise level with the grid resistor short-circuited; this is, effectively, the noise level of the amplifiers. Record *B* is the noise level with the grid resistor in the circuit at 70° F., while record *C* is the same as *B* but with the receiver temperature reduced with dry ice. The reduction in noise caused by the refrigeration is somewhat larger than one would expect from the temperature effect on the thermal noise of the grid resistor, and it may be caused partly by a reduction in grid current of the 5800 tube. The pulses visible on records *B* and *C* are caused by cathode fluctuation noise in the 5800 tube. Not counting the amplitude of the pulses, which are of short duration, the r.m.s. noise level of record *C* is about 250 microvolts, equal within

the observational error to the theoretical thermal noise level of the input resistor, of value 2.5×10^{13} ohms. The best operating potential for the photocell is found by applying increasing photocell voltage until the noise level appreciably increases. Under these conditions the photocell, if its conduction current is not unduly high, will be operating under conditions closely approximating those obtained by means of secondary-emission multiplication. Record *D* was obtained with a CE-25 in the circuit operating at a gas-multiplying factor of 24; the additional noise due to the cell is about 1000 microvolts. Of the 1000 microvolts, about 120 are caused by the shot component of the conduction

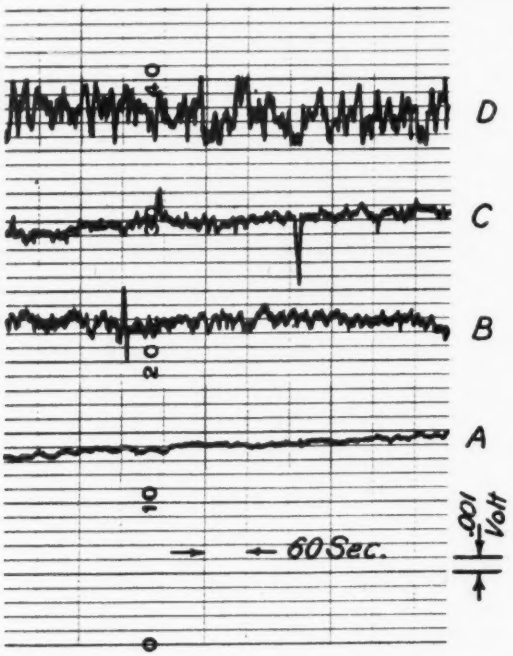

FIG. 6.—Noise-level records of the complete infrared photocell photometer, made with a Brown recorder. The significance of the various records is described in detail in the text.

current, which was about 10^{-15} amperes at the cell voltage required to give a gas-multiplying factor of 24. Thus, since random noise combines as the square root of the sum or difference of the amplitudes, about 980 (or let us say 1000) microvolts are caused by the multiplied dark-emission current; dividing this value by 24, we get about 40 microvolts of noise originating from the unmultiplied dark-emission current, which must, therefore, have been a current of about 5×10^{-17} amperes or less. The cathode area is about 3 cm^2, so the dark emission per square centimeter of cathode area is less than 2×10^{-17} amperes when the cathode is at the temperature of dry ice.

SPECIAL PHOTOCELLS

The problem of measuring small photocurrents without introducing extraneous noise is simplified if the gas-multiplying factor can be brought to values approaching 100 without a decrease in S/N of the photocell and without damage to the photocell cathode ma-

terial. As shown earlier in this report, a cell with a gas multiplication of 39 would contribute noise equal to that of the largest input resistor that would allow operation of the photometer without feedback; thus the operating S/N would be poorer than perfection only by a factor of $\sqrt{2}$. A cell with a gas-multiplying factor of 100 would therefore operate at least as well as a multiplier and without the circuit complications required for feedback. In the present investigation, the feedback method and the use of high gas multiplication were under development contemporaneously.

E. Steinke[17] has shown that a potassium hydride gas-filled photocell can be operated at gas-multiplying factors up to 50 without a decrease in S/N, and up to 600 without damaging the photocell. Furthermore, it is well known that the potassium hydride photocells made by Professor Jacob Kunz could be operated at gas-multiplying factors up to 70 without loss of S/N, which explains why they could be used with success in circuits with grid resistors as low as 10^{11} ohms. The foregoing is evidence that photocells exist that can be operated at high gas-multiplying factors, although they are not red-sensitive.

The low gas-multiplying factor allowable with *CsO-Ag* infrared-sensitive photocells usually is explained by sensitiveness of the cathode surface to ionic bombardment. The ions released during the gas-multiplying process are collected by the negative cathode surface; the effect of the impacts in some way increases the noise level disproportionately to the signal, and they can even cause a temporary change in the characteristics of the surface, usually an increase in the infrared sensitivity. Clearly, if the difficulty with high gas-multiplying factors is caused by ionic bombardment, then construction of a useful high-multiplication cell should be possible if the cathode could in some way be shielded from positive ions. The designers of high-power gas triodes ("Thyratrons") have a similar problem, which was solved by carefully protecting the cathode from the ions. The photocell problem is more difficult because shielding must not interfere with the passage of light to the cathode and, furthermore, it must not result in only partial collection of the primary photoelectrons, for loss of the primary electrons, if it occurs before the multiplying process, is equivalent to loss in sensitivity of the surface.

Special photocells[18] of several designs were constructed in an attempt to find an electrode configuration for accomplishing the desired purpose. The design shown in Figure 7 was decided upon, and ten sample cells were made. Laboratory tests, made by measuring the distribution of current drawn by all three of the electrodes in the tube, indicated that approximately 70 per cent of the ions were gathered by the ion collector. Most of the remaining 30 per cent of the ions must bombard the cathode, but the electrostatic shielding of the cathode by the ion-collector insures that the ions will arrive at the cathode at a velocity lower than they would have in an equivalent diode cell. The cathode thus operates under conditions like those in a low-voltage cell, even though the anode voltage may be high enough (150 volts) to cause the complete breakdown of a diode cell.

All the sample cells had a cathode sensitivity of about half that of a good CE-25 photocell, probably due to the lack of a wider selection. Tests were made only in the refrigerated condition. It was found that all cells would give quiet gas multiplication for factors up to 40, that three cells could exceed 70, and one could be operated at over 100. The best potential for the ion collector was found to be the same as the cathode potential, a fact that contributes to simplicity of circuit connections. It was found that the S/N of the cell deteriorated if the anode current exceeded 10^{-12} amperes, a condition that does not restrict the value of the cell in astronomical applications.

By the time the experiments with the special cells were completed, the feedback circuit for employing high grid resistors had been developed and was in use. The relatively low cathode sensitivities of the sample cells discouraged their adoption in our general

[17] *Zs. f. Phys.*, **38**, 378, 1936.

[18] The special cells were made by the Continental Electric Company, Geneva, Ill., through courtesy of the chief engineer, Dr. S. Paksweг.

photometric work. Nevertheless, the success of the principle makes the special cell of continuing interest and of potential value. Because of this possibility, the foregoing description of the special cells was included in this paper.

CONCLUSION

Practical experience with the inverse-feedback circuit, gathered during more than two years of routine use, indicates that it is superior in sensitivity and practicability to non-

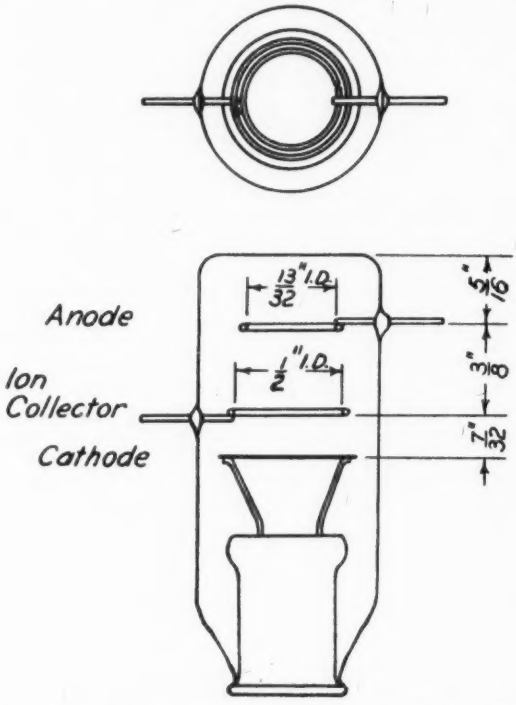

FIG. 7.—Design for a special high gas-multiplication photocell. Detailed description of the cell and its performance is given in the text.

feedback circuits. The photometer illustrated in Figure 4 and employed with the 36-inch Crossley reflector or the 36-inch refractor of the Lick Observatory can be used to carry a two-color red-infrared magnitude system to stars of 12th to 15th photographic magnitude, depending upon color. A six-color photometer employing a Western Electric D-97087 photocell and the feedback circuit has been built for the use of Dr. Joel Stebbins. When used on the Crossley reflector, the feedback six-color photometer compares favorably with the photometer formerly employed by Stebbins and Whitford[19] on the 60-inch reflector at Mount Wilson.

The performance obtained with photoelectric cells employed with the feedback circuit is about equivalent to the best to be expected from a constant-deflection method em-

[19] *Ap. J.*, **98**, 20, 1943.

ploying a Hoffman electrometer.[20] It is unlikely that further improvement in performance can be accomplished by employing a multiplier, although the advantage to be gained in simplicity and response time (where required) is obvious.

I am indebted to Messrs. A. E. Whitford, H. L. Johnson, and J. Lynn Smith for their helpful suggestions and co-operation during the course of this work, and to the Continental Electric Company for their willingness to construct the special cells. The work was made possible by financial assistance from the Office of Naval Research.

[20] Sinclair Smith, *Ap. J.*, **76**, 286, 1932.

A PHOTOELECTRIC STUDY OF U PEGASI IN TWO COLORS*

ROBERT LAFARA
Goethe Link Observatory, Indiana University
Received July 13, 1951

ABSTRACT

Photoelectric observations of the light- and color-variations of a W Ursae Majoris type eclipsing binary are presented. In addition, all available spectroscopic information is included. A brief discussion is made of the peculiarities of the system, and the approximate elements of the orbit are given, in addition to the precise light-elements.

The system of U Pegasi[1] has been observed numerous times, both visually and photographically, since it was discovered to be variable in 1894 by S. C. Chandler.[2] Since only a few W Ursae Majoris type stars have been investigated photoelectrically, the present study is an attempt to define the light-curve accurately and to investigate the color-variation of the system by means of simultaneous photoelectric observations in two colors.

Although this system has been observed photometrically many times,[3] the spectroscopic observations have been few. The spectrum has been classified by different observers from F3 to G3. Adams, Joy, and Sanford[4] found double lines and gave the velocity range as -60 to $+135$ km/sec. Struve and Horak[5] have found $K_1 = 165$ km/sec and $K_2 = 205$ km/sec on the basis of four spectrograms and the times of minima as presented in this paper. From this, they conclude that the more massive star is eclipsed at secondary and the mass ratio is 1.25. The mass ratio could possibly be greater if the radial velocity of the system is not zero. Struve also comments:

> Our photographs show quite definitely that the violet component of the double lines is stronger at phases $0.646P$ and $0.790P$. Unfortunately, we do not have spectrograms near phase $0.25P$, and we are not able to ascertain whether the positions of the stronger and of the weaker components are reversed. However, it has been my experience in the case of other stars of the W Ursae Majoris type that the violet component often remains the stronger, despite the fact that one normally expects to see their position reversed. This unusual appearance has been discussed by me on various occasions, and it also has been commented upon by D. M. Popper. It is a purely physical effect and is, in fact, the observational reason why I believe that each component carries in front of it a fairly thick mass of gas belonging to an unsymmetrical envelope.

U Pegasi was observed with a photoelectric photometer attached to the 36-inch telescope of the Goethe Link Observatory. The photometer contains a set of filters and a field lens that throws an out-of-focus image on the cathode of an unrefrigerated 1P21 photomultiplier tube. The yellow filter is a Corning 3385, 1 mm thick, of effective wave length 5350 A, and the blue filter consists of a Corning 3060, 1 mm thick, cemented to a Corning 5543, 2.5 mm thick, the combination having an effective wave length of 4500 A. Each normal point in Table 1 is the average of at least four observations made

* *Publications of the Goethe Link Observatory, Indiana University*, No. 4.

[1] BD+15°4915, $\alpha = 23^h55^m26^s$, $\delta = +15°40'$ (1950); $m_v = 9.5$–10.1.

[2] *A.J.*, **15**, 181, 1895.

[3] For a complete list of references see *Contr. Princeton U. Obs.*, No. 22, 1947.

[4] *Pub. A.S.P.*, **36**, 139, 1924.

[5] Private communication.

on different nights. Each observation is the mean of four deflections. These differential magnitudes were corrected for sky background and differential extinction, the latter amounting to 0.009 mag., at the most. The Δm's are given in the sense of comparison *minus* variable, the color is yellow *minus* blue, and the phase is in fractions of a period. The comparison star used was BD+15°4912, whose constancy was checked by other stars in the field as well as with reference to the North Polar Sequence.

Figure 1 is a plot of the light- and color-variations. It may be noted that the light-curve is relatively smooth, not showing the deformations reported by other observers of W Ursae Majoris type systems. The color becomes redder at both eclipses, which indicates that the hemispheres of both stars which face away from each other are redder than those which do face each other. This is what would be expected because of mutual heating and gravity darkening in such highly distorted stars.

TABLE 1

NORMAL LIGHT- AND COLOR-CURVES OF U PEGASI

Phase	$\Delta m_{(c-v)}$		Color	Phase	$\Delta m_{(c-v)}$		Color
	Yellow	Blue			Yellow	Blue	
0.0184	0.580	0.441	0.139	0.4998	0.616	0.496	0.120
.0307	0.648	0.516	.132	.5174	0.631	0.503	.128
.0563	0.734	0.616	.118	.5288	0.664	0.541	.123
.0752	0.809	0.691	.108	.5454	0.729	0.609	.120
.0939	0.891	0.771	.120	.5675	0.821	0.701	.120
.1147	0.954	0.834	.120	.5910	0.912	0.793	.119
.1342	0.983	0.868	.115	.6276	1.002	0.890	.112
.1596	1.026	0.912	.114	.6694	1.077	0.964	.113
.1825	1.066	0.957	.109	.7111	1.117	1.011	.106
.2135	1.102	0.993	.109	.7585	1.122	1.013	.109
.2452	1.109	1.002	.107	.7945	1.099	0.993	.106
.2780	1.117	1.000	.117	.8279	1.058	0.950	.108
.3066	1.099	0.992	.107	.8597	1.012	0.902	.110
.3354	1.065	0.956	.109	.8813	0.962	0.854	.108
.3650	1.028	0.918	.110	.9042	0.897	0.783	.114
.3973	0.950	0.838	.112	.9304	0.782	0.656	.126
.4248	0.860	0.745	.115	.9592	0.658	0.531	.127
.4445	0.783	0.671	.112	.9779	0.568	0.438	.130
.4675	0.687	0.557	.130	0.9960	0.536	0.398	0.138
0.4851	0.631	0.504	0.127				

An attempt was made to determine the elements of the system, but when the minima are of nearly equal depth, as in this case, there are numerous solutions that fit the data. The yellow curve was first rectified by Russell's method,[6] and the resulting curve was solved by Kopal's method for partial eclipses.[7] The various possible solutions indicate that the radii of both stars are about 0.4 of the distance between their centers and that the inclination of the orbit to the celestial sphere is about 70°. The solutions fit the data with a probable error of ± 0.004 mag.

In Table 2 are listed the heliocentric times of minima, the epoch, and the residual from:

$$\text{JD of minimum} = 2430260.6790 + 0.3747821575E,$$

the initial epoch being the last primary minimum observed by Recillas and Woodward.[8]

[6] *Ap. J.*, **108**, 388, 1948.

[7] *An Introduction to the Study of Eclipsing Variables* (Cambridge: Harvard College Observatory, 1946), eq. (79), p. 70.

[8] *A.J.*, **51**, 101, 1945.

The probable error of a time of minimum is ± 0.0004 days.

A new and more complete theory of the W Ursae Majoris type stars must be worked out in order to explain the peculiar color-variation as well as the highly distorted light-curves. Other W Ursae Majoris systems should be investigated more thoroughly in order to determine whether they show the same variation of period[8] as that exhibited by U Pegasi.

This investigation was made at the suggestion of Dr. John B. Irwin. I wish to express my thanks to the faculty and staff of the Indiana University astronomy department for their aid in the observations of U Pegasi and for their suggestions and assistance in the reduction of the data. I also wish to thank Dr. Otto Struve for the information he has contributed on the mass ratio and radial velocities of this system.

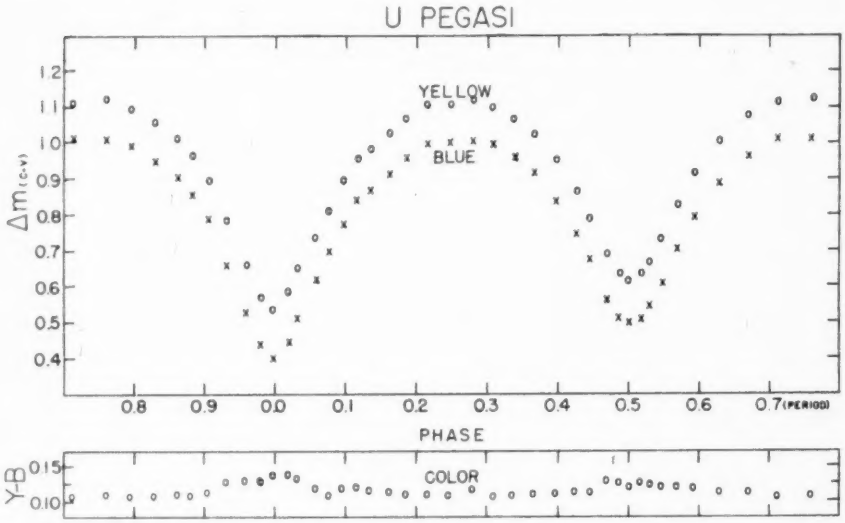

FIG. 1.—Light- and color-variations of U Pegasi

TABLE 2

TIMES OF OBSERVED MINIMA OF U PEGASI

Date	Time of Minimum JD 2433000+	Epoch	Residual (O−C)
1949 Sept. 23	182.8561	7797.0	+0.0006
Oct. 1	190.7262	7818.0	+ .0003
1	190.9132	7818.5	− .0001
13	202.7181	7850.0	− .0008
Nov. 10	230.6408	7924.5	+ .0006
24	244.5075	7961.5	+ .0004
Dec. 5	255.5630	7991.0	− .0002
1950 Oct. 4	558.7624	8800.0	+ .0004
7	561.7592	8808.0	−0.0010

THE LUNAR ECLIPSE OF SEPTEMBER 26, 1950*

JAMES CUFFEY
Goethe Link Observatory, Indiana University
Received July 13, 1951

ABSTRACT

Photoelectric light-curves in red and ultraviolet light for a small region of the moon centered on the crater Tycho were obtained under unusually good observing conditions. The light-curves (Fig. 1) give the intensity of the region of Tycho plus the intensity of the scattered light from the uneclipsed parts of the moon. In the present set of observations it was not possible satisfactorily to eliminate the scattered component (see text). The present results are to be regarded as provisional and not of high accuracy.

Tycho was dimmed at totality by 8.01 mag. in red light and by 14.05 mag. in ultraviolet. The essentially flat portions at the bottoms of the eclipse-curves lasted approximately 100 minutes (red) and 40 minutes (ultraviolet). Some observations in blue and yellow light were also obtained for purposes of calibration. Color indices, on the International System, obtained for Tycho were, during eclipse, $C_{int} = +2.97$ and, outside eclipse, $+0.60$. In ultraviolet and red light the color indices were $C_{uv-r} = +4.03$ for eclipsed Tycho, and -2.11 for uneclipsed Tycho. Details concerning calibration of the C_{uv-r} in terms of C_{int} are given.

OBSERVATIONAL DETAILS

The unusually favorable circumstances of the eclipse of September 26, 1950, led us to obtain experience, a few nights previously, in using the photoelectric equipment for observing small areas of the moon. It became evident that modifications were necessary for preventing scattered light within our photometer and that small diaphragms would be needed for the 36-inch mirror. An extension tube, with several baffles for eliminating scattered light in the photometer, and suitable diaphragms for the 36-inch mirror were therefore constructed. Experiments had shown that accurate guiding could be accomplished with a relatively small photometer diaphragm centered on the crater Tycho. This crater was chosen because of its conspicuousness and because it would pass closer to the center of the earth's shadow than would the moon's center. The technique of guiding on Tycho through the photometer aperture selected during these trials (0.′4) proved satisfactory during the first part of the eclipse. However, as the eclipse approached totality, guiding on Tycho became increasingly difficult, partly because of the smallness of the photometer aperture and partly because of the moon's rapid motion in declination. During the second half of the eclipse, therefore, a larger photometer aperture (3.′3) was used.

The equipment used included a 36-inch $f/5$ aluminized reflector with 5- and 3-inch off-axis apertures; a 1P21 photomultiplier with d.c. amplifier of the Kron type, and a Brown Electronik 0-10 MV recorder. The filters had the characteristics shown in the accompanying tabulation.

RESULTS OF THE OBSERVATIONS

The lunar eclipse light-curves, corrected for extinction to a point outside the earth's atmosphere, are shown in Figure 1. Magnitudes based on single deflections are plotted. Since the extreme intensity range in the ultraviolet greatly exceeded the 10-mag. range of our amplifier, it became necessary to make auxiliary zero-point determinations from the observations themselves. Originally, we had planned to calibrate the telescope apertures on an intensity basis, but this did not prove practicable. Therefore, the light-curve was obtained by integration of the slopes found in a given set of observations. Evalua-

* *Publications of the Goethe Link Observatory, Indiana University*, No. 5.

tion of the zero-point shifts by this method proved satisfactorily accurate for the observations of egress, but quite uncertain for those of ingress. They were necessary, however, only at five points in the light-curves. In general, the magnitudes rest upon a careful calibration of the amplifier resistors.

It must be borne in mind that Figure 1 represents the apparent brightness of Tycho. That is, it includes the light from Tycho as, usually, the main component but also, as smaller contributions, the light scattered by the earth's atmosphere from other parts of the moon into the air in front of Tycho plus a very small contribution from the light of the night sky. The necessity for including these intensities and the difficulties attendant upon any attempts to correct for them will be evident from the following discussion of the observations.

During eclipse the light-changes took place with great rapidity, and the use of a comparison star as a control on the extinction was impracticable. A more serious difficulty, however, arose from the impossibility of measuring accurately at a given instant,

Filter	No. (Corning, Jena)	Thickness	λ Band	λ Effective*
Ultraviolet	UG 1 BG 9780†	1 mm 1 mm	3500–3900	3700
Blue	3850 (0–51) 5850 (7–59)†	⅔ standard ⅓ standard	3700–4700	4250
Yellow	9780 (4–76) 3384 (3–70)	½ standard ¼ standard	5000–6200	5400
Red	2418	2.6 mm	6000——	6200

* Estimated from published sensitivity-curves and commercially available transmission-curves of the filters, assuming the 1P21 cell used is not abnormally red-sensitive.

† Second component cemented to first with Canada balsam. Eliminates red transmission in case of ultraviolet filter.

and at a given region near the partially eclipsed moon, the atmospheric background of scattered light plus the amount of light from the night sky. Mean extinction coefficients determined on other nights provided sufficient accuracy, since the sky was of excellent quality all through the major part of the eclipse. Measurements of night-sky light, made on other nights with the filters used here, showed that the maximum error to be expected from its neglect is less than 0.005 mag. The scattered-light component, however, became very important during certain phases of eclipse, and, as a result, uncertainties amounting to several tenths of a magnitude are possible in the present light-curves.

The light-curves show considerable asymmetry, which originates in the scattered-light component rather than in a real asymmetry in the earth's shadow. The scattered light comes from parts of the moon undergoing phases of eclipse radically different from those being experienced by Tycho at a given instant. Thus the light-curve represents composites of two different phenomena superposed—the eclipse of Tycho and the eclipse of the moon in general. Tycho's eclipse was not symmetrical with the eclipse of the moon as a whole, and its light-curve was considerably distorted by the scattered-light component. An illustration of the manner in which distortion in the slopes of the light-curves of Tycho resulted from scattered light from other regions of the moon is evident near U.T. 0350. Here it is evident that the light from Tycho is decreasing, in spite of the fact that Tycho is deep in the umbra and would be expected to be nearly constant in brightness. A plot of the moon's position relative to the umbra (Fig. 1, *C*) shows that the slope is due entirely to the rapid decrease in the scattered light coming from the brilliantly

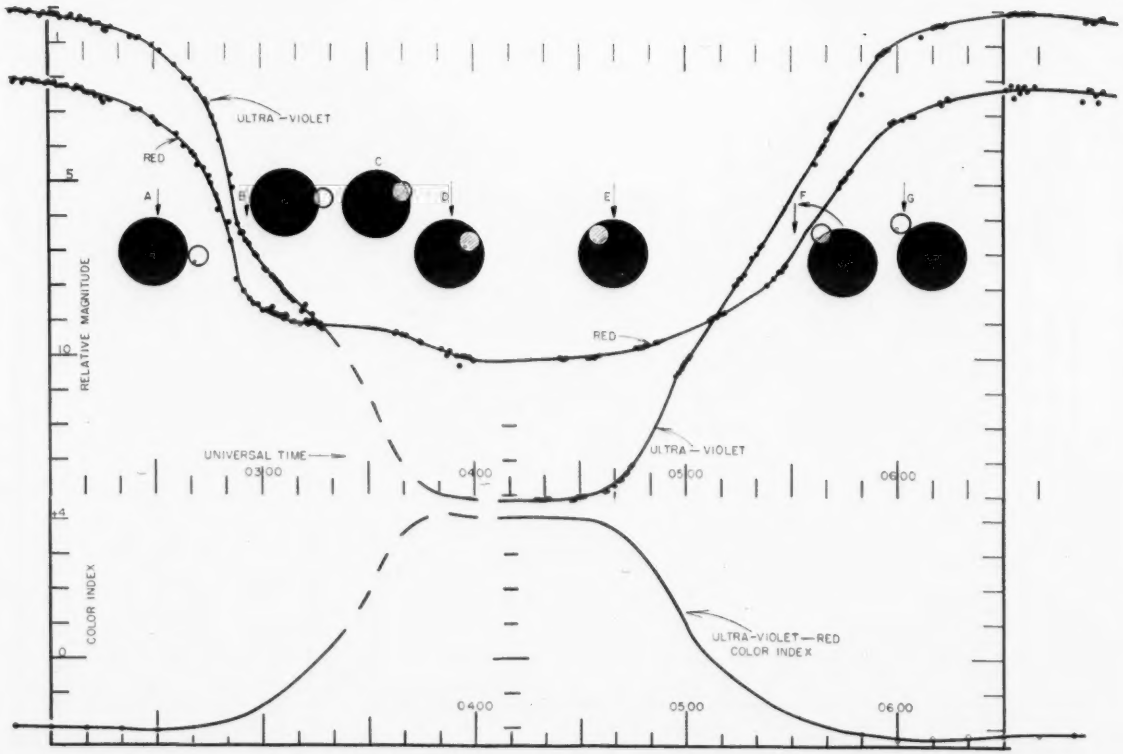

FIG. 1.—Ultraviolet and red light-curves of crater Tycho, lunar eclipse of September 26, 1950. Insets show situation of moon and Tycho relative to umbra. Distortion of curve near 0350 results from rapid decrease in scattered light from moon in general (see inset *C* and text for details).

illuminated edge of the moon, at that time rapidly disappearing into the umbra. A similar, but somewhat less obvious, effect raises the light-curve above that expected for Tycho alone in the interval 0430–0500.

Elimination of the influence of atmospheric scattering from the present observations of Tycho is, unfortunately, impracticable. An estimate of its importance may be obtained from the discussion by H. C. van de Hulst[1] of observations of the light-intensity near the limb of the sun. Scattering produces an aureole which has a brightness between 100 and 500×10^{-6} of the brightness of the disk itself. In this case the light scattered by the air is less than 0.1 per cent of the disk intensity. Thus, if similar values hold for

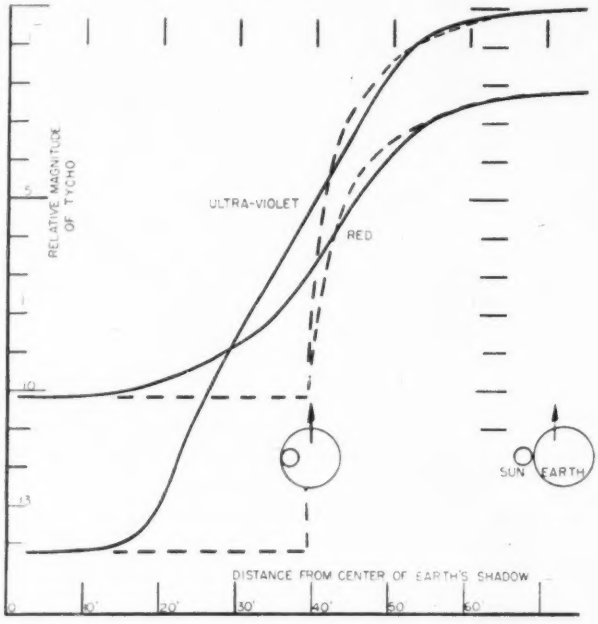

FIG. 2.—Comparison of observed light-curves with those expected from an eclipse of the sun by an "atmosphereless" earth, as viewed from Tycho.

the moon, we may expect the scattered light in front of Tycho to be less than 0.1 per cent of the light from Tycho itself, provided that the moon is either entirely out of, or entirely obscured by, the earth's shadow. Therefore, the depths of eclipses obtained from the present light-curves are probably correct. However, when Tycho is in the shadow and other parts of the moon are still bright, the scattered light they contribute becomes very important relative to that from Tycho. When Tycho enters the umbra, its brightness suddenly decreases by 8 mag. in red light. The background of scattered light, however, has not altered appreciably during this short interval and, on the basis of the numerical values used above, becomes approximately 0.6 as bright as Tycho itself. An attempt was made to evaluate corrections for the scattered light, taking into consideration the scattering law and the varying distance of Tycho from the center of light of the

[1] *The Atmospheres of the Earth and Planets*, ed. G. P. Kuiper (Chicago: University of Chicago Press, 1949), pp. 59–68.

still illuminated area of the moon, but was abandoned because of the number of undetermined functions involved. Among these were the radial-intensity distribution in the umbra, the influence of the penumbra on the illuminated part of the moon, the uneven brightness of the moon's face, and the atmospheric scattering coefficient on the occasion in question.

The manner in which a more satisfactory series of observations may be obtained is suggested by the above discussion. Instead of making continuous settings on one region of the moon, it is essential that a number of regions scattered over the moon's face should be observed. During totality, these observations are especially important and can give an accurate determination of the radial-intensity distribution in the umbra, free from appreciable interference by scattered light. Outside totality, similar observations will give the radial-intensity distribution in the penumbra, and outside eclipse they will evaluate the uneven brightness of the lunar disk. Knowing these functions plus the law of atmospheric scattering, which could be determined earlier or later on the same night, we

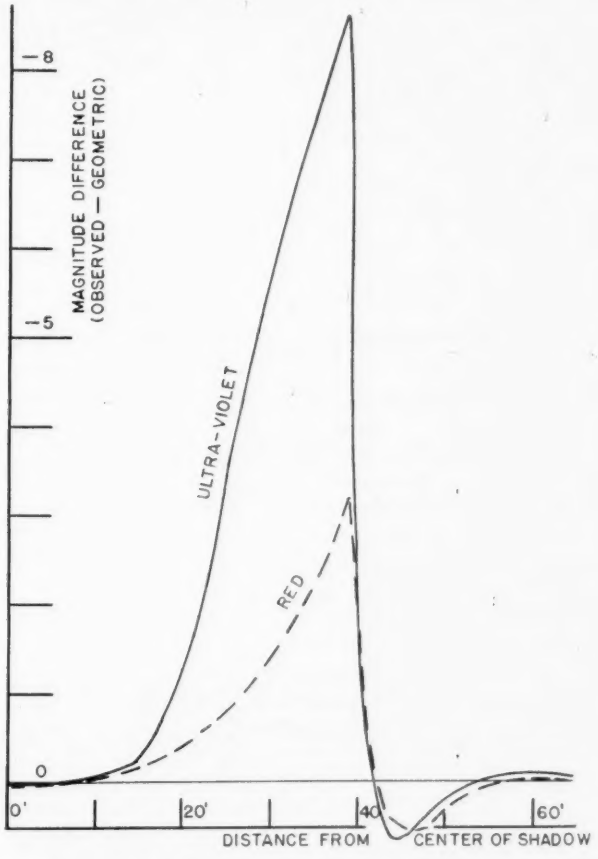

FIG. 3.—Magnitude differences, observed curve *minus* geometric eclipse-curve

could then evaluate with fair accuracy the intensity of the scattered component and apply the corrections necessary to obtain a corrected light-curve for a given point on the moon's face.

In Figure 2 the magnitudes are plotted as a function of the radial separation of Tycho from the geometrical center of the shadow. Auxiliary curves in Figure 2 show the characteristics, as viewed from Tycho, of the simple geometrical eclipse of the sun by an

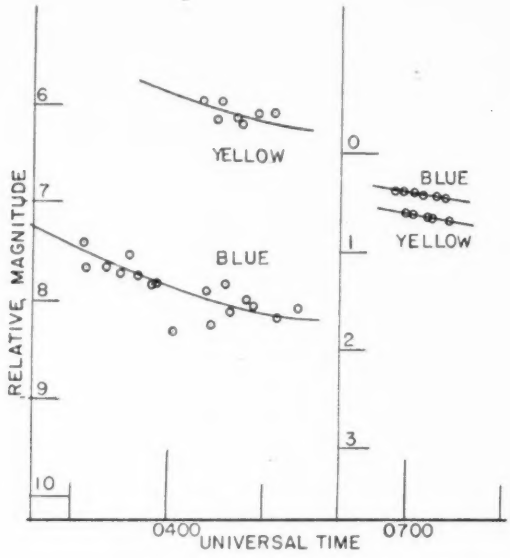

FIG. 4.—Yellow and blue measurements, near totality, and at end of eclipse

TABLE 1*

DATA ON COLORS

Object	C_{uv-r}	C_{int}
Eclipsed moon (Tycho)	−3.74	+2.97
Uneclipsed moon (Tycho)	−2.15	+0.60
Earthshine on moon (Oct. 7, 1950)	−1.81:	+0.72:
Asteroid Vesta	−1.965	+0.677
	−2.070	+0.677
Comparison star B, for Vesta (BD+8°511)	−1.785	+0.780
	−1.805	+0.774
Comparison star A, for Vesta (BD+9°427)	−2.899	+0.266
North Polar Seq. 1s	−2.414	+0.47
North Polar Seq. 5	−3.397	+0.03
North Polar Seq. 8	−2.985	+0.23

* In some cases the values have less accuracy than that indicated by the decimals present in the formal reduction to C_{int}. Not many polar stars are bright enough to be measured with our photometer in ultraviolet and in red light. That is why NPS 1s was included, in spite of its known variability.

atmosphereless earth. Depths of the eclipses have been assumed, for convenience, to be equal to the depths shown in the light-curves. This assumption, of course, endows the "atmosphereless" earth with a fictitious, constant luminosity equal to that which the atmosphere contributes to a point at the moon at the center of the shadow. The geometrical eclipse-curves were computed from the eclipsing-star tables of J. E. Merrill.[2] Solar limb-darkening coefficients of 0.56 and 0.85 were used for red and ultraviolet light, respectively.

Several of the properties of the illumination of the umbra and penumbra are evident, in spite of the presence of scattered light in the observations. Agreement between the geometrical and the observed light-curves is good only up to the point at $r = 52'$, where the atmosphere's effect upon the shadow becomes noticeable. Between $r = 52'$ and $r = 43'$ the observed intensity is fainter than that which we should expect from a geometrical eclipse. Here the atmosphere refracts part of the light that should appear, were there no atmosphere, toward the central regions of the shadow. Extinction acts in the same sense, while the presence of scattered light in the observations tends to mask the effect somewhat. After the geometrical eclipse has become total, the atmosphere is the only contributor to the umbra, and the shadow becomes darker and redder as the sun sinks farther below the rim of the earth. Figure 3 illustrates these effects further, by plotting differences in magnitude, observed curve minus computed curve, as a function of distance from the center of the earth's shadow. To some extent, the high peaks of intensity result from the scattered light, which is most serious between $r = 17'$ and $r = 54'$ and is quite negligible in the ranges $r = 0$ to $r = 17'$ and $r = 54'$ to $r = 70'$.

Figure 4 shows the yellow and blue measurements made during totality and at the end of the eclipse for purposes of calibrating the ultraviolet-red color indices in terms of the familiar color index on the International System, C_{int}. With the present cell and filters, the reduction from C_{b-y} to C_{int} is performed by an empirical relation derived from pole-star observations (see note to Table 1), or

$$C_{\text{int}} = 1.121\, C_{b-y} + 0.836 .$$

Here all values have been referred to a point outside the earth's atmosphere. The blue-yellow color calibration in terms of C_{int} is based on observations of ten North Polar Sequence stars, each on three to five different nights. The ultraviolet-red calibration, based upon the data of Table 1 only, is less accurately defined.

Calibration of the ultraviolet-red color data in terms of C_{int} obtained from our blue-yellow measures and from other data is illustrated in Figure 5. Several fundamentally different kinds of objects are involved, and the information is listed, for greater accuracy, in Table 1. Appropriate relations converting ultraviolet-red color indices into International color indices are:

$$C_{uv-r} = 2.182\, C_{\text{int}} - 3.47 \qquad (\text{Range}, C_{\text{int}}\ 0\text{–}0.80),$$

$$C_{uv-r} = 2.502\, C_{\text{int}} - 3.73 \qquad (\text{Range}, C_{\text{int}}\ 0.80\text{–}3.0).$$

It is a pleasure to acknowledge the assistance of Mr. Don M. Bubeck in obtaining the observations, and of Mr. Kenneth L. Hallam in making the reductions.

[2] *Contr. Princeton U. Obs.*, No. 23, 1950.

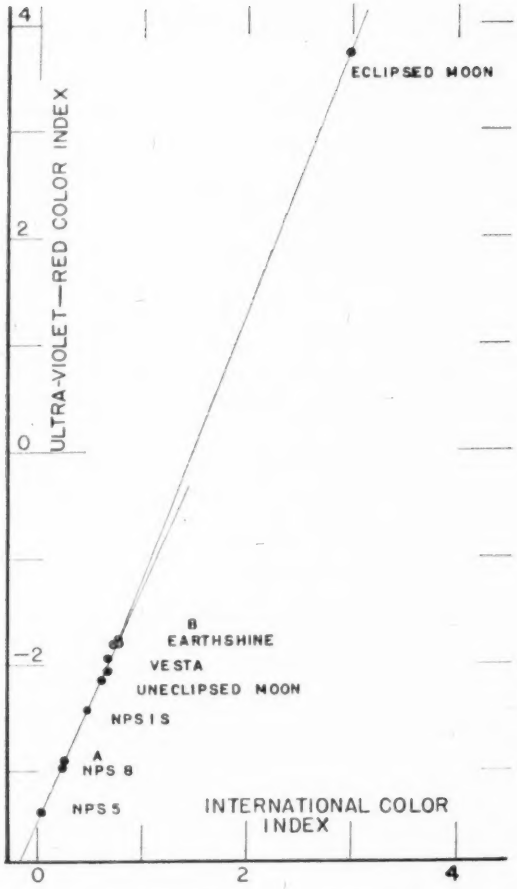

FIG. 5.—Calibration of ultraviolet-red color indices in terms of International color index

THE SEMIREGULAR VARIABLE STARS OF THE RV TAURI AND RELATED CLASSES

ALFRED H. JOY
MOUNT WILSON AND PALOMAR OBSERVATORIES
CARNEGIE INSTITUTION OF WASHINGTON
CALIFORNIA INSTITUTE OF TECHNOLOGY
Received September 20, 1951

ABSTRACT

Observations.—A spectroscopic survey of the F, G, and K semiregular variables was based on Mount Wilson spectrograms of thirty-eight stars.

Physical characteristics.—Strong ionized lines indicate that many of the stars are as bright as, or brighter than, the long-period cepheids. The mean spectral type is about G0 at maximum and K0 at minimum light. Titanium oxide bands occur in twenty-one stars and are seen on spectra as early as G4. The mean radial-velocity range during a cycle is 36 km/sec, but irregularities are so great that mean velocity-curves are impossible. The relation of velocity changes to light-variations is similar to that of the cepheids. Hydrogen emission is present in twenty-five stars at times of increasing light. The G band of *CH* becomes stronger with decreasing light and later spectral type.

Subdivisions.—If the stars are divided according to radial velocity, the fast and slow groups are found to differ also in mean luminosity, spectral type, intensity of carbon bands, and distribution in the sky. The fast-moving group is undoubtedly of type II population, but the exact relationship of the slow group to Baade's populations is uncertain.

In order to investigate the spectroscopic characteristics of the semiregular variablet with intermediate spectral types and periods, thirty-eight stars have been observed as Mount Wilson with low dispersion. Nearly all the observable RV Tauri variables and most of the irregular variables of types F, G, and K have been included.

Among variable-star observers there is general agreement as to the standard behavior of RV Tauri variables, but, unfortunately, few stars meet all the requirements over any considerable length of time. The changes and irregularities are often most confusing. Cyclic variations are seldom repeated exactly, and the statistical use of suggested periods is unsatisfactory.

The strange fluctuations of light of these variables have been investigated by numerous observers. Particularly valuable results have been obtained from the Harvard photographs covering periods of time sufficiently long to show the extreme irregularities at different epochs.The painstaking work of Payne-Gaposchkin, Brenton, and Gaposchkin[1] giving light-curves for fourteen RV Tauri stars is most illuminating.

General data pertaining to the stars observed are in Table 1. The photographic magnitudes are mostly from Kukarkin and Parenago's *Catalogue of Variable Stars*. The classification according to Payne-Gaposchkin, Brenton, and Gaposchkin; Kukarkin and Parenago; and L. Rosino[2] ("RV" = RV Tauri class, "SR" = semiregular, "LP" = long period) is indicated in the eighth to the tenth columns. From observations of the light-changes, all three sources assign thirteen stars of the list to the RV Tauri class. Two place six other stars in this class, while for five stars the RV Tauri designation is from one only of these sources. The remaining thirteen stars are semiregular variables which are not recognized as RV Tauri stars, although in period, light-range, and spectroscopic characteristics they seem to be rather closely related to them. One star, AB Leonis (BD+20°2337), is the new variable whose light-changes were found by Miss D. Hoffleit[3] to be of the RV Tauri type.

[1] *Harvard Ann.*, Vol. 113, No. 1, 1943.
[2] *Ap. J.*, 113, 60, 1951.
[3] *Harvard Bull.*, No. 919, p. 11, 1949.

Five stars of the list—DF Cyg, SU Gem, U Mon, AI Sco, and RV Tau—have long-period light-variations of 690–2320 days superposed upon the short-period (50–90 days) light-curves. For U Mon, R. F. Sanford[4] discovered a variation of 40 km/sec in the γ velocity in a period of 2320 days, and the same period was later found by E. Loreta[5] in

TABLE 1

DATA CONCERNING VARIABLES OBSERVED

STAR	DESIGNATION	l	b	m_{pg}		PERIOD (DAYS)	CLASS			NO. PLATES
				Max.	Min.		Gap.	K. and P.	Rosino	
WY And	233647	79°	−14°	9.5	10.6	109	.....	SR	SR	10
BL Aqr	210902	17	−33	11.0	12.3	85	.....	SR	.....	8
TW Aql	194613	20	− 8	10.6	12.7	96:	.....	SR:	.....	5
DY Aql	194111	357	−19	10.2	12.9	131	RV	RV	.....	7
EZ Aql	193408	14	− 8	12.4	14.6	39	RV	RV	RV	3
KK Aql	194314	20	− 7	11.5	12.8	89	RV	SR	.....	7
Z Aur	055353	127	+16	9.7	12.9	111	.....	LP	.....	9
AG Aur	062047	135	+17	10.0	13.1	98	.....	RV	SR	16
TW Cam	041257	116	+ 6	10.4	11.5	86	.....	RV	RV	6
RX Cap	200913	358	−26	11.6	13.7	68	RV	RV	RV	5
RU Cep	010884	91	+22	9.3	10.4	109	.....	SR	.....	7
TZ Cep	001973	88	+11	9.8	12.0	83	.....	SR	.....	6
AV Cyg	191629	30	+ 6	11.2	13.0	90	RV	SR	.....	7
DF Cyg	194542	44	+ 8	10.8	15.2	50	RV	RV	RV	10
V360 Cyg	210630	45	−12	10.8	13.3	63	RV	RV	RV	10
SS Gem	060222	156	+ 3	9.2	10.7	89	RV	RV	RV	13
SU Gem	060727	152	+ 6	10.7	13.2	50	.....	RV	RV	5
SX Her	160325	9	+45	9.0	11.1	103	.....	SR	SR	21
UU Her	163238	28	+41	8.5	10.6	71	RV	SR	SR	18
AC Her	182621	18	+13	7.1	9.4	75	RV	RV	RV	73
AB Leo	092720	179	+46	10.7	13.2	103	.....	.....	.....	12
W LMi	103926	176	+63	11.3	14.5	117	.....	LP	.....	13
UW Lib	142516	303	+39	10.4	11.0	85	.....	SR:	.....	17
U Lup	155429	313	+16	10.8	13.2	87	.....	SR	.....	7
U Mon	072609	194	+ 6	6.8	8.5	92	RV	RV	RV	68
TT Oph	164403	349	+27	9.8	11.7	61	RV	RV	RV	14
TX Oph	165905	352	+25	9.8	12.1	138:	RV	RV:	SR	11
UZ Oph	171707	356	+22	10.5	13.1	87	RV	RV	RV	9
TX Per	024136	116	−19	11.1	13.7	76	.....	SR	.....	10
S Sge	200916	26	−11	9.0	11.5	71	RV	RV	RV	29
AR Sgr	185323	340	−14	9.6	11.5	88	RV	RV	.....	8
AI Sco	174933	325	− 6	9.4	12.6	72	.....	RV	RV	3
R Sct	184205	355	− 3	6.5	9.6	144	RV	RV	RV	12
RV Tau	044025	143	−11	9.8	13.3	79	RV	RV	RV	18
WW Tau	035529	133	−16	9.9	12.9	125:	.....	SR	.....	6
SV UMa	104055	119	+55	9.8	11.3	76	.....	SR	SR	11
S Vul	194427	31	0	10.1	11.4	69	RV	SR	.....	18
V Vul	203226	37	− 9	9.0	11.0	76	RV	RV	RV	31

[4] *Mt. W. Contr.*, No. 465; *Ap. J.*, **77**, 120, 1933.

[5] *A.N.*, **267**, 399, 1938.

the light-variations. On account of insufficient spectroscopic observations, this important correlation between light and velocity measures has not been traced in other stars. These five stars have a short mean double period of 69 days, and their mean total light-range is over 3 mag. They are high-luminosity stars with mean galactic latitude of 7°. Emission is weak or absent.

SPECTROSCOPIC OBSERVATIONS

Our knowledge of the detailed spectroscopic behavior of the RV Tauri variables is based on the extensive studies of AC Herculis,[6] U Monocerotis,[4] R Sagittae,[7] and V Vulpeculae[8] by R. F. Sanford at Mount Wilson and of R Scuti[9] by D. B. McLaughlin at Michigan. Their observations cover the whole period of light-variations and indicate that the fundamental behavior is related to that of the cepheids. Under the most favorable circumstances the double period is clearly seen in spectrographic and radial-velocity changes,[10] as well as in the light-variations.

L. Rosino[2] has recently estimated the spectral type and luminosity class of thirteen of the stars of Table 1. McLaughlin and Rosino have added greatly to the value of their spectrographic data by determining simultaneous light-curves.

Spectra of two of the variables of Table 1 obtained at Mount Wilson have already been described.[11] Data for the hitherto unpublished Mount Wilson observations are in Table 2, together with the spectrographic results for each plate. The photometric elements (mostly from the *Variable Star Catalogue* [1948], by Kukarkin and Parenago) used in computing the phases (fourth column) are in the notes following Table 3. The letters in the table indicate whether the phases are reckoned from maximum (M) or from minimum (m). In the last four columns are rough intensity estimates of the strongest emission lines, the titanium oxide bands, the general absorption effect of *CH* at the G band, and (M II) the relative strength of the lines of ionized metallic atoms as compared with those of neutral atoms. A dash is used to indicate that the photograph was not properly exposed to show the feature in question, but a zero indicates that the feature is not visible, even though the plate is competent to show it.

These observational results are summarized in Table 3, where the stars are separated into low- and high-velocity groups. In the last three columns are the mean or γ velocity, the approximate velocity range, and the residual velocity, assuming the usual solar motion of 20 km/sec.

The spectral types generally vary from about G0 somewhat before maximum light to about K0 near minimum. Near minimum light the titanium oxide bands appear in spectra which otherwise would be classed as G or K. The classification on the basis of the *TiO* bands is given in parentheses. This peculiar phenomenon, which was first noticed in R Sct,[11] seems to be characteristic of these stars and is especially outstanding among the members of group 2. In SV UMa an intensity of 4 in the titanium bands is observed on two spectrograms of types G5 and G8.

Rosino[2] has noted the presence of carbon bands in AC Her. On the Mount Wilson plates, as reported by Sanford,[6] the G band attains great strength as the light decreases to minimum. The λ 4215 *CN* band and the λ 4737 C_2 bands are faintly visible for a few days preceding minimum. Doubtless the total carbon absorption is responsible for a part of the loss of light. The small change in color index[1] at different phases indicates that the cyanogen absorption plays a minor role.

[6] *Mt. W. Contr.*, No. 424; *Ap. J.*, **73**, 364, 1931.

[7] *Mt. W. Contr.*, No. 481; *Ap. J.*, **79**, 81, 1934.

[8] *Mt. W. Contr.*, No. 481; *Ap. J.*, **79**, 82, 1934.

[9] *Pub. Obs. U. Michigan*, **7**, 57, 1938.

[10] D. B. McLaughlin, *Ap. J.*, **94**, 94, 1941.

[11] A. H. Joy, R Scuti, *Pub. A.S.P.*, **34**, 349, 1922; SX Herculis, *Mt. W. Contr.*, No. 443; *Ap. J.*, **75**, 127, 1932.

TABLE 2

SPECTROSCOPIC OBSERVATIONS OF RV TAURI AND SEMIREGULAR VARIABLES

Star	Plate	Date JD 24	Phase (Days)	Spectrum	Velocity (Km/Sec)	Disp. at $H\gamma$ (A/Mm)	Intensity			
							Em.	*TiO*	*CH*	M II
WY And	γ 19195	26993	M 108	G6	−176	70	0	0	2	1
	19262	7021	27	G8	−191	70	0	0	2	1
	C 6348	7431	2	—e	−192	35	4	0	—	—
	6351	7432	3	—e	−207	35	3	0	—	—
	γ 23000	9894	72	K2	−188	70	0	2	2	1
	23144	9932	1	G8e	−185	70	3	—	1	3
	Ce 3262	31038	19	—e	−197	20	1	—	—	—
	E 1455	1662	99	G2e	−179	70	3	0	1	2
	1492	1698	26	G3e	−197	70	1	0	1	2
	γ 27057	1724	52	K2	−198	70	0	3	1	2
					−191					
BL Aqr	γ 19769	27287	M 17	G4	+ 34	110	0	0	1	2
	C 7521	9826	6	G5	+ 46	110	0	0	2	2
	γ 22856	9857	37	G4	+ 36	70	0	0	2	2
	E 209	30209	49	K0	+ 52	110	0	1	3	1
	γ 23640	0220	60	G5	+ 39	110	0	1	2	2
	E 1441	1638	33	G8	+ 51	110	0	2	2	2
	1463	1665	60	G8	+ 55	70	0	2	2	2
	γ 27922	2053	23	G2	+ 47	110	0	0	1	2
					+ 45					
TW Aql	C 5156	27018	—	G5	+ 14	110	0	0	2	2
	γ 21862	9413	—	G6	+ 34	70	0	0	3	3
	22855	9857	—	G0	+ 35	70	0	0	0	3
	23639	30220	—	G4	+ 2	110	0	0	3	3
	E 268	0266	—	K0	+ 20	110	0	0	3	3
					+ 21					
DY Aql	C 7490	29766	m 109	K0	+ 3	110	0	3	2	1
	γ 22742	9804	15	G8	0	110	0	0	3	2
	C 7520	9826	37	K0	+ 30	110	0	2	3	2
	E 39	9896	107	—	—	110	0	2	—	—
	57	9913	124	G5e	+ 14	110	5	0	2	3
	146	30147	95	G6	+ 24	110	0	2	2	3
	259	0251	68	K0	+ 25	110	0	1	4	2
					+ 15					
EZ Aql	C 7348	29452	m 31	G5	—	110	0	0	2	2
	7351	9471	11	G8	+ 48	110	0	0	3	3
	7539	9853	7	K0	+ 49	110	0	0	2	3
					+ 48					
KK Aql	C 6168	27020	M 43	G6	−245	110	0	1	1	1
	6445	7611	13	—	−256	70	0	0	—	2
	γ 21160	8734	72	G2e	−280	110	4	0	1	2
	E 255	30250	80	G4	−231	110	0	0	2	2
	γ 27066	1727	49	G6	−246	110	0	2	2	2
	27703	1980	36	G4	−240	110	0	1	1	1
	27919	2052	19	G6	−262	110	0	0	0	1
					−252					

TABLE 2—*Continued*

Star	Plate	Date JD 24	Phase (Days)	Spectrum	Velocity (Km/Sec)	Disp. at $H\gamma$ (A/Mm)	Intensity			
							Em.	*TiO*	*CH*	M II
Z Aur	γ 23030	29898	M 46	G4e	−155	70	5	0	2	1
	23163	9945	93	G6e	−187	110	4	0	2	2
	23339	30071	8	G2	−157	110	0	0	1	1
	E 258	0251	65	G2e	−152	110	3	0	1	1
	γ 23842	0302	5	G0e	−154	70	3	0	1	1
	23929	0334	37	G0	−160	110	0	0	1	1
	27176	1755	17	G5e	−157	110	5	1	1	1
	27503	1894	45	G4e	−168	110	4	2	1	1
	E 1688	1922	73	G3e	−170	110	2	0	2	2
					−165					
AG Aur	C 4695	25305	M 30	G6	+182	70	0	0	1	2
	4717	5342	67	—	—	70	0	2	—	1
	4729	5344	69	—	+196	70	0	2	—	1
	5364	5956	92	G8e	+199	70	2	0	2	2
	5568	6256	97	G4e	+190	70	1	0	2	2
	5584	6267	10	G4e	+190	70	1	0	1	2
	5602	6283	26	G4	+192	70	0	1	1	1
	5624	6311	54	G8	+206	70	0	3	1	1
	5664	6340	83	G2e	+197	35	5	0	2	1
	5665	6340	83	G2e	+195	70	5	0	1	1
	V 94	6647	95	G5e	+195	35	2	0	2	2
	C 6347	7403	82	—	+201	35	4	—	—	—
	6349	7431	12	G4e	+186	70	4	0	1	2
	γ 27177	31756	12	G4e	+183	110	4	0	1	2
	27504	1894	53	K0	+189	110	0	1	2	1
	E 1689	1922	81	G8	+200	110	0	2	2	1
					+193					
TW Cam	γ 23137	29927	m 82	G8	− 69	110	0	0	0	3
	23197	9957	27	G8	− 44	110	0	0	1	3
	C 7642	9971	41	G5	− 51	70	0	0	1	3
	E 257	30250	63	G2	− 59	110	0	0	1	3
	γ 27171	1754	26	G3	− 61	70	0	0	0	3
	27971	2076	6	G4	− 40	110	0	0	1	3
					− 55					
RX Cap	C 7515	29825	m 47	G3	−135	110	0	0	0	1
	γ 22848	9856	10	G0	−122	110	0	0	1	2
	23132	9927	13	G3	−148	110	0	0	1	2
	23509	30180	62	G2	−156	110	0	0	1	1
	26939	1696	15	G0	−135	110	0	0	0	2
					−135					
RU Cep	γ 22107	29505	M 62	—	− 13	70	0	0	—	1
	22199	9560	7	—	− 18	70	0	0	—	2
	22415	9647	94	K0	− 4	70	0	1	1	2
	23027	9898	16	—	− 17	70	0	2	—	2
	23029	9898	16	K2	− 17	70	0	2	2	1
	27170	31754	11	K0	− 18	35	0	1	1	2
	27924	2053	91	G6	− 8	70	0	2	2	1
					− 12					
TZ Cep	γ 19188	26992	M 74	K0e	− 15	70	1	0	3	3
	21971	9450	42	G6	− 5	110	0	2	2	3

TABLE 2—*Continued*

Star	Plate	Date JD 24	Phase (Days)	Spectrum	Velocity (Km/Sec)	Disp. at $H\gamma$ (A/Mm)	Intensity			
							Em.	*TiO*	*CH*	M II
TZ Cep	γ 23028	29898	M 75	G8e	− 7	70	4	1	3	3
	23136	9927	21	K1	0	110	0	2	2	2
	23636	30219	64	K2e	+ 4	110	3	1	3	1
	27974	2077	13	K0	+ 6	110	0	0	0	1
					− 5					
AV Cyg	γ 18899	26878	M 77	G4	− 28	70	0	0	3	1
	C 7305	9410	8	G3e	− 16	110	3	0	3	3
	7549	9855	4	G2e	− 30	110	3	0	3	2
	γ 23453	30151	31	G6	− 11	110	0	0	3	3
	E 1416	1600	45	G0e	− 32	110	1	0	2	2
	γ 26744	1633	78	G3	− 19	70	0	0	2	2
	C 7708	1958	44	G2e	− 28	110	2	0	3	2
					− 23					
DF Cyg	γ 18070	26401	m 12	K0	− 5	110	0	0	2	3
	C 5751	6495	7	K2	+ 4	70	0	0	1	3
	5758	6516	28	G6	− 10	70	0	0	1	3
	5841	6606	18	K2	− 35	110	0	0	3	3
	7064	8702	23	K4	− 7	110	0	0	3	3
	7086	8731	2	K0	+ 8	110	0	0	1	3
	7100	8763	34	G6	− 9	110	0	0	2	2
	γ 21218	8793	14	G8	− 4	110	0	0	3	3
	21231	8821	42	G8	+ 7	110	0	0	4	3
	C 7193	9144	16	G5	− 16	110	0	0	3	3
					− 5					
V360 Cyg	C 7507	29806	m 57	F5	−260	110	0	0	0	1
	γ 22758	9824	11	F8e	−247	110	1	0	1	1
	C 7540	9853	40	G0	−238	110	0	0	0	1
	E 40	9896	20	G0e	−238	110	2	0	0	2
	313	30297	41	F8	−264	110	0	0	1	1
	1417	1600	16	F5	−258	110	0	0	0	1
	1433	1635	51	G0	−255	70	0	0	1	2
	γ 27056	1724	13	F8e	−240	110	1	0	0	1
	27173	1755	44	G0e	−264	110	1	0	0	1
	27920	2052	25	F5	−281	110	0	0	0	2
					−250					
SS Gem	C 1677	23179	m 36	G5	+ 23	70	0	0	3	2
	3238	4249	35	—	+ 30	70	0	0	—	2
	3661	4539	57	G5	− 19	70	0	0	2	3
	4221	4984	55	G4	+ 9	70	0	0	3	2
	4560	5217	20	G8	− 17	70	0	0	4	2
	4740	5347	61	G4	− 14	70	0	0	—	2
	5610	6285	17	G5	− 14	35	0	0	3	2
	5630	6312	44	G2	− 19	70	0	0	1	3
	5647	6316	48	G0	− 15	70	0	0	2	2
	γ 17978	6322	54	G2	− 8	70	0	0	2	3
	C 5652	6338	70	G0	− 7	70	0	0	1	2
	5674	6342	74	G0	− 5	70	0	0	1	2
	γ 18035	6346	78	G2	− 23	70	0	0	1	2
					− 6					

TABLE 2—*Continued*

Star	Plate	Date JD 24	Phase (Days)	Spectrum	Velocity (Km/Sec)	Disp. at $H\gamma$ (A/Mm)	Intensity			
							Em.	*TiO*	*CH*	M II
SU Gem.....	γ 21440	29176	—	G2	+ 16	110	0	0	1	3
	23159	9944	—	G4	+ 2	70	0	0	1	2
	C 7661	30029	—	G2	− 7	110	0	0	2	3
	E 339	0324	—	F5	+ 7	110	0	0	0	2
	γ 26392	1463	—	G6	− 26	110	0	0	2	3
					− 2					
UU Her.....	C 2742	23889	—	F5	−128	70	0	0	0	2
	2766	3916	—	F6	−142	70	0	0	0	2
	2796	3926	—	F8	−137	70	0	0	0	2
	3512	4417	—	F5	−121	70	0	0	0	2
	3980	4750	—	G0	−130	70	0	0	1	2
	4197	4956	—	F2	−132	70	0	0	0	2
	4224	4984	—	F5	−130	70	0	0	0	1
	4254	5011	—	F7	−127	70	0	0	0	2
	4285	5040	—	F4	−132	70	0	0	0	2
	4308	5048	—	G0	−139	70	0	0	0	1
	4370	5079	—	F6	−126	70	0	0	0	2
	5205	5777	—	F5	−131	70	0	0	0	2
	5234	5809	—	F6	−117	70	0	0	0	1
	5390	6018	—	F8	−141	70	0	0	0	2
	5415	6048	—	F8	−139	70	0	0	0	2
	5464	6135	—	F7	−144	35	0	0	0	2
	5740	6493	—	F7	−125	70	0	0	0	1
	5756	6516	—	F6	−125	70	0	0	0	1
					−131					
AB Leo.....	E 1681	31919	M 47	G0e	+208	110	4	0	1	2
	1690	1923	51	G0e	+188	110	5	0	1	1
	Ce 4231	1929	57	—e	+182	20	4	—	—	—
	γ 27603	1930	58	F6e	+166	70	3	0	0	1
	27651	1952	80	F5e	+163	70	3	0	0	1
	E 1707	1976	1	G3e	+194	110	1	0	1	1
	γ 27705	1981	6	G0	+172	110	0	0	1	1
	29272	2555	64	F8	—	110	0	0	1	1
	E 1951	2582	91	G0e	+180	110	5	0	1	2
	γ 29383	2611	17	F5e	+189	110	1	0	1	2
	E 1969	2636	42	G2e	+178	110	1	0	1	1
	γ 29524	2671	77	F5e	+182	110	6	0	0	1
					+182					
W LMi.....	C 7176	29379	M 101	—	—	110	3	1	0	—
	γ 21784	9380	102	K0e	—	70	3	1	2	1
	C 7664	30030	48	G4e	+ 57	110	10	2	1	1
	γ 23340	0071	90	G6e	+ 55	110	3	0	2	1
	E 87	0090	109	K0e	+ 94	110	2	1	3	1
	γ 23450	0151	53	G2e	+ 48	110	6	0	2	1
	24024	0397	64	G2e	+ 64	110	8	0	1	1
	E 422	0443	110	K0e	+ 96	110	3	1	3	1
	γ 26394	1464	76	G4e	+ 71	110	4	0	2	1
	E 1354	1546	41	G5e	+ 41	110	5	2	2	1
	1397	1568	63	G3e	+ 46	70	5	0	2	1
	1595	1844	104	K2e	—	110	0	3	2	1
	C 7715	1960	104	K0e	+ 90	110	1	2	1	1
					+ 66					

TABLE 2—*Continued*

Star	Plate	Date JD 24	Phase (Days)	Spectrum	Velocity (Km/Sec)	Disp. at $H\gamma$ (A/Mm)	Intensity			
							Em.	*TiO*	*CH*	M II
UW Lib	γ 22735	29803		G7e	+155	70	0	0	1	1
	22756	9824		G8	+186	110	0	1	1	1
	C 7538	9853		G6e	+164	110	4	0	1	2
	γ 23341	30071		G4	+146	110	0	1	2	1
	E 106	0119		G7e	+169	110	2	2	2	2
	151	0149		G2e	+194	110	1	0	2	2
	γ 23510	0181		G8	+155	110	0	1	1	1
	24025	0398		K0	+142	110	0	0	2	2
	24054	0423		G6	+176	110	0	2	2	1
	E 423	0443		G7e	+179	110	4	3	2	2
	442	0471		G6e	+136	110	2	0	2	1
	1396	1567		G4e	+161	70	2	0	1	2
	γ 26612	1595		G6e	+169	110	1	1	1	1
	26742	1633		G5e	+171	70	1	0	1	2
	27642	1948		G8e	+174	110	2	0	2	2
	C 7707	1958		G6e	+146	110	1	0	2	2
	γ 27706	1981		G8	+145	110	0	0	2	1
					+163					
U Lup	C 7485	29765		K0	−134	110	0	2	2	1
	7502	9806		—	—	110	0	1	—	1
	E 93	30091		G6e	−134	110	2	0	2	1
	107	0119		K0e	−141	110	1	0	2	1
	171	0178		K0	−124	110	0	2	2	1
	1428	1634		G2	−109	110	0	0	2	2
	C 7716	1960		G6e	−141	110	4	0	2	1
					−130					
TT Oph	γ 6870	21711	m 13	G4e	− 64	70	1	0	2	2
	C 340	2414	43	G6e	− 43	35	2	0	3	3
	386	2443	12	—	—	35	3	0	—	—
	441	2473	42	G5e	− 41	35	1	0	—	3
	476	2483	52	K0	− 62	35	0	0	3	3
	504	2507	15	G4e	− 53	70	2	0	3	3
	1075	2866	8	G8	− 49	35	0	0	3	2
	1114	2882	24	G5	− 58	70	0	0	2	3
	1218	2918	59	K0	− 57	35	0	0	3	3
	1265	2940	20	G6	− 67	70	0	0	2	3
	1367	2970	50	G8	− 81	70	0	0	2	3
	1640	3136	33	K0	− 39	70	0	0	3	2
	2297	3592	0	G8	− 34	70	0	0	3	3
	3881	4715	24	G7	− 61	70	0	0	2	3
					− 50					
TX Oph	C 4225	24984	—	G2e	−157	70	1	0	1	3
	4251	5010	—	G0	−166	70	0	0	0	3
	4399	5129	—	G2	−172	70	0	0	1	3
	4739	5346	—	G3	−170	70	0	0	1	3
	4928	5458	—	G6e	−158	70	1	0	1	3
	5227	5786	—	G4e	−161	70	1	0	1	2
	5435	6078	—	G0e	−155	70	1	0	1	2
	γ 24129	30484	—	F8	−165	110	0	0	0	3
	24151	0504	—	G3	−178	110	0	0	—	3
	26613	1595	—	G6	−164	110	0	0	1	2
	E 1683	1919	—	F5e	−177	110	1	0	0	2
					−165					

TABLE 2—*Continued*

Star	Plate	Date JD 24	Phase (Days)	Spectrum	Velocity (Km/Sec)	Disp. at H_γ (A/Mm)	Intensity			
							Em.	*TiO*	*CH*	M II
UZ Oph	C 4899	25439	m 24	G6e	− 99	70	1	0	2	3
	5149	5688	11	G6	− 58	70	0	0	2	3
	5460	6133	19	G4e	− 99	70	1	0	0	2
	γ 21968	9450	15	G5e	− 80	70	2	0	1	2
	23345	30087	41	G4	− 87	110	0	0	2	2
	23637	0220	86	G8	− 76	110	0	2	2	2
	E 443	0471	75	G2	−120	110	0	0	3	2
	γ 24130	0484	1	G8	− 90	110	0	1	2	2
	E 1415	1600	68	G2e	− 92	110	2	0	2	2
					− 85					
TX Per	γ 19263	27021	M 6	K2	− 15	70	0	1	4	2
	22109	9506	48	G7	− 7	110	0	0	3	2
	C 7432	9646	36	K0e	+ 7	110	1	2	2	1
	E 43	9896	58	K0	− 6	110	0	1	2	2
	54	9912	74	—	—	70	0	2	—	2
	261	30251	31	G8e	+ 22	110	2	1	4	2
	1493	1698	28	K2	− 6	70	0	3	1	2
	γ 27174	1755	9	G6	− 13	110	0	1	3	2
	27251	1786	40	G5	+ 21	110	0	0	2	1
	E 1762	2082	31	G6e	− 2	110	3	1	2	1
					0					
AR Sgr	C 4995	25518	m 31	G6	−101	70	0	0	1	2
	5487	6164	62	G2	−101	70	0	0	1	1
	5557	6242	52	F8	− 90	70	1	0	0	1
	E 50	9912	31	G0	−101	70	0	0	0	2
	γ 23508	30180	36	G0	−108	70	0	0	1	2
	23634	0219	75	G2	−102	110	0	0	1	2
	26616	1596	46	G3e	−105	70	2	0	0	1
	E 1430	1634	84	F5e	− 88	70	1	0	1	1
					−100					
AI Sco	C 6261	27254	—	K2	− 3	110	0	0	1	3
	6268	7256	—	G0	− 40	110	0	0	2	—
	E 274	30267	—	G5	− 8	110	0	0	2	2
					− 15					
RV Tau	C 4511	25183	m 63	K1	+ 46	70	0	0	4	3
	5150	5690	19	G4	+ 39	70	0	0	2	3
	5329	5875	48	K0e	+ 34	70	1	0	3	2
	5617	6310	11	G8e	+ 48	70	2	0	1	3
	5658	6339	40	G8	+ 44	70	0	1	3	2
	5702	6431	53	G5e	+ 33	70	1	0	3	2
	5843	6606	71	G8	+ 41	70	0	0	3	3
	γ 19122	6964	36	G5	+ 32	70	0	0	2	1
	19199	6993	65	G4	+ 18	70	0	0	3	3
	C 6173	7020	13	G5e	+ 33	70	1	0	2	3
	E 47	9897	61	G6	+ 39	110	0	0	2	3
	279	30267	38	G6	+ 28	110	0	1	4	3
	1498	1710	66	G4	+ 25	110	0	0	2	3
	γ 27059	1724	1	G6	+ 41	70	0	0	3	2
	E 1524	1744	21	G4	+ 22	110	0	0	2	2
	γ 27175	1755	32	G6	+ 5	110	0	0	3	2

TABLE 2—*Continued*

Star	Plate	Date JD 24	Phase (Days)	Spectrum	Velocity (Km/Sec)	Disp. at $H\gamma$ (A/Mm)	Intensity			
							Em.	*TiO*	*CH*	M II
RV Tau	γ 27347	31881	m 29	G5	+ 25	70	0	0	3	3
	E 1908	2496	66	G4e	+ 24	110	1	0	3	2
					+ 35					
WW Tau	γ 22473	29678	—	G5	− 99	110	0	0	2	2
	E 48	9897	—	G4e	−113	110	5	2	1	2
	γ 23161	9945	—	K2	−102	110	0	3	2	1
	23196	9957	—	K0	−109	110	0	3	1	2
	E 284	30268	—	K0	−109	110	0	—	1	2
	γ 27068	1727	—	G4e	−120	110	2	1	2	2
					−110					
SV UMa	C 4667	25278	—	G5e	− 80	70	6	0	1	2
	4738	5346	—	G4e	− 86	70	3	0	2	3
	4761	5353	—	G5e		70	1	0	1	2
	4764	5362	—	G6	− 99	70	0	0	1	2
	4804	5380	—	G8	−101	70	0	1	3	3
	4822	5394	—	G5	− 97	70	0	4	2	3
	4841	5410	—	G8	− 85	70	0	4	—	2
	4850	5422	—	G6	− 90	70	0	3	3	2
	5148	5688	—	G8	− 90	70	0	1	2	2
	5164	5723	—	G2e	− 85	70	1	0	2	1
	5393	6018	—	G3	−101	70	0	0	2	3
					− 90					
S Vul	C 2937	24377	M 56	G6	− 14	70	0	0	1	2
	3950	4744	28	G6	+ 1	70	0	0	1	2
	4400	5129	35	K2	+ 10	70	0	1	4	3
	4983	5515	14	K0	− 5	70	0	0	3	3
	5180	5751	47	K0	− 1	70	0	0	3	3
	5211	5779	7	G0	− 13	70	0	0	1	2
	5237	5809	37	G8	+ 6	70	0	0	3	2
	γ 16781	5836	64	G4	− 10	70	0	0	2	2
	17544	6154	44	G6	− 3	70	0	0	3	2
	17545	6155	45	G6	− 3	70	0	0	—	2
	17576	6169	59	G4	− 2	70	0	0	1	3
	C 5556	6241	62	G2	− 9	70	0	0	—	2
	γ 17855	6285	39	K0	+ 4	70	0	0	3	2
	C 5615	6310	63	G6	− 5	70	0	0	1	3
	5801	6554	37	G8	+ 8	70	0	0	2	2
	5819	6580	63	G5	− 4	70	0	0	1	3
	5846	6607	22	G6	− 13	70	0	0	2	3
	6046	6879	23	G4	− 6	70	0	0	1	3
					− 2					

TABLE 3

SUMMARY OF SPECTROSCOPIC RESULTS

Star	Spectrum (Atomic Lines *TiO*)	Max. Emission Int.	*CH* G band Int.	Max. M II Int.	Velocity		
					Meas. (Km/Sec)	Range (Km/Sec)	Resid. (Km/Sec)
	Group 1: Velocities < 70 Km/Sec						
BL Aqr	G2 –K0 (M2)	0	1–3	2	+ 45	20	+ 57
TW Aql	G0 –K0	0	0–3	3	+ 21	35	+ 39
DY Aql	G5e–K0 (M3)	5	1–3	3	+ 15	30	+ 29
EZ Aql	G5 –K0	0	2–3	3	+ 48	–	+ 66
TW Cam	G2 –G8	0	0–1	3	– 55	30	– 56
RU Cep	G6 –K2 (M2)	0	1–2	2	– 12	15	– 3
TZ Cep	G6 –K2e (M2)	4	0–3	3	– 5	20	+ 4
AV Cyg	G0e–G6	3	2–3	3	– 23	20	– 4
DF Cyg	G5 –K4	0	1–4	3	– 5	45	+ 13
SS Gem	G0 –G8	0	0–4	3	– 6	55	– 19
SU Gem	F5 –G6	0	0–2	3	– 2	40	– 13
SX Her	G3e–K0 (M3)	8	0–3	2	+ 20	15	+ 38
AC Her	F1 –K4e	4	0–4	3	– 30	60	– 10
U Mon	F8e–K2 (M2)	5	1–4	3	+ 35	45	+ 17
TT Oph	G2e–K0	3	2–3	3	– 50	45	– 33
UZ Oph	G2e–G8 (M2)	2	1–3	3	– 85	70	– 67
TX Per	G5e–K2 (M3)	3	1–4	2	0	40	– 3
R Sge	G2 –K0	0	1–4	3	+ 10	40	+ 27
AI Sco	G0 –K2	0	1–2	3	– 15	35	– 6
R Set	G5e–K2 (M3)	3	2–3	3	+ 40	35	+ 56
RV Tau	G4e–K1 (M1)	2	1–4	3	+ 35	45	+ 24
S Vul	G0 –K2 (M1)	0	1–4	3	– 2	25	+ 17
V Vul	G4 –K3 (M2)	1	1–4	3	– 15	40	+ 2
	Group 2: Velocities > 70 Km/Sec						
WY And	G2e–K2 (M3)	4	1–2	3	–191	55	–183
KK Aql	G2e–G6 (M2)	4	1–2	2	–252	50	–234
Z Aur	G0e–G6e (M1)	5	1–2	2	–165	35	–167
AG Aur	G2e–K0 (M3)	5	1–2	2	+193	25	+188
RX Cap	G0 –G3	0	0–1	2	–135	35	–123
V360 Cyg	F5 –G0e	2	0–1	2	–250	45	–235
UU Her	F2 –G0	0	0–1	2	–131	25	–114
AB Leo	F5e–G3e	6	0–1	2	+182	50	+175
W LMi	G2e–K2e (M3)	10	1–3	1	+ 66	55	+ 70
UW Lib	G2e–K0 (M3)	4	1–2	2	+163	60	+176
U Lup	G2 –K0e (M2)	4	2–2	2	–130	30	–122
TX Oph	F5e–G6e	1	0–1	3	–165	20	–147
AR Sgr	F5e–G6	2	0–1	2	–100	10	– 88
WW Tau	G4e–K2 (M3)	5	1–2	2	–110	20	–119
SV UMa	G2e–G8 (M4)	6	1–3	3	– 90	20	– 86

NOTES TO TABLES 2 AND 3

WY And — Max. = JD 2428408.9 + 108^{d}8E. On plates C 6348, C 6351, and Ce 3262 the stellar D1 and D2 sodium lines are well separated by velocity from the interstellar lines. Ce 3262 was taken and measured by R. F. Sanford. On this plate the $H\alpha$ emission is symmetrically divided by a strong, deep absorption line.

BL Aqr — Max. = JD 2430160 + 85^dE.

TW Aql — P = 96? days. Sharp lines.

DY Aql — Min. = JD 2428344 + 131^{d}42E.

NOTES TO TABLES 2 AND 3—*Continued*

EZ Aql	Min. = JD 2428611.05 + 38^{d}61*E*. Extensive light-observations by Taylor and Olivier (*Pub. Obs. U. Pennsylvania*, Vol. **6**, Part 5, 1941). The spectrum is much like that of DF Cyg.
KK Aql	Max. = JD 2428308.4 + 88^{d}7*E*.
Z Aur	Max. = JD 2432072 + 110^{d}96*E*.
AG Aur	Max. = JD 2425766.5 + 98^{d}26*E* (*Schneller*, 1939).
TW Cam	Min. = JD 2428647 + 85^{d}6*E*.
RX Cap	Min. = JD 2420741.4 + 67^{d}95*E*. Only maximum phase was observed.
RU Cep	Max. = JD 2430649 + 109^{d}5*E*. Observed by P. C. Keenan, M0 III (*Ap. J.*, **95**, 462, 1942). The Mount Wilson observations are poorly distributed and do not cover the minimum phases.
TZ Cep	Max. = JD 2425840 + 83^{d}0*E*.
AV Cyg	Max. = JD 2430659 + 89^{d}7*E*. Except for λ 4077 and λ 4215 *Sr* II, the lines are weak.
DF Cyg	Min. = JD 2414883.5 + 49^{d}808*E*. The spectrograms were all obtained at the brighter phases of the long-period variation of 782 days. The remarkable light-variations of this star were discovered and extensively observed by Miss M. Harwood (*Harvard Ann.*, **105**, 521, 1937).
V360 Cyg	Min. = JD 2426967 + 63^{d}26*E*. The emission lines are double, with shortward component stronger; separation 160 km/sec. The absorption lines are weak.
SS Gem	Min. = JD 2430020 + 89^{d}31*E*.
SU Gem	*P* = 50.12 days, with an additional long-period variation of 689.6 days. The absorption lines show large changes in intensity.
SX Her	The spectroscopic behavior of this star resembles that of the Mira stars in some particulars. Hydrogen emission occurs for about 30 days before and after maximum light. *TiO* bands attain considerable strength at minimum light.
UU Her	Alternating periods of 90.40 and 71.06 days have been found. The G band is usually absent. Spectral changes and velocity variations are small and uncertain. The star is unlike other stars of the group. The mean of the Mount Wilson and McCormick trigonometric parallaxes is 0".010. The observations were made at the times when the period of 90 days prevailed.
AC Her	Sanford (*Mt. W. Contr.*, No. 424; *Ap. J.*, **73**, 364, 1931) found that during increasing light the hydrogen lines have emission edges. The velocity-curve shows a double maximum corresponding to the double minimum of the light-curve. The spectral type at maximum is earlier than that of any other star in the list and has a large range (F1–K4), although no *TiO* bands appear. The G band shows remarkable changes with phase. L. Rosino (*Ap. J.*, **113**, 60, 1951) calls attention to the strength of the carbon bands during decreasing light and classifies the star as Rp at this phase.
AB Leo = BD + 20°2337	Max. = JD 2428880 + 103^{d}2*E*. A. Vyssotsky found emission lines of hydrogen in objective-prism spectra of this star. From Harvard plates Miss Hoffleit discovered light-changes which resemble those of the semiregular or RV Tauri variables. She determined the elements used here. The light-curve seldom shows alternating bright and faint minima, but the period seems to hold, even though the epoch may shift. At times the light-fluctuations become irregular and of small range. The bright lines are strong and persistent, showing slow decrement shortward, but the type is too early to permit *TiO* bands. The star is evidently one of the semiregular variables of high velocity and moderate luminosity. Plate Ce 4231 was taken by R. F. Sanford. On this plate the emission at *Hα* is symmetrically divided by a narrow central reversal. In general, the absorption lines are sharp, and the spectrum resembles that of UU Her, but, on the plates showing the earliest estimated spectral type, the lines seem weak, although no certain veiling effect is observable.
W LMi	Max. = JD 2428303 + 117^{d}2*E*. The light-changes and period are poorly determined. The range of light-variation is large. The hydrogen emission lines are strong and persistent, but the enhanced lines are weak. This star should certainly be placed among the high-velocity stars.
UW Lib	*P* = 84.73 days. No epoch. This period does not seem to satisfy the velocity and spectral variations. Small light-range.
U Lup	The period is variable between 75 and 95 days, according to D. J. K. O'Connell (*Harvard Bull.*, No. 893, 1933).
U Mon	Sanford (*Mt. W. Contr.*, No. 465; *Ap. J.*, **77**, 120, 1933) found that the velocity-curve shows a double minimum, corresponding to the double maximum of the light-curve. Hydrogen emission and *TiO* bands were observed.
TT Oph	Min. = JD 2428723 + 61^{d}08*E*. This star, which was at first thought to be an eclipsing binary, is one of the best examples of the RV Tauri type of variation. The light-

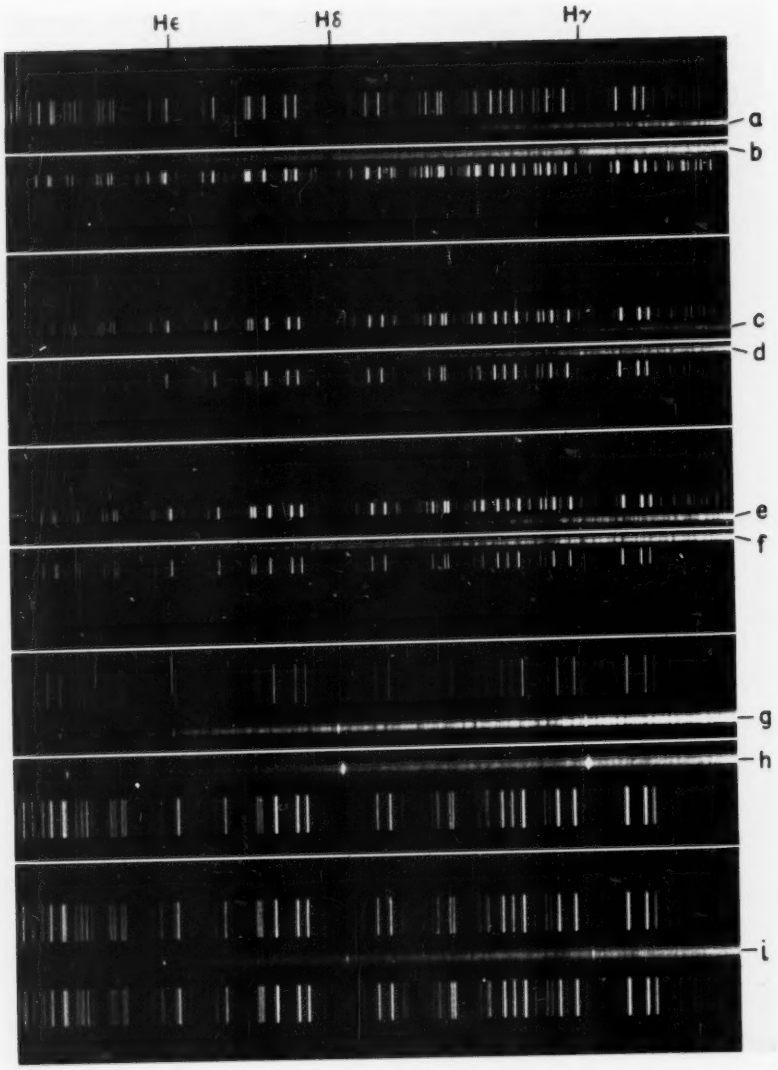

FIG. 1.—Spectra of semiregular variables. *a*, K2 (M3), TX Persei; *b*, F4, UU Herculis; *c*, G5 (M4), SV Ursae Majoris, strong titanium bands on G5 spectrum; *d*, G8e, RV Tauri, *CH* weak; *e*, K0, RV Tauri, *CH* strong; *f*, G6, TW Camelopardalis, ionized metallic lines strong; *g*, G2e, WY Andromedae, ionized metallic lines weak, slow decrement of bright lines, $H\epsilon$ weakened; *h*, G5e (M2), W Leonis Minoris, all absorption lines weak, $H\epsilon$ absent; *i*, G0e, AB Leonis, lines weak.

NOTES TO TABLES 2 AND 3—*Continued*

	minima are usually well defined and of nearly equal depth. Emission lines of hydrogen appear during increasing light and reach greatest intensity 2 days before maximum light. The velocity-curve shows definite correlation with the light-curve. No *TiO* bands have been observed. The enhanced lines are strong.
TX Oph	P = 138? days. The range in velocity and spectral type is small. The enhanced lines are strong and indicate the highest luminosity of the high-velocity stars.
UZ Oph	Min. = JD 2422531.84 + 87^d39E. This star may belong to the high-velocity group.
TX Per	Max. = JD 2428466 + 76^d3E.
R Sge	Sanford found (*Mt. W. Contr.*, No. 481; *Ap. J.*, **79**, 81, 1934) that the radial velocities show little correlation with the light-curve, but D. B. McLaughlin (*Ap. J.*, **94**, 94, 1941) discovered that, by omitting velocities obtained when light-variations were irregular, a reasonable correlation could be determined. No *TiO* bands or emission lines were found. The G band strengthens at minimum light.
AR Sgr	Min. = JD 2426103 + 87^d87E (*Harvard Ann.*, **113**, 39, 1943). Observed minimum.
AI Sco	P = 71.78 days, with superposed period of 960 days.
R Sct	The appearance of *TiO* bands at spectral type G9 was noted (*Pub. A.S.P.*, **34**, 349, 1922) in 1922. This fine example of RV Tauri variation has been thoroughly studied by D. B. McLaughlin (*Pub. Obs. U. Michigan*, **7**, 57, 1938).
RV Tau	Min. = JD 2429290 + 78^d6E (*Harvard Ann.*, **113**, 49, 1943). Observed minimum. A superposed period of 1227 days has been suggested. The G band and the enhanced lines are strong, but the emission lines and *TiO* bands are weak and rarely seen.
WW Tau	The period varies from 113 to 138 days. The velocity range is small, but there is considerable variation in spectral type.
SV UMa	P = 76 days. The light-variations are quite irregular, and the period is variable. The star was spectroscopically observed in 1930 by R. O. Redman (*M.N.*, **92**, 116, 1931) at Victoria. A series of seventeen spectrograms covering more than a cycle failed to show, at that time, the strong emission lines of hydrogen and the *TiO* bands observed later at Mount Wilson. A McDonald spectrogram in 1941 by P. C. Keenan was classified as K3p: Ia (*Ap. J.*, **95**, 463, 1942) with weak lines.
S Vul	Max. = JD 2423671.7 + 67^d77E (*Schneller*, 1939). The period is variable. Velocity and spectral variations are small, but the strength of the G band shows large fluctuations with phase. The spectrum resembles that of cepheids of intermediate period.
V Vul	Sanford (*Mt. W. Contr.*, No. 481; *Ap. J.*, **79**, 82, 1934) reported weak *TiO* bands but no emission.

The *CH* absorption is an outstanding feature of the stars of group 1, reaching its greatest strength at the times of later spectral type. At other phases the band becomes weak or disappears. In group 2, *CH* seldom attains great intensity. In all the stars, marked changes in the bands take place in a few days' time. The λ 4215 *CN* band has also been found for a short period preceding minimum in the luminous stars DF Cyg, SS Gem, U Mon, RV Tau, and SV UMa.

Emission lines of hydrogen occur, especially at times of increasing light, in a majority of the stars of both groups. The bright lines are stronger and more persistent in group 2. The decrement toward the violet is usually gradual. The bright hydrogen line *Hε* is often greatly reduced in intensity by the absorption of the H line of calcium (Fig. 1, *g*, *h*, and *i*).

With further observation, hydrogen emission or titanium bands may yet be found at favorable phases in some of the stars in which these features were not observed.

The irregular behavior of the stars makes it impossible to draw useful velocity-curves from scattered observations. The mean measured velocity range of 36 km/sec is somewhat less than that of the most luminous cepheids, but this may be due to periods of inactivity which occur from time to time among the semiregular variables. The mean velocity range is the same for both groups of Table 3.

In studies of variable stars the period of variation has usually been an important factor in the discussion. This parameter has rendered little help with the irregular stars discussed in this paper. Various correlations with period have been tried, but they have not seemed significant.

SUBGROUPS

Since the stars of the present list were included largely on the basis of their spectral characteristics, considerable study was given to their spectroscopic behavior, in order to detect the presence of physically defined subgroups. Such an analysis points to a division (Table 3 and Fig. 3) into high- and low-velocity groups as the most natural and fruitful means of bringing together the stars of like physical characteristics. Only five stars of the list have residual velocities between 57 and 114 km/sec, and none are found between 70 and 86 km/sec. A value of 70 km/sec was set as the lower limit of the velocities of group 2. It is near the minimum frequency of velocities and corresponds well with the values used by Oort and others in separating stars of low and high velocity. If the maximum strength of the ionized lines (fifth column of Table 3) or that of the G band (fourth column) had been taken as criteria, the grouping would have been practically the same,

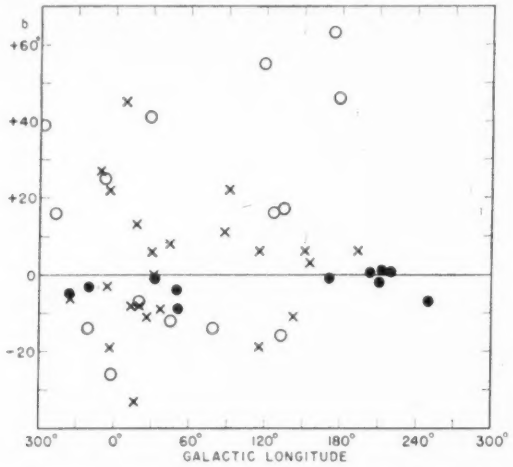

FIG. 2.—Galactic latitude and longitude of semiregular variables. Circles are high-velocity stars (Group 1); crosses, low-velocity stars (Group 2); and filled circles, cepheids with period > 20 days.

except that it might have been necessary to place TW Cam in group 2 with the high-velocity stars.

The evidence for two physical groups among these semiregular variables is strong in several respects: (1) The mean galactic latitudes of groups 1 and 2 (13° and 27°) indicate a difference in distribution (Fig. 2), although in neither group is the concentration toward the galactic equator as marked as in the δ Cephei variables, for which the average distance from the equator is less than 5°. (2) Mean proper motions determined by R. E. Wilson are 0".018 for thirteen stars of group 1 and 0".035 for seven stars of group 2. Since these values are, respectively, two and three times the mean proper motions of cepheids with periods greater than 20 days, it seems unlikely that either group has close kinetic relationship with the long-period cepheids. (3) Mean residual radial velocities (Table 3) without regard to sign: group 1, 28 km/sec; group 2, 154 km/sec. (4) A plot of radial velocities according to galactic longitude (Fig. 3) shows a distinct difference in the distribution of velocities in the two groups. The high velocities of group 2 are widely separated from those of group 1. A solar-motion solution for group 2 from the radial velocities indicates a group motion of 263 km/sec in nearly the same direction as that of RR Lyrae

stars[12] and the high-velocity R-type stars.[13] The smaller velocities of group 1, unlike those of the δ Cephei stars, show little galactic-rotation effect. (5) The average spectral type of group 2 is slightly earlier than that of group 1: at maximum F9 for group 2, G2 for group 1; at minimum G7 and K0, respectively. (6) The ionized lines of metals are distinctly stronger in group 1, and the absorption spectrum is more clearly defined, indicating higher luminosity. (7) The G band (*CH*) reaches greater intensity in group 1, but this may be, in part, due to the effect of later spectral type in the low-velocity stars. (8) Emission lines of hydrogen are often found in both groups at certain phases but occur more frequently and in greater strength among the high-velocity stars (eleven of twenty-three stars in group 1; thirteen of fifteen stars in group 2). (9) The double period with two unequal minima of light, typical of the more regular RV Tauri stars, seldom occurs in group 2.

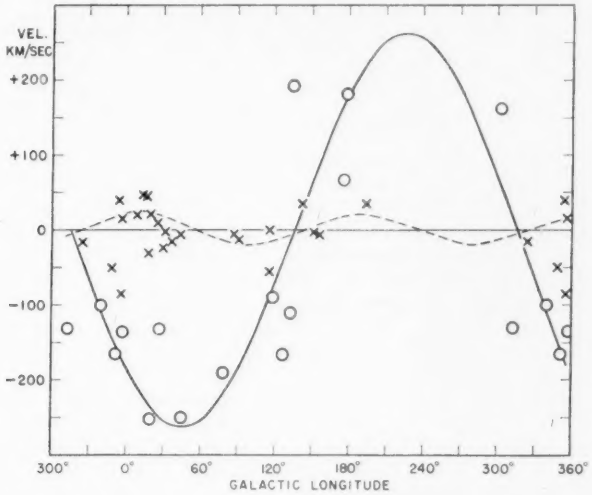

FIG. 3.—Radial velocity and galactic longitude of semiregular variables. Circles are high-velocity stars (Group 1); crosses, low-velocity stars (Group 2). The solid curve shows the radial velocity of Group 2 with reference to the sun; the dashed curve is the theoretical galactic rotation effect having a maximum of 25 km/sec.

The stars of group 2 are doubtless of type II population and might be expected to resemble those of groups 4 and 5 of the globular clusters.[14] This similarity prevails with regard to luminosity, period, and the occasional appearance of emission lines in our group 2 as compared with group 5 of the clusters. On the other hand, in the clusters the mean range of light-variation is smaller, 0.8 mag. compared to 2.2 mag. Also, in the clusters the G band is stronger and the spectral type somewhat later, although the *TiO* bands apparently are less frequent.

High-luminosity variables such as those of group 4 in the clusters seem to be few or absent among the high-velocity stars of the galaxy. Perhaps TX Oph may be an exception. Several of the low-velocity stars of our group 1 are similar to those of group 4 in the

[12] J. H. Oort, *B.A.N.*, **8**, 337, 1939; O. Struve, *Pub. A.S.P.*, **62**, 217, 1950.

[13] N. W. McLeod, *Ap. J.*, **105**, 390, 1947.

[14] A. H. Joy, *Ap. J.*, **110**, 105, 1949.

clusters, except that the group 1 stars are later in spectral type and have strong G bands, while *CH* in group 4 of the clusters is weak or absent.

From these considerations it seems evident that these semiregular variables may well comprise two groups based on distribution, motions, luminosity, or the intensity of the G band of *CH*. The relationship of these two groups to the variables of the δ Cephei class, on the one hand, and to the red M-type variables, on the other, is yet uncertain. Group 2 definitely should be included in population II, but the place of group 1 is not clear. Since the peculiar motions of group 1, which includes many of the best-known RV Tauri variables, such as U Mon, R Sct, and V Vul, are large as compared with the long-period cepheids but yet are much smaller than is generally found for type II stars, and their galactic latitude agrees with neither, it seems best, at present, to consider these stars as an anomalous group of population I stars. Possibly they may be related to the widely scattered giant K stars whose rapid velocities were first found by W. W. Campbell.

Most of the stars of group 2 are irregular variables which cannot meet the rigid requirements usually set up for the RV Tauri class. TX Oph and RX Cap have most of the RV Tauri characteristics and may correspond to the RV Tauri group in the clusters.

ABSOLUTE MAGNITUDE AND DISTANCE

On account of the great distances, trigonometric parallaxes of these stars are few and unreliable. Spectroscopic estimates of the visual absolute magnitude have been published for SX Her[11] (−1.5) and U Mon[15] (−2.0), and comparisons with the spectra of cepheids of the same spectral type indicate clearly that the luminosity of the brightest stars is as high as, or perhaps higher than, that of any of the cepheids. This conclusion is confirmed by the distances determined from the strength of the interstellar lines of sodium[16] in three of the less luminous stars (WY And, AG Aur, and UU Her), from which absolute magnitudes brighter than −2.2 may be deduced. In the globular clusters the absolute photographic magnitudes of the RV Tauri and semiregular groups are −3.0 and −1.5, respectively. Using the proper motions of sixteen stars (eleven belonging to these groups), P. P. Parenago[17] found a mean absolute visual magnitude of −0.4, but this value is of low weight on account of the small proper motions (mean about 0″.02) involved.

Rosino[2] has classified eleven of the stars (eight of group 1 and three of group 2) and assigned the luminosity class Ia or Ib, indicating visual absolute magnitudes as high as −4 or −5 according to the Yerkes system.

While none of these methods of determining absolute magnitude are precise, they indicate that the RV Tauri and related stars are among the most highly luminous stars and that they are comparable with the cepheids of similar spectra and periods of from 20 to 40 days for which Shapley's period-luminosity curve gives photographic absolute magnitudes as bright as −3.0.

Judging by the strength of their ionized lines, many of the stars of group 1 appear to be somewhat more luminous than the brightest cepheids. Absolute photographic magnitudes −3.0 for group 1 and −1.5 for group 2 seem to be reasonable mean values.

Neglecting space absorption, the distances of the stars of group 1, as determined from this value of the absolute magnitude and their median apparent magnitudes, average about 7 kpc. Since only twelve stars of this group are within 10° of the galactic equator, large corrections to their apparent magnitudes on account of interstellar absorption are probably limited to a few stars of the group. Some of the stars, such as BL Aql, SX Her, TT Oph, and UZ Oph are distant 2.5–5 kpc from the galactic plane. With these assumptions, the mean distance of the stars of group 2 is about 4 kpc.

[15] W. S. Adams *et al.*, *Mt. W. Contr.*, No. 511; *Ap. J.*, **81**, 225, 1935.

[16] A. H. Joy, *Pub. A.S.P.*, **46**, 51, 1934.

[17] *A.J.U.S.S.R.*, **11**, 95, 1934.

CONCLUSIONS

As a result of spectroscopic observations it is evident that the semiregular variables with pseudo-periods between 39 and 144 days and spectral types F, G, and K do not form a homogeneous group. In motion, luminosity, and spectral behavior no standard pattern is rigorously followed. The RV Tauri stars, well known to observers of variable stars for their irregular light-changes, are the accepted models for the group, but wide deviations in the behavior and characteristics of the individual stars are present.

On the basis of velocity, of absolute magnitude as determined by the strength of the ionized lines, and of the maximum intensity of the G band (*CH*), the thirty-eight stars observed may be separated into two groups, group 1 having velocities less than 70 km/sec, brighter absolute magnitudes, and greater maximum intensities of the G band. Within these two groups marked differences among the stars are found.

The stars of group 2 evidently belong to the type II population and correspond closely with the semiregular variables of the globular clusters. In luminosity and in radial-velocity variations the members of group 1 are similar to the long-period cepheids, but they are more scattered with reference to the plane of the galaxy and fail to show clearly the effect of galactic rotation. Also, these stars frequently have hydrogen emission and titanium oxide bands which have not been found in the cepheids. The place of the group 1 stars with reference to Baade's population types is not yet clear.

The veiling and absorption effects of titanium and carbon bands must contribute toward dimming the light of the semiregular stars at certain phases. On the other hand, increases in light may be, in part, due to flare effects, which are accompanied by hydrogen emission and a marked diminution in the visibility of the absorption spectrum at times in many of the stars. Such outbursts must be quite different in size and duration from those encountered in the faint dwarfs of extremely low temperatures.

SPECTRA OF TWO STARS WITH STABLE SHELLS

PAUL W. MERRILL
MOUNT WILSON AND PALOMAR OBSERVATORIES
CARNEGIE INSTITUTION OF WASHINGTON
CALIFORNIA INSTITUTE OF TECHNOLOGY
Received September 11, 1951

ABSTRACT

The stars HD 193182 and HD 195325 (1 Delphini) have shells which appear stable. Spectroscopic observations indicate no considerable change in HD 193182 since 1921, or in 1 Delphini since 1929. In both stars all lines yield the same velocity within narrow limits.

The shell spectrum of HD 193182 is one of the most striking thus far photographed. Lines in the Balmer series were measured down to *H*42. Lines of ionized metals are numerous and extraordinarily sharp. Lines of *He* I and *Mg* II are weak and diffuse.

The spectrum of 1 Delphini resembles that of HD 193182, but the dark lines are somewhat weaker. In both stars *Hα* is a wide emission line with a strong dark core.

Most stars whose spectra indicate the presence of an absorbing gaseous "shell" high above the level of the usual reversing layer[1] show marked changes in intervals not exceeding a few years in the appearance or the position of the lines. Stability is the exception rather than the rule. In the two stars listed in Table 1, however, no changes have been

TABLE 1

TWO STARS WITH STABLE SHELLS

STAR	HD	MWC	1900		MAG.	HARVARD SPECT.
			R.A.	Decl.		
	193182	632	20^h13^m8	$+39°16'$	6.6	A0
1 Del	195325	1019	20 25.5	+10 34	5.9	A0

detected, although both have been observed over a term of many years.

HD 193182.—Bright *Hα* was discovered[2] on objective-prism spectrograms taken at Mount Wilson in September, 1920. W. W. Morgan[3] classified the spectrum as cA0 but called attention to the absence of the expected space reddening. Miss Burwell and I[4] then noted that the spectrum resembled that of Pleione photographed on November 27, 1941, and that the object was thus a shell star or, as we said, a "false c star"; and our observation was confirmed by O. Struve.[5] Since a shell star is much nearer than a supergiant of the same apparent magnitude, the lack of space reddening is understandable.

Slit spectrograms obtained at Mount Wilson and at Palomar are listed in Table 2. Several of the earliest were taken and measured by M. L. Humason; and the plate with

[1] For a description of a typical shell spectrum see P. W. Merrill, *Pub. A.S.P.*, **61**, 38, 1949. A revised partial list of shell stars will be found in the *Second Supplement* to the Mount Wilson catalogue of Be stars, Merrill and Burwell, *Mt. W. and P. Obs. Reprint* No. 8; *Ap. J.*, **110**, 412, 1949.

[2] P. W. Merrill, *Pub. A.S.P.*, **35**, 263, 1923.

[3] *Ap. J.*, **90**, 632, 1939.

[4] *Mt. W. Contr.*, No. 682; *Ap. J.*, **98**, 153, 1943.

[5] *Ap. J.*, **99**, 205, 1944.

the highest dispersion, Pa 8, was taken with the coudé spectrograph of the 200-inch telescope by I. S. Bowen and O. C. Wilson. I am indebted to these colleagues for this valuable material.

The shell spectrum is one of the most striking thus far photographed with high dispersion. The Balmer lines near the limit of the series, together with numerous metallic lines, are well shown in a large halftone in *Physics Today*, **2**: 10, 1949. The hydrogen lines of longer wave length have strong central dark cores with remarkably well-defined edges. The dark core of *Hα* is about 3.5 A wide, centered in emission whose total width is 25 A (see Fig. 1). It would be interesting to study the profile of *Hα* in HD 193182 and other shell stars with the aid of equations similar to those developed by Cowan and Dieke[6] in their investigation of self-absorption in laboratory spectra. The dark core of *Hδ* is 2 A wide, with weak dark wings extending to a total width of 26 A. The core of *Hζ* is slightly narrower than that of *Hδ*, but the wing spread appears to be 25 A. Toward

TABLE 2

SPECTROGRAMS OF HD 193182

PLATE	DATE	DISP. (A/MM)	RADIAL VELOCITY (KM/SEC)				
			H	No.	M II	No.	Adopt.
γ 10135	1921 Apr. 27	35	−19.4	3	−18.1	26	−17.9
γ 10196	June 13	35	−18.4	3	−20.4	11	−20.0
γ 10495	Sept. 20	35	−25.4	3	−23.8	16	−24.1
γ 10986	1922 Apr. 13	35	−20.4	3	−18.0	10	−18.4
γ 11924	1923 July 3	35	−23	1	−15.3	12	−15.9
C 7692	1941 Aug. 7	35	−18.7	3	−17.4	24	−17.5
γ 23886	Nov. 26	35	−20.2	5	−21.9	5	−21.0
γ 23896	27	35	−19.6	7	−18.0	30	−18.3
Ce 3056	1943 May 26	10	−21.1	36	−20.8	65	−20.9
Ce 3572	1944 Sept. 8	10	−21.1	39	−21.0	103	−21.0
Ce 5350*	1948 Oct. 13	20	−22	1	−19.3	2	−20.1
Pa 8†	1950 Sept. 21	2.3	−18.6	36	−20.2	78	−19.8

* Red region.

† Comparison spectrum slightly imperfect.

the limit of the Balmer series the cores become narrow, while the wings are inconspicuous. Thus an exceptional number of lines is visible; *H*42 was measured on two plates with dispersion 10 A/mm, and *H*43 seems recognizable. This, I think, is a record number of observed Balmer lines. A contrasty emulsion with sufficiently fine grain should do better than the IIa-O emulsion actually employed.[7] It is probable that additional lines could be detected also with higher dispersion; the density of plate Pa 8 near the limit of the series is too low for a test of this point.

The fact that various lines of the Balmer series yield the same radial velocity, shown by the horizontal progression-curve in Figure 2, indicates that atoms of hydrogen are not appreciably accelerated within the observable zones above the star's photosphere. This stability is not always present in shell stars.

Lines of ionized metals are numerous and extraordinarily sharp. With some exceptions, notably λ 4481 *Mg* II and several lines of *Si* II, they correspond to the lines of α Cygni but are much sharper. The general correspondence and the greater sharpness

[6] *Rev. Mod. Phys.*, **20**, 418, 1948.

[7] The IIa-O emulsion, prepared by the research laboratory of the Eastman Kodak Company, is a remarkable one. It has high speed, fine grain, and low contrast.

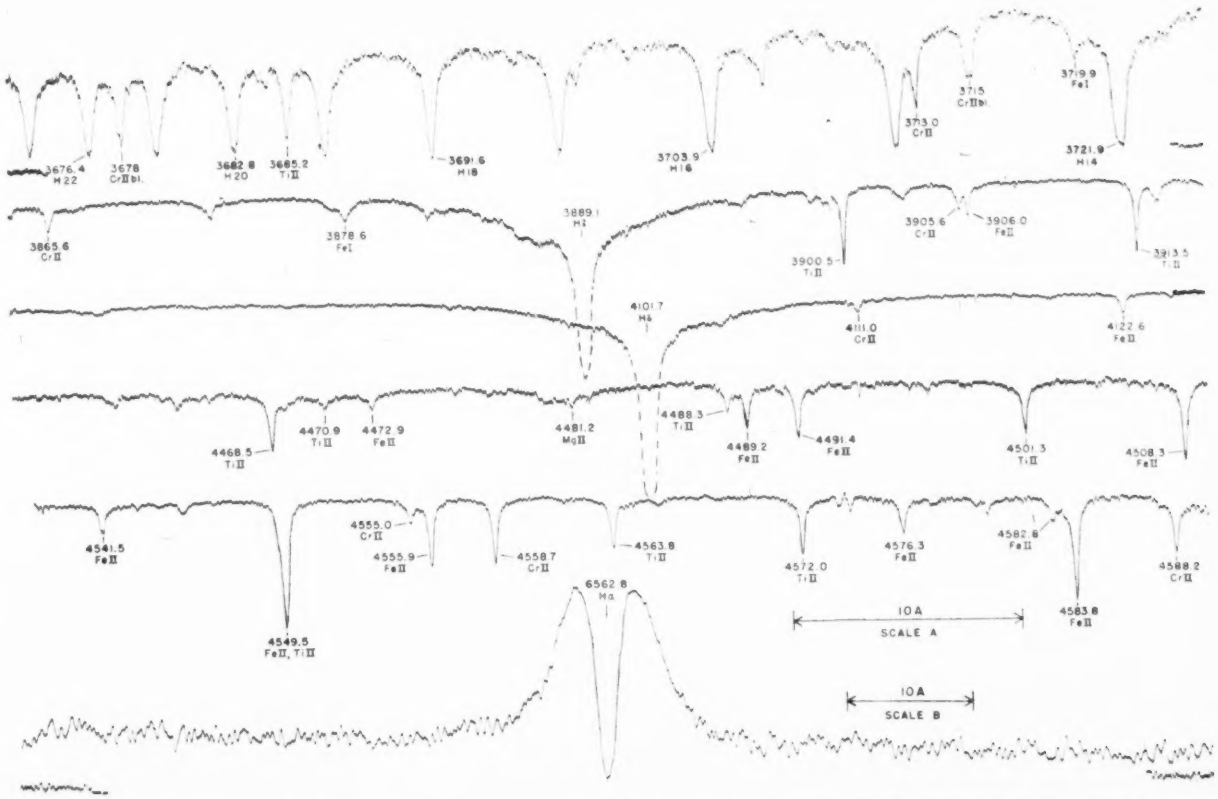

FIG. 1.—Tracings of lines in the spectrum of HD 193182. The *Hα* line is from plate Ce 5350, scale *B*; all others from Pa 8, scale *A*

are especially striking in the rich ultraviolet region from λ 3100 to λ 3500. The resemblance to Pleione, photographed on February 25, 1943, is very close, but the lines in HD 193182 are slightly sharper. The star is an outstanding one for detailed study of lines of ionized metals and lines of hydrogen near the limit of the Balmer series.

Several of the larger residuals from the progression-curve in Figure 2 are due to blending lines of ionized metals:

*H*35 λ 3657.93 may be slightly affected by blending with *Cr* II λ 3658.19.
*H*28 λ 3664.68 is probably affected by blending with *Cr* II λ 3664.95.
*H*14 λ 3721.94 is affected by blending with *Ti* II λ 3721.63.
*H*11 λ 3770.63. The measurement of this line may possibly be affected by *Ni* II λ 3769.46 close by (but well resolved) on the shortward side.

The relatively small values of the velocity residuals of these hydrogen lines indicate that in HD 193182 the Balmer lines are considerably stronger with respect to lines of *Ti* II and *Cr* II than in 1 Delphini or in Pleione (1944).

The *Mg* II line λ 4481 is shallow and inconspicuous. Its width measured on a tracing is about 5 A. The *He* I lines λ 4026 and λ 4471 are probably present as very shallow lines, 5 or 6 A wide; their measurement is made difficult by superposed metallic lines. The velocity residuals of the lines of the various elements are given in Table 3.

1 Delphini = HD 195325.—In describing three spectrograms taken at the Dominion Astrophysical Observatory in 1929, W. E. Harper[8] remarked: "Numerous lines like

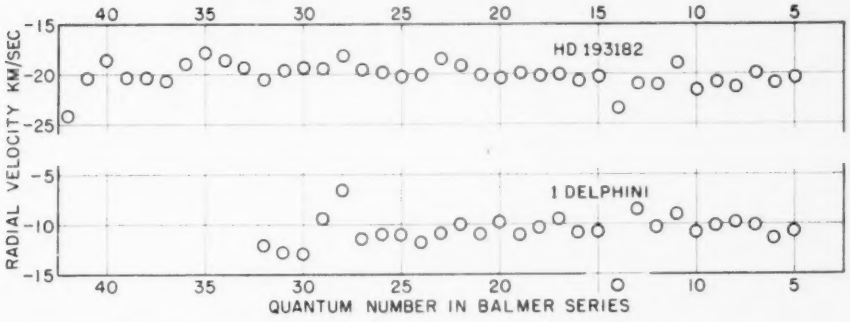

FIG. 2.—Displacements of hydrogen lines. HD 193182: means from plates Ce 3056, Ce 3572, and Pa 8. 1 Delphini: means from plates Ce 5749, 5807, 5918, 6019, 7078, and 7088.

TABLE 3

HD 193182: VELOCITY RESIDUALS OF LINES OF VARIOUS ELEMENTS
(Km/Sec)

PLATE	ADOPTED VEL.	RESIDUALS							
		H	*Fe* II	*Ti* II	*Cr* II	*Ca* II	*Ni* II	*Mn* II	*Mg* I
Ce 3056	−20.9	−0.2	+0.4	+0.1	−0.2	+0.1	(+2.8)	(+2.5)	.....
Ce 3572	−21.0	−0.1	+0.1	+0.4	−0.5	+0.6	(+2.2)	(+1.0)	(−0.3)
Pa 8	−19.8	+1.2	+0.4	0.0	−0.7	+0.8	(+0.2)	.....	.....

[8] *Pub. D. m. Ap. Ob., Victoria*, 7, 83, 1937.

α Cygni spectrum." He obtained a mean radial velocity of −16.7 km/sec (corrected by R. E. Wilson to −15.7 km/sec). Four plates obtained at the Simeis branch of the Pulkovo Observatory during the summer months of 1929 and 1930 were described by Shajn and Albitzky[9] as having many good lines. The mean radial velocity was −15.3 km/sec. Low-dispersion spectrograms obtained by W. P. Bidelman[10] at the Yerkes and McDonald Observatories in 1948 showed the object (brighter component of the visual binary ADS 13920) to be a shell star. On plates taken at Mount Wilson in May and June, 1949, *Hα* was found to have a sharp dark core with weak bright borders of nearly equal intensity.[11] The Mount Wilson spectrograms are listed in Table 4. Most of the measures were by Miss Sylvia Burd.

TABLE 4

SPECTROGRAMS OF 1 DELPHINI

Plate	Date	Disp. (A/Mm)	Radial Velocity (Km/Sec)				
			H	No.	M II	No.	Adopted
γ 30692	1949 May 8	35	− 5	2	− 9.7	20	− 9.2
Ce 5680*	June 11	20	−16	1	− 8.3	4	− 9
5749	July 12	10	− 9.6	29	− 9.8	73	− 9.8
5807	Aug. 3	10	−10.3	29	−10.5	82	−10.5
5918	Sept. 9	10	−10.0	29	− 9.9	75	− 9.9
6019	Nov. 11	10	−11.0	28	−10.1	68	−10.0
7078	1951 June 22	10	−11.3	25	− 9.6	86	−10.0
7088	24	10	−12.3	25	−11.4	72	−11.6
7089*	24	15	−12	1	− 9	3	− 9.4

* Red region.

The spectrum resembles that of HD 193182, but the dark lines, especially those of hydrogen, are weaker. Hydrogen lines of longer wave length have narrow cores and weak, wide wings. The shell of 1 Delphini, like that of HD 193182, appears to be stable. The hydrogen lines (Fig. 2) and the metallic lines all yield practically the same velocity, with little variation with time. The core of *Hδ* is about 1.7 A wide, with a total wing spread of 23 A. The apparent difference of about 5 km/sec between measures in 1929, dispersion 30–36 A/mm, and those in 1949, 10 A/mm, may possibly be within the limits of observational error; certainly any changes are small.

The D lines of sodium are strong and sharp, as they are characteristically in shell spectra. Because of the high galactic latitude, −17°, it is improbable that interstellar sodium makes a large contribution.

[9] *M. N.*, **92**, 771, 1932; *Pub. Central Obs. Pulkovo*, Ser. II, **41**, 1, 1933.

[10] *Pub. A.S.P.*, **61**, 32, 1949.

[11] Merrill and Burwell, *Mt. W. and P. Obs. Reprint* No. 8; *Ap. J.*, **110**, 410, 1949.

THREE STARS WITH HELIUM SHELLS

PAUL W. MERRILL
MOUNT WILSON AND PALOMAR OBSERVATORIES
CARNEGIE INSTITUTION OF WASHINGTON
CALIFORNIA INSTITUTE OF TECHNOLOGY

Received October 4, 1951

ABSTRACT

In the B-type stars HD 172694, HD 184279, and HD 195407 absorption lines from metastable levels of the neutral helium atom indicate a cloud of gas at high excitation far above the usual reversing layer. Observations over many years show that all three stars have variable spectra. Many details are given. These helium shells are probably similar to the commoner type showing numerous metallic lines, but differ in having higher excitation.

In shell stars an abnormally large amount of absorbing gas lies far above the usual reversing layer. The conspicuous lines in spectra of typical shell stars are those of hydrogen and of ionized metals; helium lines, if present at all, are usually weak and diffuse as if formed in a low-lying stratum and not in the shell. In a few stars, however, the presence of a helium shell is indicated by narrow lines (chiefly λλ 3888, 3965, and 5016) arising from metastable levels in the helium atom. In these stars the metallic lines are absent or very weak, presumably because the excitation required for the helium lines is sufficient to remove a second electron from the metallic atoms. Three stars of this kind, listed in Table 1, are described in this paper.

TABLE 1

THREE STARS WITH HELIUM SHELLS

HD	MWC	1900		Mag.	HARVARD SPECT.
		R.A.	Decl.		
172694	303	18^h36^m5	−15°57′	8.3	B3
184279	319	19 28.6	+ 3 34	6.8	B5
195407	346	20 26.0	+36 39	7.7	B5

HD 172694 = MWC 303.—A strong bright *Hα* line was found in the spectrum of HD 172694 at Mount Wilson[1] on an objective-prism spectrogram taken with the 10-inch telescope on August 2, 1921. The ultraviolet Balmer lines seen in absorption in many Be stars were weak or absent. Additional objective-prism plates, showing *Hα* bright, were obtained in 1926, 1927, and 1928[2] and in later years. Slit spectrograms taken at Mount Wilson are listed in Table 2.

On four one-prism spectrograms taken during the years 1921–1925 the *Hβ* line has a strong dark core, with conspicuous emission on the shortward edge; *Hγ* is similar, except that the emission is weaker. Other lines are wholly dark. The line *He* I λ 4471 is well marked. Other lines visible are *He* I λ 4388, λ 4713; *Fe* II λ 4352, λ 4549. Lines of *H*, *He* I, and *Fe* II yielded the same radial velocity, within errors of measurement, with the

[1] Merrill, Humason, and Burwell, *Mt. W. Contr.*, No. 294; *Ap. J.*, **61**, 389, 1925.

[2] Merrill, Humason, and Burwell, *Mt. W. Contr.*, No. 456; *Ap. J.*, **76**, 156, 1932.

exception that the velocity from $H\gamma$ averaged 11 km/sec less than the over-all mean velocity of +52 km/sec.

Six one-prism plates taken by F. J. Neubauer[3] at Lick Observatory in August and September, 1938, yielded the radial velocity -29.0 ± 3.3 km/sec. The value from interstellar K was −15 km/sec. On these plates, kindly sent to me for examination by Director C. D. Shane, the emission at $H\beta$ is fairly strong, but the dark core is not distinctly seen; it and the dark core of $H\gamma$ appear to be weaker than they were on the earlier Mount Wilson plates.

Two low-dispersion spectrograms obtained by Swings and Struve[4] at the McDonald Observatory in July, 1942, showed the usual shell lines to be weak, but they brought out for the first time an additional feature of great interest, namely, the strong sharp line λ 3889 from the metastable 2^3S level of *He* I. The sharp *H* and *He* I lines yielded the radial velocity +26 km/sec; the broad *He* I line λ 4026, +6 km/sec.

TABLE 2

SPECTROGRAMS OF HD 172694

PLATE	DATE	DISP. AT $H\gamma$ (A/MM)	RADIAL VELOCITY (KM/SEC)	
			Stellar	Interst. H and K
γ 10358	1921 Aug. 14	35	+47	.....
γ 11922	1923 July 3	35	+58	.....
γ 12692	1924 May 25	35	+52	.....
C 3347	1925 June 15	35	+54	.....
Ce 3502	1944 July 9	10	+16.2	− 9.5
Ce 4369	1946 Aug. 16	10	+13.5	−10.2
Ce 5227	1948 July 18	10	+11.2	− 8.8
Ce 6442	1950 Aug. 7	10	+ 4.4	− 8.6
Ce 7219	1951 Aug. 1	10	+ 9.1	−11.1
Mean	.....	.....	.....	− 9.6

On five spectrograms, dispersion 10 A/mm, taken at Mount Wilson from 1944 to 1951 (Table 2), *He* I λ 3888 is a strong, well-defined dark line, and λ 3965 from another metastable level 2^1S of *He* I is weaker but very sharp. On plates with suitable exposure in the λ 5000 region, *He* I λ 5016 appears as a strong narrow line. Other lines of *He* I are weak and indistinct, although λ 4471 was measured on two plates. Metallic lines are absent or extremely weak, and the dark cores of the *H* lines are probably weaker than on the early one-prism plates. The fairly wide emission edges at $H\beta$ are about equally intense on either side of the dark core. On a given plate all measurable lines, except the interstellar *Ca* II lines, yield the same velocity, but there is a slight variation from year to year.

The velocity pattern (Table 3) is peculiar and not easy to interpret. Perhaps there has been a general decrease in velocity (due to orbital motion?) since 1924, with an atmospheric outburst in 1938; but this hypothesis is insecure. A satisfactory understanding of this interesting object will probably require many additional observations.

HD 184279 = MWC 319.—A bright $H\alpha$ line was found in the spectrum of HD 184279 at Mount Wilson[5] on an objective-prism photograph taken on July 11, 1929. The first

[3] *Ap. J.*, **97**, 300, 1943.

[4] *Ap. J.*, **97**, 194, 1943.

slit spectrograms on record[5] were taken at Victoria in 1925. The hydrogen lines were described as "abnormally strong and narrow"; but nothing was said about emission. The Mount Wilson series began in 1929. On plates taken at the McDonald Observatory in July, 1942, Swings and Struve[4] noted that the lines were probably broader and less intense than on earlier plates taken at Mount Wilson. Since 1942, even greater changes have occurred.

The Mount Wilson spectrograms are listed in Table 4. I am indebted to W. S. Adams, W. C. Miller, and R. F. Sanford for permission to use plates taken by them.

The lines in the spectrum of HD 184279, wholly dark except for *Hα*, are subject to marked changes, as indicated in Table 5.

TABLE 3

RADIAL VELOCITIES OF HD 172694

Year	Radial Velocity (Km/Sec)	Observatory	Year	Radial Velocity (Km/Sec)	Observatory
1921–1925	+52	Mt. Wilson	1946	+14	Mt. Wilson
1938	−29	Lick	1948	+11	Mt. Wilson
1942	+26	McDonald	1950	+ 4	Mt. Wilson
1944	+16	Mt. Wilson	1951	+ 9	Mt. Wilson

TABLE 4

SPECTROGRAMS OF HD 184279

Plate	Date	Observer	Disp. at $H\gamma$ (A/Mm)	Radial Velocity (Km/Sec)		
				H	*He* I	Interst.
C 5268	1929 Aug. 17	P. W. Merrill	35	(− 3)	(−18)	(−13)
G 1057*	1934 July 31	P. W. Merrill	34*	(−13)	− 6	−11.2
V 1459†	1936 July 28	R. F. Sanford	39			
Ce 3151	1943 Aug. 17	R. F. Sanford	10			− 6.2
Ce 3217	Oct. 6	P. W. Merrill	10			− 9.9
Ce 3441	1944 June 3	P. W. Merrill	10	−12.1	−13.4	− 9.7
γ 26846	1945 July 28	W. C. Miller	35	−14	−13	− 7.1
Ce 3921	Aug. 28	W. S. Adams	10	−10.4	− 5.6	− 9.5
Ce 7224	1951 Aug. 1	P. W. Merrill	10			− 9.9
Mean						− 9.3

* Yellow and red region.
† Underexposed.

TABLE 5

BEHAVIOR OF *H* AND *He* I LINES IN THE SPECTRUM OF HD 184279

Year	Character of Lines	Year	Character of Lines
1925, 1927, 1929, 1934	Strong and well defined	1944	Somewhat stronger
1936, 1942	Weaker	1945	Fairly strong and narrow
1943	Extremely weak and diffuse	1951	Extremely weak and diffuse

[5] J. S. Plaskett, *Pub. Dom. Ap. Obs. Victoria*, **5**, 1, 1931.

The only plate of the red region, G 1057, shows *Hα* to have a strong dark core, with symmetrical bright edges of moderate intensity on either side. The dark D3 line of *He* I is narrow and extremely strong.

The sensitive lines λλ 3888, 3965, and 5015 are so weak that it is only by courtesy that this star can be said to have a helium shell. On some of the plates, however, these lines are present, and on the earlier plates other lines of *He* I, together with the *H* lines, were unusually well defined. (It is unfortunate that no observations in the blue and violet were obtained in 1934, when D3 was strong and well defined.) Perhaps one might say that at times the star has had a rudimentary shell or that the reversing layer was abnormally extended.

The measured radial velocities are included in Table 4. The stellar lines are not sufficiently numerous or well defined to yield highly accurate values. The Mount Wilson

TABLE 6

SPECTROGRAMS OF HD 195407

Plate	Date	Disp. at $H\gamma$ (A/Mm)	Radial Velocity (Km/Sec)		
			H	*He* I	Interst. H and K
C 1327*	1921 Sept. 19	35	−69	.....	.....
γ 12596*	1924 Apr. 21	35	−82	.....	.....
γ 12688*	May 24	35	(−86)	.....	.....
γ 12726	June 15	35	−80	.....	.....
C 3072	Nov. 8	35	−70	.....	−15
Ce 3287	1943 Nov. 14	10	−72	−71	−10.6
Ce 3498	1944 June 8	10	−65	−67	− 9.9
Ce 4367	1946 Aug. 15	10	−76	−78	−10.0
Ce 5316	1948 Sept. 12	10	−69	−74	−10.7
Ce 5317	Sept. 12	21†	−72†	.....	.....
Ce 7226	1951 Aug. 2	10	−71	−68	−10.2
Mean	.....	.....	−72	−72	−10.3

* These plates were taken by M. L. Humason, to whom I am indebted for permission to use them.

† *Hα*.

values probably agree among themselves within errors of measurement, but they differ from Plaskett's value (1925–1927) of -2.9 ± 0.5 km/sec. The mean for the years 1944–1945 was -11.0 ± 1.0 km/sec. The rare type of change in this spectrum would seem to warrant further observation.

HD 195407 = MWC 346.—A strong bright *Hα* line was found in the spectrum of HD 195407 at Mount Wilson[1] on an objective-prism photograph taken on September 11, 1920. The slit spectrograms obtained at Mount Wilson (Table 6) fall into two groups: five one-prism plates taken in 1921 and 1924 and six coudé plates taken in the years 1943–1951. Four one-prism plates were taken by Swings and Struve[4] at McDonald Observatory in July, 1942.

On the early Mount Wilson plates the *Hβ* and *Hγ* emission lines were fairly strong but of variable intensity. The absorption cores were quite weak except on γ 12596, the first plate taken in 1924; even on this plate the cores were not outstanding. In 1942, however, the McDonald spectrograms showed "a remarkably strong shell-absorption spectrum of *H* and *He* I." In 1943 the Mount Wilson plates showed the *H* cores again to be very weak. There was not much change in 1944, 1946, and 1948. The *He* I line

λ 3888 was strong and well defined, while λ 3965 was weak and narrow. In 1951 (plate Ce 7226), all the dark lines were considerably stronger, but the *H* cores were probably not nearly so intense as in 1942. Variations in the structure of *Hβ* are illustrated in Figure 1.

The radial velocity has been nearly constant; it is not certain that differences from year to year exceed errors of observation. Hydrogen and helium lines yield the same mean value, −72 km/sec. The residual radial velocity, −55 km/sec, is high for a B-type star.

Discussion.—The spectral variability of these three stars indicates that with helium shells, as with the commoner type of shells showing numerous metallic lines, stability is

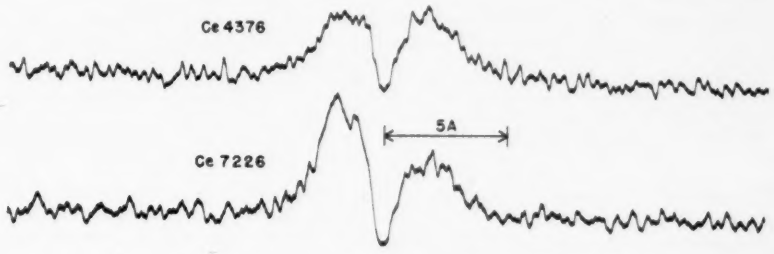

FIG. 1.—Variations in the structure of *Hβ* in HD 195407

TABLE 7

DATA FROM INTERSTELLAR LINES

Star	Vis. Mag.	*l*	*b*	Radial Vel. (Km/Sec)	Resid. Vel. (Km/Sec)	Distance (Parsecs)	Abs. Mag.
HD 172694	8.3	345°	−7°	−9.6	+4.1	770	−1.1
HD 184279	6.8	8	−8	−9.3	+7.4	860	−2.9
HD 195407	7.7	44	−2	−10.3	+6.8	1970	−3.8

the exception rather than the rule. The two types of shells appear similar in another respect, namely, that changes tend to be measured in months and years rather than in days and weeks. Probably the two types of shells differ chiefly in the excitation to which they are subjected. One would expect the helium shells to lie above the hotter photospheres, but the broad lines of the reversing layer do not clearly indicate spectral types earlier than those of stars with metallic shells. This point should have further study. Possibly the helium shells lie nearer to the photosphere, where the radiation is more intense.

The interstellar H and K lines of *Ca* II are strong and accurately measurable in all three stars. They are of about equal intensity in HD 172694 and HD 195407 and are slightly more intense in HD 184279. In HD 184279, the only star observed in the yellow, the D lines of *Na* I are very strong. In this star, in addition, there are traces of the following interstellar lines: λ 3383.78 *Ti* II, λ 3957.71 *CH* II, λ 4232.57 *CH* II, λ 4300.31 *CH* I, λ 5780.55, and λ 6283.91.

Radial velocities measured from interstellar lines (Table 7) are nearly the same for all three stars but differ substantially when corrected for solar motion. The distances

and absolute magnitudes in Table 7 are derived from the equations

$$V = 17.7\, r \sin 2\,(l - 326^\circ) \cos^2 b\,,$$

$$M = m - 5 \log r + 5\,.$$

According to the usual practice, V is put equal to twice the measured residual interstellar velocity. If allowance were made for space reddening, the absolute magnitudes would be somewhat brighter. If, on the other hand, we should apply the negative correction to the measured velocities suggested by W. S. Adams,[6] the computed distances would become considerably less and the magnitudes fainter. While this method of determining stellar distances would doubtless yield valuable statistical results, the data in Table 7 suggest that distances for individual stars are subject to considerable error because of irregularities in the distribution and motion of interstellar clouds of gas.

[6] *Mt. W. Contr.*, No. 760; *Ap. J.*, **109**, 354, 1949.

THE SPECTROSCOPIC BINARY BOSS 4496

JORGE SAHADE AND JORGE LANDI DESSY
Observatorio Astronómico de Córdoba, Argentina
Received August 14, 1951

ABSTRACT

The star Boss 4496 is a double-lined spectroscopic binary. A period of 3.170 days for the velocity variation has been derived. The velocity-curves for *H* and *He* I are different; the orbital elements and the behavior of the spectral lines suggest that the results from *He* I represent orbital motion and that there is a stream of *H* gas which flows toward the advancing hemisphere and away from the receding hemisphere of each star, relative to the *He* I atoms. The orbital elements and their probable errors, as derived from *He* I, are as follows: $\gamma = -6 \pm 1.2$ km/sec; $K_1 = 154 \pm 2.0$ km/sec; $K_2 = 181 \pm 2.0$ km/sec; $e = 0.04 \pm 0.011$; $\omega = 29° \pm 13°7$; $T_0 = 0.700 \pm 0.0022P$; $a_1 \sin i = 6.7 \times 10^6$ km; $a_2 \sin i = 7.9 \times 10^6$ km; $\mathfrak{M}_1 \sin^3 i = 6.7\odot$; $\mathfrak{M}_2 \sin^3 i = 5.7\odot$.

The spectroscopic binary Boss 4496[1] was discovered by Neubauer[2,3] from three spectrograms taken at Santiago, Chile, in 1928, which show double lines and indicate a range in radial velocity of the order of 300 km/sec. With the purpose of determining the period of the velocity variation and the orbital elements, the star was observed at Bosque Alegre during the intervals July–October, 1949, and March–July, 1950, with the Wood-grating spectrograph attached to the 154-cm reflector; the linear dispersion is about 42 A/mm. Prior to April, 1950, the exposures were made on Eastman 103*a*-O emulsion with a projected slit-width of 0.019 mm and thereafter on Eastman II*a*-O emulsion with a projected slit-width of 0.015 mm, except two rather long exposures which were taken on Eastman 103*a*-F plates.

In good seeing conditions the exposure times were of the order of 30 minutes on the 103*a*-O plates and 45 minutes on the II*a*-O plates. Ninety-four measurable plates were secured for the present investigation.

From the 1949 spectrograms a period of 3.170 days was derived for the variation in radial velocity of B 4496, and, accordingly, the phases used for the analysis of the results obtained have been computed with this period, taking as an arbitrary origin the Julian date 2433112.5, quite close to the epoch of our first spectrogram. Near the completion of our work, Neubauer's original paper[3] with his radial velocities for B 4496 came to our attention. The consideration of Neubauer's velocities indicates that all the figures of our period are significant and that it could be further improved to 3.17035 days. The possibility of periods smaller than 1 day and between 1 and 2 days is ruled out by the distribution of our observations.

Except at or around opposition, the spectrum of B 4496 shows two sets of sharp lines of different relative intensities and the interstellar line of *Ca* II K. The stronger set of lines corresponds to a spectral type of about B3 and the fainter set to a spectral type somewhere around B5. The *He* I lines are strong and show no change with phase or with cycle; their intensities look normal. The relative intensities of both sets of *He* I lines are, roughly, of the order of 2.5. The *Mg* II lines are relatively faint, and the ratio of the intensities of both components is about 0.9. Relative to *He* I 4471, the ratio is of the order

[1] $\alpha = 17^h46^m4$; $\delta = -53°36'$ (1950.0). 77 G. Arae = BS 6622 (5.90 mag.) = CD−53°7423 = CPD−53°8799 = h 4978 = HD 161783 (Sp. B3). In Moore's *Fourth Catalogue of Spectroscopic Binary Stars* (*Lick Obs. Bull.*, No. 483, p. 34, 1936) the revised spectral type indicated for this star is B3s.

[2] *Pub. A.S.P.*, **42**, 235, 1930.

[3] *Lick Obs. Bull.*, No. 429, p. 76, 1930.

of 1:3 in the stronger set, and 1:1.5 in the fainter set. The first ratio may be variable.

The *H* lines are strong, and, near maximum positive and negative velocities, both components are distinctly separated (Fig. 1). The fainter component does not show noticeable changes with phase or with cycle, but the stronger component is sharper and deeper around maximum velocity of recession. At the other half of the cycle the ratio of the intensity of both components of *H* is about 1.3. The Balmer series is seen up to *H*16.

The radial velocities of B 4496 were determined by measuring the lines of *H* and *He* I in the wave-length interval λλ 3795–4490 and, whenever it was possible, *Mg* II 4481 and *C* II 4267. On a few plates the spectral region measured was extended shortward to λ 3720 or longward to λ 4925. The adopted wave lengths are listed in Table 1.

TABLE 1

ADOPTED WAVE LENGTHS FOR THE RADIAL-VELOCITY DETERMINATION

H	*He* I	*Mg* II	*Ca* II	*C* II
3721.94	3819.64	4481.23	3933.67	4267.15
3734.37	3867.53*			
3750.15	4009.27			
3770.63	4026.22			
3797.90	4143.76			
3835.39	4387.93			
3889.05	4471.51			
3970.08	4921.93			
4101.74				
4340.47				
4861.33				

* This line was measured on only one plate.

From the beginning of our work it was evident that *He* I and *H* give different velocities; hence separate plots were made for each element. The individual values are given in Table 2, and the plots are shown in Figures 2 and 3. The plots for *Mg* II and *C* II indicate that these elements behave like *He* I; but, in view of the scatter of the individual points arising from the difficulty of measuring the lines, it was decided to base all the discussion only on the results from *He* I and *H*. The interstellar line of *Ca* II gives a radial velocity of $+1 \pm 1.8$ (p.e.) km/sec, as a mean of twenty-eight values.

The plots of the radial velocities from *H* and *He* I showed at once that the amplitude is different for both elements, smaller for *H* than for *He* I, a feature which has been previously found in two eclipsing systems, namely, BD+55°616[4] and RY Persei.[5] The possibility that the difference in amplitude between *He* I and *H* may come from a difference in the appearance of the lines from both elements is out of the question in the present case because of the sharpness of the *H* lines and their distinct separation when double. In order completely to eliminate any possible doubt, the separations of both components of *H* and *He* I, at phases corresponding to maximum positive and negative velocities, were measured on photoelectric tracings, and, of course, the agreement with the results obtained with the measuring machine was excellent. Therefore, the difference in the amplitude of the radial velocities from *H* and *He* I is undoubtedly real.

As to the orbital elements, independent applications of the Wilsing-Russell method were made for each of the four sets of points. The results obtained are shown in

[4] Deutsch, *Ap. J.*, **102**, 496, 1945; *McDonald Contr.*, No. 119.

[5] Hiltner, *Ap. J.*, **104**, 396, 1946; *McDonald Contr.*, No. 129.

FIG. 1.—Spectrograms of Boss 4496

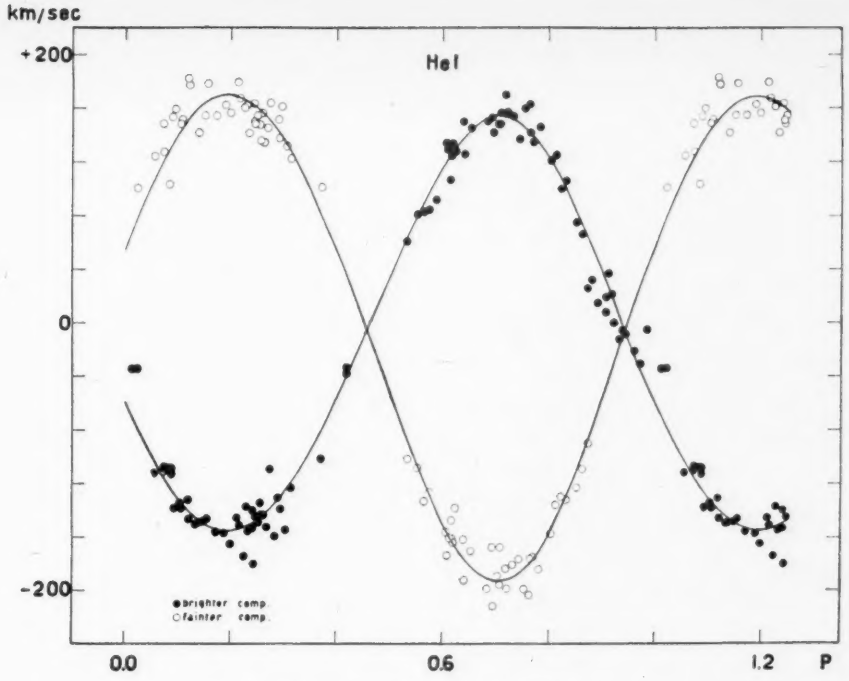

FIG. 2.—Velocity-curve for Boss 4496 from *He* I lines

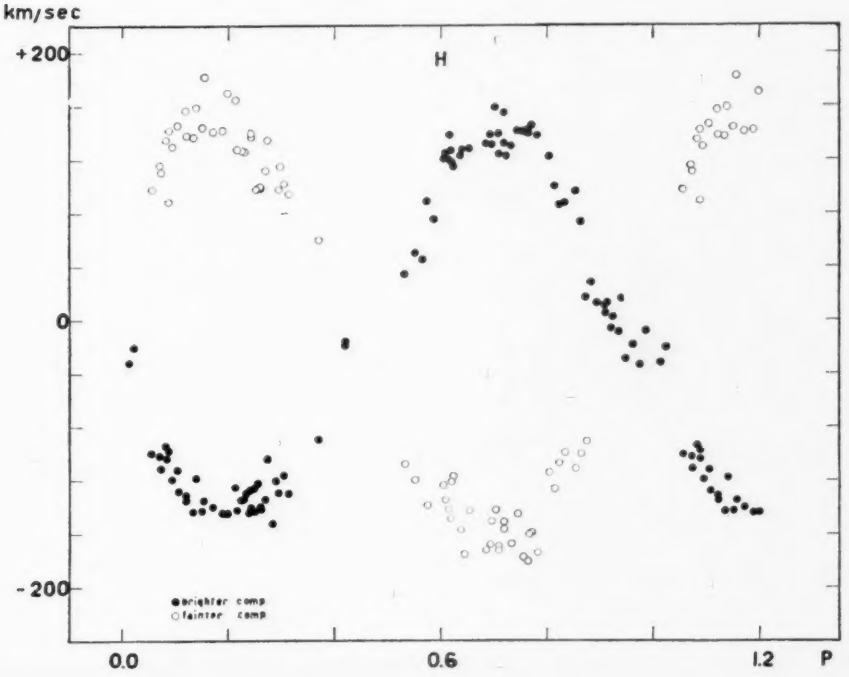

FIG. 3.—Velocity-curve for Boss 4496 from *H* lines

TABLE 2

RADIAL VELOCITIES OF BOSS 4496

DATE	U.T.	PHASE* (PERIOD)	RADIAL VELOCITIES (KM/SEC) FROM†							
			H		*He* I		*C* II		*Mg* II	
			I	II	I	II	I	II	I	II
1949 Sept. 10	2:20	0.012	− 32	....	− 34	....	....	....	− 25	.....
10	3:07	.022	− 21	....	− 34	+101	....	....	....	.....
1950 May 9	3:40	.055	−100	+ 98	−112	+125	−107	+113	−127	+ 72
9	4:54	.071	−102	+116	−111	+149	....	....	−120	.....
1949 Oct. 31	0:14	.073	−111	+111	−107	+128	....	....	− 98	+ 82
31	0:55	.082	− 94	+135	−108	+104	....	....	−118	+104
1950 May 9	6:04	.087	−104	+142	−113	+154	−100	....	−106	+165
1949 July 15	6:37	.087	− 98	+ 89	−108	....	....	....	.....	.....
1950 May 6	2:31	.094	−119	+130	−138	+160	....	....	−136	+167
9	7:21	.104	−112	+146	−134	+149	....	....	−129	+138
6	3:28	.106	−128	....	−138	+152	−113	....	−161	+154
9	8:30	.119	−131	+157	−132	+183	−133	+212	−131	+166
6	4:37	.121	−135	+138	−146	+178	....	....	.....	.....
9	9:38	.134	−143	+137	−150	....	....	....	−133	.....
6	5:55	.138	−118	+159	−149	+142	....	+159	−106	+162
1949 Sept. 4	4:39	.149	−143	+144	−148	+155	....	....	.....	.....
1950 May 6	7:09	.155	−135	+182	−146	+179	....	....	−108	+120
6	8:24	.171	−140	+141	−156	+155	....	....	.....	.....
6	9:42	.188	−144	+142	−157	+163	....	....	−127	+157
Apr. 30	2:20	.199	−144	+170	−165	+157	....	....	−180	+138
30	3:27	.213	−125	+167	−145	+180	....	....	−124	+138
Mar. 7	6:20	.216	−142	+128	−151	+168	....	....	−154	+190
7	6:58	.225	−134	+127	−174	+161	....	....	.....	.....
Apr. 30	4:34	.228	−134	+126	−137	+163	....	....	.....	.....
Mar. 7	7:34	.233	−129	....	−155	+142	....	....	−160	.....
7	8:11	.241	−127	+140	−153	+164	....	....	−117	+ 99
Apr. 30	5:41	.243	−144	+138	−140	+151	....	....	−170	+124
1949 Aug. 25	23:38	.244	−140	....	−180	+148	....	....	.....	.....
1950 Mar. 7	8:46	.248	−126	....	−145	+155	....	....	−110	+159
1949 Aug. 26	0:13	.252	−143	+ 98	−149	+148	....	....	.....	.....
1950 Mar. 7	9:16	.255	−122	....	−135	+136	....	....	−150	+173
Apr. 30	6:53	.258	−140	+ 99	−143	+157	....	....	.....	.....
1949 Aug. 26	0:54	.261	−141	+100	−143	+135	....	....	.....	.....
26	1:30	.269	−134	+112	−152	+146	....	....	.....	.....
1950 Apr. 30	8:06	.274	−104	+135	−109	+165	....	....	−138	+135
1949 Sept. 10	23:01	.284	−152	....	−159	+152	....	....	.....	.....
1950 Apr. 30	9:18	.290	−120	+ 99	−130	+138	....	....	.....	.....
1949 Aug. 26	3:28	.295	−129	+115	−139	+162	....	....	−148	+199
26	4:10	.304	−116	+102	−154	+132	....	....	.....	.....
26	4:50	.313	−130	+ 97	−123	+123	....	....	.....	.....
July 16	4:10	.370	− 89	+ 60	−101	+102	....	....	.....	.....
Sept. 5	1:02	.407	− 19	....	− 38	....	....	....	.....	.....
July 16	7:52	.419	− 16	....	− 33	....	....	....	− 59	.....
1950 Mar. 8	6:22	.532	+ 34	−107	+ 61	−102	....	....	.....	.....
June 5	2:08	.553	+ 50	−119	+ 81	−108	....	....	.....	.....
Mar. 8	8:52	.565	+ 45	....	+ 83	−133	....	....	+ 90	−108
8	9:33	.574	+ 89	−138	+ 85	−126	....	....	.....	.....
1949 Aug. 27	1:39	.586	+ 75	....	+ 92	....	....	....	.....	.....
1950 July 13	7:11	.605	+121	−124	+134	−156	+124	−134	+114	−165
June 5	6:22	.608	+125	−134	+129	−174	....	....	+127	−149
1949 Aug. 27	3:46	.614	+120	−141	+107	−161	....	....	.....	.....
1950 July 13	8:00	.616	+138	....	+125	−147	....	....	+113	−182
Mar. 5	8:48	.618	+118	−121	+134	−164	....	....	+113	.....
June 5	7:12	.619	+127	−148	+133	−161	....	....	.....	.....
1949 Aug. 27	4:26	.623	+117	−117	+128	−138	....	....	.....	.....
1950 Apr. 28	7:36	0.637	+123	−156	+150	−162	....	....	+140	−193

* The origin was arbitrarily taken at JD 2433112.5.

† "I" designates the stronger component; "II," the fainter component.

TABLE 2—*Continued*

Date	U.T.	Phase* (Period)	Radial Velocities (Km/Sec) from†							
			H		*He* I		*C* II		*Mg* II	
			I	II	I	II	I	II	I	II
1950 June 5	8:57	0.642	+128	−175	+126	−192	+157	−142	+147	−136
5	9:52	.654	+128	−142	+145	−170	.....	.....	.....	.....
May 11	3:28	.684	+132	−172	+150	−199	+135	−184	+124	−213
1949 Sept. 9	2:02	.692	+138	−168	+153	−168	.....	.....	+147	−113
1950 May 11	4:22	.695	+131	−150	+142	−212	.....	.....	+125	−168
1949 Sept. 9	2:52	.703	+159	−142	+148	−189	.....	.....	.....	.....
1950 May 11	5:20	.708	+139	−169	+148	−168	+163	−169	+162	−203
1949 Sept. 5	23:14	.709	+124	−172	+156	−196	.....	.....	+235	−218
5	23:56	.718	+132	−156	+170	−184	.....	.....	.....	.....
July 17	6:36	.718	+155	−151	+156	−184	.....	.....	.....	.....
1950 May 11	6:18	.721	+122	.....	+158	−199	.....	.....	.....	.....
11	7:07	.732	+130	−167	+154	−181	+188	−174	+148	−205
11	8:02	.744	+141	−145	+137	−177	.....	.....	.....	.....
1949 Oct. 30	0:00	.754	+141	−177	+160	−199	.....	.....	+166	.....
30	0:40	.763	+142	−181	+163	−203	.....	.....	.....	−154
1950 May 11	9:40	.765	+139	−160	+142	−176	+146	−173	+130	−212
8	5:57	.770	+145	−159	+135	−175	.....	.....	+130	−192
1949 Sept. 6	4:40	.781	+138	−174	+146	−184	.....	.....	+190	.....
1950 June 9	1:20	.804	+122	−114	+121	−158	+115	−161	+ 52	−160
9	2:06	.814	+100	−126	+125	−136	.....	.....	+ 55	−140
9	2:50	.824	+ 86	−107	+100	−130	.....	.....	.....	.....
9	3:32	.833	+ 87	− 99	+106	−132	+101	−107	+ 81	−139
6	1:00	.853	+ 96	−111	+ 75	−123	+ 62	− 94	+ 73	−146
6	1:48	.864	+ 73	−100	+ 66	−109	.....	.....	+ 69	.....
6	2:34	.874	+ 17	− 91	+ 26	− 90	.....	.....	+ 54	.....
6	3:18	.883	+ 28	.....	+ 32	.....	.....	.....	.....	.....
6	4:06	.894	+ 13	.....	+ 15	.....	.....	.....	+ 37	.....
3	1:00	.907	+ 11	.....	+ 8	.....	+ 48	.....	+ 16	.....
Apr. 29	4:19	.909	+ 5	.....	+ 19	.....	.....	.....	.....	.....
1949 Aug. 28	2:26	.912	+ 13	.....	+ 37	.....	.....	.....	.....	.....
28	3:00	.920	− 6	.....	+ 21	.....	.....	.....	.....	.....
1950 Apr. 29	5:18	.922	+ 2	.....	0	.....	− 5	.....	− 3	.....
29	6:14	.934	− 19	.....	− 12	.....	.....	.....	.....	.....
Mar. 6	9:12	.939	+ 16	.....	− 6	.....	.....	.....	.....	.....
Apr. 29	7:12	.947	− 30	.....	− 9	.....	+ 2	.....	− 25	.....
29	8:12	.960	− 19	.....	− 21	.....	.....	.....	.....	.....
29	9:10	.973	− 34	.....	− 31	.....	.....	.....	+ 8	.....
1949 Sept. 10	0:18	0.985	− 8	.....	− 5	.....	.....	.....	+ 3	.....

Table 2*a*. In view of the elements and of the behavior of the *H* lines with phase, it seems safe to conclude that the radial velocities from *He* I, or rather from all lines except *Ca* II and *H*, do result from the orbital motion of the two components of the system.

At the suggestion of Dr. O. Struve, a least-squares solution was carried out for *He* I. The method suggested by Sterne[6] was followed and the following were considered as preliminary elements:

$$e = 0\,,\ \gamma = -2 \text{ km/sec}\,,\qquad K_1 = 152.0 \text{ km/sec}\,,\qquad K_2 = 182.2 \text{ km/sec}\,,$$
$$T_{0_1} = 0.715P\,.$$

[6] *Proc. Nat. Acad. Sci.*, **27**, 175, 1941.

For the least-squares solution, we grouped the observations in nineteen normal points—ten corresponding to component I and nine to component II—and each one was given a weight equal to the square root of the number of individual values considered. The nineteen equations were solved as one set. The radial velocities corresponding to those phases at which the components were not seen unblended—except the results for phases 0.934, 0.939, and $0.947P$—were disregarded in the formation of the normal points. The final results are given in Table 3, and the corresponding velocity-curves are drawn

TABLE 2*a*

	He I		*H*	
	Brighter Component	Fainter Component	Brighter Component	Fainter Component
γ	−3.9	−4.0	−3.8	−9.3 km/sec
K	151.6	182.2	142.8	155.9 km/sec
e	0.04	0.04	0.05	0.03
ω	36°.4	211°.6	350°.6	321°.1
T*	0.802	0.790	0.680	$0.079P$

* The origin was arbitrarily taken at JD 2433112.5.

TABLE 3

ORBITAL ELEMENTS OF BOSS 4496 AND PROBABLE ERRORS (FROM *He* I)

P	3.170 days	T_0*	$0.700 \pm 0.0022P$ ($\therefore T = 0.781P$)
γ	-6 ± 1.2 km/sec	$a_1 \sin i$	6.7×10^6 km
K_1	154 ± 2.0 km/sec	$a_2 \sin i$	7.9×10^6 km
K_2	181 ± 2.0 km/sec	$\mathfrak{M}_1 \sin^3 i$	$6.7\odot$
e	0.04 ± 0.011	$\mathfrak{M}_2 \sin^3 i$	$5.7\odot$
ω	$29° \pm 13°.7$		

* The origin was arbitrarily taken at JD 2433112.5.

in Figure 2. $O-C^2$ lowered from 18,678 to 13,106 for component I, and from 28,248 to 14,728 for component II.

We believe that the orbital motion of the two stars is represented by *He* I and, therefore, that the radial velocities given by *H* show distortion. As in so many other cases in which a distortion of the velocity-curve is not shared by all the elements, *H* is the only element affected. In the present case we have a smaller amplitude for *H*, suggesting the existence of a mass of *H* gas moving toward the advancing hemisphere and away from the receding hemisphere of each star of the system, relative to the rest of the atoms—a phenomenon which is just the contrary of the one suggested by the observations of UX Monocerotis.[7]

The Wilsing-Russell solutions suggest that the distortion which affects the *H* radial velocities is also shown in the fact that the T_0's[8] and the ω's for both components of *H* differ by quantities which are different from $0.5P$ and 180°, respectively. In fact, the solutions give

$$T_{0_1} = 0.715P\,, \qquad \omega_1 = 351°\,,$$

$$T_{0_2} = 0.187P\,, \qquad \omega_2 = 321°\,.$$

[7] Struve, *Ap. J.*, **106**, 255, 1947; *McDonald Contr.*, No. 138.

[8] T_0 represents the time at which the mean longitude $M + \omega$ is equal to zero.

The smallness of the eccentricities obtained is certainly against considering the difference in the ω's as significant, but the visual inspection of the radial velocities points toward the possibility that both differences are real. The plot suggests, for both components of H, velocity-curves narrower at maximum positive velocity than at maximum negative velocity, thus pointing to slightly eccentric orbits with different values for ω_1 and $\omega_2 - 180°$. It also suggests a slight difference between the times at which component I shows the maximum velocity of approach and component II the maximum velocity of recession.

In order to determine the probable errors affecting the elements, least-squares solutions—according to Sterne's[6] suggestions—were independently made for both components of H, starting from the preliminary circular elements given in Table 4 and per-

TABLE 4

PRELIMINARY CIRCULAR ELEMENTS

	Component I	Component II
e	0	0
γ	0 km/sec	0 km/sec
K	143 km/sec	158 km/sec
T_0	$0.715P$	$0.185P$

TABLE 5

FINAL ELEMENTS (FROM H)

	Component I	Component II
γ	-11 ± 3.2 km/sec	-11 ± 5.8 km/sec
K	143 ± 1.8 km/sec	158 ± 2.6 km/sec
e	0.10 ± 0.018	0.07 ± 0.020
ω	$358° \pm 8°2$	$293° \pm 27°6$
T_0	$0.708 \pm 0.0030P$	$0.186 \pm 0.0044P$

forming second approximations. The final elements and their probable errors are listed in Table 5, the $O-C^2$ having been reduced from 19,088 to 11,362 in the case of component I, and from 28,796 to 15,799 in the case of component II. The actual eccentricities should be smaller than those obtained because the normal points at about phase $0.55P$ are based upon three plates of less than average quality. The criteria for selecting, grouping, and weighing the H radial velocities were the same as for *He* I. We have, then, in the case of H,

$$T_{0_1} - (T_{0_2} + 0.5P) = 0.022 \pm 0.0053P$$

and

$$\omega_1 - (\omega_2 - 180°) = 115° \pm 28°9 .$$

The probability that these differences will be affected by errors of their same order of magnitude is rather small—5:1000 and 7:1000, respectively—so we may conclude that the differences found in the T_0's and the ω's are almost certainly also distortion effects. It is somewhat surprising that the scatter of the H radial velocities is not very large and,

in fact, not larger than for *He* I. The star probably deserves attention from the photoelectric observers.

We are indebted to Dr. O. Struve for a valuable discussion concerning this star; to Dr. R. Platzeck for setting up a provisory photoelectric photometer for the analysis of some of the spectra of B 4496; and to Mr. Julio Albarracín and Miss Nélida Keller for assistance in the reduction of the plate measurements.

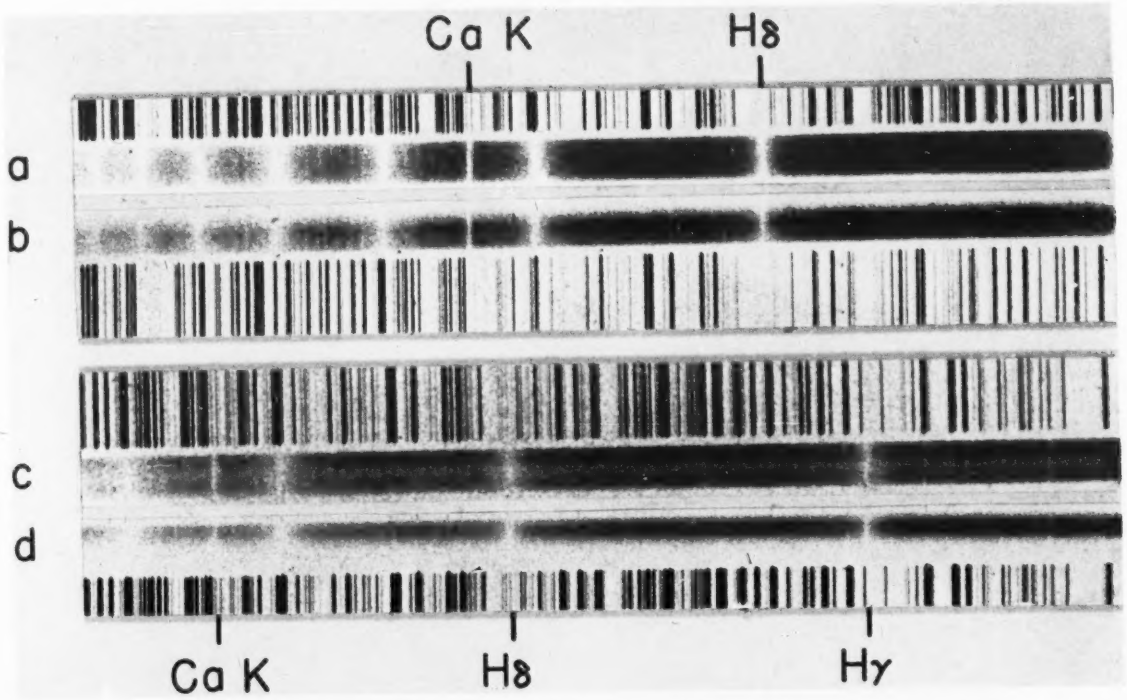

FIG. 1.—Spectrograms taken at the following phases: (*a*) 0.819, (*b*) 0.983, (*c*) 0.971, (*d*) 0.668

A SPECTROGRAPHIC STUDY OF RZ CASSIOPEIAE*

HENRY G. HORAK
University of Kansas, Lawrence, Kansas
Received July 11, 1951

ABSTRACT

Eighty-nine spectrograms of RZ Cassiopeiae were obtained with the 82-inch reflector of the McDonald Observatory; the radial velocities were determined, and the orbit computed by least squares. The spectral lines of only the A-type component could be observed. The velocity-curve shows the rotational-velocity effect.

The Algol-type variable RZ Cassiopeiae was discovered by Müller and Kempf on May 24, 1906. The earliest spectroscopic observations were made by Hartmann[1] that same year. Jordan[2] made a detailed study of this binary in 1914, and his orbital elements were rediscussed by Luyten,[3] who gives the following elements with mean errors: $P = 1.19525$ days, $\gamma = -39 \pm 1.4$ km/sec, $K = 69.1 \pm 2.0$ km/sec, $\omega = 170° \pm 35°$, $e = 0.048 \pm 0.030$ (71 observations). He also states: "From photometric observations

TABLE 1

LIST OF STAR LINES

Element	Wave Length (Angstroms)	Element	Wave Length (Angstroms)	Element	Wave Length (Angstroms)
*H*9	3835.39	*Ca* II	3933.67	*Ca* I	4226.73
Fe I + *Ni* II	3849.86	*Fe* I	4045.82	*Fe* II	4233.16
Si II	3856.02	*Fe* I	4063.62	*Fe* I	4271.44
Fe I	3878.34	*Fe* I	4071.74	*H*γ	4340.47
*H*8	3889.05	*H*δ	4101.74	*Mg* II	4481.23

we have every reason to believe that the eccentricity, if any, must be less than 0.01, yet we must accept the spectroscopic values for the moment." More recent photometric observations by various observers[4] also indicate an eccentricity of near zero. Now an inconsistency in the value of the eccentricity as determined spectroscopically and photometrically has been found in connection with other stars, notably U Cephei.[5] It was therefore considered desirable to study RZ Cassiopeiae in detail; hence it was placed on the observing program of the McDonald Observatory. During the period from December 24, 1949, to January 23, 1950, a series of eighty-nine spectrograms was taken by O. Struve. The quartz-prism spectrograph was used at the Cassegrain focus of the 82-inch reflector. The combination gave a dispersion of 40 A/mm at λ 3933. The spectrum (Fig. 1) shows only the lines of the brighter component and indicates a normal A0 star. No evidence for the secondary could be found.

The list of star lines measured is given in Table 1. The results of the measurements are given in Table 2. All plates were measured by Horak except the first two, which

* *Contributions from the McDonald Observatory, University of Texas*, No. 202.

[1] *A.N.*, **173**, 101, 1906.

[2] *Pub. Allegheny Obs.*, **3**, 137, 1914.

[3] *Ap. J.*, **84**, 85, 1936.

[4] See, e.g., Walter, *A.N.*, **277**, 159, 1949.

[5] Struve, *Ap. J.*, **99**, 222, 1944; *M.N.*, **109**, 487, 1949 (Darwin Lecture); and Hardie, *Ap. J.*, **112**, 542, 1950.

TABLE 2

RADIAL VELOCITIES OF RZ CASSIOPEIAE

DATE	U.T.	PHASE		RADIAL VELOCITIES (KM/SEC)
		Days	Period	
1949 Dec. 24	6:14	0.960	0.803	+ 23.2
24	6:40	0.977	.817	+ 21.9
24	6:58	0.990	.828	+ 6.1
24	7:12	1.000	.837	+ 12.6
24	10:20	1.131	.946	− 13.6
24	10:56	1.156	.967	+ 13.9
24	11:38	1.185	.991	− 65.0
24	12:06	0.009	.008	− 97.0
25	2:41	0.617	.516	− 42.3
25	3:16	0.641	.536	− 35.5
25	3:53	0.667	.558	− 7.4
25	4:10	0.679	.568	− 5.5
25	4:31	0.693	.580	− 12.0
26	4:18	0.487	.407	− 67.1
26	4:36	0.500	.418	− 66.4
26	5:17	0.529	.443	− 54.1
27	4:36	0.305	.255	−113.5
27	4:48	0.314	.263	−113.9
27	4:52	0.316	.264	−106.3
27	5:08	0.328	.274	−102.1
27	5:29	0.342	.286	−102.2
27	5:44	0.352	.294	−106.4
27	5:59	0.363	.304	−103.7
28	1:28	1.175	.983	− 39.5
28	1:48	1.189	.995	− 59.9
28	2:18	0.015	.013	− 78.3
28	2:46	0.034	.028	− 86.4
28	3:02	0.045	.038	− 88.8
31	7:01	0.820	.686	+ 22.1
31	7:20	0.834	.698	+ 26.5
31	7:28	0.839	.702	+ 25.8
31	7:41	0.848	.709	+ 28.5
31	7:55	0.858	.718	+ 26.9
1950 Jan. 1	2:40	0.444	.371	− 83.3
1	3:04	0.460	.385	− 91.6
1	3:18	0.470	.393	− 85.5
1	3:35	0.482	.403	− 90.8
1	4:08	0.505	.423	− 63.4
5	5:10	0.962	.805	+ 26.8
5	5:18	0.968	.810	+ 11.0
5	5:26	0.973	.814	+ 15.7
5	5:34	0.979	.819	+ 19.5
5	5:50	0.990	.828	+ 24.3
7	5:53	0.602	.504	− 42.9
7	6:08	0.613	.513	− 29.7
7	6:16	0.618	.517	− 28.6
7	6:32	0.629	.526	− 24.8
8	1:02	0.205	.172	−108.9
8	1:31	0.225	.188	−100.3
8	2:22	0.261	.218	−114.3
9	5:27	0.193	.161	−105.7
9	5:42	0.203	.170	− 90.6
9	6:00	0.216	.181	− 91.1
10	6:18	0.033	.028	− 83.5
10	6:44	0.052	.044	− 76.9
10	7:00	0.062	.052	− 80.0
11	4:47	0.970	.812	+ 28.4
11	5:01	0.980	0.820	+ 35.2

TABLE 2—*Continued*

Date	U.T.	Phase		Radial Velocities (Km/Sec)
		Days	Period	
1950 Jan. 11	5:15	0.990	0.828	+ 23.8
14	4:17	0.363	.304	−108.1
14	4:33	0.375	.314	− 98.1
14	4:48	0.385	.322	−107.8
15	4:06	0.160	.134	− 86.0
15	4:18	0.169	.141	− 97.3
15	4:34	0.180	.151	−102.9
16	3:19	1.128	.944	− 1.4
16	3:26	1.133	.948	− 0.4
16	3:35	1.139	.953	− 1.6
16	3:40	1.143	.955	+ 0.1
17	3:33	0.943	.789	+ 20.9
17	3:40	0.948	.793	+ 33.1
18	3:38	0.751	.628	+ 17.2
18	3:48	0.758	.634	+ 14.2
18	3:58	0.765	.640	+ 9.8
19	3:30	0.549	.459	− 60.6
19	3:37	0.555	.464	− 48.7
19	3:46	0.560	.469	− 48.7
20	3:10	0.341	.285	−114.8
20	3:23	0.350	.293	−109.0
20	3:35	0.358	.300	−101.1
20	3:44	0.365	.305	− 98.0
21	3:36	0.164	.137	− 98.9
21	3:48	0.172	.144	− 93.1
22	3:32	1.161	.971	− 27.0
22	3:49	1.173	.981	− 29.4
22	4:06	1.184	.991	− 35.9
23	3:04	0.947	.792	+ 24.7
23	3:20	0.957	.801	+ 21.6
23	3:37	0.970	0.812	+ 28.8

were measured by Struve. The columns give, in order, the date, the U.T., the phase in days and as fractions of the period, and the radial velocities. The phases were computed from the following photometric formula:[6] Principal minimum = JD 2416886.8806 + $1^d.195253065E$.

The radial-velocity-curve (Fig. 2) does not appear to be very unusual. The observations fall along a nearly sinusoidal curve, except during primary minimum (phases 0.94–1.06), where the rotational-velocity effect is quite apparent; $v_0 \sin i$ is estimated to be about 60 km/sec. The eclipse is not total, as is shown by the measures clustered close to the γ-axis at phase $\sim$1.0; also the line which can be drawn connecting the observations between phases 0.97 and 1.0 shows an appreciable slope. The cluster of points near phase 0.8 has a higher dispersion of velocities than is consistent with the remainder of the curve. There is an indication that the hydrogen lines at these phases are slightly asymmetric.

The orbital elements were computed by least squares. The observations during eclipse were omitted, and the remainder were converted into nine normal points (the open circles in Fig. 2). Sterne's formula for a nearly circular orbit was used.[7] The results (with mean errors) give $e = 0.01 \pm 0.03$, $\omega = 240° \pm 160°$, so that the following circular

[6] Kukarkin and Parenago, *General Catalogue of Variable Stars* (1948); De Sitter, *B.A.N.*, **7**, 119, 1933.

[7] *Proc. Nat. Acad. Sci.*, **27**, 179, 1941.

orbit has been adopted: $P = 1^d.195253065$ (assumed), $K = 68 \pm 2$ km/sec, $\gamma = -40 \pm 2$ km/sec, σ_1 = mean error of one observation = ± 6.5 km/sec, $a_1 \sin i = 935{,}000$ km, mass function = $0.023 \odot$. These elements differ slightly from Luyten's;[3] it seems quite definite now that the orbit is circular and therefore consistent with the photometric observations.

C. M. Huffer and Z. Kopal[8] recently completed a very exact photometric study of

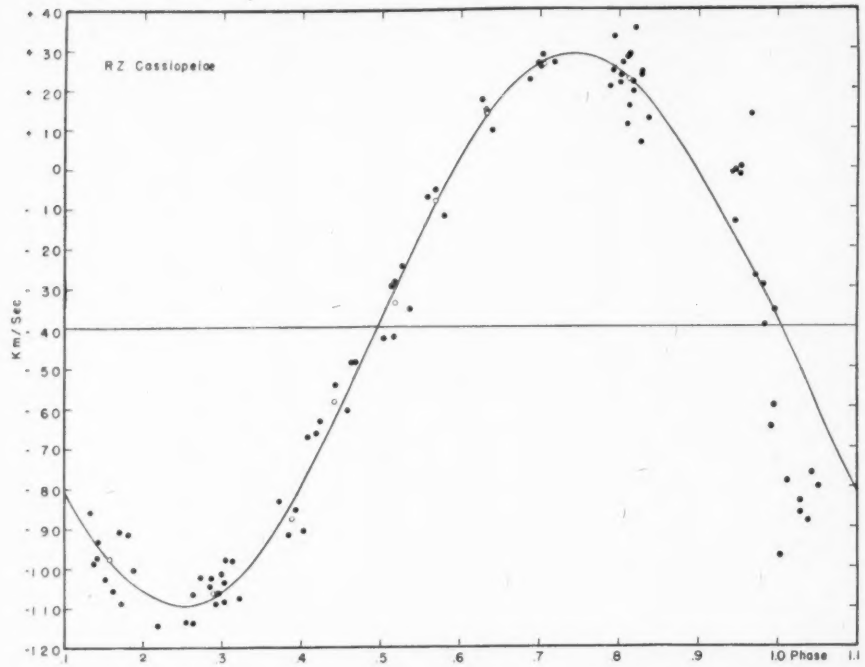

FIG. 2.—The radial-velocity-curve of RZ Cassiopeiae. The theoretical curve is computed from the elements $e = 0.01$, $\omega = 240°$, $K = 69$ km/sec, $\gamma = -40$ km/sec.

RZ Cassiopeiae. They obtained the following photometric elements:

$P = 1.1952519$ (var)	$r_2 = 0.284 \pm 0.002$
$i = 82°.14 \pm 0°.06$	$L_1 = 0.926 \pm 0.004$
$r_1 = 0.241 \pm 0.002$	$L_2 = 0.074 \pm 0.003$

Using this period, it is necessary to shift the time scale in Figure 1 to the left by 0.013 day (0.011 phase-period) which is perhaps more satisfactory, since two plates at phase $\sim$0.99 give strongly negative velocities.

Combining the photometric with the spectrographic data, we get $a_1 = 944{,}000$ km. Further, if we assume that the brighter component obeys the mass-luminosity relation, i.e., $L_1 = 10 \odot$ and $M_1 = 2 \odot$, we get $M_2 = 0.53 \odot$. This gives a mass-ratio $a \sim 4$, which shows that this binary is a rather normal type of eclipsing variable. The fainter component does not obey the mass-luminosity relation.[9]

[8] *Ap. J.*, **114**, 297, 1951.

[9] Struve, *Stellar Evolution* (Princeton: Princeton University Press, 1950), p. 27.

In the systems U Cephei and U Sagittae the primary eclipse is total, and it is possible to observe the profiles of spectrum lines on two limbs (before mid-eclipse and after mid-eclipse). Redman[10] and Struve[11] have shown that the hydrogen (and some other) lines of U Cephei and U Sagittae become weaker at the limbs. In the case of RZ Cassiopeiae the primary minimum is a partial eclipse, and Figure 1 (*b*, *c*) shows two plates taken at phases 0.983 and 0.971. Equivalent-width measurements of $H\gamma$, $H\delta$, and *Ca* K were made at these phases and compared with the same lines at phase 0.286. The hydrogen lines did not show any appreciable change, but the equivalent width of *Ca* K decreased at mid-eclipse to 0.7 times the value at phase 0.286.

I wish to express my thanks to Dr. O. Struve for obtaining the spectrograms and for valuable discussion and guidance. Also I wish to thank Miss Alice Johnson for computing the phases and solar reductions.

[10] *M.N.*, **96**, 488, 1936.

[11] *M.N.*, **109**, 498, 1949 (Darwin Lecture).

RAPID CHANGES IN LINE INTENSITIES IN THE SPECTRUM OF GAMMA CASSIOPEIAE

E. MARGARET BURBIDGE, G. R. BURBIDGE, AND S. K. WANG
University of London Observatory
Received June 11, 1951

ABSTRACT

Equivalent widths of the hydrogen and *He* I lines and two *O* II blends in the photographic region were measured in the spectrum of γ Cassiopeiae during July and August, 1949. An apparent drop and subsequent increase in equivalent width were found. Radial-velocity measures are also given.

In July and August, 1949, two of the authors (E. M. B. and G. R. B.) obtained a series of spectrograms of the B0e star γ Cassiopeiae at the Haute Provence Observatory, France. The four-prism Tremblot spectrograph (dispersion = 53 A/mm at $H\gamma$), attached to the 80-cm reflecting telescope, was used. The first two spectra were taken on Ilford Zenith plates and the remainder on Ilford Special Rapid plates. Microphotometer tracings were made by E. M. and G. R. Burbidge with the Chalonge microphotometer at the Institute of Astrophysics in Paris, and their reduction was carried out at the University of London Observatory. Further details and the method of standardization of the plates are given in an earlier paper.[1]

The equivalent widths of the hydrogen, helium, and oxygen lines for each spectrogram are given in Tables 1 and 2, the unit being the total absorption over 1 A. It will be seen that on the nights of July 28–29, July 30–31, and July 31–August 1 the hydrogen, and to a lesser extent the helium, line intensities were lower than on the other nights. We have not been able to explain this in terms of instrumental effects, and hence we conclude that the intensity variation is probably real. Seven spectrograms of ε Cassiopeiae (B3) were obtained, in an attempt to provide a check on the line-intensity measures of γ Cassiopeiae, but unfortunately the later ones were rather overexposed and consequently not suitable for spectrophotometric measurement. The individual measures of equivalent width for the four spectra which were reduced are given in Table 3. The scatter is seen to be small, and agreement with the measures by E. G. Williams,[2] which are also given in the table, is good except for $H\gamma$.

In Figure 1 the means ($H\gamma$, $H\delta$, $H\epsilon$), (λ 4471, λ 4026 of the $2^3P^o-n^3D$ series of *He* I) and (λλ 4388, 4144, 4009 of the $2^1P^o-n^1D$ series of *He* I) are plotted against time for each separate spectrum for which measures were made of all the lines included in each mean. The curves for hydrogen and the helium triplets have been broken at the night July 29–30 because it is not certain whether the single high value there is real or not. Means could not be formed for the other spectrum obtained on that night, because scratches across the spectrum made it impossible to measure the intensities of $H\gamma$, *He* I 4471, and *He* I 4388. However, careful examination of the spectrum has shown that there is no criterion other than that of low weight which will allow the result to be excluded.

From the mean values for (*a*) July 28–29, 30–31, and July 31–August 1, when the absorption line intensity was low, and (*b*) the remainder of the nights, excluding July 29–30, the percentage decrease in equivalent width of *a* from *b* was found to be: ($H\gamma$), 40.1; ($H\delta$), 27.1; ($H\epsilon$), 24.7; (*He* I 4471, 4026), 24.6; (*He* I 4388, 4144, 4009), 16.7.

[1] *Ap. J.*, **113**, 84, 1951.

[2] *Ap. J.*, **83**, 279, 1936.

Mean percentage deviations are shown in the accompanying tabulation. $H\gamma$ appears

	$H\gamma$	$H\delta$	$H\epsilon$	He I 4471, 4026	He I 4388, 4144, 4009
a	10.0	5.8	8.1	9.3	7.8
b	6.2	5.5	10.4	7.0	9.9

to show the largest decrease, and the percentage decrease for the helium singlet lines, in view of the mean percentage deviations, is hardly significant. Measures of the *O* II blends are too few and show too much scatter for a significant estimate of a possible decrease to be made.

The theory of Be stars originally due to the work of O. Struve[3] suggests that the emission lines of hydrogen and other elements, which are often double, arise in an equatorial ring which forms about those stars rotating so fast as to be near rotational instability.

TABLE 1

EQUIVALENT WIDTHS OF THE HYDROGEN AND OXYGEN LINES

	Date	Time (U.T.)	Hydrogen Lines				*O* II Blends	
			$H\gamma$	$H\delta$	$H\epsilon$	$H\zeta$	λ 4416	λ 4318
1	July 26	23h 26m	2.05	2.99	2.10	.....	.....	0.49
2	27	1 1	1.81	2.54	2.22	.....	.....	.....
3	28	23 1	1.18	2.02	1.58	.....	.....	.35
4	29	0 13	1.46	2.08	1.90	.....	.....	.....
5	29	1 58	1.27	2.27	1.73	1.79	0.16	.11
6	29	3 12	1.52	2.00	1.83	.....	.21	.23
7	30	1 19	.....	2.40	2.17	1.88	.....	.....
8	30	2 55	2.30	3.09	2.31	2.22	.....	.....
9	30	23 12	1.10	1.74	1.83	1.63	.16	.29
10	31	0 18	1.59	2.23	2.01	2.00	.23	.22
11	31	1 20	1.39	1.99	2.24	1.74	.28	.29
12	Aug. 1	1 56	1.21	.....	1.61	.....	.....	.28
13	1	2 58	1.35	1.95	1.73	.....	.....	.34
14	2	23 5	2.36	2.86	2.54	.....	.16	.22
15	3	0 51	2.24	2.75	2.75	.....	.14	.32
16	3	1 53	2.40	3.10	2.80	2.26	.....	.33
17	3	2 36	2.02	2.74	2.62	.....	.27	.31
18	3	3 37	2.18	2.98	2.68	1.97	.28	.33
19	3	23 36	2.16	2.47	2.12	.....	.28	.....
20	4	0 19	2.34	2.60	2.13	2.36	.31	.33
21	4	1 49	2.32	2.78	2.16	2.14	.33	.24
22	4	2 13	2.27	2.77	2.19	2.10	.31	.29
23	4	2 25	2.20	3.04	2.37	2.15	.23	.30
24	4	2 38	2.39	2.74	2.00	.....	.35	.42
25	4	2 59	2.16	2.60	2.29	2.08	.40	.41
26	4	3 11	2.53	2.81	2.18	2.16	.32	.30
27	5	22 39	2.36	2.83	2.47	.....	.38	.24
28	6	0 25	2.50	3.03	2.56	2.26	.24	.32
29	6	2 3	2.20	2.54	2.67	.....	.20	.26
30	6	3 25	2.00	3.03	2.88	.....	0.34	.34
31	6	3 31	2.32	2.64	2.82	.....	.....	0.35

[3] *Ap. J.*, **73**, 93, 1931.

γ Cassiopeiae is well known as a star which undergoes spasmodic violent outbursts, three having been observed in detail in 1934, 1937, and 1939. Baldwin[4] has explained most of the observed features by postulating an expansion of the photosphere and ring, angular momentum being conserved as the gas spreads outward. From 1941 until the

TABLE 2

EQUIVALENT WIDTHS OF THE HELIUM LINES

	Date	Time (U.T.)	λ 4471	λ 4026	λ 4388	λ 4144	λ 4009	λ 3927
1	July 26	23h26m	...	0.56	...	0.55	0.32	...
2	27	1 1	0.79	.64	0.53	.50	...	...
3	28	23 1	.49	.67	...	...	.28	0.35
4	29	0 13	.34	.49	.28	...	.20	...
5	29	1 58	.46	.52	.31	.40	.32	.31
6	29	3 12	.43	.57	.29	.41	.28	.38
7	30	1 19	...	.78	...	.40	.32	.44
8	30	2 55	.70	.74	.28	.39	.34	.29
9	30	23 12	.42	.49	.26	...	.28	.36
10	31	0 18	.55	.67	.30	.57	.31	.39
11	31	1 20	.42	.51	.29	.39	.23	.39
12	Aug. 1	1 56	...	.49	...	.39	.22	...
13	1	2 58	.44	.55	...	...	.20	...
14	2	23 5	.59	.76	.41	.37	.27	...
15	3	0 51	.52	.71	.31	.40	.28	.41
16	3	1 53	.75	.75	.42	.59	.35	.51
17	3	2 36	.61	.62	.41	.39	.34	.40
18	3	3 37	.80	.78	.45	.68	.37	.50
19	3	23 36	.58	.64	.37	.51	.30	...
20	4	0 19	.65	.67	.33	.52	.35	.35
21	4	1 49	.58	.59	.42	.42	.26	.26
22	4	2 13	.58	.62	.39	.46	.27	.23
23	4	2 25	.75	.63	.37	.49	.32	.39
24	4	2 38	.78	.59	.43	.50	.35	...
25	4	2 59	.70	.68	.34	.42	.32	.38
26	4	3 11	.56	.65	.47	.45	.35	.43
27	5	22 39	.70	.65	.49	.49	...	.42
28	6	0 25	.60	.75	.43	.55	.29	.34
29	6	2 3	.65	.74	.35	.51	.48	.43
30	6	3 25	.70	.74	.40	.56	.51	.47
31	6	3 31	0.47	0.70	0.53	0.37	0.49	0.45

TABLE 3

EQUIVALENT WIDTHS IN ε CASSIOPEIAE

Date	Time (U.T.)	Hydrogen Lines			Helium Lines				
		$H\gamma$	$H\delta$	$H\epsilon$	λ 4471	λ 4026	λ 4388	λ 4144	λ 4009
July 28	23h29m	4.64	5.56	5.08	0.87	0.93	0.58	0.67	0.46
29	2 17	4.61	5.69	5.59	.91	1.08	.49	.58	.54
30	1 39	4.60	5.91	6.08	.79	1.01	.46	.58	.58
30	23 55	4.48	5.83	5.79	.78	1.06	.46	.50	.50
E. G. Williams	...	5.60	5.90	6.20	0.87	1.14	0.49	0.55	0.51

[4] *Ap. J.*, 92, 82, 1940.

time of the observations reported here, γ Cassiopeiae has been in a relatively quiescent state. Late in 1940 Baldwin[5] found the equivalent width of $H\delta$ to be greater than 5 A. At the end of 1944 it was reported by Belorizky[6] that the Balmer series, including $H\alpha$, was in absorption. In September, 1946, Belorizky and Fehrenbach[7] observed that $H\alpha$, $H\beta$, and D3 were in emission. In 1948 Miczaika[8] reported that the equivalent widths of $H\gamma$, $H\delta$, $H\epsilon$, and $H\zeta$ were 2.5, 1.6, 1.9, and 1.6 A, respectively. Spectra of the visual region were obtained by E. M. and G. R. Burbidge in August, 1949, with the large four-prism Tremblot spectrograph attached to the 120-cm reflector at Haute Provence. Emission at $H\alpha$ was strong, and double emission lines were present at $H\beta$ and *He* I 5876.

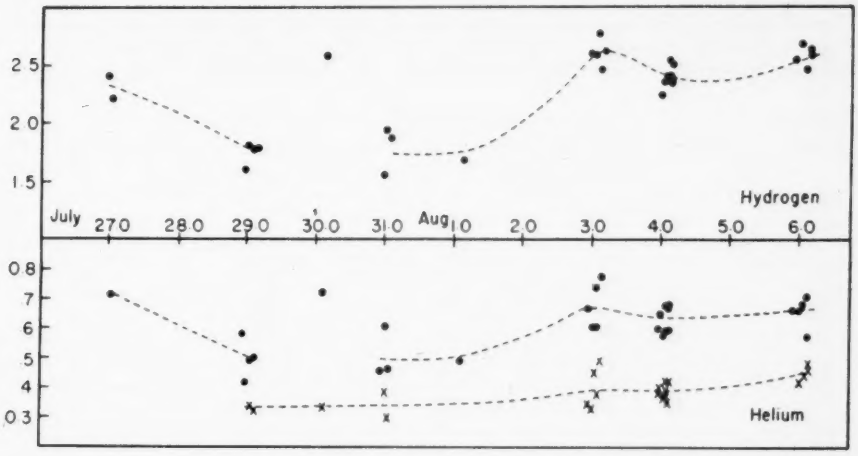

FIG. 1.—Mean equivalent width of ($H\gamma$, $H\delta$, $H\epsilon$) plotted against time in the upper part of the figure; mean equivalent widths of (*He* I λ 4471, λ 4026) (*dots*) and (*He* I λλ 4388, 4144, 4009) (*crosses*) plotted against time in the lower part. Unit = 1 equivalent angstrom.

These spectra were obtained for descriptive purposes and were not suitable for spectrophotometric measurement.

It is unlikely that the star has lost an appreciable amount of its angular momentum by the ejection of material in recent outbursts, and it can still be considered to be near rotational instability, though the equatorial ring of gas may not be so extensive as when the star was in a highly disturbed state. There may be continuous or spasmodic interaction between the ring and the photosphere, in which material is ejected from the star by means of flarelike outbursts and accumulates in the ring. It is suggested that the observed phenomenon may be such an outburst. An increase in the electron density outside the photosphere would reduce the absorption-line intensity by increased opacity through electron scattering and perhaps continuous emission—an increase in the "veiling" which normally causes lines in this star to be much weaker than those in an absorption-line star of the same spectral type. The hydrogen-line emission might increase temporarily, and the steepness of the Balmer decrement might cause the absorption-line intensity of $H\gamma$ to decrease more than the later series members.

For a stellar radius of order 10 solar radii and an equatorial rotational velocity of 300–400 km/sec,[4] the rotational period of the star would be 40–30 hours. If the disturbed

[5] *Ap. J.*, **94**, 283, 1941.
[6] *J. d. phys.*, **6**, ser. 8, No. 12, 39, 1945.
[7] *Ann. d'ap.*, **10**, 39, 1947.
[8] *Zs. f. Ap.*, **25**, 77, 1948.

area were localized in extent, we could expect that fairly rapid fluctuations in line intensity might take place. However, since the velocity of rotation of the ring is less than that of the star, ejected material would interact with a larger area of the ring than the area of the original disturbance in the star's equatorial zone. It will be important to see whether future observations verify the occurrence of line-intensity variations in this star.

Mrs. Mayall, recorder of the A.A.V.S.O., has kindly supplied visual observations of γ Cassiopeiae over the period discussed here, with an estimated error of 0.2 mag. No brightness fluctuations over this period and outside this error were found.*

Twelve spectrograms have been measured for radial velocity. Eleven were chosen as representative of the thirty-one used for the line-intensity measures, and the twelfth was too strongly exposed to be suitable for spectrophotometric measurement. The results are shown in Table 4. There is some scatter, probably owing to the width and

TABLE 4

RADIAL VELOCITIES OF γ CASSIOPEIAE

	Date	Time (U.T.)	Velocity
5	July 29	1^{h}58^m	−13.2
7	30	1 19	− 8.3
11	31	1 20	−10.6
14	Aug. 2	23 5	− 9.7
18	3	3 37	− 5.4
23	4	2 25	−14.2
26	4	3 11	+ 1.6
27	5	22 39	− 6.2
28	6	0 25	− 6.7
	6	1 2	− 8.1
29	6	2 3	− 3.3
30	6	3 25	− 7.8

shallowness of the spectrum lines, and there is no correlation with the intensity measures. Only the strongest lines were used in the determinations, namely, $H\gamma$, $H\delta$, $H\epsilon$, $H\zeta$, $H9$, $H10$, $H11$; *He* I λλ 4388, 4144, 4121, 4026, 4009, 3820. The radial velocities obtained may be compared with those published by Burke Smith and O. Struve[9] for the period 1940–1947.

In addition to the *O* II blends at λ 4416 and λ 4318, the following *O* II lines were visible: λλ 4367, 4351–4346, 4304, 4276, 4190, 4185, 4153, 4133, 4105, 4076, 4072–4070, 3983, 3973, 3954, 3919, 3912, 3907, and 3882. The remaining elements present in the spectrum were: *Si* IV (λ 4089), *N* III (λ 4097), *N* II (λλ 3995, 4041, 4044), *S* III (λ 4254, λ 4285), *Si* III (λ 3807), *C* II (λ 4267), and ?*S* II (λ 4153, blended with *O* II λ 4153).

It is a pleasure to express our thanks for the facilities provided and help given by M. Dufay, director, and M. Fehrenbach, associate director, of the Haute Provence Observatory, and by M. Chalonge, M. Barbier, and M. Laffineur at the Institute of Astrophysics in Paris. We are grateful also to Mr. C. C. L. Gregory, former director of the University of London Observatory, who has suspected the occurrence of line-intensity variations in this star and who enabled E. M. Burbidge to take part in these observations.

* *Footnote added in proof:* R. Rigollet has kindly sent magnitude observations over this period by G. Florsch and L. Rébuffat. These observations have an accuracy of 0.05 mag., and no rapid fluctuations in brightness were evident.

[9] *Ap. J.*, **112**, 192, 1950.

A STUDY OF THE NEBULAR [*N* II] LINES IN SELECTED GASEOUS NEBULAE

MARVIN LEE WHITE*
University of Michigan Observatory
Received March 3, 1951

ABSTRACT

A spectrophotometric survey is undertaken of typical planetary nebulae accessible with the 37-inch reflector at Ann Arbor, as well as of several regions of the Orion Nebula, for the purpose of determining the intensity ratios [*N* II] 6584/*Hα* and [*N* II] 6548/*Hα*. The results of the observations are summarized in tabular form.

The aim of this investigation was to make photometric measurements of the intensities of the red nebular lines of singly ionized nitrogen. Emphasis was placed on the objects observed by Wyse,[1] although additional planetaries have been observed.

The [*N* II] 6548 and 6584 lines consist of transitions from the $^1D_2$ level to $^3P_1$ and $^3P_2$. Thus the lines are analogous to the forbidden green "N_1" and "N_2" lines of doubly ionized oxygen which are frequently the strongest features of the spectra of the gaseous nebulae. The incentive for this program came from the theoretical investigations by Aller, Hebb, and Menzel[2] and by the writer and Aller,[3] in which it was shown how the relative intensities of the forbidden lines of doubly ionized oxygen and singly ionized nitrogen may be used to estimate the abundance ratio of nitrogen to oxygen. Before this ratio can be calculated, however, it is necessary to know the target areas for collisional excitation of ionized nitrogen from the ground ^3P to the metastable ^1D term. The target areas were computed[4] by the method of Hebb and Menzel;[5] and it was found that these values differed from the corresponding target areas for *O* III by a constant factor of 0.46. Unfortunately, the theory was found to be unsatisfactory for collisions in which a change of electron spin is involved, predicting cross-sections that are too large.[6] Thus, at present, we have only an upper limit to the collisional cross-sections of ionized nitrogen, and exact values for the abundance ratio of nitrogen to oxygen must await further theoretical developments. However, it should be of considerable value to have available more accurate observations of the relative intensities of the nebular lines of ionized nitrogen, on the one hand, and of *Hα*, on the other.

The observational work on this program was carried on from the autumn of 1948 up to and including the summer of 1949 and was resumed and concluded in the summer of 1950. The two-prism spectrograph was used with cameras of focal lengths 6 and 12 inches, the former giving a dispersion of 355 A/mm in the *Hα* region and 124 A/mm in the *Hβ* region, while the corresponding dispersion for the 12-inch camera differed by a factor of $\frac{1}{2}$. With these dispersions, *Hα* was adequately separated from the closely neighboring [*N* II] 6584 and [*N* II] 6548 lines. Previous estimates of the relative intensities of *Hα* and *Hβ* with low-dispersion material suffered in certain instances from the blending

* Now of Army Map Service, Geodetic Division, Research and Analysis Section, Washington, D.C.

[1] *Ap. J.*, **95**, 365, 1942.

[2] *Ap. J.*, **102**, 239, 1945.

[3] *A.J.*, **54**, 181, 1949.

[4] *Ibid.*

[5] *Ap. J.*, **92**, 408, 1940.

[6] This difficulty was pointed out by Bates, Fundaminsky, Massey, and Leech, *Phil. Trans. R. Soc. London, A*, **243**, 93, 1950. The astrophysical implications are discussed by L. H. Aller, *Ap. J.*, **111**, 609, 1950.

of these nebular lines with *Hα*. (Considerations of the Balmer decrement, as well as of the relative intensities of the forbidden [*O* III] N_1 and N_2 lines, will be left for a future paper.) The characteristic curve was determined individually for each plate. This involved exposing each plate in the calibration spectrograph twice, one exposure for 15 seconds and another for 2 minutes. A slightly modified version of the wedge-slit calibrating spectrograph previously used by Williams[7] was employed during all but the first few months of the program. At that time a spot photometer was used in conjunction with a red filter as a temporary expedient. Fortunately, the 103*a*-F plates that were employed exclusively before 1950 had negligible reciprocity failure. The 103*a*-F3 plates were slightly less satisfactory in this respect, in addition to being slower. Finally, tracings were made of the emission spectra, as well as of the calibration spectra, with a conventional self-recording Moll microphotometer.

The results of these observations are given in Tables 1 and 2; the latter table is con-

TABLE 1

INTENSITIES OF [*N* II] LINES IN TYPICAL PLANETARY NEBULAE

OBJECT	DATE	TOTAL TIME EXPOSURE	LINE-INTENSITY RATIOS		REMARKS*
			[*N* II] 6584/*Hα*	[*N* II] 6548/*Hα*	
NGC 40	Oct. 4–5, 1948	3 hr. 34 min.	0.76	.....	1
IC 351	Oct. 25–26, 1948	2 hr.	0	0	11
IC 2003	Oct. 26–27, 1948	2 hr.	0.0	0.0	10
NGC 2440	Mar. 29–30, 1949	1 hr. 30 min.	3.3	.76	
IC 418	Oct. 14–15, 1948	1 hr. 43 min.	0.38	.06	1, 8
	Dec. 12–13, 1948	1 hr. 25 min.	Present	.07	6, 7
II 2149	Oct. 26–27, 1948	55 min.	0.04	.....	1, 10
	Jan. 1–2, 1949	25 min.	0.07	.....	8
NGC 3242	Jan. 7, 1949	4 hr. 4 min.	0.00	.00	9
IC 3568	Apr. 4–5, 1949	3 hr. 40 min.	0.0	.0	10
IC 4593	Apr. 7–8, 1949	2 hr. 40 min.	0.00	.00	
NGC 6210	July 31, 1949	3 hr. 52 min.	0.00	.00	7
NGC 6543	July 2–3, 1950	1 hr. 30 min.	0.03	.....	5
NGC 6572	Aug. 15–16, 1949	25 min.	0.27	.....	3
	July 2–3, 1950	30 min.	0.10	.....	5
NGC 6720	Aug. 13–14, 1950	3 hr. 40 min.	1.8	.63	5
NGC 6790	Aug. 6–7, 1950	2 hr.	0.0	.....	
HD 184738	July 30–Aug. 1, 1949	25 min.	1.17	.42	3
	July 6–7, 1950	2 min. 40 sec.	1.20	.25	5
NGC 6826	June 25–26, 1949	1 hr. 10 min.	0.0	.0	
NGC 6891	June 27–28, 1949	3 hr.	0.0	.0	9
IC 4997	July 4–5, 1949	3 hr. 12 min.	0.00	.00	7
NGC 7009	July 30, 1949	2 hr.	0.00	0.00	10
NGC 7026	July 9–10, 1950	2 hr. 30 min.	0.44	.....	5
NGC 7027	Oct. 4–5, 1948	10 min.	0.33	.....	1
	Aug. 15–16, 1949	12 min.	0.28–0.35	.....	2, 4
Anon (21^h31^m)	July 28–29, 1949	3 hr.	0.92	.....	

* Numbers in this column have the following meanings:

1. Spot photometer employed.
2. Wedge-slit calibrating spectrograph.
3. Plate overexposed.
4. 0.28 and 0.35 represent values for eastern and western regions, respectively.
5. 103*a*-F3 plate used.
6. 0.07 found from [*N* II] 6548/[*N* II] 6584 ratio and [*N* II] 6584/*Hα*.
7. *Hα* overexposed.
8. [*N* II] 6584 underexposed.
9. *Hα* well exposed.
10. *Hα* strongly exposed, but not overexposed.
11. *Hα* rather weak.

[7] *Pub. U. Michigan Obs.*, **7**, 98, 1938.

FIG. 1. Photograph of the Orion Nebula, showing where observations of [N II] lines were made. Curtis Schmidt telescope; photo by Freeman D. Miller.

cerned only with certain selected regions of the Orion Nebula. These regions were selected because guide stars were available and spectra could be obtained in a reasonable exposure time. For exposures on the Orion Nebula, the slit was lengthened to about 1 cm (corresponding to 2′ in the sky), and tracings were made across three separate points in the spectral lines. In this manner a comparison of neighboring points in the Orion Nebula could be obtained from a single exposure. The locations of these regions are marked on the accompanying photograph of the Orion Nebula (Fig. 1). The intensities of the [*N* II] 6584 and [*N* II] 6548 lines listed in the fourth and fifth columns, respectively, of

TABLE 2

DATA ON THE ORION NEBULA

Region	Plate No.	Date	Total Exposure Time	Line-Intensity Ratios		Remarks*
				[*N* II] 6584/*Hα*	[*N* II] 6548/*Hα*	
1	S 17593 A	Dec. 6–7, 1948	45 min. (cloudy)	0.12	.....	1
2*a*	S 17612 A	Dec. 30–31, 1948	1 hr. 32 min.	.25	.....	
2*b*	.....	.....	.....	.23	.....	2
2*b*	S 17690 A	Mar. 6–7, 1949	1 hr. 25 min.	.35	.....	
2*c*	.....	.....	.....	.33	.....	3
3*a*	S 17616 A	Jan. 1–2, 1949	45 min.	.21	.....	
4	S 17621 A	Jan. 2–3, 1949	3 hr.	0.19	.....	

* Numbers in this column have the following meanings:

1. Opposite end of spectrum showed no [*N* II], while *Hα* fell off to 0.646 of the original intensity.
2. Same exposure as 2*a*.
3. Same exposure as 2*b* on plate No. S 17690 A.

Table 1 are given in terms of the intensity of the *Hα* line as unit. In many instances the [*N* II] 6548 line was too faint to be seen, while, for approximately half the planetary nebulae investigated, both forbidden nitrogen lines, 6584 and 6548, were undetectable. In these instances, rough estimates of the upper limits of the intensity ratios are indicated. In the "Remarks" column is listed information concerning the type of plate used in the event that a 103*a*-F plate was not employed; similarly, whenever the spot sensitometer was used instead of the wedge-slit calibration spectrograph, this information is also recorded. It is noted that the two methods of calibration give consistent results.

The wide range in the intensities as we proceed from object to object is striking. Objects such as NGC 2440, NGC 6720 (Ring Nebula), and HD 184738 (Campbell's star), for which the forbidden line λ 6584 is more intense than the neighboring *Hα* line, are definitely in the minority.

In conclusion, I should like to thank Dr. L. H. Aller for suggesting this problem and for his continued encouragement, as well as Dr. Dean B. McLaughlin and Mr. Edwin Weston for their spirit of friendly co-operation.

THE SPECTRA OF COMETS 1950b (MINKOWSKI) AND 1951a (PAJDUSAKOVA)*

P. SWINGS AND THORNTON PAGE
University of Liége, Yerkes, and McDonald Observatories
Received August 4, 1951

ABSTRACT

The spectrum of Comet 1950b at heliocentric distance 2.65 A.U. shows a strong solar continuum concentrated in the nucleus and *CN* emission over a coma forty times larger. Comet 1951a at heliocentric distance 0.91 A.U. is very unusual in showing a strong nuclear continuum and extremely weak *CN* emission over a coma only eight times larger than the nucleus. The former seems normal for a comet distance from the sun; the latter is probably a "fresh" comet, newly arrived near the sun from the swarm of cometary material postulated by Oort at the outer confines of the solar system.

I. INTRODUCTION

Since 1940 a program of spectroscopic observations of comets has been carried on at the McDonald Observatory, with the aim of increasing our knowledge of the physical, chemical, and dynamical processes at play in comets.[1,2,3,4] It was expected that new observational data would help in erecting a satisfactory theory of the origin and development of comets, a matter of importance in itself and in relation to theories of the origin and history of the solar system. The McDonald observers have tried to gather information on as many comets as possible. Special attention was devoted to the discovery of new cometary molecules (*OH*, *NH*, CH^+, CO_2^+, NH_2, and probably OH^+ were found), the establishment of the excitation mechanism (pure resonance fluorescence due to solar radiation), the spectroscopic differences between individual comets (e.g., in the intensity ratio of *OH* and *NH*), the behavior of band intensities with distance to the sun, and the distribution of molecules within the coma and tail. Various laboratory investigations have been undertaken in conjunction with these cometary observations.

From recent theoretical investigations by Oort, van Woerkom, and Schmidt[5] it appears that comets come from a swarm of material at the outer confines of the solar system. This swarm is definitely a part of the solar system, although it extends to distances of the order of several thousand times the distance of the farthest planet. It is through stellar perturbations of this swarm that "fresh" comets continue to come into the central parts of the solar system. The observational material permitting a spectroscopic comparison between "fresh," or new comets, and old ones, which have passed near the sun previously, is still rather scanty. This is due partly to the fact that sufficiently accurate data on the original orbits described before the comets came into the region of the planets are available only for comets observed before 1940. It is highly desirable that similar orbit calculations be performed for comets which have been well covered spectroscopically in recent years.

* *Contributions from the McDonald Observatory, University of Texas*, No. 206.

[1] Swings, Elvey, and Babcock, *Ap. J.*, **94**, 320, 1941.

[2] Swings and Page, *Ap. J.*, **108**, 526, 1948.

[3] Jose and Swings, *Ap. J.*, **111**, 41, 1950.

[4] Swings and Page, *Ap. J.*, **111**, 530, 1950.

[5] J. H. Oort, *B.A.N.*, **11**, 91, 1950; van Woerkom, *B.A.N.*, **10**, 445, 1948; M. Schmidt, *B.A.N.*, **11**, 253, 1951; J. H. Oort and M. Schmidt, *B.A.N.*, **11**, 259, 1951; J. H. Oort, *Observatory*, **71**, 129, 1951 (Halley Lecture).

According to Oort and Schmidt,[6] these spectroscopic data, scanty as they are, seem to indicate that comets showing an unusually strong continuous spectrum, not connected with outbursts or division, are new comets. In other words, the amount of dust relative to the observable gas appears to be larger in new comets. The photometric observations also indicate that the brightness of the new comets increases more slowly with diminishing heliocentric distance r than in the case of older comets. The development of a comet's head would be due to at least two different processes: one causing the expulsion of dust and meteorites (process 1), the other giving rise to gases and hence to the usual emission bands (process 2). These processes vary differently with r. At large heliocentric distances, process 1 prevails, while process 2 dominates for distances below about 3 A.U. "The relative intensity of the two processes appears to vary considerably with the 'age' of the comet. In new comets process 1 is relatively much stronger, so that the continuous spectrum prevails even down to $r = 1$, while the emission only begins to exceed it for still smaller r."[6] A theoretical treatment along the general lines of Levin's discussion[7] indicates that the new comets deteriorate markedly during their first, or first few, perihelion passages. The complex physical mechanisms causing the production of dust and gas are still mostly unknown; their investigation by A. Delsemme and one of the authors (Swings) is under way.

In the coma of all comets—and especially so in new comets—the continuous spectrum prevails at large heliocentric distances. The few available observations indicate that at very large r the spectra of comets are essentially continuous. This is the case for Comet Schwassmann-Wachmann I at $r = 5.5$ after outbursts.[8] Similarly, Halley's Comet at $r = 2.8$ showed only a continuous spectrum[9] with suspected CN and possibly C_2. In Comet 1948l, at $r = 2.21$, only the CN and λ 4050 emissions remained conspicuous on a strong solar spectrum.

The data reported here on two recent comets, 1950b (Minkowski) and 1951a (Pajdusakova), have a direct bearing on Oort and Schmidt's theoretical discussions. The first comet, observed at $r = 2.63$, provides data on comet spectra at fairly large heliocentric distances; moreover, it had the unusually large perihelion distance, $q = 2.59$ A.U. The latter comet, observed at $r = 0.92$, reveals an intense continuous spectrum, despite the small heliocentric distance and the small perihelion distance, $q = 0.72$.

II. THE OBSERVATIONAL MATERIAL

Six spectra have been obtained with the B spectrograph and one with the quartz Cassegrain spectrograph attached to the 82-inch reflector of the McDonald Observatory. The instruments and procedure have been described previously.[4] Detailed data are given in Table 1.

III. THE SPECTRUM OF COMET 1950b (MINKOWSKI)

At heliocentric distances between 2.62 and 2.66 A.U. the (0, 0) band of CN is of fair intensity, while there is no trace of C_2. The solar spectrum is so intense in the central parts of the coma that no definite decision can be taken as to a possible weak emission near λ 4050; at any rate, if any λ 4050 emission is present in the central regions, it must be much weaker than CN. On the spectrogram at $r = 2.64$ there may be a trace of λ 4050 emission extending faintly on one side of the nuclear region. In Comet 1948l at $r = 2.21$, λ 4050 was still conspicuous,[3] being about as strong as the R branch of CN (0, 0) near the nucleus.

[6] *Op. cit.*, p. 267.

[7] *A.J. U.S.S.R.*, **20**, 48, 1943; see also B. Vorontsov-Velyaminov, *Ap. J.*, **104**, 232, 1946; M. Minnaert, *Proc. Kon. Ned. Akad. Wetensch.*, **50**, 833, 1947; F. L. Whipple, *Ap. J.*, **111**, 385, 1950.

[8] N. U. Mayall, *Pub. A.S.P.*, **53**, 340, 1941; R. Minkowski, private communication.

[9] N. T. Bobrovnikoff, *Pub. Lick Obs.*, **17**, 447, 1931.

The ultraviolet spectrogram of Comet 1950b at $r = 2.66$ reveals no trace of *OH* or *NH*, although *CN* appears fairly strongly. There is no definite NH_2 emission in the central part of the coma; however, the λ 6300 line of NH_2 may be hidden by the strong airglow line (the main lines of the airglow are strong on all spectrograms). The continuous spectrum is purely solar, as is revealed by the strength of H, K, and other absorption lines. The molecular emission in the comet is an extremely small fraction of the continuous emission.

Owing to difficulties in guiding, the diameter of the region of the coma showing a solar spectrum cannot be determined accurately. A rough estimate from spectrograms B371 and B445 gives a maximum value of 8000 km. On the other hand, the diameter of the *CN* emission, which extends to large distances from the nucleus in regions where no continuous background appears, may be estimated fairly accurately from B376 to be of the order of 315,000 km. This may be compared with the diameters in Comet 1948l,[3]

TABLE 1

COMET SPECTRA

Comet and Film No.	Mar., 1951, Date (U.T.)	Exp. (Min.)	Emulsion	Mid-Alt.	Slit			Region λλ	r (A.U.)	Remarks
					w (Min.)	l (″Arc)	p.a.			
1950b:										
B306	1.42	60	103*a*-F*	27°	0.10	290	52°	3600–6700	2.62	
B371	10.38	70	103*a*-F*	20	.20	290	41.5	3600–6700	2.64	Clouds
B376	11.43	95	103*a*-F*	22	.20	290	29	3600–6700	2.64	Clouds
B445	19.38	30	103*a*-O	23	.20	290	20	3500–5000	2.66	Clouds
Of/1 13108	20.28	(60)	103*a*-O	27	.012	17	20	3200–4000	2.66	Clouds
1951a:										
B307	1.49	45	103*a*-F	13	.10	290	174	3600–6500	0.92	
B315	2.50	40	103*a*-F*	13	0.20	290	172	3600–6700	0.93	Clouds

* Ammonia hypersensitized.

at $r = 2.21$: for *CN*, 166,000 km; for λ 4050, approximately 22,000 km (the continuous spectrum extending to somewhat smaller distances[10] than λ 4050).

This emphasizes once more the fact that the dimension of the coma has no meaning if it is not referred to definite spectral emissions. In practically all comets the solid particles reflecting the solar spectrum are present only in the central part of the coma, and each molecule has its specific extension. Whenever the *CH*, NH_2, and λ 4050 emissions appear, they are found approximately in the same central regions as the continuous spectrum, although the latter is still more confined to the regions close to the nucleus. A comet may therefore have a very large coma in the ultraviolet (*CN* emission) and an extremely small one in the visual region (continuous spectrum).

The present observations of Comet 1950b show that the evolution toward a pure continuous spectrum, as the comet recedes from the sun, continues beyond $r = 2.21$ (Comet 1948l) to $r = 2.66$. *CN* declines in intensity relative to the solar spectrum, the NH_2 and λ 4050 emissions practically disappear before $r = 2.6$, and no trace remains of C_2, *CH*, *OH*, and *NH*. More extensive material is needed before we may definitely state that the increase of the intensity ratio λ 4050/*CN* with increasing heliocentric distance,

[10] Jose and Swings, *op. cit.*, Fig. 1, facing p. 42, spectrum of February 2, 1949.

which has been observed[4] to $r = 2.21$, ceases before $r = 2.6$. CN may have been unusually abundant in Comet 1950b, around $r = 2.6$.

Of course, a comparison between Comet 1948l at $r = 2.21$ and Comet 1950b at $r = 2.66$ may not be fully justified: one object may be old and the other new. However, it appears safe to conclude that a comet at large heliocentric distance has a continuous spectrum, apparently due to the reflection of solar radiation by solid particles. It may be of interest to pursue this matter further, especially by determining colors. Parent-molecules, such as CH_4, NH_3, CO_2, N_2, O_2, and CO, which are chemically stable and have no fluorescence spectrum in the observable region, may add their Rayleigh scattering to the reflection by solids. This could be checked by careful determination of the colors of a few distant comets.

IV. THE SPECTRUM OF COMET 1951a (PAJDUSAKOVA)

Two spectrograms were obtained at heliocentric distances 0.92 and 0.93. The airglow emissions are strong. While CN is present, there is no evidence for C_2; there may be a trace of NH_2 and of the λ 4050 emission. The main characteristic of the spectrograms is the strong continuous spectrum, confined to the central part of the coma; the contribution of the molecular emission to the brightness of the comet is extremely small compared with that of the continuous spectrum. The diameter of the CN region is of the order of 46,000 km, while that of the continuum is smaller than 6400 km.

Comet 1951a appears unusual. To our knowledge, no other comet observed at a heliocentric distance less than 1 A.U. has ever shown such a strong continuum relative to the gaseous emission. On the basis of Oort's theory, this comet would be placed among the new ones, which, coming from the confines of the solar spectrum, have entered for the first time into the region near the sun. It is a striking example of a case where Oort's process 1 remains much more efficient than process 2, even at the small heliocentric distance $r = 0.92$. It is hoped that photometric determinations and more extensive spectroscopic observations of this comet have been made at other observatories; also, that accurate positions are available for a determination of the original orbit.

On the basis of Baldet's compilation of observational data, Oort and Schmidt did not find any conspicuous difference between new and old comets with regard to intensity ratios of different emission bands. While our material on 1951a is not sufficient to make any definite statement, it seems that the intensity ratios C_2/CN and CH/CN are abnormally low for $r = 0.92$. In this comet, probably a new one, C_2 and CH would therefore be deficient relative to CN. This point will be kept in mind for our future observations. It may be that 1950b is also a new comet and that the strength of CN relative to λ 4050—compared to 1948l—is a result of the "freshness" of the comet.

THE LIMB FLARE OF MAY 8, 1951*

HELEN W. DODSON AND ROBERT R. MCMATH
McMath-Hulbert Observatory, University of Michigan
Received October 2, 1951

ABSTRACT

Published data indicate that flares have been observed at the limb of the sun with elevations above the chromosphere of 8000–80,000 km. Continuous records of the solar limb and disk secured on *Hα* spectroheliograms at the McMath-Hulbert Observatory show the outbreak and development of a number of these flarelike prominences. They range in form from relatively small cap-type prominences to the great flare prominence of May 8, 1951. This latter object rose to a height of 50,000 km in less than 90 seconds. During this interval the *Hα* lines of the spectrum were 8–10 A wide and showed large Doppler displacements. Throughout the remainder of the flare the change in height was negligible, and the *Hα* spectrum lines were 5–6 A wide and symmetrical. This flare prominence was four times as bright as the undisturbed *Hα* disk, was accompanied by an increase in 200-Mc/sec radiation from the sun, and was associated with a sudden disturbance of the earth's ionosphere.

INTRODUCTION

Solar flares, from an observational point of view, are primarily disk phenomena. They range from small bright dots to large, ropelike filaments of great brilliance. The brighter and more intensive flares are often accompanied simultaneously by a sudden disturbance of the earth's ionosphere.

The limb aspect of a flare is especially challenging. The apparent absence of Doppler shift for the greatly widened *Hα* emission lines of disk flares has been considered by many investigators to indicate that, in general, there is no appreciable outward motion and that flares are essentially low-level phenomena. Furthermore, there are many pitfalls inherent in any attempt to identify, on the basis of intensity, an elevated phenomenon as the limb aspect of a flare.

REVIEW OF DATA IN LITERATURE

Although the *Quarterly Bulletin on Solar Activity* of the I.A.U. reports the occurrence of a large number of flares very close to the sun's limb, the literature seems to carry descriptions of only a small number of these phenomena. Six are described by Ellison[1] as being "lesser flares" and to have appeared as "luminous dome-shaped elevations rising to heights of no more than 10,000 km."

An apparently similar object was observed by Giovanelli[2] on December 19, 1938. The latter observer also reports[3] a brilliant prominence that appeared on the west limb of the sun on March 14, 1939, as a flare of importance 2. This flare is described as having been similar in form and motion to the great surges photographed by McMath and Pettit.[4] Its mean velocity is given as 78 km/sec and its maximum height as of the order of 80,000 km. The Mount Wilson Observatory also reported this object as a flare. This flare prominence was accompanied by a weakening of the *E*-echoes but not by a complete fade-out.

* Work supported in part by Contract N6-onr-232-V with the Office of Naval Research.

[1] *M.N.*, **109**, 12, 1949.

[2] *Ap. J.*, **91**, 348, 1940.

[3] *Ibid.*, p. 349; R. G. Giovanelli and A. J. Higgs, *Terr. Mag.*, **44**, 187, 1939.

[4] *Ap. J.*, **85**, 296, 1937; **88**, 269, 1938.

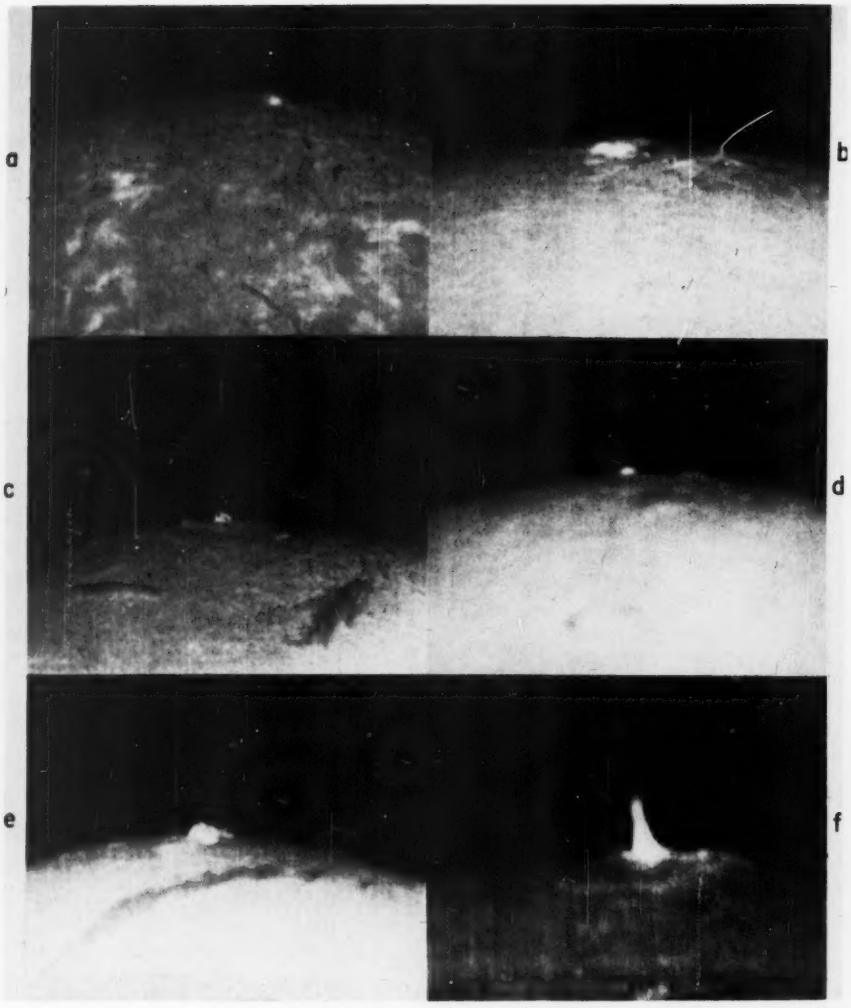

FIG. 1.—$H\alpha$ spectroheliograms, showing flarelike phenomena near the limb of the sun. *a*, April 29, 1949, 1630 U.T.; *b*, June 8, 1950, 1601 U.T.; *c*, October 7, 1949, 1820 U.T.; *d*, June 25, 1951, 1519 U.T.; *e*, July 10, 1949, 1718 U.T.; *f*, June 11, 1949, 1909 U.T.

A flare of importance 2 or greater was observed by Ellison[5] on August 23, 1947, and is described as "detached from the limb at a height of 30,000 km, connected by fainter prominence streamers to the chromosphere below." This probably represents a somewhat late stage in the development of the phenomenon, since the observation was made a half-hour after the onset of the sudden ionospheric disturbance associated with the flare.

A limb flare of importance 3 was observed on February 21, 1942, at Meudon. A photographic record of its development was obtained and is described in the literature.[6] This object had the form of an extended prominence that rose from the chromosphere to a height of 40,000 km. The rate of ascent during the 1^h32^m interval in which it was observed was of the order of 7 km/sec. In the later stages of development the flarelike brilliance appeared only as an upper fringe on the prominence. There was a sudden ionospheric disturbance associated with this flare prominence. On February 11, 1949, a flare of importance 2+ was photographed at Meudon. The brilliant material appears both on the disk and beyond the limb.[7]

PHOTOGRAPHIC RECORD OF LIMB FLARES, McMATH-HULBERT OBSERVATORY

During the last two years at the McMath-Hulbert Observatory there has been included in the observing program a technique by which the development of flares at or near the limb can be recorded photographically. With slits transmitting 0.4 A centered on *Hα*, with suitably chosen exposure times, and with the occulting disk removed, it has been possible to record simultaneously the activity of the brighter prominences and the accompanying disk features and changes. The Stone radial-velocity spectroheliograph has been used concurrently to photograph the *Hα* spectra of the prominences. The films so taken record the outbreak and development of a large number of flares.

Certain of the flares on the above series of films occurred very close to the solar limb but showed no changes other than those that can best be described as a brightening of a portion of the disk (Fig. 1, *a*, *b*). Some of these flares were accompanied by sudden disturbances of the earth's ionosphere, and some were not. The outbreaks were often followed by the appearance of surge-type prominences at the limb or by active dark flocculi on the adjacent disk. The latter appear as absorption markings, usually with negative radial velocities during the initial stages and with positive radial velocities during the later development. In those somewhat rare cases in which the motion of the dark flocculus carried it beyond the limb, it appeared as a surge or a more complicated form of active prominence.

The dome-shaped elevations described by Ellison appear on these films as small flares or brightenings. Had they been photographed with an occulting disk over the photosphere, they would probably have been called very bright loops (Fig. 1, *c*) or cap-type prominences (Fig. 1, *d*, *e*). Although the small flare of June 25, 1951, shown in Figure 1, *d*, was of very short duration (1519–1523 U.T.), a sudden ionospheric disturbance was reported from Meudon as starting at 1520 U.T. An increase in atmospherics was recorded at Paris at 1520 U.T., with maximum at 1525 U.T.[8]

The films also include the development of a certain number of exceptionally bright surge-type prominences (Fig. 1, *f*). These may or may not be the limb aspect of features that would appear as small flares or flarelike brightenings if seen in projection on the disk. In each case these prominences began on the disk or in the chromosphere and moved outward to heights of some tens of thousands of kilometers. After the first few minutes

[5] *Op. cit.*, p. 10; *Observatory*, **67**, 206, 1947; **68**, 70, 1948.

[6] L. d'Azambuja, *Bull. Soc. Astr. France*, p. 97, 1942; and Newton, *J. British Astr. Assoc.*, **57**, 54, 1947.

[7] L. d'Azambuja, *Bull. Soc. Astr. France*, p. 241, 1949.

[8] *Central Radio Propagation Laboratory of the National Bureau of Standards Solar Flare Report*, June 26, 1951.

the outward velocities were small. These limb phenomena appeared suddenly, brightened to intensities greater than that of the undisturbed *Hα* disk, and subsided within intervals of the order of the lifetime of flares. The width of the *Hα* emission lines of these prominences was about 5 A. There were no fade-outs reported at the times these prominences developed. However, some of these objects were very similar to the prominence of March 14, 1939, which was reported by Giovanelli[4] as having caused a weakening of the *E*-layer reflections. It is not known whether or not such minor disturbances of the ionosphere accompanied the prominence-like objects here described.

LIMB FLARE OF MAY 8, 1951

The films also contain a very small number of major prominence phenomena which are believed to be the limb aspects of important flares. The most clear-cut case is that of the flare prominence of May 8, 1951. This "flare," if it be suitable to use that term, was associated with the great sunspot group that crossed the solar disk in the middle of May, 1951. At the time of the occurrence of the flarelike prominence, the spot itself was entirely behind the limb and did not appear on the disk until the following day.

Hα spectra and spectroheliograms taken at 20–30-second intervals show the principal stages of the development of the flare (see Figs. 2 and 3). It appeared first as a low cap-type prominence and within 30 seconds became a series of complicated brilliant elevations, no higher than 10,000 km. During the next 90 seconds a portion of the very brilliant formation rose with a velocity of the order of 700 km/sec and reached a height of 50,000 km. During this period, *Hα* was 8–10 A wide and showed large Doppler shifts. Gases 5000 km above the photosphere had a negative radial velocity greater than 300 km/sec, while at a height of 45,000 km the radial velocity was equally great but in the opposite direction. These Doppler shifts indicate that motion tangential to the sun's surface was taking place at the same time at the outward elevation of the very brilliant formation. After the first 90 seconds both the outward and the tangential velocities diminished, and the *Hα* line became 5–6 A wide and relatively symmetrical. In the later stages of the activity the upward motion of the flarelike object was negligible.

Above the brilliant flare there appeared rapidly ascending prominence material which was fainter and for which the spectrum lines were only 2 A wide. Doppler shifts as great as 5 A, representing line-of-sight velocities of 228 km/sec, were present. If seen in projection on the disk, these gases would probably have appeared as an active dark flocculus. This fainter material rose to heights greater than 200,000 km, with outward velocities of the order of 500 km/sec (see Fig. 4).

The light-curve showing the intensity of this elevated flare indicates that at maximum it was four times as bright as the undisturbed *Hα* disk. This is the intensity reached at maximum by some of the brightest disk flares when photographed with the same instrumental adjustments. The May 8 limb flare was accompanied by a sudden ionospheric disburbance that began within 1 minute of the time of maximum intensity in the flare.

Records of solar radio emission at 200 Mc/sec secured at the Radio Astronomy Observatory of Cornell University showed a disturbance at the time of the limb flare that can best be described as an increase in the power flux. The 200-Mc/sec disturbance lasted for 23 minutes and had two maxima. The initial maximum came when the flare prominence first appeared. Its value was at least five times that of the quiet sun. The second maximum coincided with the period of maximum intensity of the optical flare and reached a value of six times the quiet sun.

The very lowest levels of the solar regions associated with this limb flare were in all probability occulted by the sun itself. These observations could therefore provide a possible case for a consideration of the levels at which phenomena attendant upon flares take place. On the other hand, as the observational material increases, it becomes ever more clear that the sudden brightenings observed on the disk—called "flares" of one

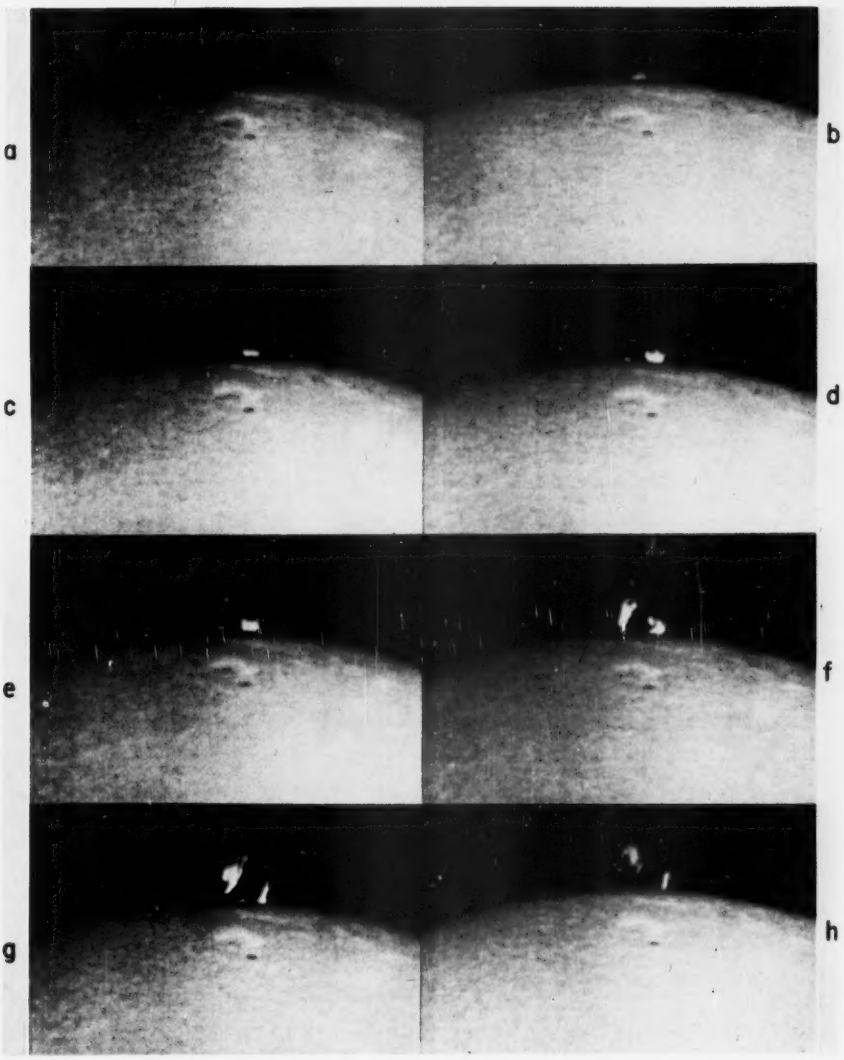

FIG. 2.—*Hα* spectroheliograms, showing outbreak and development of flare prominence, May 8, 1951. A prominence of average intensity appears to the left of the flare. On the disk a sunspot and small plage area can be seen. *a*, 1500.7 U.T.; *b*, 1503.5 U.T.; *c*, 1505.2 U.T.; *d*, 1505.7 U.T.; *e*, 1506.3 U.T.; *f*, 1507.4 U.T.; *g*, 1510.0 U.T.; *h*, 1511.9 U.T.

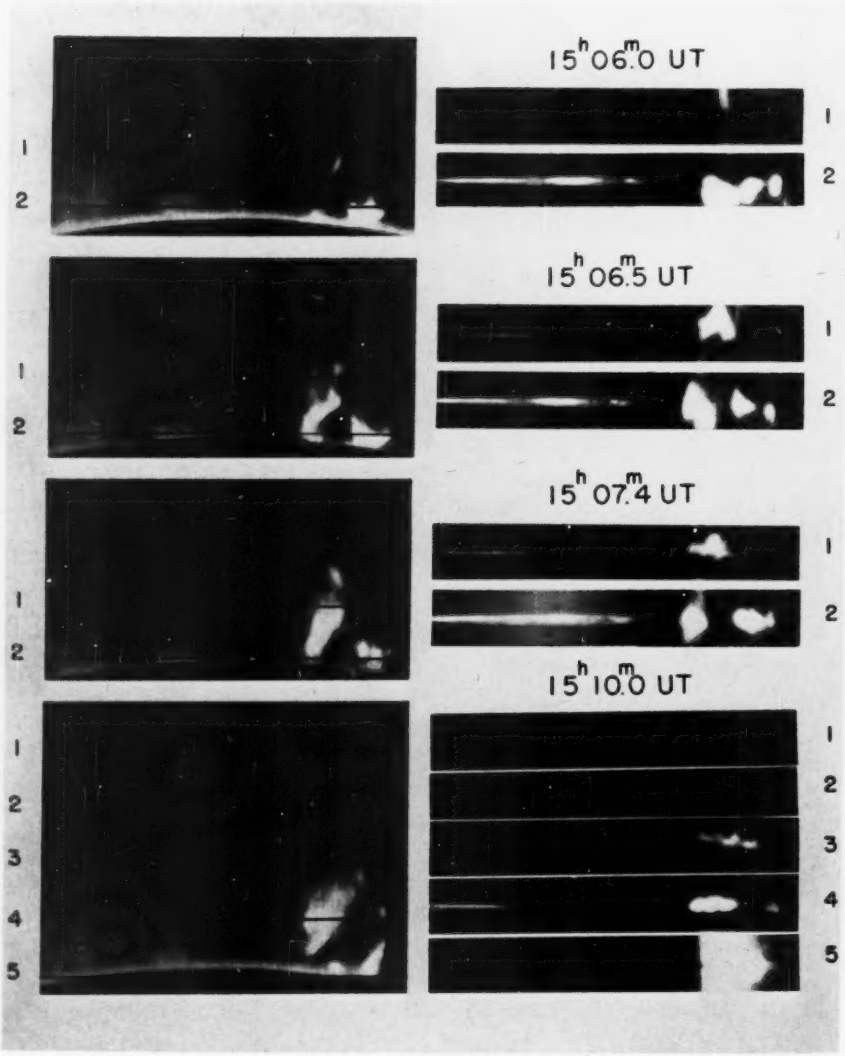

FIG. 3. *Hα* spectra of flare prominence, May 8, 1951. Full black line shows orientation of slit of spectrograph when spectrum was secured. Each portion of spectrum in column at right includes 13 A centered on *Hα*. Position of *Hα* is indicated by emission from neighboring quiescent prominence or by superposed dotted lines. Dispersion runs vertically; wave lengths increase upward. Spectrum 5 for 1510 U.T. shows the emission of the flare prominence superposed on the continuous spectrum of the photosphere.

importance or another—probably include a number of different physical forms at a number of different levels in the sun.

The writers acknowledge gratefully the part played by all members of the Observatory staff in the preparation of this paper. They also wish to thank McGregor Fund of Detroit for their continued support of the work of the Observatory.

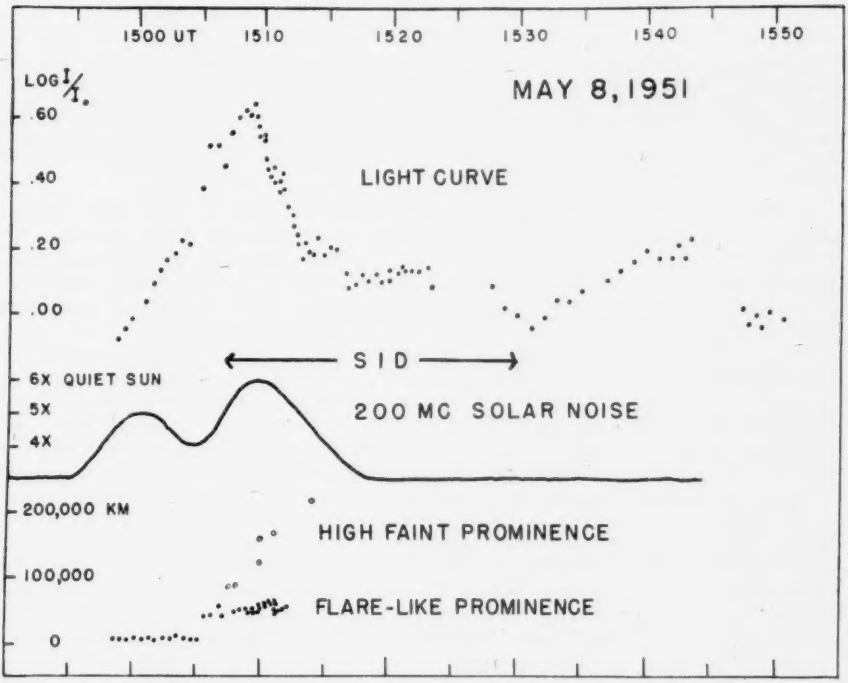

FIG. 4.—Light-curve for flare of May 8, 1951; time of ionospheric and 200-Mc/sec radio-noise disturbance; heights of flare and associated fainter prominence.

AN INFRARED SYSTEM OF BANDS OF *VO* IN M-TYPE STARS*

PHILIP C. KEENAN AND LEON W. SCHROEDER†
Perkins Observatory‡
Received September 6, 1951

ABSTRACT

Several groups of strong bands in the λλ 7400–8600 region of late M-type stars are identified as members of a new infrared system of the *VO* molecule. Measurements on laboratory arc spectra allow a provisional vibrational analysis of the infrared system into sets of eight main components. Like the well-known yellow bands (system A), the bands of the new system originate from the ground level of the molecule. The infrared *VO* bands appear to be present in all M-type stars of type M7 or later and become very strong in the coolest long-period variables. As the temperature decreases, they increase in strength relative to the adjacent *TiO* bands.

In 1949 a number of unidentified bands were reported in the λλ 7400–8000 region of the spectra of long-period variables of late M type.[1] Observations of these bands with the Perkins grating spectrograph have since been extended to a number of additional stars, including irregular variables. All the observed stars which are classified M7 or later from the strength of the usual *TiO* bands show the new bands, which become very prominent in the coolest of the stars.

Progress toward the identification of these bands has been hindered by the incompleteness of laboratory data on molecular spectra in the photographic infrared. Consequently, it was decided to photograph the arc spectra of a number of diatomic oxides on plates having a scale (49 A/mm) identical with that of the stellar spectrograms. Direct comparisons of these plates of moderate dispersion is of value in studying the stellar behavior of even the well-analyzed band systems; for the published laboratory intensity data, based on spectra of varying scales and conditions of excitation, are frequently confusing.

Out of some twenty-seven compounds included in the preliminary survey made here, the only one which proved important in the present problem was vanadium oxide. When powdered V_2O_5 is introduced into the lower electrode of an iron arc (burning at about 800 volts and 0.5 amperes), the complete set of unknown bands observed in the stars is produced. The correspondence of the stellar and arc bands can be seen in Figure 1, *b–d*, which shows the strongest bands of the λ 7400 and λ 7900 groups. In addition, several weaker stellar bands near 8500 A match arc bands of the less conspicuous group marked −1 in Figure 1, *a*.

In Table 1 the wave lengths and estimated intensities of the bands as observed in both stellar and laboratory spectra are collected. The stellar data for the region from 7300 A to 8000 A refer to *o* Ceti, S CrB, and T Cas and are taken from the earlier report.[1] For the weaker bands longward from 8500 A, the stellar wave lengths were measured on spectrograms of *o* Ceti, T Cas, and R Aql. The measurement of wave lengths of the arc lines was carried out on a set of spectrograms having a dispersion of 25 A/mm, about twice as great as on the plates from which the enlargements of the illustration were made. All the negatives were made on Eastman Spectrographic I-N plates. The arc spectra could be measured down to 6700 A, but, owing to the extreme redness of these cool stars, the stellar data extend only to 7300 A.

* *Contributions from the Perkins Observatory*, No. 32.

† This work was carried out while the second author was on leave from the Department of Physics, Oklahoma Agricultural and Mechanical College.

‡ This research was aided by an Office of Naval Research contract.

[1] Nassau, van Albada, and Keenan, *Ap. J.*, **109**, 333, 1949.

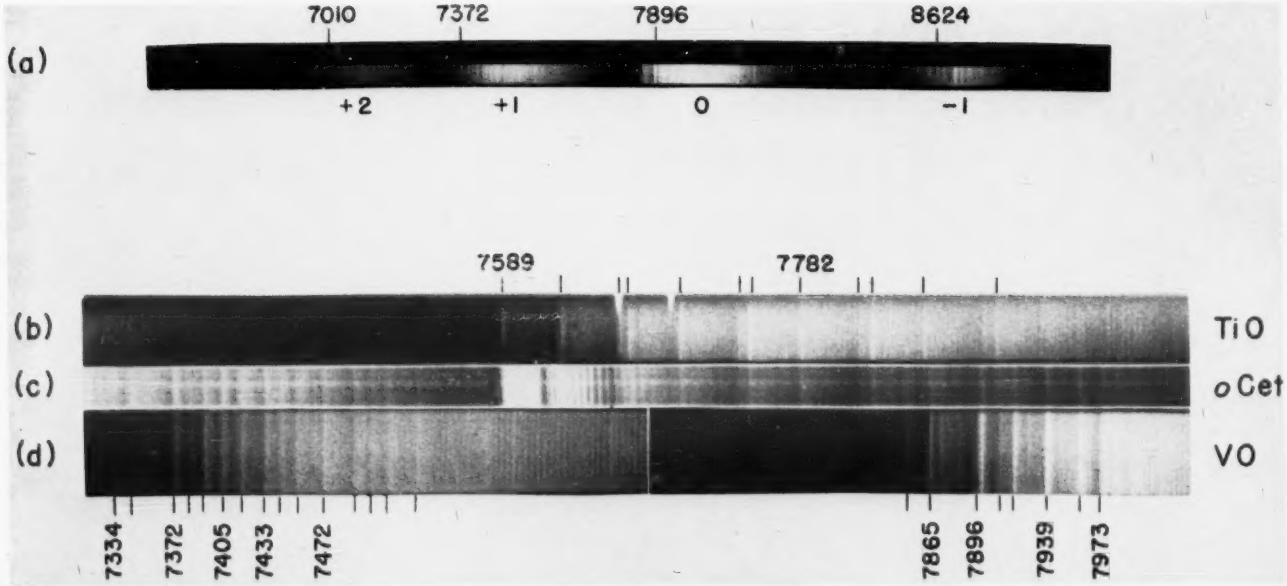

FIG. 1.—*a*, Four sequences of the infrared system of *VO*, positive reproduction. Neon comparison spectrum is shown above the *VO* arc spectrum. *b*, Positive of *TiO* arc spectrum. $\Delta v = -1$ sequence of red system. *c*, Negative of spectrum of *o* Ceti near faint maximum, December 7, 1946. The very strong absorption near 7590 A is the A band of atmospheric O_2. *d*, Positive of *VO* arc spectrum. $\Delta v = +1$ and $\Delta v = 0$ sequences of the infrared system.

TABLE 1

BAND HEADS OF VO IN THE NEAR INFRARED

STARS		LABORATORY					
λ	Int.	λ	Int.	ν_{vac}	Transition	$\Delta\nu$	Remarks
		6477.47:	3	15,433.9	A 0,2		
		6531.21	5	15,306.8	A 1,3		Bl with V I 6531
		6585.79	0 n	15,180.0	A 2,4		
		6626.77	2 s	15,086.1			
		6782.74	0	14,739.3			
		6901.64	0	14,483.2			
		6917.83	2 nn	14,451.4	A 0,3		
		6957.00	3	14,370.1	B 3,1 (2)	-4.6	
		6973.51	3	14,336.0	B 2,0 (7) A 2,5 ?	+1.7	Start of wide group
		6978.20	3 n	14,324.3	B 2,0 (8) B 3,1 (3)	-0.9 -1.6	
		6985.87	1	14,310.7			Short
		6996.14	2 -	14,289.6	B 3,1 (5)	-0.4	Short
		7010.38	3	14,260.3	B 3,1 (6)	+2.8	
		7037.27	2 n	14,206.1	B 3,1 (7) B 3,1 (8) B 4,2 (3)	-6.5 +2.6 +0.7	
		7069.83	2	14,140.7	B 5,3 (2)	+0.6	
		7096.82	1 n	14,086.9	B 5,3 (3)	-3.4	
7333:	2:	7333.83	3	13,631.7	B 1,0 (1)	-0.4	Short
7342.5	1						Not VO
7344.4	3 w	7344.88	4	13,611.2	B 1,0 (2)	+2.0	
		7353.87	2	13,594.5			
7372.6	4	7372.45	4	13,560.3	B 1,0 (3)	+0.9	
7382:	0	7383.53	0	13,540.0	B 1,0 (4)	+2.5	
7393.7	2	7393.19	5	13,522.2	B 1,0 (5) B 2,1 (1)	-1.3 +1.8	
		7397.26	0	13,514.8			
7404.7	3	7405.16	4	13,500.4	B 2,1 (2)	+2.9	
7415.1	2 w	7414.08	0	13,484.1	B 1,0 (6)	-6.1 (?)	
7417.4	2	7417.95	4	13,477.1			?

TABLE 1

BAND HEADS OF VO IN THE NEAR INFRARED

STARS		LABORATORY					
λ	Int.	λ	Int.	ν vac	Transition	$\Delta\nu$	Remarks
		7425.77	1 -	13,462.9			
7433.4	3	7433.29	4	13,449.3	B 2,1 (3)	+1.6	Short
Bl with 7433		7435.38	3	13,445.5	B 1,0 (7)	-0.6	
7443.7	1	7443.69	3 n	13,430.5	B 1,0 (8)? B 2,1 (4)	-6.5 +4.7	
7453.9	2 w	7453.61	4 -	13,412.6	B 2,1 (5)	+0.8	
7472.2	2	7472.13	5	13,379.4	B 2,1 (6)	+0.1	
7490.0 7491.8	0 2	7491.80	2	13,344.2	B 3,2 (3)?	+5.6	
7503.3:	1	7503.91:	1 +	13,322.7	B 2,1 (8)	-2.6	Wide
7514.9:	1 n	7514.27:	2:	13,304.4	B 3,2 (5)	+1.7	Diffuse
7534.0:	2	7533.44	3 -	13,270.5	B 3,2 (6)	+0.3	
7850.7	2	7850.87	4	12,733.9	B 0,0 (1)	0	
7865.1	3	7866.04	7	12,711.0	B 0,0 (2)	0	
		7872.03	1 n	12,699.7	B ?		Weak branch
7896.2	2	7895.97	8	12,661.2	B 0,0 (3)	0	
Bl with 7896		7898.32	3:	12,637.4			Second head
Bl with Ti0 7907		7909.65	2	12,639.3	B 0,0 (4)	0	
7918.8	2	7918.44	4	12,625.3	B 0,0 (5)	0	
		7928.13	1 -	12,609.8	B 1,1 (2)	-0.1	
7939.3	4	7938.88	5	12,592.8	B 0,0 (6)	0	
7960.5	2 n	7960.39	4 n	12,558.8	B 1,1 (3)	-0.8	
		7967.26	2	12,547.9	B 0,0 (7)	0	Short
7974.3	4	7973.08	5 n	12,538.8	B 0,0 (8) B 2,2 (1)	0 +5.7	
Observed diffuse		7981.46	3:	12,525.6	B 1,1 (5)	+2.0	
		Higher bands too closely packed to be measured with this dispersion.					
		8518.22	3	11,736.3	B 0,1 (1)	+2.3	
8537.8	2	8537.66	5	11,709.6	B 0,1 (2)	-1.5	
Bl with Ti0 8570		8572.58	4	11,661.9	B 0,1 (3)	+0.4	
" " " "		8575.25	6	11,658.3	B		Secondary head
		8584.39	1	11,645.9	B 1,2 (1)	+0.9	

TABLE 1

BAND HEADS OF VO IN THE NEAR INFRARED

STARS		LABORATORY					
λ	Int.	λ	Int.	ν vac	Transition	$\Delta\nu$	Remarks
8591.0 (Bl with TiO 8591)	1	8590.56	2	11,637.5	B 0,1 (4)	-2.0	
Bl with 8591		8592.48	1	11,634.9			Secondary head
8597.5	0	8597.88	2	11,627.6	B 0,1 (5)	-2.1	
8603.8	0 n	8603.98	3	11,619.7	B 1,2 (2)	+2.3	
8624.4[4]	3	8624.00	5	11,592.4	B 0,1 (6)	-0.5	
Observed diffuse		8641.93	3 n	11,568.3	B 1,2 (3)	-3.9	Blend
Observed diffuse		8657.44	2	11,547.6	B 0,1 (7)	-0.4	
8667.6:	1 n	8666.58	3	11,535.4	B 0,1 (8)	-3.5	
		Higher bands blended and overexposed.					

4 This is the strongest of these bands in stellar spectra, and was actually observed as early as 1934 by Merrill in R Hya; Ap.J. 79, 183, Table 8, 1934.

The new infrared bands could be assigned almost at once to the *VO* molecule, for the well-known visual system of *VO* bands was excited simultaneously in the arc and the two groups appeared with comparably high intensity. The visual bands have been classified by W. F. C. Ferguson[2] and by P. C. Mahanti[3] into a single system, which we shall designate as "system A." A number of the infrared bands also had been observed by Ferguson, but the absence from his list of several of the stronger stellar bands and the discrepancies between the relative strength of the bands in the stars and the general indications of intensity which he had given prevented us from making a definite identification of the stellar bands on the basis of his data.

Since neither Ferguson nor Mahanti had found it possible to analyze the infrared bands satisfactorily, it seems worth while to attempt at least a rough vibrational analysis from our more extensive table of frequencies. Inspection of Figure 1, *a*, suggests at once that we are dealing with one system (which we shall term the "infrared system"). The fact that the λλ 7000, 7400, and 7900 groups have roughly equal frequency differences, while the distance from the λ 7900 group to the λ 8500 group is greater, implies that the group at 7900 A is the $\Delta v = 0$ sequence. This interpretation is further supported by the high intensity of the bands in this group.

TABLE 2

WAVE-NUMBER DIFFERENCES FOR THE LOWER LEVEL OF SYSTEM B

Component	Δv	Component	Δv
1	999.6	6	1000.4
2	1001.4	7	1000.3
3	998.3		
4	1001.8	Mean $\Delta G'' = 999.4 \pm 0.6$ cm^{-1}	
5	997.6		

Recognition of the corresponding band heads in the different sequences, however, is difficult, for it is evident from Figure 1, *d*, that we are dealing with a rather complex system. The best representation of the data appears to be given by assuming eight components for each band. Below Figure 1, *d*, these eight heads are indicated for the 0, 0 bands, and in Table 1 the corresponding heads in each sequence are shown in the column headed "Transition" by the numbers in parentheses. The letter "B" is used to indicate bands belonging to the infrared system. The reality of the set of components numbered 8 is somewhat questionable, for these bands are somewhat diffuse in each sequence and their positions are close to those of some of the bands from the higher vibrational levels of component 3. Consequently, the frequencies of component 8 have not been used in deriving the vibrational constants.

The values of $\Delta G'' = \omega_0'' - \omega_0'' x_0''$ found from the bands of the λ 7900 and λ 8500 sequences are given in Table 2.

The values of $\Delta G''$ for the lower level of the visual system, as given by Ferguson and by Mahanti, were 1001.7 cm^{-1} and 1002.9 cm^{-1}, respectively. The close agreement with our result, 999.4 cm^{-1}, makes it probable that the *infrared bands observed in both the stellar and the laboratory spectra are due to transitions from the same lowest level of the VO molecule from which the yellow bands arise.*

$\Delta G'$ is found from the differences from the +1 and 0 sequences as 897.6 ± 1.5 cm^{-1}. The accuracy here is less, largely because the 1, 0 band of component 6 is surprisingly weak and has to be taken as the faint head to the violet of the intensity peak at λ 7418. In a system of so many components, no accurate determination of even the vibrational constants is possible from plates of the scale employed here, particularly since the +2 sequence of the infrared system is overlapped by the −3 bands of system A. Consequent-

[2] *J. Res. Nat. Bur. Stand.*, **8**, 381, 1932.

[3] *Proc. Phys. Soc. London*, **47**, 433, 1935.

ly, the values given for the infrared system in Table 3 are merely approximate; a rotational analysis of this system is needed. The value of ω_e'' given in the table has been assumed from the rotational analysis of the yellow bands. The ν_e for the infrared system refers to the first component. For system A the constants given by both Ferguson[2] and Mahanti[3] are listed.

The constants given for the infrared system in Table 3 were used to compute the predicted wave numbers, starting from the eight observed 0, 0 heads, and the column headed "$\Delta\nu$" in Table 1 gives the differences, observed *minus* computed.

TABLE 3

VIBRATIONAL CONSTANTS OF *VO*

System	ν_e	ω_e'	$\omega_e'x_e'$	ω_e''	$\omega_e''x_e''$
A (Ferguson)	17,498.8	864.9	5.7	1012.3	5.3
A (Mahanti)	17,501.3	863.5	5.4	1012.7	4.9
Infrared	11,788.1	908.2	5	(1012.6)	6.3

In the *VO* molecule, doublet and quartet levels would be expected. The lowest electronic level, which is common to the two systems, is presumably a doublet, and Mahanti considers system A as a $^2\Delta - ^2\Delta$ transition. The greater complexity of the bands of the infrared system suggests the possibility that the transition involves quartet terms. In this connection it is interesting to note that the band systems of *VO* appear to be analogous to the systems of *CbO* (*NbO*), which have been investigated by Rao,[4] who found that these *CbO* bands also exhibit complex structure, which led him to suggest that his systems B and C involve quartet terms. It is possible that the infrared system of *VO* corresponds to system C of *CbO*.[5]

The astrophysical interest of the infrared *VO* bands lies chiefly in the fact that they occur in a fairly clean region of the spectrum, where the only other strong absorption features are bands of *TiO*. Consequently, the situation is favorable for comparing the relative strengths of *TiO* and *VO*. In Figure 1 the closely adjacent heads, 7861 A of *TiO* and 7865 A of *VO*, can be seen to be particularly sensitive criteria. On the exposure of Figure 1, *c*, taken during the faint maximum of Mira in 1946, the *VO* band is somewhat stronger than *TiO* 7861, though at a normal bright maximum the *VO* bands are missing, as remarked before.[1] In a cooler atmosphere, however, *VO* 7865 is much the stronger, and in some cases *TiO* 7861 is scarcely visible, presumably because of the general *VO* absorption in this region. This was the situation in the spectrum of R Aql (M7e) on July 8, 1951, when the visual brightness was about 2 mag. below maximum.

The behavior of the infrared *VO* bands agrees fully with the following conclusion of Merrill, based on observations of the yellow bands: "The *VO* bands appear to increase in intensity with advancing spectral type. Thus, at time of maximum light they are stronger in R Leonis than in *o* Ceti and in a given variable become stronger as the light declines. The astrophysical data suggest that the dissociation energy of *VO* is less than that of *TiO*."[6] This astrophysical evidence for a lower dissociation energy of *VO* is of some importance in view of the uncertainties in present laboratory data. Herzberg's extrapolation of the spectroscopic data gives $D_0 = 6.9$ e.v. for *TiO* and $D_0 = 6.4$ e.v. for *VO*, whereas Gaydon estimated the dissociation energy as 5.5 e.v. for each of the mole-

[4] *Indian J. Phys.*, **24**, 35, 1950; and *Ap. J.* (in press).

[5] This suggestion was made tentatively by Dr. Rao in correspondence.

[6] P. W. Merrill, *Spectra of Long-Period Variable Stars* (Chicago: University of Chicago Press, 1940), p. 36.

cules.[7] The behavior of the stellar bands is in better accord with the values given by Herzberg.

When more accurate laboratory values of the dissociation energies are available, it will be of interest to reverse the argument and use the stellar intensity ratios to estimate differences in the atmospheric temperatures.

It is a pleasure to express our appreciation to Professor C. E. Hesthal for the loan of the 1400-volt transformer used to supply current to the d.c. arc.

[7] G. Herzberg, *Molecular Spectra and Molecular Structure*, Vol. 1, *Spectra of Diatomic Molecules* (2d ed.; New York: D. van Nostrand Co., Inc., 1950), Table 39.

THE NEAREST *H* II REGIONS

STEWART SHARPLESS AND DONALD OSTERBROCK*
Yerkes Observatory
Received August 23, 1951

ABSTRACT

Distances and linear dimensions are given for hydrogen emission regions visible on plates taken in the *Hα* region with the Greenstein-Henyey wide-angle camera. Two new large *H* II regions were found surrounding the stars λ Orionis and ζ Ophiuchi and having apparent diameters of about 7° and 10°, respectively.

A survey in *Hα* of the brightest hydrogen emission regions has recently been made with the Greenstein-Henyey wide-angle camera.[1] A Corning 2403 filter was used with Eastman 103*a*-F plates. This combination isolates a spectral band about 300 A wide, centered approximately on *Hα*. The night-sky lines at λ 6300 and λ 6363 are cut out by the filter, and exposures up to 2 hours can be made without objectionable sky background. Comparison exposures were made with no filter on Eastman 103*a*-F plates.

Emission regions were found by comparing the *Hα* and panchromatic photographs, both in a blink microscope and on prints. Many of these regions have been previously detected with the nebular spectrograph[2] at the McDonald Observatory.

For each emission region appearing on the plates an attempt was made to identify the exciting stars. The criteria for this identification were early spectral type (O–B0) and apparent association with the nebulosity. In some cases the excitation is due to a single star, while in others it is due to an entire cluster. Spectral types and luminosity classes for most of these stars were kindly furnished by W. W. Morgan. Spectroscopic parallaxes were computed and then corrected for interstellar absorption by means of the colors of Stebbins, Huffer, and Whitford.[3] The angular sizes of the emission regions were measured from the plates, and their linear dimensions then computed.

Table 1 lists the emission regions, their designations in the catalogue of Struve and Elvey,[2] their galactic co-ordinates, the adopted distance moduli corrected for interstellar absorption, and the measured angular sizes of the emission regions and their computed linear dimensions.

Photographs of the Milky Way from Sagittarius to Cepheus and from Cepheus to Canis Major in *Hα* are reproduced in Figures 2 and 3. In Figures 1 and 4 the emission objects are identified according to their numbers in Table 1. Aside from the discrete emission regions listed here, it appears from the photographs that the Milky Way from Sagittarius to Cygnus is considerably brighter in the spectral interval observed than from Cepheus to Canis Major. This enhancement is relatively greater on the *Hα* plate than on the panchromatic comparison plate, and thus is probably due, at least in part, to a general *Hα* illumination, consisting of a great number of overlapping emission regions.

Two new large *H* II regions were recorded in this survey and are shown in detail in Figure 5. They are excited by the stars ζ Ophiuchi and λ Orionis, respectively. The λ Orionis *H* II region is about 7° in diameter, while the ζ Ophiuchi region is about 10° in length. The lower part of the λ Orionis nebulosity appears on a photograph by H. A.

* Atomic Energy Commission Pre-doctoral Fellow in Astrophysics.

[1] O. Struve, *Sky and Telescope*, **10**, 215, 1951.

[2] O. Struve, C. T. Elvey, and W. Linke, *Contr. McDonald Obs.*, No. 9, 1939.

[3] *Ap. J.*, **91**, 20, 1940.

FIG. 1.—The location of the emission regions appearing in Figure 2. Numbers *10* through *16*, except *15*, lie along the Milky Way from top to bottom.

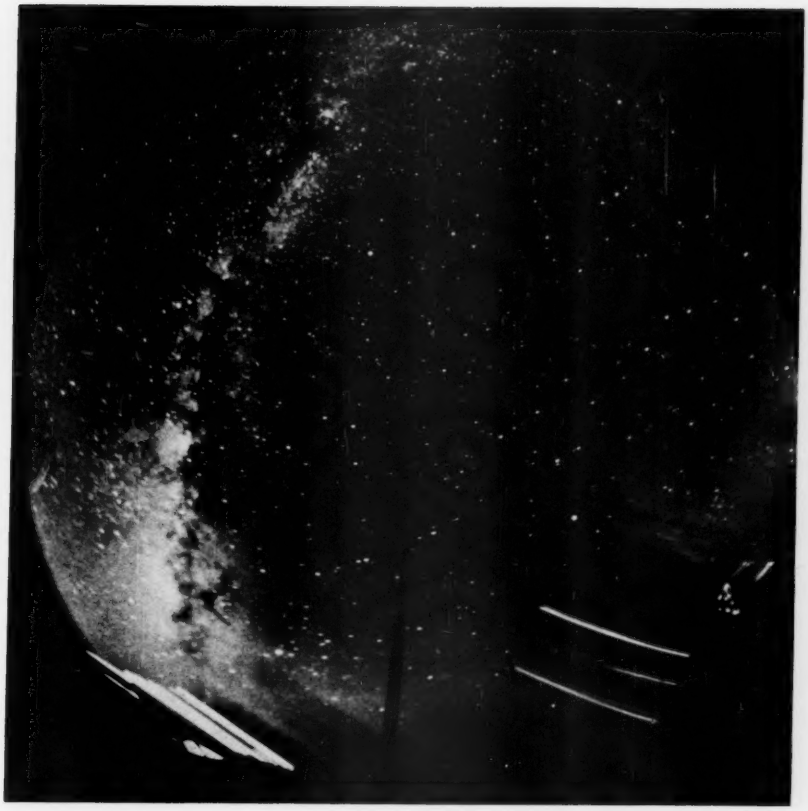

FIG. 2.—The Milky Way from Sagittarius to Cepheus in *Hα*. Exposure, 2 hours on Eastman 103*a*-F emulsion, Corning 2403 filter. The bright lines at the bottom are due to trailed horizon lights.

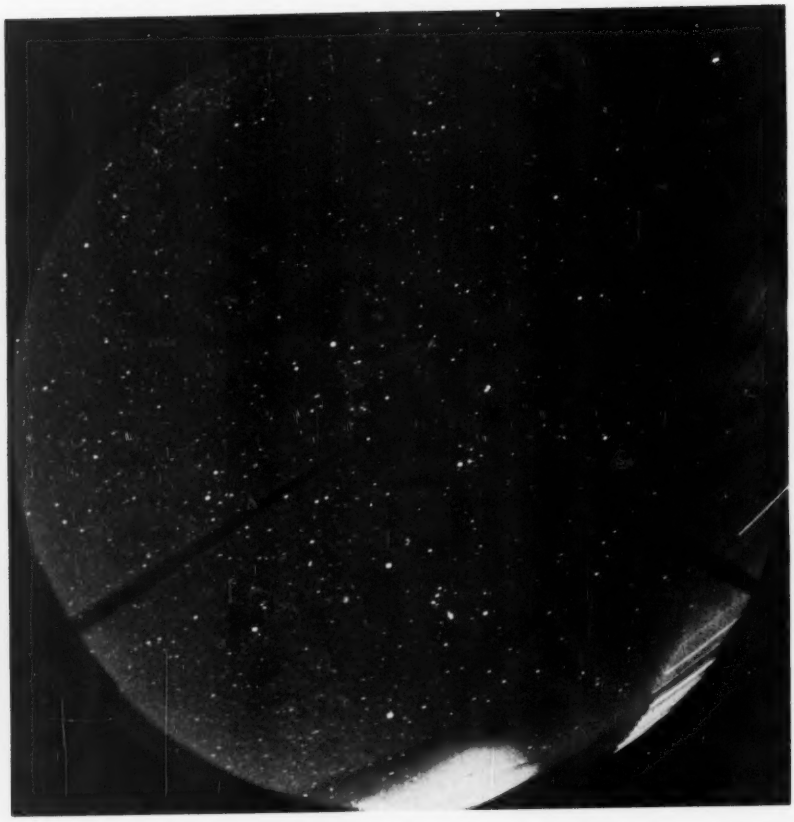

FIG. 3.—The Milky Way from Cepheus to Canis Major in *Hα*. Exposure, 2 hours on Eastman 103*a*-F emulsion, Corning 2403 filter.

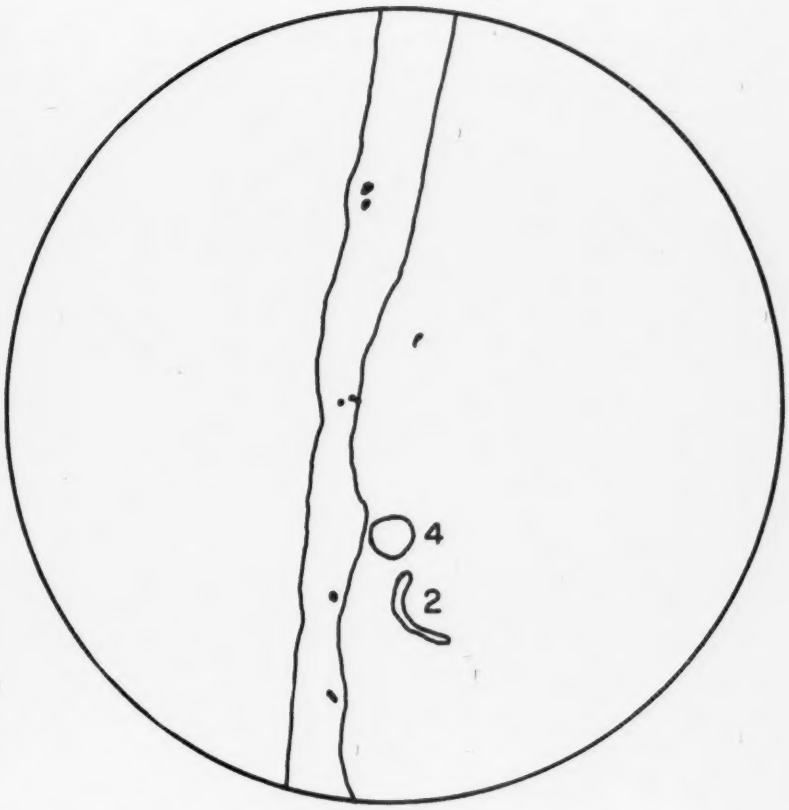

FIG. 4.—The location of the emission regions appearing in Figure 3. Numbers *1* through *9*, except *4* and *2*, lie along the Milky Way from bottom to top.

Lower.[4] The fact that they both appear at intermediate galactic latitude is probably a selection effect, since similar regions near the galactic circle would be lost in the general illumination of the Milky Way. These two emission regions seem to resemble most closely the idealized *H* II regions investigated by Strömgren,[5] since they appear homogeneous and approximately spherical about the exciting star. The apparent irregularities in the ζ Ophiuchi nebulosity are due to foreground obscuring material which can be traced on the blue-sensitive photographs of this region taken by Ross.[6] Knowing the diameters of these regions and the spectral types of the exciting stars, one can use Strömgren's tables[5] to obtain an estimate of the density of hydrogen. The quantity tabu-

TABLE 1

HYDROGEN EMISSION REGIONS

	Object	McD.	l	b	$m_0 - M$	Angular Dimension	Linear Dimension (Parsecs)	Remarks
1	IC 2177	45	192°	+ 1°	10.2	2°.5×1°.3	48×25	
2	Orion Loop	41	177	−18	8.0	12×7.2	84×50	Barnard's Great Curved Nebula
3	NGC 2244	55	173	+ 1	10.0	1.2	21	12 Mon Cluster
4	λ Ori	4	162	−10	8.9	6.8	71	
5	IC 410	...	141	− 1	12.7:	0.6	37	
6	IC 405	...	140	− 1	8.6	1.4	13	Excited by AE Aur
7	NGC 1499	5	127	−13	7.4	2.4×0.8	13×4	Excited by ξ Per
8	BD+59°522	29	105	+ 1	11.5*	1.8×0.8	63×28	
9	NGC 1027	27	103	+ 1		2.1×1.6	73×56	
10	IC 1396	22	67	+ 3	9.5	2.8	39	Excited by HD 206267
11	NGC 7000	...	53	− 1	9.8	2.1	33	North America Nebula; excited by HD 199579
12	NGC 6604	...	346	0	10.7	1.2	29	
13	NGC 6611	...	345	− 1	12.6:	0.7	40	M 16
14	NGC 6523	...	334	− 3	10.3	1.0×0.5	20×10	M 8
15	ζ Oph	...	334	+23	5.8	9.6	24	
16	IC 4628	69	323	− 1	9.4	2.5	33	Excited by HD 159176

* Assumed to be at the same distance.

lated by Strömgren is $s_0 \times N_H^{2/3}$, where s_0 is the radius of the emission region and N_H is the number of hydrogen atoms or ions per cubic centimeter. The results of the computations are given in Table 2. The computed values of N_H are tabulated under the two assumptions: A, that the hydrogen is uniformly distributed, and B, that the hydrogen is nonuniformly distributed but with 5 per cent of the volume occupied by small clouds. These results agree fairly well with other determinations[5, 7] of the density of hydrogen in interstellar space.

It should be noted that HD 199579 has been taken to be the exciting star in the case of the North America Nebula, rather than α Cygni, as has been previously assumed. The former is a sixth-magnitude O6 star near the densest part of the nebulosity. Assuming that HD 199579 is the exciting star, one finds a density of hydrogen of 15 ions/cc and an emission measure,[5] which is proportional to the surface brightness, of about 8000. For the faintest nebulosities, around λ Orionis and ζ Ophiuchi, the emission measures are

[4] *Ap. J.*, **89**, 137, 1939.

[5] *Ap. J.*, **89**, 526, 1939; **108**, 242, 1948.

[6] Unpublished photographs in Yerkes plate collection.

[7] R. Minkowski, *Pub. A.S.P.*, **61**, 151, 1949.

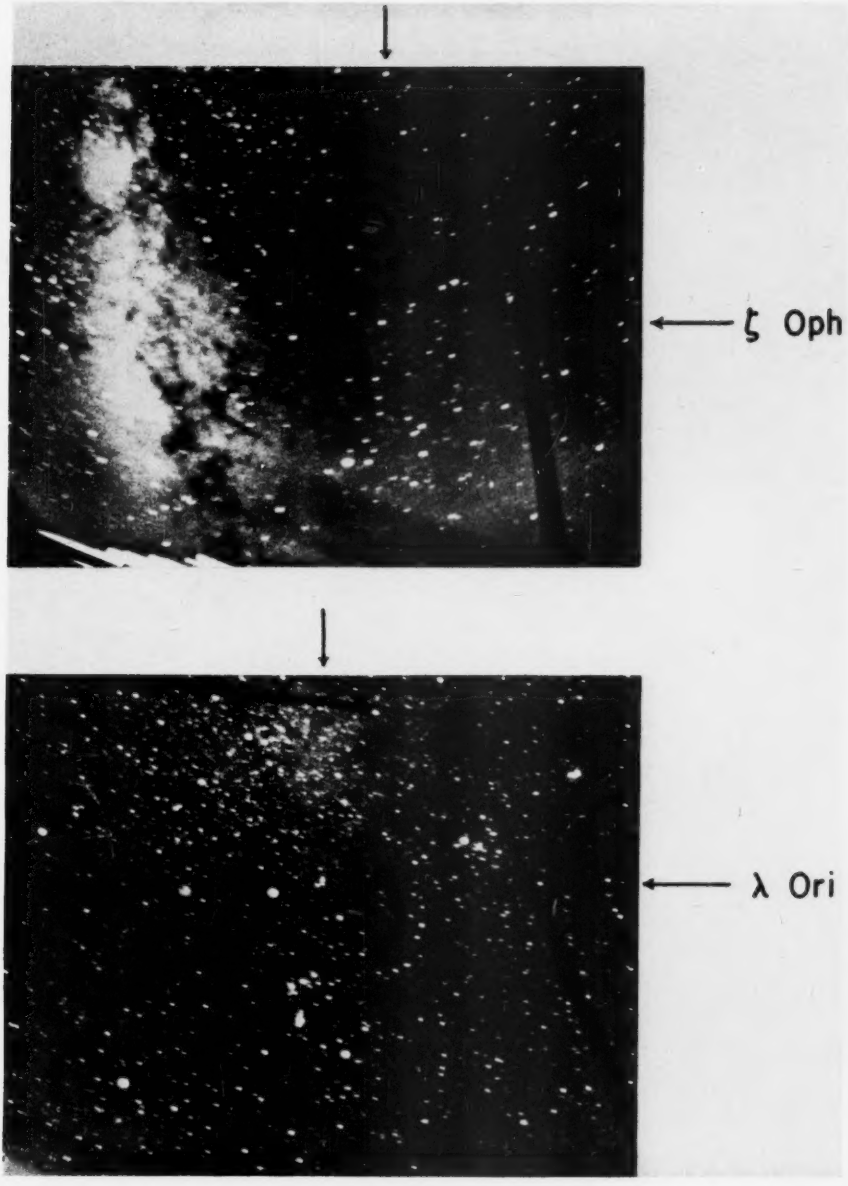

FIG. 5.—Enlargements of the regions of the ζ Ophiuchi nebulosity (*upper*) and the λ Orionis nebulosity (*lower*). These reproductions have been copied to higher contrast.

about 500. The assumption of α Cygni as the exciting star, however, leads to a density of 0.3 ions/cc and an emission measure of 3, which would make the nebula too faint to be observed.

TABLE 2

DENSITY OF HYDROGEN

OBJECT	SPECTRUM*	DIAMETER (PARSECS)	$s_0 \times N_H^{2/3}$	N_H (CM^{-3})	
				A	B
λ Ori	O8	71	66	2.5	11
ζ Oph	O9.5 V	24	36	5.2	24

* W. W. Morgan, unpublished.

The emission regions listed in Table 1 seem to be identical in nature with those in the Andromeda nebula studied by Baade and Mayall.[8] Their sizes are, on the average, the same, and they are associated in both cases with high-luminosity objects of population I.

We are indebted to W. W. Morgan for his advice regarding this investigation.

[8] *Problems of Cosmical Aerodynamics* (Dayton, Ohio: Central Air Documents Office), p. 185.

THE THEORY OF THE FLUCTUATIONS IN BRIGHTNESS OF THE MILKY WAY. IV

G. MÜNCH AND S. CHANDRASEKHAR
Yerkes Observatory
Received April 27, 1951

ABSTRACT

In this paper the integral equation governing the fluctuations in brightness of the Milky Way is solved, quite generally, for the case when the system of the stars and clouds extends to infinity in the direction of the line of sight and the transparency factor, q, characterizing the clouds is governed by an arbitrary frequency function, $\psi(q)(0 \leqslant q \leqslant 1)$. The solution is obtained in the form of a series in Laguerre polynomials with coefficients depending only on the moments of $\psi(q)$. It is further shown that the solutions found in Paper II for two particular forms of $\psi(q)$ can be obtained as special cases of the general solution given here.

1. *Introduction.*—In this paper, which is a continuation of three earlier papers[1] devoted to the theory of the fluctuations in brightness of the Milky Way, we shall return to the case considered in Paper II, namely, when the system of the stars and interstellar clouds extends to infinity in the direction of the line of sight. In this case the integral equation governing the distribution of brightness is (I, eq. [17], or III, eq. [3])

$$f(u) + \frac{df}{du} = \int_0^1 f\left(\frac{u}{q}\right)\psi(q)\,dq\,, \tag{1}$$

where u is a measure of the observed brightness, $f(u)$ is the probability that the brightness (in the chosen units) exceeds the assigned value u, and q is the transparency factor which is assumed to occur with a frequency given by $\psi(q)$. Regarding the solution of equation (1), we know that the moments of the distribution,

$$\mu_n = -\int_0^\infty u^n df(u)\,, \tag{2}$$

are given by

$$\mu_n = n! \prod_{j=1}^{n} (1 - \varpi_j)^{-1}\,, \tag{3}$$

where

$$\varpi_j = \int_0^1 q^j \psi(q)\,dq\,. \tag{4}$$[2]

In Paper II we showed how equation (1)—or, rather, the equation

$$g(u) + \frac{dg}{du} = \int_0^1 g\left(\frac{u}{q}\right)\psi(q)\frac{dq}{q}\,, \tag{5}$$

governing the corresponding frequency function of u—can be solved for the two cases in which all the clouds are equally transparent and when $\psi(q) = (n+1)q^n$. In this paper we shall show how equation (1) can be solved quite generally.

[1] *Ap. J.*, **112**, 380, 393, 1950; **114**, 110, 1951. These papers will be referred to as "Papers I, II, and III," respectively.

[2] In Papers I and II we denoted the moments of q by q_j. We are now denoting them by ϖ_j, since we wish to retain q_1, q_2, etc., for denoting the running variable when integrating over q (cf. eqs. [12] and [13] below).

2. *The solution of equation (1) by the method of successive iterations.*—Letting

$$f(u) = e^{-u}F(u), \tag{6}$$

we can write equation (1) more conveniently in the form

$$\frac{dF(u)}{du} = \int_0^1 e^{-(1-q)u/q} F\left(\frac{u}{q}\right) d\phi(q), \tag{7}$$

where, for the sake of brevity, we have further written

$$d\phi(q) = \psi(q)\, dq\,. \tag{8}$$

[In eq. (7) the integral on the right-hand side may now be regarded as a Stieltjes integral.]

Equation (7) can be formally integrated to give

$$F(u) = 1 + \int_0^1 d\phi(q) \int_0^u dt\, e^{-(1-q)t/q} F\left(\frac{t}{q}\right), \tag{9}$$

where the constant of integration has been chosen to satisfy the normalizing condition,

$$F(0) = f(0) = 1\,. \tag{10}$$

According to equation (9), we have

$$F\left(\frac{t}{q}\right) = 1 + \int_0^1 d\phi(q_1) \int_0^{t/q} dt_1\, e^{-(1-q_1)t_1/q_1} F\left(\frac{t_1}{q_1}\right). \tag{11}$$

Substituting this expression for $F(t/q)$ in equation (9), we obtain

$$\begin{aligned} F(u) = 1 &+ \int_0^1 d\phi(q_1) \int_0^u dt_1\, e^{-(1-q_1)t_1/q_1} \\ &+ \int_0^1 d\phi(q_2) \int_0^1 d\phi(q_1) \int_0^u dt_2\, e^{-(1-q_2)t_2/q_2} \int_0^{t_2/q_2} dt_1\, e^{-(1-q_1)t_1/q_1} F\left(\frac{t_1}{q_1}\right). \end{aligned} \tag{12}$$

In this last equation, we can again substitute for $F(t_1/q_1)$ according to equation (11), and in the resulting equation we can again make the same substitution. In this manner, after m such substitutions, we shall obtain

$$\begin{aligned} F(u) = 1 &+ \sum_{n=1}^{m} \int_0^1 d\phi(q_n) \int_0^1 d\phi(q_{n-1}) \int_0^1 \cdots \int_0^1 d\phi(q_1) \int_0^u dt_n\, e^{-(1-q_n)t_n/q_n} \\ &\times \int_0^{t_n/q_n} dt_{n-1}\, e^{-(1-q_{n-1})t_{n-1}/q_{n-1}} \int_0^{t_{n-1}/q_{n-1}} \cdots \int_0^{t_2/q_2} dt_1\, e^{-(1-q_1)t_1/q_1} \\ &+ \int_0^1 d\phi(q_{m+1}) \int_0^1 d\phi(q_m) \int_0^1 \cdots \int_0^1 d\phi(q_1) \int_0^u dt_{m+1}\, e^{-(1-q_{m+1})t_{m+1}/q_{m+1}} \\ &\times \int_0^{t_{m+1}/q_{m+1}} dt_m\, e^{-(1-q_m)t_m/q_m} \cdots \int_0^{t_2/q_2} dt_1\, e^{-(1-q_1)t_1/q_1} F\left(\frac{t_1}{q_1}\right). \end{aligned} \tag{13}$$

By defining the sequence of functions

$$K_1(u;\, q_1) = \int_0^u dt_1\, e^{-(1-q_1)t_1/q_1} = \frac{q_1}{1-q_1}\left[1 - e^{-(1-q_1)u/q_1}\right], \tag{14}$$

$$K_2(u;\, q_2,\, q_1) = \int_0^u dt_2\, e^{-(1-q_2)t_2/q_2} K_1\left(\frac{t_2}{q_2};\, q_1\right), \tag{15}$$

and

$$K_n(u;\, q_n, \ldots, q_1) = \int_0^u dt_n\, e^{-(1-q_n)t_n/q_n} K_{n-1}\left(\frac{t_n}{q_n};\, q_{n-1}, \ldots, q_1\right) \tag{16}$$
$$(n = 2, 3, \ldots),$$

we can rewrite equation (13) in the form

$$F(u) = 1 + \sum_{n=1}^{m} \int_0^1 d\phi(q_n) \int_0^1 \cdots \int_0^1 d\phi(q_1)\, K_n(u;\, q_n, \ldots, q_1) + R_m(u), \tag{17}$$

where $R_m(u)$ stands for the last term in equation (13) involving $F(t_1/q_1)$.

We shall now show that the infinite series,

$$F(u) = 1 + \sum_{n=1}^{\infty} \int_0^1 d\phi(q_n) \int_0^1 \cdots \int_0^1 d\phi(q_1)\, K_n(u;\, q_n, \ldots, q_1), \tag{18}$$

obtained by letting $m \to \infty$ in equation (17), actually converges uniformly for all $0 \leqslant u < \infty$ to the required solution of equation (7). In order to establish this, we need the following two lemmas.

Lemma 1.—The functions $K_n(u; q_n, \ldots, q_1)$ defined by equations (14) and (16) satisfy the recurrence relation,

$$K_n(u;\, q_n, \ldots, q_1) = \frac{q_1}{1-q_1}\left[K_{n-1}(u;\, q_n, \ldots, q_3,\, q_2)\right. \tag{19}$$
$$\left. - K_{n-1}(u;\, q_n,\, q_{n-1}, \ldots, q_3,\, q_2 q_1)\right] \qquad (n = 2, 3, \ldots).$$

Proof.—The proof is by induction. From equations (14) and (15) it follows that

$$K_2(u;\, q_2,\, q_1) = \frac{q_1}{1-q_1} \int_0^u e^{-(1-q_2)t_2/q_2}\left[1 - e^{-(1-q_1)t_2/q_2 q_1}\right] dt_2 \tag{20}$$
$$= \frac{q_1}{1-q_1}\left[\int_0^u e^{-(1-q_2)t_2/q_2} dt_2 - \int_0^u e^{-(1-q_2 q_1)t_2/q_2 q_1} dt_2\right].$$

Hence

$$K_2(u;\, q_2,\, q_1) = \frac{q_1}{1-q_1}\left[K_1(u;\, q_2) - K_1(u;\, q_2 q_1)\right]. \tag{21}$$

This verifies the lemma for $n = 2$. Now assume that the lemma is true for $n - 1$ and consider the integral expression (eq. [16]) for K_n in terms of K_{n-1} and substitute for K_{n-2} in accordance with the lemma. We obtain

$$K_n(u;\, q_n, \ldots, q_1) = \frac{q_1}{1-q_1}\left[\int_0^u dt_n\, e^{-(1-q_n)t_n/q_n}\right. \tag{22}$$
$$\left.\times\left\{K_{n-2}\left(\frac{t_n}{q_n};\, q_{n-1}, \ldots, q_3,\, q_2\right) - K_{n-2}\left(\frac{t_n}{q_n};\, q_{n-1}, \ldots, q_3,\, q_2 q_1\right)\right\}\right];$$

and, again using equation (16) (for $n - 1$), we can rewrite the foregoing as

$$K_n(u;\, q_n, q_{n-1}, \ldots, q_1) = \frac{q_1}{1-q_1}\left[K_{n-1}(u;\, q_n, \ldots, q_2)\right. \tag{23}$$
$$\left. - K_{n-1}(u;\, q_n, \ldots, q_3,\, q_2 q_1)\right];$$

this establishes the lemma for n. The general truth of the lemma now follows by induction.

Lemma 2.—The function $K_n(u;q_n, \ldots, q_1)$ $(0 \leqslant u < \infty$ and $0 \leqslant q_i < 1, j = 1, \ldots, n)$ has a uniformly convergent expansion in terms of the Laguerre polynomials, $L_k(u)$, given by

$$K_n(u; q_n, \ldots, q_1) = q_n q_{n-1} \cdots q_1 - \sum_{k=1}^{\infty} p_k(n; q_n, \ldots, q_1) L_k(u), \tag{24}$$

where

$$p_k(n; q_n, \ldots, q_1) = \sum_{j=0}^{k-1} (-1)^j \binom{k-1}{j} q_n^{j+2} \sum_{i_{n-1}=1}^{j+2} q_{n-1}^{i_{n-1}} \sum_{i_{n-2}=1}^{i_{n-1}} q_{n-2}^{i_{n-2}} \times \cdots \sum_{i_2=1}^{i_3} q_2^{i_2} \sum_{i_1=1}^{i_2} q_1^{i_1}, \tag{25}$$

are polynomials in the q_i's.

Proof.—One definition of the Laguerre polynomials, $L_k(u)$, is in terms of the generating function $\exp[-ux/(1-x)]/(1-x)$. Thus,[3]

$$e^{-ux/(1-x)} = (1-x) \sum_{k=0}^{\infty} x^k L_k(u). \tag{26}$$

This expansion is uniformly convergent for $0 \leqslant u < \infty$ and $0 \leqslant x < 1$. Letting $x = 1 - q_1$ and remembering that $L_0(u) \equiv 1$, we can rewrite equation (26) in the form

$$e^{-(1-q_1)u/q_1} = q_1 + q_1(1-q_1) \sum_{k=1}^{\infty} (1-q_1)^{k-1} L_k(u). \tag{27}$$

Using this expansion in equation (14), we obtain the following representation for $K_1(u; q_1)$:

$$K_1(u; q_1) = q_1 - \sum_{k=1}^{\infty} p_k(1; q_1) L_k(u), \tag{28}$$

where

$$p_k(1; q_1) = q_1^2(1-q_1)^{k-1} = \sum_{j=0}^{k-1} (-1)^j \binom{k-1}{j} q_1^{j+2}. \tag{29}$$

Equations (28) and (29) verify the lemma for $n = 1$.

Now, assuming that the lemma is true for n, we can establish its validity for $n+1$. For, expressing K_{n+1} in terms of K_n in accordance with lemma 1 and using the polynomial representation given by equations (24) and (25) for K_n, we have

$$K_{n+1}(u; q_{n+1}, \ldots, q_1) = \frac{q_1}{1-q_1}[K_n(u; q_{n+1}, \ldots, q_2) - K_n(u; q_{n+1}, \ldots, q_3, q_2 q_1)] = \frac{q_1}{1-q_1}\Big[q_{n+1} q_n \cdots q_3 q_2 (1-q_1) - \sum_{k=1}^{\infty} L_k(u) \sum_{j=0}^{k-1} (-1)^j \binom{k-1}{j} q_{n+1}^{j+2} \sum_{i_n=1}^{j+2} q_n^{i_n} \sum_{i_{n-1}=1}^{i_n} q_{n-1}^{i_{n-1}} \cdots \sum_{i_2=1}^{i_3} q_2^{i_2}(1-q_1^{i_2})\Big]$$

[3] See, e.g., G. Szego, *Orthogonal Polynomials* ("American Mathematical Society Colloquium Publications," Vol. XXIII [1939]), p. 97.

$$= q_{n+1}q_n \cdots q_2 q_1 - \sum_{k=1}^{\infty} L_k(u) \sum_{j=0}^{k-1} (-1)^j \binom{k-1}{j} q_{n+1}^{j+2} \sum_{i_n=1}^{j+2} q_n^{i_n} \tag{30}$$

$$\cdots \sum_{i_2=1}^{i_3} q_2^{i_2} \frac{q_1(1-q_1^{i_2})}{1-q_1} = q_{n+1} \cdots q_1 - \sum_{k=1}^{\infty} L_k(u) \sum_{j=0}^{k-1} (-1)^j \binom{k-1}{j}$$

$$\times q_{n+1}^{j+2} \sum_{i_n=1}^{j+2} q_n^{i_n} \sum_{i_{n-1}}^{i_n} q_n^{i_{n-1}} \cdots \sum_{i_2=1}^{i_3} q_2^{i_2} \sum_{i_1=1}^{i_2} q_1^{i_1}.$$

The truth of the lemma now follows by induction.

Returning to equation (18), we can now substitute for K_n its expansion as a power series in the q_i's. According to equations (24) and (25), the general term in the series on the right-hand side of equation (18) is

$$\int_0^1 d\phi(q_n) \int_0^1 d\phi(q_{n-1}) \int_0^1 \cdots \int_0^1 d\phi(q_1)\, K_n(u; q_n, \ldots, q_1)$$

$$= \varpi_1^n - \sum_{k=1}^{\infty} L_k(u) \sum_{j=0}^{k-1} (-1)^j \binom{k-1}{j} \varpi_{j+2} \sum_{i_{n-1}=1}^{j+2} \varpi_{i_{n-1}} \sum_{i_{n-2}=1}^{i_{n-1}} \varpi_{i_{n-2}} \cdots \sum_{i_1=1}^{i_2} \varpi_{i_1}; \tag{31}$$

we thus have

$$F(u) = 1 + \sum_{n=1}^{\infty} \varpi_1^n$$

$$- \sum_{n=1}^{\infty} \sum_{k=1}^{\infty} L_k(u) \sum_{j=0}^{k-1} (-1)^j \binom{k-1}{j} \varpi_{j+2} \sum_{i_{n-1}=1}^{j+2} \varpi_{i_{n-1}} \sum_{i_{n-2}=1}^{i_{n-1}} \varpi_{i_{n-2}} \cdots \sum_{i_1=1}^{i_2} \varpi_{i_1}. \tag{32}$$

Letting

$$a_k = \sum_{n=1}^{\infty} \sum_{j=0}^{k-1} (-1)^j \binom{k-1}{j} \varpi_{j+2} \sum_{i_{n-1}=1}^{j+2} \varpi_{i_{n-1}} \sum_{i_{n-2}=1}^{i_{n-1}} \varpi_{i_{n-2}} \cdots \sum_{i_1=1}^{i_2} \varpi_{i_1}, \tag{33}$$

we can rewrite equation (32) in the form

$$F(u) = \frac{1}{1-\varpi_1} - \sum_{k=1}^{\infty} a_k L_k(u). \tag{34}$$

The expression for the coefficient a_k in equation (34) can be simplified in the following manner: By inverting the order of the summations over n and j in equation (33), we have

$$a_k = \sum_{j=0}^{k-1} (-1)^j \binom{k-1}{j} \varpi_{j+2} \Big\{ 1 + \sum_{i_1=1}^{j+2} \varpi_{i_1} + \sum_{i_2=1}^{j+2} \varpi_{i_2} \sum_{i_1=1}^{i_2} \varpi_{i_1}$$

$$+ \cdots + \sum_{i_n=1}^{j+2} \varpi_{i_n} \sum_{i_{n-1}=1}^{i_n} \varpi_{i_{n-1}} \cdots \sum_{i_2=1}^{i_3} \varpi_{i_2} \sum_{i_1=1}^{i_2} \varpi_{i_1} + \cdots \Big\}. \tag{35}$$

The quantity in braces on the right-hand side is clearly

$$\prod_{i=1}^{j+2} (1 + \varpi_i + \varpi_i^2 + \cdots + \varpi_i + \cdots) = \prod_{i=1}^{j+2} (1-\varpi_i)^{-1}. \tag{36}$$

Hence

$$a_k = \sum_{j=0}^{k-1} (-1)^j \binom{k-1}{j} \varpi_{j+2} \prod_{i=1}^{j+2} (1-\varpi_i)^{-1}. \tag{37}$$

By some rearranging of the terms, we can simplify the foregoing expression for a_k still further to the form

$$a_k = -\sum_{j=0}^{k} (-1)^j \binom{k}{j} \prod_{i=1}^{j+1} (1-\varpi_i)^{-1}. \tag{38}$$

The fact that we have been able to carry out, explicitly, the summation over n in the expression for a_k establishes the convergence of the series on the right-hand side of equation (18); and from lemma 2 it follows that the convergence is uniform for $0 \leqslant u < \infty$. The series (18), therefore, represents the required solution of equation (7).

With a_k given by equation (37), equation (34) becomes

$$F(u) = \frac{1}{1-\varpi_1} + \sum_{k=1}^{\infty} L_k(u) \sum_{j=0}^{k} (-1)^j \binom{k}{j} \prod_{i=1}^{j+1} (1-\varpi_i)^{-1}; \tag{39}$$

or, since $L_0(u) \equiv 1$, we can also write

$$F(u) = \sum_{k=0}^{\infty} L_k(u) \sum_{j=0}^{k} (-1)^j \binom{k}{j} \prod_{i=1}^{j+1} (1-\varpi_i)^{-1}. \tag{40}$$

The solution for $f(u)$ is therefore given by

$$f(u) = e^{-u} \sum_{k=0}^{\infty} L_k(u) \sum_{j=0}^{k} (-1)^j \binom{k}{j} \prod_{i=1}^{j+1} (1-\varpi_i)^{-1}; \tag{41}$$

or, using expression (3) for the moments μ_j, we can write, alternatively,

$$f(u) = e^{-u} \sum_{k=0}^{\infty} L_k(u) \sum_{j=0}^{k} \frac{(-1)^j}{(j+1)!} \binom{k}{j} \mu_{j+1}. \tag{42}$$

3. *Relation with a formal solution of the problem of moments.*—It is of interest to verify that the solution for $f(u)$ obtained in § 2 is in agreement with a formal solution of the classical problem of moments in mathematics.[4]

If a function $f(u)$ $(0 \leqslant u < \infty)$ can be expanded in a series in Laguerre polynomials of the form

$$f(u) = e^{-u} \sum_{k=0}^{\infty} a_k L_k(u), \tag{43}$$

then the coefficients a_k in the expansion will be given by

$$a_k = \int_0^{\infty} f(u) L_k(u)\, du. \tag{44}$$

[4] J. A. Shohat and J. D. Tamarkin, *The Problem of Moments* (New York: American Mathematical Society, 1943), esp. § 10, p. 96.

Since

$$L_k(u) = \sum_{j=0}^{k} \frac{(-1)^j}{j!}\binom{k}{j} u^j, \tag{45}$$

we have

$$\begin{aligned} a_k &= \sum_{j=0}^{k} \frac{(-1)^j}{j!}\binom{k}{j}\int_0^\infty f(u)\, u^j du \\ &= -\sum_{j=0}^{k} \frac{(-1)^j}{(j+1)!}\binom{k}{j}\int_0^\infty u^{j+1} df(u), \end{aligned} \tag{46}$$

or

$$a_k = \sum_{j=0}^{k} \frac{(-1)^j}{(j+1)!}\binom{k}{j}\mu_{j+1}. \tag{47}$$

The last expression for a_k is in agreement with the coefficient of L_k in equation (42). It should, however, be emphasized that the foregoing analysis, giving a solution of the Stieltjes problem of moments, is purely formal: it is known that, in general, such solutions converge only in some "mean" sense (cf. Shohat and Tamarkin, *op. cit.*).

4. *Special forms of the solution (41).*—We shall now show how the solutions found in Paper II for two particular forms of $\psi(q)$ can be derived as special cases of the general solution obtained in § 2.

i) *The case when all the clouds are equally transparent.*—In this case

$$\varpi_i = q^i; \tag{48}$$

and in the general solution given by equation (41) we must write

$$\prod_{i=1}^{j+1}(1-\varpi_i)^{-1} = \prod_{i=1}^{j+1}(1-q^i)^{-1}. \tag{49}$$

In virtue of the identity,

$$\prod_{i=1}^{\infty}(1-q^{i+j}) = \sum_{n=0}^{\infty}(-1)^n q^{nj}\prod_{r=1}^{n}\frac{q^r}{1-q^r}, \tag{50}$$

established in Paper II (eq. [18]), we can also write

$$\begin{aligned} \prod_{i=1}^{j+1}(1-\varpi_i)^{-1} &= \Big[\prod_{i=1}^{\infty}(1-q^i)\Big]^{-1}\prod_{i=1}^{\infty}(1-q^{i+j+1}) \\ &= \Big[\prod_{i=1}^{\infty}(1-q^i)\Big]^{-1}\sum_{n=0}^{\infty}(-1)^n q^{n(j+1)}\prod_{r=1}^{n}\frac{q^r}{1-q^r}. \end{aligned} \tag{51}$$

Now letting (cf. III, eqs. [49] and [51])

$$K = \Big[\prod_{i=1}^{\infty}(1-q_i)\Big]^{-1} \quad \text{and} \quad Q_n = (-1)^n\prod_{r=1}^{n}\frac{q^r}{1-q^r}, \tag{52}$$

we can express equation (51) in the form

$$\prod_{i=1}^{j+1} (1-\varpi_i)^{-1} = K \sum_{n=0}^{\infty} Q_n q^{n(j+1)} . \tag{53}$$

Hence, in this case, the general solution reduces to

$$f(u) = K e^{-u} \sum_{k=0}^{\infty} L_k(u) \sum_{n=0}^{\infty} Q_n q^n \sum_{j=0}^{k} (-1)^j \binom{k}{j} q^{nj}$$

$$= K e^{-u} \sum_{n=0}^{\infty} Q_n q^n \sum_{k=0}^{\infty} (1-q^n)^k L_k(u) . \tag{54}$$

But (cf. eq. [27])

$$q^n \sum_{k=0}^{\infty} L_k(u) (1-q^n)^k = e^{-(1-q^n)u/q^n} . \tag{55}$$

Hence

$$f(u) = K e^{-u} \sum_{n=0}^{\infty} Q_n e^{-(1-q^n)u/q^n} . \tag{56}$$

This is in agreement with the solution found in Paper II (eq. [21]).

ii) *The case* $\psi(q) = (n+1)q^n$.—In this case

$$\varpi_i = \frac{n+1}{n+i+1} , \tag{57}$$

$$\prod_{i=1}^{j+1} (1-\varpi_i)^{-1} = \prod_{i=1}^{j+1} \left(1 - \frac{n+1}{n+i+1}\right)^{-1} = \binom{n+j+2}{n+1}$$

$$= \sum_{r=0}^{n+1} \binom{r+j}{r} , \tag{58}$$

and the coefficient of L_k in the solution (41) becomes

$$\sum_{r=0}^{n+1} \sum_{j=0}^{k} (-1)^j \binom{k}{j} \binom{r+j}{r} . \tag{59}$$

Now from combinatorial analysis it is known[5] that

$$\sum_{j=0}^{k} (-1)^j \binom{k}{j} \binom{r+j}{r} = (-1)^k \binom{r}{k} \quad \text{if} \quad k \leqslant r$$

$$= 0 \qquad \text{otherwise} . \tag{60}$$

Hence, by combining equations (41), (59), and (60) we have

$$f(u) = e^{-u} \sum_{r=0}^{n+1} \sum_{k=0}^{r} (-1)^k \binom{r}{k} L_k(u) . \tag{61}$$

[5] W. Feller, *An Introduction to Probability Theory and Its Applications* (New York: John Wiley & Sons, 1950), **1**, 48, problem 10.

But the expansion of u^r in Laguerre polynomials is

$$u^r = r! \sum_{k=0}^{r} (-1)^k \binom{r}{k} L_k(u). \tag{62}$$

Hence

$$f(u) = e^{-u} \sum_{r=0}^{n+1} \frac{u^r}{r!}. \tag{63}$$

By differentiating this last expression, we obtain

$$g(u) = -\frac{df}{du} = \frac{u^{n+1}}{(n+1)!} e^{-u}. \tag{64}$$

And again this is in agreement with the solution found in Paper II (eq. [33]).

THE THEORY OF THE FLUCTUATIONS IN BRIGHTNESS OF THE MILKY WAY. V

S. CHANDRASEKHAR AND G. MÜNCH
Yerkes Observatory
Received June 18, 1951

ABSTRACT

In this paper a new picture of the distribution of the interstellar matter is proposed which may be considered as an alternative to (or a refinement of) the current picture, which visualizes the interstellar medium as consisting of a distribution of discrete clouds. On this new picture the distribution of density is considered to be continuous but exhibiting fluctuations of a statistical character. More particularly, it is assumed that the volume absorption coefficient $\kappa\rho(r)$ at any point in the medium can be written in the form $\kappa\rho(r) = \overline{\kappa\rho}[1 + \delta(r)]$, where $\delta(r)$ is a chance variable whose mean expectancy is zero. The following additional assumptions regarding $\delta(r)$ are made:

$$\overline{\delta^2(r)} = a^2 \qquad \text{and} \qquad \overline{\delta(r_1)\,\delta(r_2)} = a^2 R(|r_1 - r_2|),$$

where a^2 is a constant throughout the medium and R represents the correlation coefficient of the fluctuations $\delta(r)$ at two different points; according to our assumption, this latter correlation depends only on the distance r between the two points considered. The correlation function $R(r)$ defines a micro-scale, r_0, such that for $r > r_0$ the correlation rapidly becomes negligible. On the picture of continuous distribution, the parameters a^2 and r_0 replace the parameters ν and τ_* (giving the number of clouds per unit distance and the optical thickness per cloud) on the discrete picture.

The various problems of stellar statistics, such as the fluctuations in the counts of extragalactic nebulae and in the brightness of the Milky Way, are rediscussed in terms of this new picture, and it is shown that the observations can be interpreted equally in terms of it. Indeed, it appears that $2a^2\int_0^\infty R(\tau/\tau_0)d\tau = 2a^2\tau_0\int_0^\infty R(\xi)d\xi$ (where τ denotes the optical thickness in $\overline{\kappa\rho}$ and τ_0 is the micro-scale measured in optical thickness) replaces the optical thickness τ_* of a single cloud on the discrete picture. However, the particular advantage of the continuous picture over the discrete picture is that the angular correlations in the brightness of the Milky Way in two neighboring directions can be discussed without any additional assumptions. This latter problem is discussed in some detail, and it is shown that, by combining the results of the fluctuations in the brightness itself with the results of the angular correlations, it is possible to infer the order of magnitudes of both a^2 and τ_0. The results of Pannekoek's survey of the southern Milky Way are analyzed with this in view, and it is found that $\tau_0 \simeq 0.01$ and that $a^2 \simeq 14$. A value of $a^2 \simeq 14$ implies that the root mean square of the deviations in the density is about three to four times the mean density itself.

1. *Introduction.*—In the earlier papers of this series[1] we examined certain basic problems in stellar statistics arising from the irregular distribution of the interstellar absorbing matter. In these papers the assumption was made that interstellar matter occurs in the form of discrete clouds; that these clouds are characterized by a certain average optical thickness τ_*; and, finally, that they occur with a certain average frequency, ν, per unit distance. This idealized picture of the interstellar medium was first advanced by Ambarzumian[2] and has since been generally accepted.[3] And during recent years there

[1] *Ap. J.*, **112**, 380, 393, 1950; **114**, 110, 1951; **115**, 94, 1952; these papers will be referred to as "Papers I, II, III, and IV," respectively. After these papers were written, a paper by G. E. Rusakov was received (*Utchenia Zapiske*, Ser. Math., **13**, 53, 1949) in which the solution found in Paper II for the integral equation governing the fluctuations in brightness of the Milky Way for the case when the system extends to infinity in the direction of the line of sight and all the clouds are equally transparent is also given. However, the solution for the case (also given in Paper II) when the transparency factor of the clouds is governed by the frequency function $\psi(q) = (n + 1)q^n$, as well as all the other results contained in Papers I, III, and IV, has not, so far as we know, been anticipated by the Russian writers.

[2] V. A. Ambarzumian and S. G. Gordeladse, *Bull. Abastumani Obs.*, No. 2, p. 37, 1938; also V. A. Ambarzumian, *Bull. Abastumani Obs.*, No. 4, p. 17, 1940.

[3] J. H. Oort and H. C. van de Hulst, *B.A.N.*, No. 376, 1946; B. Strömgren, *Ap. J.*, **108**, 242, 1948; L. Spitzer, *Ap. J.*, **108**, 276, 1948.

have been many attempts, particularly by the Russian writers, to determine the average optical thickness τ_* of a cloud. But it would appear that the only direct determination is that which follows from ascribing to the clouds an optical thickness which will account for the known coefficient of interstellar absorption of 1.5 mag. per kiloparsec. Thus, on the assumption that the stars and the clouds are randomly distributed and that the reason why early-type stars are generally associated with diffuse nebulae is due to the larger volumes of space they illuminate, it can be deduced that a line of sight will, on the average, intersect about six to seven clouds per kiloparsec.[2,3] On the picture of discrete clouds, we must therefore suppose that the average optical thickness of a cloud is about 0.25. We believe that it may be stated with fairness that all the other attempts to determine τ_* have served only to show that the other data used for this purpose, such as the fluctuations in brightness of the Milky Way and the counts of stars and extragalactic nebulae, are *consistent* with this value of $\tau_* = 0.25$ and the picture of discrete clouds. We wish to emphasize this point, since a tendency to argue in circles can be noted in the literature, in that confirmation for the *picture* of interstellar matter as occurring in the form of discrete clouds is sought in the data analyzed. In saying this, we are not suggesting that the picture of interstellar matter as occurring in discrete clouds may not be true; but we are suggesting that it may be worth while to inquire whether the observed fluctuations in the brightness of the Milky Way and the associated phenomena cannot also be analyzed in terms of a picture of interstellar matter as continuously distributed with a fluctuating (*albeit* a "wildly" fluctuating) density distribution. From one point of view such a picture may indeed recommend itself as being more consistent with the view which regards the irregular distribution of interstellar matter as an exemplification of large-scale turbulence. And it should be remembered in this connection that so far no satisfactory explanation has been given from gas dynamics for the relative permanence of the interstellar gas clouds which must be attributed to them on the picture of discrete clouds.[4] In this paper we shall therefore present an alternative picture of the interstellar medium as a fluctuating continuous distribution of matter and shall show how all the phenomena, such as the fluctuations in brightness of the Milky Way, etc., can be interpreted equally well on this basis. Moreover, it will appear that the correlations in the brightness of the Milky Way in different directions can be analyzed much more readily in terms of the continuous picture than in terms of the discrete picture, as has recently been attempted by Rusakov[5] on the basis of a formula due to Ambarzumian.[6]

2. *A picture of the interstellar medium as a fluctuating continuous distribution of matter.*—We shall suppose that the coefficient of general absorption, κ, and the density, ρ, of the interstellar medium are continuous functions of position ($\mathbf{r}$) but that they are subject to fluctuations. We shall accordingly write

$$\kappa\,\rho\,(\mathbf{r}) = \overline{\kappa\rho}\,[1 + \delta\,(\mathbf{r})]\,, \tag{1}$$

where the mean coefficient of volume absorption, $\overline{\kappa\rho}$, is assumed to be constant throughout the medium and $\delta(\mathbf{r})$ is a chance variable whose expectation value is zero:

$$\overline{\delta\,(\mathbf{r})} = 0\,. \tag{2}$$

[4] Cf. J. M. Burgers, *Kon. Ned. Akad. Wetensch.*, **49**, 588, 1946. A referee, commenting on the present paper, has written: "There can be no doubt about the reality and individuality of these large clouds and complexes of clouds [like those in Taurus and Ophiuchus] nor about the relative sharpness of their boundaries. . . . We must probably conclude that there is the small scale irregular structure the authors use as a starting point, as well as a large cloud formation." We are in substantial agreement with this comment.

[5] *Op. cit.*

[6] V. A. Ambarzumian, *Doklady Acad. Nauk Armenian S.S.R.*, **1**, 9, 1944.

Regarding $\delta(r)$ we shall make the following additional assumptions:

$$\overline{\delta^2(r)} = a^2 , \tag{3}$$

and

$$\overline{\delta(r_1)\,\delta(r_2)} = a^2 R(|r_1 - r_2|) , \tag{4}$$

where a^2 is a constant independent of position and R represents the correlation coefficient of the fluctuations $\delta(r)$ at two different points; according to equation (4), the correlation coefficient is assumed to depend only on the distance between the two points considered.

The foregoing assumptions concerning the fluctuations in $\kappa\rho$ will be valid if the conditions in the interstellar medium are those expected to prevail in homogeneous isotropic turbulence.

It follows from definitions (3) and (4) that

$$R(0) = 1 . \tag{5}$$

It is also clear that we must require

$$R(r) \to 0 \qquad \text{as} \qquad r \to \infty . \tag{6}$$

Now the correlation function, $R(r)$, defines a *scale of length;* this may be defined, for example, as the distance r_0 at which R decreases to the value $1/e$. On the picture of a continuously distributed fluctuating density of matter, the two basic parameters are, therefore, a^2, which is a measure of $\overline{\delta^2\rho}/\overline{\rho}^2$ (cf. eq. [25] below) and r_0, which is a measure of the "micro-scale" of the turbulent eddies.[7] The parameters a^2 and r_0 of the present picture replace the parameters ν and τ_* of the picture of discrete clouds.

3. *The equivalent optical thickness of a cloud.*—The two pictures of the interstellar medium described, respectively, in terms of the parameters ν and τ_* and a^2 and r_0 can be formally related by considering the optical thickness,

$$\tau(s) = \int_0^s \kappa\rho\, ds , \tag{7}$$

on the two pictures.

On the picture of discrete clouds we have

$$\overline{\tau}(s) = \overline{n}(s)\,\tau_* \qquad \text{and} \qquad \overline{\tau^2}(s) = \overline{n^2}(s)\,\tau_*^2 , \tag{8}$$

where $n(s)$ and $\overline{n^2}(s)$ are the mean and the mean square of the number of clouds to be expected in a distance s. For the assumed uniform Poisson distribution of the clouds, we have

$$\overline{n}(s) = \nu s \qquad \text{and} \qquad \overline{n^2}(s) = \nu^2 s^2 + \nu s . \tag{9}$$

Hence

$$\overline{\tau}(s) = \nu s\,\tau_* \qquad \text{and} \qquad \overline{\tau^2}(s) = (\nu^2 s^2 + \nu s)\,\tau_*^2 = \overline{\tau}^2(s) + \overline{\tau}(s)\,\tau_* . \tag{10}$$

Thus we have the relation

$$\overline{\tau}(s)\,\tau_* = [\,\overline{\tau^2}(s) - \overline{\tau}^2(s)\,] . \tag{11}$$

Considering, next, $\tau(s)$ and $\tau^2(s)$ on the picture of continuous distribution, we have (cf. eqs. [1] and [2])

$$\overline{\tau}(s) = \overline{\kappa\rho}\int_0^s [\,1 + \overline{\delta}(s)\,]\, ds = \overline{\kappa\rho}\, s \tag{12}$$

[7] The length r_0 we have defined is clearly equivalent to Taylor's micro-scale in his theory of isotropic turbulence (*Proc. R. Soc. London, A*, **151**, 421, 1935).

and

$$\overline{\tau^2(s)} = \overline{\kappa\rho}^2 \int_0^s \int_0^s [1+\delta(x)][1+\delta(y)]\,dx\,dy$$
$$= (\overline{\kappa\rho}\, s)^2 + \overline{\kappa\rho}^2 \int_0^s \int_0^s \overline{\delta(x)\,\delta(y)}\,dx\,dy\,. \tag{13}$$

It is now convenient to introduce the optical thickness, τ, in the mean volume absorption coefficient $\overline{\kappa\rho}$. Thus, letting $dt_1 = \overline{\kappa\rho}dx$ and $dt_2 = \overline{\kappa\rho}dy$, we can rewrite the expression for $\overline{\tau^2}(s)$ in the form

$$\overline{\tau^2(s)} = \overline{\tau}^2(s) + a^2 \int_0^{\overline{\tau}(s)} \int_0^{\overline{\tau}(s)} R(|t_1 - t_2|)\,dt_1 dt_2\,, \tag{14}$$

where we have further substituted for $\overline{\delta(t_1)\delta(t_2)}$ in terms of the correlation coefficient R (cf. eq. [4]). Since the integrand is symmetrical in t_1 and t_2, an alternative form of equation (14) is

$$\overline{\tau^2(s)} = \overline{\tau}^2(s) + 2a^2 \int_0^{\overline{\tau}(s)} dt_1 \int_{t_1}^{\overline{\tau}(s)} dt_2 R(t_2 - t_1)\,. \tag{15}$$

Letting $t = t_2 - t_1$ as the variable of integration in place of t_2 and inverting the order of the integrations, we have

$$\overline{\tau^2}(s) - \overline{\tau}^2(s) = 2a^2 \int_0^{\overline{\tau}(s)} dt R(t) \int_0^{\overline{\tau}(s)-t} dt_1\,, \tag{16}$$

or

$$\overline{\tau^2}(s) - \overline{\tau}^2(s) = 2a^2 \int_0^{\overline{\tau}(s)} [\overline{\tau}(s) - t] R(t)\,dt\,. \tag{17}$$

It may be noted here that in deriving equation (17) we have incidentally established the following relation:

$$\int_0^\tau \int_0^\tau \overline{\delta(t_1)\,\delta(t_2)}\,dt_1 dt_2 = 2a^2 \int_0^\tau (\tau - t) R(t)\,dt\,. \tag{18}$$

We shall find this relation useful in our subsequent work.

As we have already remarked, the correlation function $R(r)$ introduces a scale of length r_0. If τ_0 denotes the corresponding optical thickness (i.e., $\overline{\kappa\rho} r_0$), we can write

$$R(\tau) \equiv R(\tau/\tau_0) \equiv R(\xi) \quad \text{(say)}\,. \tag{19}$$

Expressing R in terms of ξ, we can rewrite equation (17) in the form

$$\overline{\tau^2}(s) - \overline{\tau}^2(s) = 2a^2 \tau_0 \int_0^{\overline{\tau}(s)/\tau_0} [\overline{\tau}(s) - \tau_0 \xi] R(\xi)\,d\xi\,. \tag{20}$$

For $\tau(s) \gg \tau_0$, the foregoing equation becomes

$$\overline{\tau^2}(s) - \overline{\tau}^2(s) \to 2a^2 \tau_0 \overline{\tau}(s) \int_0^\infty R(\xi)\,d\xi \qquad [\overline{\tau}(s) \gg \tau_0]\,. \tag{21}$$

Hence

$$[\overline{\tau^2}(s) - \overline{\tau}^2(s)] \to 2a^2 \overline{\tau}(s)\,\tau_0 R_0 \qquad [\overline{\tau}(s) \gg \tau_0]\,, \tag{22}$$

where we have written

$$R_0 = \int_0^\infty R(\xi)\,d\xi\,. \tag{23}$$

We shall see that, in the practical problems we shall consider, $\tau_0 \sim 0.01$ (cf. § 8); accordingly, in these cases the asymptotic relation (22) will provide a good approximation even for $\bar{\tau}(s) \sim 1$.

From equations (11) and (22) it would appear that, on the picture of continuous distribution, the quantity $2a^2\tau_0 R_0$ will replace τ_* of the discrete picture. We shall see that this is actually the case. Hence

$$\tau_* = 2a^2\tau_0 R_0 \tag{24}$$

provides a relation in terms of which we may pass from the picture of continuous distribution to the picture of discrete clouds. We may therefore say that $2a^2\tau_0 R_0$ gives the *equivalent optical thickness* of a cloud on the discrete picture. It is to be particularly noted that the equivalent optical thickness of a cloud is not τ_0; in other words the micro-scale should not be confused with the macro-scale!

In practice we may suppose that the mass-absorption coefficient, κ, is constant throughout the medium.[8] In that case

$$a^2 = \frac{\overline{\delta^2\rho}}{\bar{\rho}^2}, \tag{25}$$

where $\delta^2\rho$ is the mean-square deviation in the density and ρ is the mean density. The expression for the equivalent optical thickness, then, is

$$\tau_* = 2\,\frac{\overline{\delta^2\rho}}{\bar{\rho}^2}\,\tau_0 R_0\,. \tag{26}$$

In our further work we shall sometimes find it convenient to specify $R(\tau)$ more explicitly than by its micro-scale, τ_0. When the need for this arises, we shall adopt either of the two following laws:

$$R(\tau) = e^{-\tau/\tau_0} \quad \text{or} \quad R(\tau) = e^{-\tau^2/\tau_0^2}. \tag{27}$$

For these two cases,

$$\tau_* = 2a^2\tau_0 \quad \text{and} \quad \tau_* = a^2\tau_0\sqrt{\pi}, \tag{28}$$

respectively. However, it should be emphasized that it need not be required of the correlation function R that it be a monotonically decreasing function. Indeed, in the theory of turbulence, one often encounters correlation functions which change sign, pass through a minimum, and then tend to zero as the argument tends to infinity.[9]

4. *The fluctuations in the counts of extragalactic nebulae.*—The earliest determination of τ_* on the picture of discrete clouds is that due to Ambarzumian[10] based on the fluctuations exhibited by the counts of extragalactic nebulae. Ambarzumian showed that, on the picture of discrete clouds, the dispersion σ_m^2 in the number of nebulae N_m per square degree brighter than a given apparent magnitude m should exhibit the following dependence on the galactic latitude β:

$$\sigma_m^2 = \frac{\overline{N_m^2}}{\overline{N_m}^2} - 1 = 2.25\,\tau_*\tau_1 \operatorname{cosec}\beta\,, \tag{29}$$

where τ_1 is the optical thickness of the interstellar absorbing layer perpendicular to the

[8] This essentially means that in the interstellar medium it is the fluctuations in the density which are important and which outweigh any variations there may be in the composition.

[9] G. I. Taylor, *Proc. R. Soc. London*, *A*, **164**, 476, 1938; see also L. H. Aller, *Ap. J.*, **113**, 120, 1951.

[10] *Bull. Abastumani Obs.*, No. 4, p. 17, 1940; see also his later discussion in *Trans. I.A.U.*, **7**, 452–455, 1950.

galactic plane. Ambarzumian satisfied himself that the observed dispersion did show a linear dependence on cosec β as required by equation (29) and, further, that its application led to a value of τ_* in the range

$$0.20 \leqslant \tau_* \leqslant 0.30 \,. \tag{30}$$

Some doubts have recently been expressed[11] for believing that there is any real observational evidence for the linear dependence of σ_m^2 on cosec β; nevertheless, it seems desirable to derive an expression for σ_m^2 on the picture of continuous distribution.

In the absence of interstellar absorption, it is expected that the counted numbers of extragalactic nebulae, N_m, must show the proportionality

$$N_m = 10^{0.6m} N_0 \,, \tag{31}$$

where N_0 is a constant. But if there is absorbing matter of total optical thickness $\tau(s)$ in the line of sight, then we should have, instead,

$$N_m = 10^{0.6m} N_0 e^{-1.5\tau(s)} . \tag{32}$$

On the picture of the continuous but fluctuating distribution of interstellar matter (cf. eq. [12])

$$\tau(s) = \int_0^\tau [1 + \delta(t)]\, dt = \tau + \int_0^\tau \delta(t)\, dt \,, \tag{33}$$

where $\tau = \tau(s)$. With the foregoing expression for $\tau(s)$, equation (32) becomes

$$N_m = \mathfrak{N} \exp\left\{ -1.5 \int_0^\tau \delta(t)\, dt \right\} , \tag{34}$$

where

$$\mathfrak{N} = 10^{0.6m} N_0 e^{-1.5\tau} \,. \tag{35}$$

We shall assume that the exponential term in equation (34) containing the chance variable $\delta(t)$ can be expanded in a power series and that it is sufficient to retain only the first three terms in the expansion. Thus

$$\exp\left\{ -1.5 \int_0^\tau \delta(t)\, dt \right\} = 1 - 1.5 \int_0^\tau \delta(t)\, dt + \tfrac{1}{2} 2.25 \int_0^\tau \int_0^\tau \delta(t_1)\, \delta(t_2)\, dt_1 dt_2 \,. \tag{36}$$

We shall see that the validity of this approximation requires that the equivalent optical thickness $\tau_* \ll 1$ and that quantities of order τ_*^2 can be neglected.

In the framework of approximation (36),

$$\overline{N}_m = \mathfrak{N}\left[1 + \tfrac{1}{2} 2.25 \int_0^\tau \int_0^\tau \overline{\delta(t_1)\, \delta(t_2)}\, dt_1 dt_2 \right] , \tag{37}$$

and

$$\overline{N_m^2} = \mathfrak{N}^2\left[1 + 4.5 \int_0^\tau \int_0^\tau \overline{\delta(t_1)\, \delta(t_2)}\, dt_1 dt_2 \right] . \tag{38}$$

In the same approximation,

$$\frac{\overline{N_m^2}}{\overline{N}_m^2} = 1 + 2.25 \int_0^\tau \int_0^\tau \overline{\delta(t_1)\, \delta(t_2)}\, dt_1 dt_2 \,; \tag{39}$$

[11] C. Warwick, *Proc. Nat. Acad. Sci.*, **36**, 415, 1950.

or, using the result expressed by equation (18), we have

$$\sigma_m^2 = \frac{\overline{N_m^2}}{\overline{N_m}^2} - 1 = 4.5\alpha^2 \int_0^\tau (\tau - t) R(t)\, dt . \tag{40}$$

Now if τ refers to the average optical thickness of the absorbing layer in the direction of galactic latitude β, then

$$\tau = \tau_1 \operatorname{cosec} \beta , \tag{41}$$

where τ_1 is the corresponding optical thickness perpendicular to the galactic plane. Also, if τ_0 is the micro-scale defined by the correlation function $R(\tau)$, we can rewrite equation (40) in the form

$$\sigma_m^2 = 4.5\alpha^2 \tau_0 \int_0^{\tau_1 \operatorname{cosec}\beta/\tau_0} (\tau_1 \operatorname{cosec} \beta - \tau_0 \xi) R(\xi)\, d\xi . \tag{42}$$

Now it is known that $\tau_1 \sim 0.25$; also we shall see that $\tau_0 \sim 0.01$. Hence, to a sufficient accuracy (cf. eqs. [20], [21], and [23]) we may write

$$\sigma_m^2 \simeq 2.25\, (2\alpha^2 \tau_0 R_0)\, \tau_1 \operatorname{cosec} \beta . \tag{43}$$

Thus, on the picture of continuous distribution, the dispersion in the counts is given by a formula of exactly the same type as on the picture of discrete clouds. Indeed, we see that, in agreement with what was stated in § 3, $2\alpha^2\tau_0 R_0$ replaces τ_*. The earlier estimates of τ_* now imply that, on our present picture,

$$0.1 \leqslant \frac{\overline{\delta^2 \rho}}{\bar{\rho}^2}\, \tau_0 R_0 \leqslant 0.15 . \tag{44}$$

5. *The fluctuations in the brightness of the Milky Way.*—We shall now return to the problem which is the principal concern of this series of papers, namely, the fluctuations in the brightness of the Milky Way. On the picture of discrete clouds, the brightness, u, of the Milky Way measured in a certain suitably chosen unit is given by (cf. Paper I, eq. [4])

$$u = \int_0^\infty \prod_{i=1}^{n(r)} q_i\, dr , \tag{45}$$

where r is the linear distance also measured in a suitable unit. In writing equation (45), we have assumed that the system extends to infinity in the direction of the line of sight. (In this paper we shall restrict ourselves to this case.) From equation (45) it follows that (cf. Paper II, eq. [2])

$$\bar{u} = \frac{1}{1 - q_1} \quad \text{and} \quad \overline{u^2} = \frac{2}{(1 - q_1)(1 - q_2)} , \tag{46}$$

where $q_1 = q$ and $q_2 = q^2$. If the clouds are all assumed to be equally transparent, then $q_1 = q$ and $q_2 = q^2$, and we deduce from equations (46) that

$$\overline{u^2} = \frac{2}{1 + q} \bar{u}^2 . \tag{47}$$

Now q is related to the optical thickness τ_* by

$$q = e^{-\tau_*} = 1 - \tau_* + O(\tau_*^2) . \tag{48}$$

Hence to $O(\tau_s^2)$,

$$\frac{\overline{u^2}}{\overline{u}^2} = 1 + \tfrac{1}{2}\tau_s . \tag{49}$$

Returning to the picture of continuous distribution, we may first observe that the expression for the brightness analogous to equation (45) is now

$$u = \int_0^\infty e^{-\tau(s)} d\tau , \tag{50}$$

where, according to equation (33),

$$\tau(s) = \tau + \int_0^\tau \delta(t)\, dt . \tag{51}$$

Hence

$$u = \int_0^\infty d\tau\, e^{-\tau} \exp\left\{ - \int_0^\tau \delta(t)\, dt \right\} . \tag{52}$$

On the scheme of approximation represented by equation (36), we have

$$u = \int_0^\infty d\tau\, e^{-\tau} \left[1 - \int_0^\tau \delta(t)\, dt + \frac{1}{2}\int_0^\tau \int_0^\tau \delta(t_1)\, \delta(t_2)\, dt_1 dt_2 \right] . \tag{53}$$

We shall adopt this approximation consistently in all our future work.

From equation (53) it readily follows that (cf. eq. [18])

$$\overline{u} = 1 + a^2 \int_0^\infty d\tau\, e^{-\tau} \int_0^\tau dt\, (\tau - t) R(t) . \tag{54}$$

Inverting the order of the integrations in equation (54), we have

$$\overline{u} = 1 + a^2 \int_0^\infty dt R(t) \int_t^\infty d\tau\, (\tau - t)\, e^{-\tau} , \tag{55}$$

or

$$\overline{u} = 1 + a^2 \int_0^\infty e^{-t} R(t)\, dt . \tag{56}$$

Considering u^2 next, we have

$$\begin{aligned} u^2 = \int_0^\infty \int_0^\infty e^{-\tau_1 - \tau_2} & \left[1 - \int_0^{\tau_1} \delta(t_1)\, dt_1 + \frac{1}{2}\int_0^{\tau_1} \int_0^{\tau_1} \delta(t_1)\, \delta(t_2)\, dt_1 dt_2 \right] \\ & \times \left[1 - \int_0^{\tau_2} \delta(t_2)\, dt_2 + \frac{1}{2}\int_0^{\tau_2} \int_0^{\tau_2} \delta(t_1)\, \delta(t_2)\, dt_1 dt_2 \right] d\tau_1 d\tau_2 . \end{aligned} \tag{57}$$

Expanding the foregoing and retaining only the terms which are consistent with the adopted approximation, we have

$$\begin{aligned} \overline{u^2} = 1 + \int_0^\infty \int_0^\infty e^{-\tau_1 - \tau_2} & \left[\int_0^{\tau_1} \int_0^{\tau_2} \overline{\delta(t_1)\, \delta(t_2)}\, dt_1 dt_2 \right. \\ & \left. + \frac{1}{2}\int_0^{\tau_1} \int_0^{\tau_1} \overline{\delta(t_1)\, \delta(t_2)}\, dt_1 dt_2 + \frac{1}{2}\int_0^{\tau_2} \int_0^{\tau_2} \overline{\delta(t_1)\, \delta(t_2)}\, dt_1 dt_2 \right] d\tau_1 d\tau_2 . \end{aligned} \tag{58}$$

Of the three double integrals which occur inside the brackets on the right-hand side of equation (58), only the first requires some consideration; the other two lead to terms of

the same type which we have already encountered in the evaluation of $\bar{u}$. We thus have

$$\overline{u^2} = 1 + 2a^2 \int_0^\infty e^{-t} R(t)\, dt + a^2 \int_0^\infty \int_0^\infty d\tau_1 d\tau_2 e^{-\tau_1-\tau_2} \int_0^{\tau_1}\int_0^{\tau_2} dt_1 dt_2 R(|t_1 - t_2|)\,. \tag{59}$$

The quadruple integral on the right-hand side of equation (59) can be reduced to a single integral by successively rearranging the orders of the integrations in the following manner:

$$\begin{aligned}
&\int_0^\infty \int_0^\infty d\tau_1 d\tau_2 e^{-\tau_1-\tau_2} \int_0^{\tau_1}\int_0^{\tau_2} dt_1 dt_2 R(|t_1-t_2|) \\
&= \int_0^\infty d\tau_2 e^{-\tau_2} \int_0^{\tau_2} dt_2 \int_0^\infty d\tau_1 e^{-\tau_1} \int_0^{\tau_1} dt_1 R(|t_1-t_2|) \\
&= \int_0^\infty d\tau_2 e^{-\tau_2} \int_0^{\tau_2} dt_2 \int_0^\infty dt_1 R(|t_1-t_2|) \int_{t_1}^\infty d\tau_1 e^{-\tau_1} \\
&= \int_0^\infty dt_1 e^{-t_1} \int_0^\infty d\tau_2 e^{-\tau_2} \int_0^{\tau_2} dt_2 R(|t_1-t_2|) \\
&= \int^\infty dt_1 e^{-t_1} \int_0^\infty dt_2 R(|t_1-t_2|) \int_{t_2}^\infty d\tau_2 e^{-\tau_2} \\
&= \int_0^\infty dt_1 e^{-t_1} \int_0^\infty dt_2 e^{-t_2} R(|t_1-t_2|) = 2\int_0^\infty dt_1 e^{-t_1} \int_{t_1}^\infty dt_2 e^{-t_2} R(t_2-t_1) \\
&= 2\int_0^\infty dt_1 e^{-2t_1} \int_{t_1}^\infty dt_2 e^{-(t_2-t_1)} R(t_2-t_1) = \int_0^\infty e^{-t} R(t)\, dt\,.
\end{aligned} \tag{60}$$

Using this result in equation (59), we have

$$\overline{u^2} = 1 + 3a^2 \int_0^\infty e^{-t} R(t)\, dt\,. \tag{61}$$

Now, combining equations (56) and (61), we have, to the same order of accuracy,

$$\frac{\overline{u^2}}{\overline{u}^2} = 1 + a^2 \int_0^\infty e^{-t} R(t)\, dt\,. \tag{62}$$

Writing (cf. eq. [19])

$$R(t) \equiv R(t/\tau_0) \equiv R(\xi)\,, \tag{63}$$

we have

$$\frac{\overline{u^2}}{\overline{u}^2} = 1 + a^2 \tau_0 \int_0^\infty e^{-t\tau_0} R(\xi)\, d\xi\,. \tag{64}$$

For $\tau_0 \ll 1$, equation (64) reduces to

$$\frac{\overline{u^2}}{\overline{u}^2} = 1 + a^2 \tau_0 R_0 \qquad (\tau_0 \ll 1)\,. \tag{65}$$

Comparing this last equation with the corresponding equation on the picture of discrete clouds (eq. [49]), we again see that, on the continuous picture, $2a^2\tau_0 R_0$ replaces the

optical thickness τ_* of a single cloud on the discrete picture. It is also evident now that the adopted scheme of approximation is one which is correct to the first order in τ_*.

6. *The angular correlations in the brightness of the Milky Way.*—A problem of considerable interest in the theory of the fluctuations in brightness of the Milky Way is the angular correlation, $\overline{uu_\varphi}$, of the brightness in two directions, s_1 and s_2, which are inclined at an angle φ to each other. This problem has been considered by Ambarzumian[6] on the picture of discrete clouds. In order to evaluate the required correlation, Ambarzumian introduced the probability $Q(s_1)$ that a cloud intersecting the line of sight in the direction s_1, somewhere between 0 and s_1, will also intersect the line of sight in the direction s_2 and contribute (by the full amount) to the absorption in that direction. In terms of this probability, he showed that

$$\overline{uu_\varphi} = \frac{2}{1-q}\int_0^\infty d\,s_1 \exp\{-s_1(1-q)[2-Q(s_1)(1-q)]\}. \tag{66}$$

We should, of course, expect that, as $\varphi \to 0$, $Q(s_1) \to 1$ independently of s_1; and Ambarzumian actually assumed that

$$1-Q(s_1) = \frac{\varphi s_1}{\nu D} + O(\varphi^2) \qquad (\varphi \to 0), \tag{67}$$

where D denotes the linear diameter of a single cloud. (The occurrence of the factor ν in eq. [67] is due to the fact that s_1 measures the linear distance in the line of sight in the unit $1/\nu$.) In using a formula of type (67), we are essentially assuming that the clouds are uniform plane disks with a diameter D; otherwise, the absorption by the cloud will not be the same for all normal intersections of the cloud by a line of sight.[12] It would appear, then, that the assumption underlying equation (67) is highly restrictive. In any case, with assumption (67), the integral defining $\overline{uu_\varphi}$ (eq. [66]) can be evaluated and we obtain

$$\overline{uu_\varphi} = \frac{2}{(1-q)(1-q^2)}\left[1 - \frac{2\varphi}{\nu D(1+q)^2}\right], \tag{68}$$

or (cf. eq. [46])

$$\overline{uu_\varphi} = \overline{u^2}\left[1 - \frac{2\varphi}{\nu D(1+q)^2}\right]. \tag{69}$$

On the basis of formula (69), Rusakov[5] has recently analyzed the observed angular correlations in brightness of the Milky Way, with the object of estimating the linear diameter of the interstellar clouds. But, in view of the restrictive character of the assumptions which underlie the derivation of formula (69), it is difficult to assess the meaning we can attach to the derived diameters. Indeed, we shall see that the analysis of this problem of angular correlations on the picture of continuous distribution does not lead to a formula of type (69). And this is a serious objection, since the evaluation of uu_φ on the picture of continuous distribution requires no assumptions beyond those already made for evaluating u and u^2.

On the picture of the continuous distribution, the brightnesses u and u_φ in two directions s_1 and s_2, inclined at an angle φ to each other, are given by

$$u = \int_0^\infty d\,\tau_1 e^{-\tau_1} \exp\left\{-\int_0^{\tau_1} \delta(t_1)\,dt_1\right\}$$

and (70)

$$u_\varphi = \int_0^\infty d\,\tau_2 e^{-\tau_2} \exp\left\{-\int_0^{\tau_2} \delta(t_2)\,dt_2\right\},$$

[12] In any case it is evident that, on the picture of discrete clouds, the angular correlation cannot be discussed without some explicit assumption concerning the shapes of the clouds.

where we have written t_1 and t_2 for the arguments of δ to emphasize that the fluctuations in two different directions are considered and that therefore $|t_1 - t_2| \neq |t_1 - t_2|$.

On the scheme of approximation represented by equation (36), we have

$$u u_\varphi = \int_0^\infty \int_0^\infty e^{-\tau_1-\tau_2}\Big[1 - \int_0^{\tau_1} \delta(t_1)\, dt_1 + \frac{1}{2}\int_0^{\tau_1}\int_0^{\tau_1} \delta(t_1)\,\delta(t_2)\, dt_1 dt_2\Big] \times \Big[1 - \int_0^{\tau_2} \delta(t_2)\, dt_2 + \frac{1}{2}\int_0^{\tau_2}\int_0^{\tau_2} \delta(t_1)\,\delta(t_2)\, dt_1 dt_2\Big] d\tau_1 d\tau_2 . \tag{71}$$

On expanding and retaining only terms which are consistent with our approximation, we obtain

$$\overline{u u_\varphi} = 1 + \int_0^\infty \int_0^\infty d\tau_1 d\tau_2 e^{-\tau_1-\tau_2}\Big[\int_0^{\tau_1}\int_0^{\tau_2} \overline{\delta(t_1)\,\delta(t_2)}\, dt_1 dt_2 + \frac{1}{2}\int_0^{\tau_1}\int_0^{\tau_1} \overline{\delta(t_1)\,\delta(t_2)}\, dt_1 dt_2 + \frac{1}{2}\int_0^{\tau_2}\int_0^{\tau_2} \overline{\delta(t_1)\,\delta(t_2)}\, dt_1 dt_2\Big] . \tag{72}$$

The second and the third of the three double integrals which occur inside the brackets on the right-hand side of equation (72) are the same as those which occurred in the evaluation of u^2 (cf. eq. [58]). We can therefore write (cf. eq. [59])

$$\overline{u u_\varphi} = 1 + 2\alpha^2 \int_0^\infty e^{-t} R(t)\, dt + \alpha^2 \int_0^\infty \int_0^\infty d\tau_1 d\tau_2 e^{-\tau_1-\tau_2} \int_0^{\tau_1}\int_0^{\tau_2} dt_1 dt_2 R(|t_1 - t_2|) , \tag{73}$$

where it should be noted that now

$$|t_1 - t_2| = \sqrt{(t_1^2 + t_2^2 - 2t_1 t_2 \cos\varphi)} . \tag{74}$$

However, in spite of this last circumstance, the sequence of transformations (60), except for the last line, applies as well to the quadruple integral in equation (73). Hence we may write

$$\overline{u u_\varphi} = 1 + 2\alpha^2 \int_0^\infty e^{-t} R(t)\, dt + 2\alpha^2 \int_0^\infty dt_1 e^{-t_1} \int_{t_1}^\infty dt_2 e^{-t_2} R(|t_1 - t_2|) . \tag{75}$$

Since (eq. [56])

$$\bar{u} = 1 + \alpha^2 \int_0^\infty e^{-t} R(t)\, dt , \tag{76}$$

we can combine equations (75) and (76) (in our present approximation) to give

$$\sigma_\varphi^2 = \frac{\overline{u u_\varphi}}{\bar{u}^2} - 1 = 2\alpha^2 \int_0^\infty dt_1 e^{-t_1} \int_{t_1}^\infty dt_2 e^{-t_2} R(|t_1 - t_2|) . \tag{77}$$

Now, letting

$$t = \sqrt{(t_1^2 + t_2^2 - 2t_1 t_2 \cos\varphi)} \tag{78}$$

as the variable of integration instead of t_2, we find

$$\sigma_\varphi^2 = 2\alpha^2 \int_0^\infty dt_1 \int_{2t_1 \sin(\varphi/2)}^\infty dt R(t) \exp\{-2t\cos^2\tfrac{1}{2}\varphi + \sqrt{(t^2 - t_1^2 \sin^2\varphi)}\} \times \frac{t}{\sqrt{(t^2 - t_1^2\sin^2\varphi)}} . \tag{79}$$

Inverting the order of the integrations and introducing in place of t_1 a new variable of integration, ψ, defined by the transformation

$$t \sin(\psi - \tfrac{1}{2}\varphi) = t_1 \sin\varphi\,, \tag{80}$$

we obtain, after some further reductions,

$$\sigma_\varphi^2 = \frac{2a^2}{\sin\varphi}\int_0^\infty dt t R(t) \int_{\varphi/2}^{\pi/2} d\psi \exp\left\{-t\frac{\sin\psi}{\sin\frac{1}{2}\varphi}\right\}. \tag{81}$$

Alternative forms of this formula are:

$$\sigma_\varphi^2 = \frac{a^2}{\epsilon\sqrt{(1-\epsilon^2)}}\int_0^\infty dt t R(t) \int_\epsilon^1 \frac{dy}{\sqrt{(1-y^2)}}\, e^{-ty/\epsilon} \tag{82}$$

$$= \frac{a^2}{\epsilon\sqrt{(1-\epsilon^2)}}\int_\epsilon^1 \frac{dy}{\sqrt{(1-y^2)}}\int_0^\infty dt t R(t)\, e^{-ty/\epsilon},$$

where

$$\epsilon = \sin\tfrac{1}{2}\varphi\,. \tag{83}$$

When $\varphi \to 0$,

$$\frac{2}{\sin\varphi}\int_{\varphi/2}^{\pi/2} d\psi \exp\left\{-t\frac{\sin\psi}{\sin\frac{1}{2}\varphi}\right\} \to \frac{2}{\varphi}\int_{\varphi/2}^\infty e^{-2t\psi/\varphi} d\psi = \frac{1}{t}\, e^{-t}; \tag{84}$$

and equation (81) reduces to

$$\sigma_0^2 = a^2\int_0^\infty e^{-t} R(t)\, dt\,, \tag{85}$$

in agreement with the result obtained in § 5 (eq. [62]). For $\varphi = \pi$ we can obtain a similar expression. For this purpose it is convenient to go back to equation (75), since, for $\varphi = \pi$, $|t_2 - t_1| = t_1 + t_2$, and the equation becomes

$$\sigma_\pi^2 = 2a^2\int_0^\infty dt_1 e^{-t_1}\int_{t_1}^\infty dt_2 e^{-t_2} R(t_2 + t_1)\,. \tag{86}$$

Letting $t = t_1 + t_2$ as the variable of integration in place of t_2 and inverting the order of the integrations, we have

$$\sigma_\pi^2 = 2a^2\int_0^\infty dt e^{-t} R(t)\int_0^{t/2} dt_1 = a^2\int_0^\infty e^{-t} t R(t)\, dt \simeq a^2\tau_0^2\int_0^\infty R(\xi)\,\xi\, d\xi\,. \tag{87}$$

Thus σ_π^2 is of a higher order of smallness than the quantities we have retained; accordingly, we must consider that it vanishes in the adopted scheme of approximation.

It does not appear that the integral over ψ in equation (81) (or over y in the first form of eq. [82]) can be evaluated or expressed in terms of known functions. It does not also appear that a series expansion having a useful range of validity can be developed for $\varphi \to 0$. This will become apparent when we obtain explicit expressions for σ_φ^2 for two special forms of $R(t)$. But some light may be thrown on this peculiar behavior of σ_φ^2 for $\varphi \to 0$ by the following analysis:

Considering the moment

$$\int_0^\pi \sigma_\varphi^2 \cos^2\tfrac{1}{2}\varphi d\varphi = 2a^2\int_0^\infty dt t R(t)\int_0^\pi d\varphi \frac{\cos^2\frac{1}{2}\varphi}{\sin\varphi}\int_{\varphi/2}^{\pi/2} d\psi \exp\left\{-t\frac{\sin\psi}{\sin\frac{1}{2}\varphi}\right\}, \tag{88}$$

we can carry out the integrations over ψ and φ. Thus

$$2\int_0^{\pi} d\varphi \frac{\cos^2 \frac{1}{2}\varphi}{\sin \varphi} \int_{\varphi/2}^{\pi/2} d\psi \exp\left\{ -t \frac{\sin \psi}{\sin \frac{1}{2}\varphi} \right\} = 2\int_0^1 \frac{dx}{x} \int_{\sin^{-1} x}^{\pi/2} d\psi \, e^{-t \sin\psi/x}$$

$$= 2\int_0^{\pi/2} d\psi \int_{\operatorname{cosec}\psi}^{\infty} \frac{dy}{y} \, e^{-ty \sin \psi} = \pi E_1(t), \tag{89}$$

where $E_1(t)$ denotes the first exponential integral. Thus

$$\int_0^{\pi} \sigma_\varphi^2 \cos^2 \tfrac{1}{2}\varphi \, d\varphi = \pi a^2 \int_0^{\infty} E_1(t) \, tR(t) \, dt$$

$$= \pi a^2 \tau_0^2 \int_0^{\infty} E_1(\xi \tau_0) \, \xi R(\xi) \, d\xi . \tag{90}$$

For $\tau_0 \ll 1$, we may use the expansion

$$E_1(x) = -\gamma - \log x + O(x) \qquad (\gamma = 0.5772\ldots), \tag{91}$$

for the exponential integral $E_1(\xi\tau_0)$ in equation (90). In this manner we obtain

$$\int_0^{\pi} \sigma_\varphi^2 \cos^2 \tfrac{1}{2}\varphi \, d\varphi \simeq \pi a^2 \tau_0^2 \left[-(\gamma + \log \tau_0) \int_0^{\infty} \xi R(\xi) \, d\xi - \int_0^{\infty} \xi R(\xi) \log \xi \, d\xi \right]. \tag{92}$$

The appearance of $\log \tau_0$ in the foregoing expression is a reflection of the singular behavior of σ_φ^2.

We shall now obtain explicit expressions for σ_φ^2 for two special forms of $R(t)$.

i) *The case* $R(\tau) = e^{-\tau/\tau_0}$.—For this case

$$\sigma_0^2 = a^2 \int_0^{\infty} \exp\left\{ -t\left(1 + \frac{1}{\tau_0}\right)\right\} dt = a^2 \frac{\tau_0}{1+\tau_0}, \tag{93}$$

and (cf. eq. [82])

$$\sigma_\varphi^2 = \frac{a^2}{\epsilon \sqrt{(1-\epsilon^2)}} \int_\epsilon^1 \frac{dy}{\sqrt{(1-y^2)}} \int_0^{\infty} dt\, t \exp\left\{ -t\left[\frac{1}{\tau_0} + \frac{y}{\epsilon} \right] \right\}, \tag{94}$$

or

$$\sigma_\varphi^2 = \frac{a^2 \epsilon \tau_0^2}{\sqrt{(1-\epsilon^2)}} \int_\epsilon^1 \frac{dy}{(\epsilon + \tau_0 y)^2 \sqrt{(1-y^2)}}, \tag{95}$$

where it may be recalled that $\epsilon = \sin \frac{1}{2}\varphi$.

The integral over y in equation (95) is an elementary one; and we must distinguish the three cases: $\epsilon < \tau_0$, $\epsilon = \tau_0$, and $\epsilon > \tau_0$. We find:

$$\frac{\sigma_0^2 - \sigma_\varphi^2}{a^2} = \frac{1}{3} \frac{\tau_0 (1 + 2\tau_0)}{(1+\tau_0)^2} \qquad (\gamma = 1)$$

$$= -\frac{\epsilon\gamma}{(1-\gamma^2)} \left[\frac{\gamma}{\epsilon + \gamma} + \frac{1}{\sqrt{[(1-\gamma^2)(1-\epsilon^2)]}} \log \frac{1 + \gamma\epsilon - \sqrt{[(1-\gamma^2)(1-\epsilon^2)]}}{\gamma + \epsilon} \right] \qquad (\gamma < 1) \tag{96}$$

$$= \frac{\epsilon\gamma}{(1-\gamma^2)} \left[\frac{\gamma}{\epsilon + \gamma} - \frac{1}{\sqrt{[(1-\gamma^2)(1-\epsilon^2)]}} \left\{ \frac{\pi}{2} - \sin^{-1} \frac{1 + \gamma\epsilon}{\gamma + \epsilon} \right\} \right] \qquad (\gamma > 1),$$

where

$$\gamma = \frac{\epsilon}{\tau_0} = \frac{1}{\tau_0} \sin \tfrac{1}{2}\varphi . \tag{97}$$

From the second of equations (96) we find that, for $\varphi \to 0$,

$$\frac{\sigma_0^2 - \sigma_\varphi^2}{a^2} \to -\epsilon\gamma\,[1 + \log \tfrac{1}{2}(\gamma + \epsilon)] \qquad (\epsilon,\ \gamma \to 0) \quad (98)$$

or

$$\frac{\sigma_0^2 - \sigma_\varphi^2}{a^2} \to -\frac{\varphi^2}{4\tau_0}\left[1 + \log \frac{\varphi}{4\tau_0}\right]. \quad (99)$$

Equation (99) should be contrasted with Ambarzumian's formula (69). However, since, for the validity of equation (99), not only φ but also φ/τ_0 should be small, it is evident that the equation has no useful range of applicability.

ii) *The case* $R(\tau) = e^{-\tau^2/\tau_0^2}$.—In this case

$$\sigma_0^2 = \tfrac{1}{2}\sqrt{\pi}\, a^2 e^{\tau_0^2/4}\tau_0\,[1 - \Phi(\tfrac{1}{2}\tau_0)], \quad (100)$$

where $\Phi(x)$ stands for the error function,

$$\Phi(x) = \frac{2}{\sqrt{\pi}}\int_0^x e^{-t^2} dt. \quad (101)$$

Next, starting from equation (77), we find that, for the case on hand, the expression for σ_φ^2 can be reduced to the form

$$\sigma_\varphi^2 = \tfrac{1}{2}\sqrt{\pi}\,\frac{a^2\tau_0^2}{\sin\frac{1}{2}\varphi}\, e^{\tau_0^2/4\sin^2(\varphi/2)} \int_{\tau_0/2\sin(\varphi/2)}^{\infty} d\,z\, e^{-z^2\cos^2(\varphi/2)}\,[1 - \Phi(z\sin\tfrac{1}{2}\varphi)], \quad (102)$$

or, alternatively,

$$\sigma_\varphi^2 = \sqrt{\pi}\,\frac{a^2\tau_0^2}{\sin\varphi}\, e^{\tau_0^2/4\sin^2(\varphi/2)} \int_{\tau_0\cot(\varphi/2)/2}^{\infty} dx\, e^{-x^2}\,[1 - \Phi(x\tan\tfrac{1}{2}\varphi)]. \quad (103)$$

We shall normally be interested only in values of $\varphi \leqslant 10°$. It appears that for such small angles we may obtain a satisfactory approximation for σ_φ^2 by using, for the error function in equation (103), the series expansion,

$$\Phi(x) = \frac{2}{\sqrt{\pi}}\left(x - \frac{x^3}{3} + \frac{x^5}{10} - \ldots\right) \qquad (x \to 0). \quad (104)$$

In this manner we find that

$$\frac{\sigma_\varphi^2}{a^2} = \frac{\pi\tau_0^2}{2\sin\varphi}\, e^{\tau_0^2/4\sin^2(\varphi/2)}\,[1 - \Phi(\tfrac{1}{2}\tau_0\cot\tfrac{1}{2}\varphi)] - \tfrac{1}{2}\tau_0^2 e^{\tau_0^2/4}. \quad (105)$$

Since we shall also be interested in angles $\varphi \geqslant \tau_0$, it is clear that we cannot use any series expansion for the error function in equation (105). In other words, in this case (as in the previous case) we cannot develop any useful series expansion for σ_φ^2. And the reason for this in both cases is that, for an expansion to be valid, not only φ but also φ/τ_0 should be small; and in practice the latter condition is not fulfilled.

Using equations (96) and (105), we have evaluated σ_φ^2 for a number of values τ_0.[13] The results of these calculations are illustrated in Figures 1*a* and 1*b*.

7. *The effect of the diffuse galactic light on the fluctuations in brightness of the Milky Way.*—The analysis in the preceding sections presupposes that the brightness of the Milky Way is due, in its entirety, to the light from the stars obscured by the distribution

[13] We are grateful to Miss Donna Elbert for assistance with these calculations.

of the interstellar matter. However, as was first clearly pointed out by C. T. Elvey and F. E. Roach,[14] the observed brightness is only in part due to the light from the stars, and an appreciable fraction of it must be ascribed to the scattering of the light of the stars by the interstellar matter: this is the so-called "galactic light." While, by a suitable observational technique,[15] the two contributory sources to the brightness of the Milky Way can be distinguished, the most extensive measures we have at the present time, namely, those due to Pannekoek,[16] do not distinguish between them. We shall now show how we can allow for this admixture of the diffuse galactic light in the observed brightness.

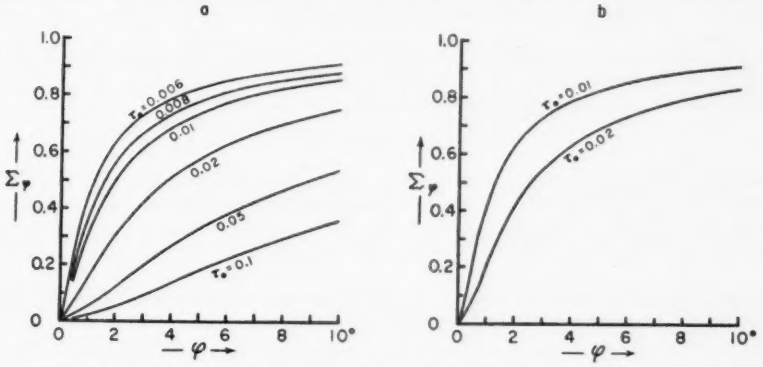

FIG. 1.—*a*, The normalized correlation function $\Sigma_\varphi = (\sigma_0^2 - \sigma_\varphi^2)/\sigma_0^2$ of the brightness in two directions making an angle φ with each other for the case $R(\tau) = e^{-\tau/\tau_0}$. The different curves are labeled by the values of τ_0 to which they refer. *b*, The normalized correlation function $\Sigma_\varphi = (\sigma_0^2 - \sigma_\varphi^2)/\sigma_0^2$ of the brightness in two directions making an angle φ with each other for the case $R(\tau) = e^{-\tau^2/\tau_0^2}$. The different curves are labeled by the values of τ_0 to which they refer. In comparing the two sets of curves in *a* and *b*, we should remember that, for equal values of τ_0, the equivalent optical thickness of a cloud on the assumption that $R(\tau) = e^{-\tau^2/\tau_0^2}$ is $\sqrt{\pi}/2 = 0.886$ times the value it has on the assumption that $R(\tau) = e^{-\tau/\tau_0}$ (cf. eq. [28]).

The contribution to the observed intensity, I, by the scattering of the light of the stars by the interstellar matter is given by

$$I_g = \int_0^\infty e^{-\tau(s)} \mathfrak{J}(s)\, d\tau(s), \tag{106}$$

where $\mathfrak{J}(s)$ denotes the source function for the galactic light. In extending the range of integration over $\tau(s)$ from zero to infinity, we are assuming, as in the preceding sections, that the system extends to infinity along the line of sight.

Now the source function $\mathfrak{J}(s)$ can be expressed in the form

$$\mathfrak{J}(s) = \int I(s, \boldsymbol{n})\, \Phi(\Theta)\, \frac{d\omega}{4\pi}, \tag{107}$$

where $I(s, \boldsymbol{n})$ is the *total* intensity (i.e., the intensity of the light from the stars plus the intensity of the diffuse galactic light) at s in the direction specified by a unit vector $\boldsymbol{n}$; Θ is the angle which the line of sight makes with the direction of $\boldsymbol{n}$; and $\Phi(\Theta)$ is the

[14] *Ap. J.*, **85**, 213, 1937.

[15] Cf. L. G. Henyey and J. L. Greenstein, *Ap. J.*, **93**, 70, 1941.

[16] *Pub. Astr. Inst. Amsterdam*, No. 3, 1933, and No. 9, 1949.

phase function governing the scattering process. In equation (107) the integration is extended over all solid angles.

For a statistically uniform distribution of matter, $\mathfrak{J}(s)$ can vary from point to point only on account of the fluctuations in $I(s, \boldsymbol{n})$. But, since $I(s, \boldsymbol{n})$ is averaged over all directions $\boldsymbol{n}$ and since, as we shall see in § 8, the correlations in the intensities in neighboring directions decreases extremely rapidly, it is evident that, to a high degree of approximation, we may ignore the statistical fluctuations in $\mathfrak{J}(s)$ and write

$$\mathfrak{J}(s) = \bar{I}\int \Phi(\Theta)\frac{d\omega}{4\pi} = \varpi_0 \bar{I}\,, \tag{108}$$

where $\bar{I}$ is the total mean intensity prevailing at any point in the system and ϖ_0 is the albedo of the interstellar particles for single scattering.

With $\mathfrak{J}(s)$ given by equation (108), equation (106) becomes

$$I_g = \varpi_0 \bar{I}\,. \tag{109}$$

According to this equation, the contribution to the observed brightness of the Milky Way near the galactic plane by the diffuse galactic light is a constant. This is in accord with the indications from observations[17] that there is no pronounced correlation between the intensity of the diffuse galactic light and the total brightness of the Milky Way.

Letting $\bar{I}_s$ denote the mean intensity of the light from the stars prevailing at any point in the system, we can rewrite equation (109) in the form

$$I_g = \bar{I}_g = \varpi_0 (\bar{I}_s + \bar{I}_g)\,, \tag{110}$$

or

$$I_g = \frac{\varpi_0}{1-\varpi_0}\,\bar{I}_s \quad \text{and} \quad \bar{I} = \frac{\bar{I}_s}{1-\varpi_0}\,. \tag{111}$$

Since I_g is a constant, the angular correlation, II_φ, in the total brightness in two directions making an angle φ to each other can be readily found. Thus,

$$\begin{aligned} \overline{II}_\varphi &= \overline{(I_s + I_g)(I_{s,\varphi} + I_g)} \\ &= \overline{I_s I_{s,\varphi}} + 2\bar{I}_s I_g + I_g^2\,; \end{aligned} \tag{112}$$

or, substituting for I_g from equation (111), we have

$$\overline{II}_\varphi = \overline{I_s I_{s,\varphi}} + \left[\frac{\varpi_0^2}{(1-\varpi_0)^2} + 2\,\frac{\varpi_0}{1-\varpi_0}\right]\bar{I}_s^2. \tag{113}$$

An alternative form of this equation is

$$\frac{\overline{I_s I_{s,\varphi}}}{\bar{I}_s^2} - 1 = \frac{\overline{II}_\varphi}{\bar{I}_s^2} - \left[\frac{\varpi_0^2}{(1-\varpi_0)^2} + 2\,\frac{\varpi_0}{1-\varpi_0} + 1\right] \tag{114}$$

or

$$\frac{\overline{I_s I_{s,\varphi}}}{\bar{I}_s^2} - 1 = \frac{\overline{II}_\varphi}{\bar{I}_s^2} - \frac{1}{(1-\varpi_0)^2}\,. \tag{115}$$

Since $\bar{I}_s = (1-\varpi_0)\bar{I}$ (cf. eq. [111]), we can also write

$$\frac{\overline{I_s I_{s,\varphi}}}{\bar{I}_s^2} - 1 = \frac{1}{(1-\varpi_0)^2}\left(\frac{\overline{II}_\varphi}{\bar{I}^2} - 1\right). \tag{116}$$

[17] Cf. Elvey and Roach, *op. cit.*, esp. Table 3, p. 238.

The quantity on the left-hand side of equation (116) can clearly be identified with σ_φ^2 of § 6 (cf. eq.[77]). And, if

$$s_\varphi^2 = \frac{\overline{I I_\varphi}}{\bar{I}^2} - 1 \tag{117}$$

represents the corresponding angular correlation in the total brightness, then it follows from equation (116) that

$$\sigma_\varphi^2 = \frac{s_\varphi^2}{(1-\varpi_0)^2}. \tag{118}$$[18]

In particular, for $\varphi = 0$ we have (cf. eq. [116])

$$\sigma_0^2 = \frac{\overline{I_s^2}}{\bar{I}_s^2} - 1 = \frac{s_0^2}{(1-\varpi_0)^2} = \frac{1}{(1-\varpi_0)^2}\left(\frac{\overline{I^2}}{\bar{I}^2} - 1\right). \tag{119}$$

From equations (118) and (119) we obtain

$$\frac{\sigma_0^2 - \sigma_\varphi^2}{\sigma_0^2} = \frac{s_0^2 - s_\varphi^2}{s_0^2} \qquad (= \Sigma_\varphi \text{ say}). \tag{120}$$

Equation (120) shows that, if the angular correlations in the total brightness are discussed in terms of the "normalized" quantity on the right-hand side, we can apply the theory of § 6 as though no galactic light were present.

8. *An analysis of the observed fluctuations in the surface brightness of the Milky Way.*— We shall now show how the theory of the preceding sections can be used to interpret the observed fluctuations in the surface brightness of the Milky Way. For this purpose we shall use the results of Pannekoek's recent survey of the southern Milky Way.[19]

It may be recalled that the observational material which formed the basis of Pannekoek's survey was a number of photographic plates taken extra-focally through a short-focus camera. The intensities measured on these plates do not, therefore, distinguish between the light of the stars and the diffuse galactic light. We must accordingly allow for this in the manner described in § 7.

Pannekoek expressed his measured brightness in the unit of one star of photographic magnitude 10 per square degree, and he presented the results of his survey in a series of beautiful charts of isophotes for the various regions. Using these charts, we can read, sufficiently accurately for our purposes, the intensities along any curve we may draw through the regions covered by the survey.

In selecting the regions for our analysis, we have tried to avoid regions which are either heavily obscured (like the region in Taurus) or which contain pronounced associations of very bright stars (such as the regions in η Carinae or near P Cygni). With these criteria in mind, the following regions were finally chosen:

Region I: $280° < l < 340°$ $(|b| \leqslant 2°)$

and (121)

Region II: $170° < l < 245°$ $(-2° \leqslant b \leqslant 0°)$.

The intensities in these regions along several parallel arcs of constant galactic latitude (b) and separated by $\frac{1}{2}°$ in b were read from Pannekoek's charts and plotted as curves

[18] A relation essentially equivalent to this was also established by Rusakov (*op. cit.*) in his analysis of the angular correlations in the brightness of the Milky Way in terms of Ambarzumian's formula (69).

[19] A. Pannekoek and D. Koelbloed, *Pub. Astr. Inst. Amsterdam*, No. 9, 1949.

against the galactic longitude (l). These curves were later approximated by step functions, in which the intensity (rounded to 5 whole units) was constant over successive intervals of $\frac{1}{2}°$ in galactic longitude. Fourteen such graphs were made (nine for region I and five for region II); a selection from these is illustrated in Figures 2 and 3.

Now the averages to which the formulae of the preceding sections apply are strictly averages over all possible complexions of the distribution of the interstellar matter. We

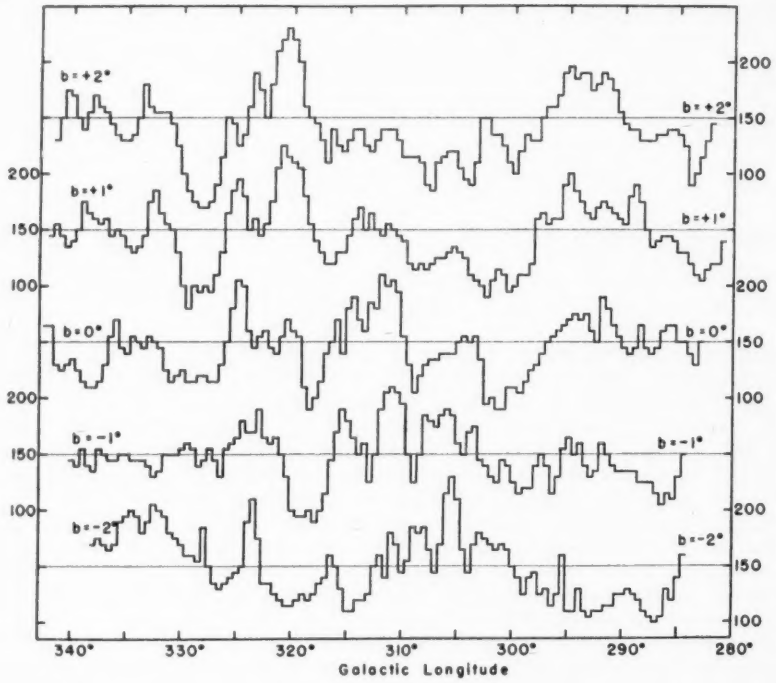

FIG. 2.—The dependence on galactic longitude of the surface brightness of the Milky Way, along arcs of constant galactic latitude b and in region I ($280° < l < 340°$; $|b| < 2°$) as read from Pannekoek's charts. The ordinates represent the intensity in the unit: brightness of one star of photographic magnitude 10 per square degree. The origin of the scale of brightness for each arc is indicated by a horizontal line at intensity 150; the values of b to which the various curves refer are also indicated.

shall suppose that we are substantially averaging over all possible complexions when we take means along various arcs of constant galactic latitude. If the available sample is sufficiently large, this will be a valid procedure; but, unfortunately, this is not the case, and this must be kept in mind when comparing the observations with the theory.

On the assumption made in the foregoing paragraph, we can write

$$\overline{II}_\varphi = \frac{1}{l_1 - l_2 + \varphi} \int_{l_2-\varphi}^{l_1} I_l I_{l+\varphi} dl\,, \tag{122}$$

where l_1 and l_2 are the limits in galactic longitude of the arc considered. When the intensity-curves are drawn as step functions (as in Figs. 3 and 4), the integral giving II_φ can be replaced by a corresponding sum. (It may be stated here that, in order to minimize

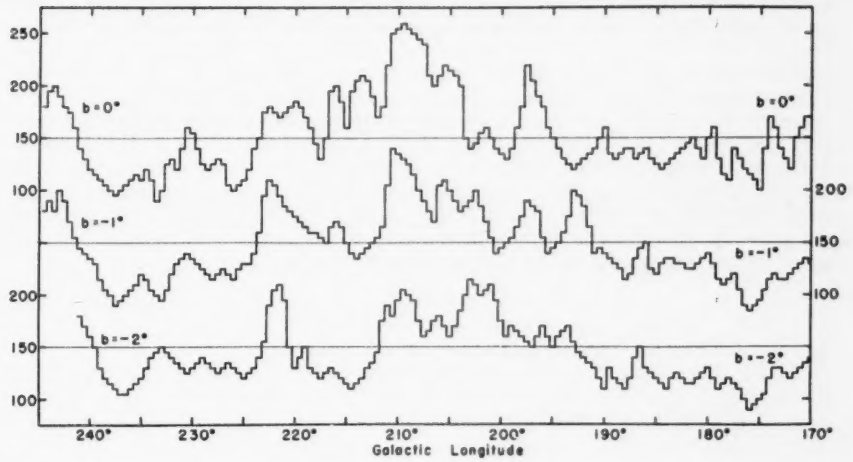

FIG. 3.—The dependence on galactic longitude of the surface brightness of the Milky Way, along arcs of constant galactic latitude b in region II ($170° < l < 245°$; $0° < b \leqslant -2°$). Otherwise the legend for Figure 2 applies to this figure also.

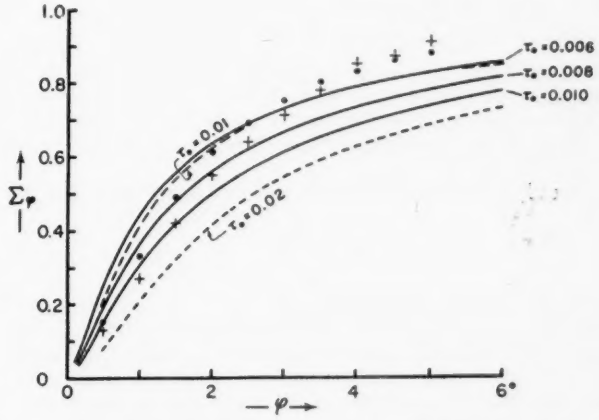

FIG. 4.—The normalized correlation function, $\Sigma_\varphi = (\sigma_0^2 - \sigma_\varphi^2)/\sigma_0^2 = (s_0^2 - s_\varphi^2)/s_0^2$, of the brightness of the Milky Way, as derived from observations in regions I (*dots*) and II (*crosses*). The curves represent the predicted dependence of Σ_φ on φ, for the various values of τ_0; the full-line curves are derived for the correlation function $R = e^{-\tau/\tau_0}$ (cf. Fig. 1, *a*), while the dashed curves are derived for $R = e^{-\tau^2/\tau_0^2}$ (cf. Fig. 1, *b*).

the effects of incomplete "waves" in the fluctuations, the limits in galactic longitudes were so chosen that I_{l_1} and I_{l_2} were in the neighborhood of $\bar{I}$.) In this manner the various quantities which occur in the definition of s_φ^2 (eq. [117]) were determined for each arc separately; they were then combined to give average values for the two regions (eq. [121]) considered. The final results of this analysis are summarized in Table 1.

It will be noticed that we have not determined the angular correlations for φ's exceeding 5°. The reason for this restriction was that it appeared that, for $\varphi > 5°$, the uncertainties resulting from the small size of the available sample became very appreciable. Indeed, the derived values of s_φ^2 are increasingly affected by sampling errors as φ increases. Nevertheless, the fact that at $\varphi = 5°$ all the calculations consistently gave, for $\Sigma_\varphi = (s_0^2 - s_\varphi^2)/s_0^2$, values in the neighborhood of 10 per cent would indicate that the derived run of this quantity for $\varphi \leqslant 5°$ is probably reliable.

TABLE 1

ANGULAR CORRELATIONS OF THE BRIGHTNESS OBSERVED IN SELECTED REGIONS OF THE MILKY WAY

φ	Region I: 280°<l<340°		Region II: 170°<l<245°		φ	Region I: 280°<l<340°		Region II: 170°<l<245°	
	s_φ^2	Σ_φ	s_φ^2	Σ_φ		s_φ^2	Σ_φ	s_φ^2	Σ_φ
0.0°	0.0381	0	0.0582	0	3.0°	0.0096	0.75	0.0169	0.71
0.5	.0325	0.15	.0508	0.13	3.5	.0076	.80	.0127	.78
1.0	.0255	.33	.0423	.27	4.0	.0063	.83	.0085	.85
1.5	.0195	.49	.0339	.42	4.5	.0054	.86	.0063	.89
2.0	.0148	.61	.0264	.55	5.0	0.0048	0.88	0.0053	0.91
2.5	0.0119	0.69	0.0212	0.64					

We should state here that the angular correlations we have derived do not agree very well with the correlations derived similarly by Rusakov for two regions in the northern Milky Way. It is possible that this discrepancy is due to the larger sampling errors in Rusakov's calculations, since he restricted himself to regions with extensions in galactic longitude even less than 25°.

As we have already remarked (cf. eq. [120]), the deduced values of

$$\Sigma_\varphi = \frac{s_0^2 - s_\varphi^2}{s_0^2} \tag{123}$$

can be compared directly with the predictions for $(\sigma_0^2 - \sigma_\varphi^2)/\sigma_0^2$ based on equation (77). It is evident that, in principle, the run of Σ_φ should give us detailed information concerning the correlation function $R(\tau/\tau_0)$. However, in view of the observational uncertainties in the deduced values of Σ_φ, it does not seem that at the present time anything more than the order of magnitude of the micro-scale, τ_0, can be derived. For this purpose it would clearly be sufficient to compare the observed run of Σ_φ with the theoretical curves derived on the two special forms of $R(\tau/\tau_0)$ considered in § 6. This comparison is made in Figure 4. From an examination of this figure, it appears that

$$\tau_0 \simeq 0.01 \ . \tag{124}$$

Returning to the absolute value of $s_0^2 (= I^2/\bar{I}^2 - 1)$, we may first observe that for $\tau_0 \simeq 0.01$ the approximation provided by equation (65) is amply sufficient and that, therefore (cf. eq. [119]),

$$s_0^2 = (1 - \varpi_0)^2 \sigma_0^2 = (1 - \varpi_0)^2 a^2 \tau_0 R_0 \ . \tag{125}$$

Since we may expect that $R_0 \sim 1$, we can write

$$a^2 \simeq \frac{s_0^2}{\tau_0 (1 - \varpi_0)^2} . \tag{126}$$

The albedo ϖ_0 of the interstellar particles is not known with any degree of precision. However, for the sake of definiteness, we shall assume that[15]

$$\varpi_0 = 0.4 . \tag{127}$$

According to Table 1, $s_0^2 \simeq 0.04$ in region I and $s_0^2 \simeq 0.06$ in region II. With these values of s_0^2 and τ_0 and ϖ_0 given by equations (124) and (127), we find that

$$a^2 \simeq 11 \text{ (region I)} \qquad \text{and} \qquad a^2 \simeq 16 \text{ (region II)} . \tag{128}$$

Since $a^2 \simeq \overline{\delta^2 \rho} / \bar{\rho}^2$ (cf. eq. [25]), the foregoing values of a^2 imply that

$$\sqrt{(\overline{\delta^2 \rho})} \simeq 3.3 \bar{\rho} \text{ (region I)} \qquad \text{and} \qquad \sqrt{(\overline{\delta^2 \rho})} \simeq 4 \bar{\rho} \text{ (region II)} . \tag{129}$$

The fact that the root mean square of the fluctuations in the density derived in this manner is of the order of three to four times the mean density itself may be taken as a quantitative confirmation of the conspicuously nonuniform distribution of the interstellar matter.

THE FORMS, ORIENTATIONS, AND MASSES OF GLOBULAR CLUSTERS

HUGH M. JOHNSON
Yerkes Observatory
Received July 3, 1951

ABSTRACT

Shapley's data on the apparent forms and orientations of globular clusters are used to test two new hypotheses about their spatial forms and orientations. The hypothesis that the equatorial planes of globular clusters pass through the galactic center is shown to be consistent with the observations, and a physical interpretation is suggested. Cluster masses $\geqslant 4 \times 10^6 \odot$ are also derived.

Globular clusters are not usually projected as circular images. This can be verified in three ways: by direct eye estimates on small-scale plates;[1] by counts of stars in sectors of a cluster;[2,3] and by photometry.[4] Some clusters are definitely asymmetric, but most are sensibly elliptical. The question arises as to whether the inferred spatial orientations are random or not. Shapley[2] has shown that his orientation data are not consistent with hypothesis A, that the clusters are oblate spheroids with axes perpendicular to the plane of the galaxy. In this paper the writer shows that one of two other hypotheses—B and C—may explain both forms and orientations of globular clusters.

Two quantities are usually derived from the observed projections: ellipse ratio,[5] $\mathfrak{E}$, here defined as ten times the ratio of apparent minor and major axes, and the orientation,[6] Ω, of the major axis. The determination of Ω becomes very uncertain for $\mathfrak{E} > 8$. The difference between the Ω's of two series of estimates[1] by Shapley and his colleagues averaged about 30°. The errors in $\mathfrak{E}$ are not so large, but it is known that $\mathfrak{E}$ depends on the distance from the center of the cluster.[2,4,7,8] Table 1 gives the number, $N(\mathfrak{E})$, of globular clusters in our galaxy which Shapley[2] finds in each $\mathfrak{E}$ class (omitting the galactic clusters[9] NGC 6235 and NGC 6535) and the number, $N(\Omega)$, therein for which Ω is assigned. These data are used to test the following new hypotheses:

TABLE 1

SHAPLEY'S GLOBULAR-CLUSTER DATA

$\mathfrak{E}$	6	7	8	9	9.5	10	Unmeasured	Totals
$N(\mathfrak{E})$	1	0	22	39	8	4	17	91
$N(\Omega)$	1	0	22	12	1	0	0	36

[1] H. Shapley and H. B. Sawyer, *Harvard Bull.*, No. 852, 1927.

[2] H. Shapley, *Star Clusters* (New York: McGraw-Hill Book Co., 1930).

[3] H. Shapley, *Handbuch der Astrophysik* (Berlin: Julius Springer, 1933), Vol. **5**, Pt. 2.

[4] J. Schilt, *A.J.*, **38**, 109, 1928.

[5] Although Shapley calls this quantity "ellipticity" (E), it will be less confusing to reserve that term for its more widely used meaning.

[6] Shapley's term for the angle the major axis makes with galactic east, measured positive through the south.

[7] J. L. Greenstein, *Ap. J.*, **90**, 387, 1939.

[8] H. Shapley and A. R. Sayer, *Proc. Nat. Acad. Sci.*, **21**, 593, 1935.

[9] N. U. Mayall, *Ap. J.*, **104**, 290, 1946.

B. The clusters are prolate spheroids with axes directed toward the galactic center (as though tidally distorted without a lag).

C. The clusters are oblate spheroids with equatorial planes containing the galactic center (a physical reason for which is added later).

Hypothesis B is discussed first. A necessary, but not sufficient, verification of the hypothesis is that the apparent major axis of a cluster is directed toward the galactic center; the angle i, defined as the absolute difference between the orientation of the apparent major axis and the direction to the galactic center, would be $i = 0°$ except for observational errors in Ω. Values of i were computed from Ω, assuming the galactic center at $l = 325°$. If the entire range $0° \leq i \leq 90°$ is divided into two, three, and four equal intervals, respectively, the numbers of clusters falling in each interval, beginning with the one nearest $i = 0°$, have the ratios 18:18, 14:5:17, and 9:9:7:11. These ratios imply that cluster frequencies according to smaller subdivisions of the range of i than the two, $0° \leq i \leq 45°$ and $45° < i \leq 90°$, have little meaning. Columns 1-4 of Table 2 detail the

TABLE 2

DISTRIBUTION OF THE INCLINATION TO THE GALACTIC CENTER OF ELLIPTICAL CLUSTERS

i (1)	$N(\mathfrak{E} \leq 8)$ (2)	$N(\mathfrak{E} \geq 9)$ (3)	N (4)	N' (5)	N_B (6)	N_C (7)	N_C' (8)
0°–45°	11	7	18	36	54	44	36
45°–90°	12	6	18	34	16	26	34
Totals	23	13	36	70	70	70	70

above results. In column 5 we try to correct the frequencies N for the lack of 34 $N(\Omega)$ data among 47 $N(\mathfrak{E} = 9$ or $9.5)$ data by assuming that the distribution of the missing clusters is the same as that of those appearing. Thus $N' = N(\mathfrak{E} \leq 8) + 47\ N(\mathfrak{E} \geq 9)/13$. The observational selection appears to have had no important effect. For comparison with N' we compute in column 6 the number N_B expected in each i-interval on the basis of the normal law of errors and probable error of 25° from $i = 0°$. Since observational errors in i cannot exceed 90°, the normal law is, at least in this respect, inappropriate here. However, for the adopted probable error, only 2 per cent of the predicted errors exceed 90°. The figures of column 6 are not compatible with those of column 5, so hypothesis B is not supported.

In a further test of hypothesis B we compute the ratio $(b/a)_p$ of real minor and major axes of the prolate spheroid from the observed $\mathfrak{E}$. It can be shown that

$$\left(\frac{b}{a}\right)_p = \left(\frac{\mathfrak{E}}{10}\right) \sin\phi \left[1 - \left(\frac{\mathfrak{E}}{10}\right)^2 \cos^2\phi\right]^{-1/2}, \tag{1}$$

where ϕ is the angle between the major axis of the spheroid and the line of sight or between the galactic center, G, and the sun, S, at the cluster C (see Fig. 1). To compute ϕ, we must know the distances SG and SC and the included angle, $\widehat{GSC}$. $SG \simeq 10$ kpc from globular-cluster data, according to Stebbins and Whitford;[10] and SC, the distance to a cluster, is known accurately[11] for only 31 clusters, of which 24 are clusters of known $\mathfrak{E}$-value. Figure 2 is a plot of $(b/a)_p$, according to equation (1), versus GC or r for these 24.

If we assume that the galactic nucleus is a point mass of $10^{11}\odot$ and assume a certain

[10] *Ap. J.*, **84**, 132, 1936.

[11] H. Shapley, *Pop. Astr.*, **57**, 203, 1949.

density distribution for globular clusters, we may compute their tidal distortion. There are reasons to believe that a polytrope of index $n \simeq 5$ is the simplest model of an observably bounded cluster to which an equilibrium tidal theory is applicable. From an equation given by Chandrasekhar[12] it can be shown that

$$\left(\frac{b}{a}\right)_p \simeq (1 + 1.5 \times 10^{11} \mathfrak{M}^{-1} R^3 r^{-3})^{-1} = (1 + 3.6 \times 10^{10} \mu^{-1} r^{-3})^{-1}, \qquad (2)$$

where the mass of the secondary body distorting the polytrope of mass $\mathfrak{M}$ has been set equal to the adopted mass of the galactic nucleus in suns; R and r are, respectively, the

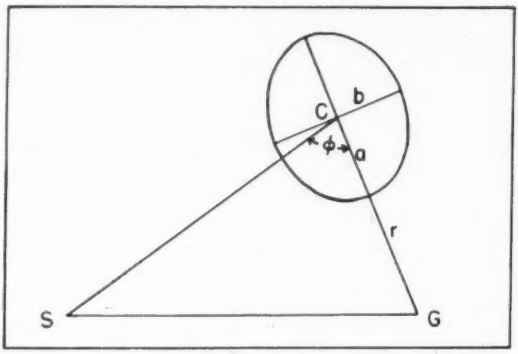

FIG. 1.—Diagram relating S, the sun; G, the galactic center; and C, the cluster center to ϕ, r, and the cluster spheroid axes a and b. For hypothesis B, $b/a = (b/a)_p$; for hypothesis C, $b/a = (b/a)_0$ (with $\psi = 90°$).

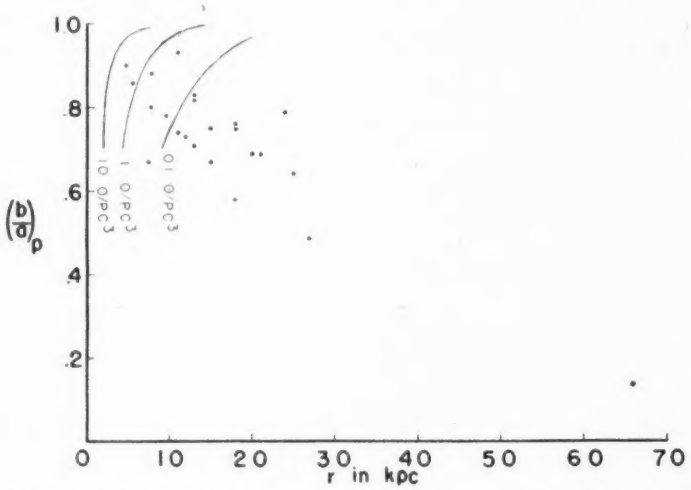

FIG. 2.—Theoretical tidal curves for different cluster densities are shown, with observed data reduced according to hypothesis B.

[12] *M.N.*, **93**, 456, eq. (41), 1933.

cluster radius and distance from the galactic nucleus in parsecs; and μ is the mean density of a cluster in $\odot/\text{psc}^3$. In Figure 2 we graph relation (2) for $\mu = 0.1$, 1, and $10\odot/\text{psc}^3$. The data extend far below a reasonable lower limit of μ. The trend toward smaller $(b/a)_p$ for large r is to be expected if $\mathfrak{E}$ is actually independent of r, since large r implies small ϕ and small ϕ in equation (1) implies strong reduction from $\mathfrak{E}/10$ to $(b/a)_p$.

However, a lower limit to the mass of a globular cluster can be derived from these data. Of the 31 clusters for which r can be found accurately, the smallest $r \simeq 5$ kpc. From the preceding paragraph we conclude that tides at 5 kpc contribute only partially to the distortion $(b/a)_p \simeq 0.9$ of a cluster (average photographic radius $R = 12$ psc). A similar conclusion can be made about the densitometric data of Shapley and Sayer,[8] where, however, the average densitometric radius $R = 32$ psc. Setting $(b/a)_p \geq 0.9$ and $R/r = 32/5000$ in equation (2), we find $\mathfrak{M} \geq 4 \times 10^5\odot$.

Hypothesis C is discussed next. Although a lower limit to cluster masses can be derived from hypothesis B, it fails to account for Shapley's data. In Figure 3 we plot $\mathfrak{E}$ versus ϕ, again for the 24 clusters for which ϕ is known. It is clear that, for an oblate spheroid defined by the ratio of axes $(b/a)_0$ and for ϕ near 90°, we have $10 \geq \mathfrak{E} \geq 10$

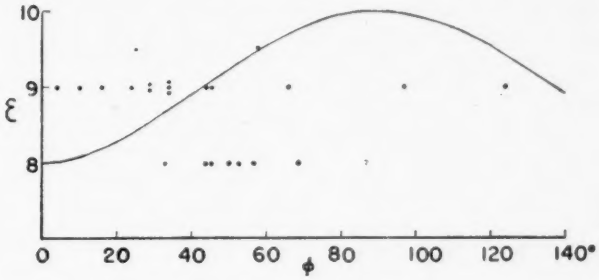

FIG. 3.—A curve of the upper limit of $\mathfrak{E}$, using $(b/a)_0 = 0.8$ in hypothesis C, is shown with observed data.

$(b/a)_0$, the value of $\mathfrak{E}$ depending on ψ, the unknown inclination of the equator of the cluster to the *GCS* plane. But for ϕ near 0° or 180°, $\mathfrak{E} \simeq 10\,(b/a)_0$. We assume for the moment that all clusters have some common $(b/a)_0 \simeq 0.8$, suggested by the apparent limit of $\mathfrak{E} \geq 8$ of all but one cluster. From the equation

$$\mathfrak{E} = 10\left[\sin^2\phi + \left(\frac{b}{a}\right)_0^2 \cos^2\phi\right]^{1/2} \tag{3}$$

we obtain the curve in Figure 3 which shows the upper limit of $\mathfrak{E}$, using $(b/a)_0 = 0.8$. Since 10 of the 24 clusters fall above the curve, we have to conclude that the assumption of a common $(b/a)_0$ is incorrect if hypothesis C is tenable.

Even if $(b/a)_0$ has a range of values, the observed values of the angle i may support hypothesis C. To check this, we compute a theoretical frequency function in i on the assumption that ψ varies randomly. It can be shown that $\tan i = \cos\phi \tan\psi$. If $N(\psi)d\psi$ is the number of spheroids with ψ between ψ and $\psi + d\psi$, and $N(i)di$ is the number of images with i between i and $i + di$, then the predicted number, N_C, of clusters between the limits j and k of i is

$$N_C = \int_j^k N\,(i)\,di = \text{const.} \sum_{l=1}^{n} \int_j^k \frac{di}{|\cos_l\phi|\cos^2 i + |\sec_l\phi|\sin^2 i}, \tag{4}$$

where $N(\psi)$ is a constant, since ψ is random. The averaging in equation (4) should be done with respect to the 70 clusters of column 5 of Table 2, but ϕ is actually known for only $n = 24$ of them. In order to compare the observed N' of the 70 clusters with N_c we assume that the distribution in ϕ is the same for the 70 as for the 24. We then get the frequencies shown in column 7 of Table 2. The sensitivity of the ratio of frequencies in the two i-intervals is such that, if, in place of 10 kpc, a distance of 8 kpc to the galactic center is used in the solutions for ϕ, the ratio would be 41:29. Finally, the adopted ratio will not express the frequencies actually expected under hypothesis C if account is taken of the different probable error which should affect Ω in the two i-intervals. For the average of $\mathfrak{E}$ over all ψ would be largest at $\phi = 90°$ where $i = 0°$, so that the greater errors in Ω should attend the images of $i = 0°$–$45°$ because they average rounder than those of $i = 45°$–$90°$. N_C can thus be transformed into a predicted N_C'—column 8 of Table 2—which agrees with the observed N' by making an approximate computation which assumes the normal law of errors and reasonable probable errors of 30° and 20° in the i-intervals 0°–45° and 45°–90°, respectively. More clusters are thrown from the former to the latter than are returned to it in the same way by errors. This indicates that hypothesis C is consistent with Shapley's data. On the other hand, it is also clear that a random distribution of i is consistent with the observations. As an observer approaches the galactic center, ϕ identically approaches zero and ψ approaches i, losing for him the observable distinction between a random orientation of clusters and the scheme of hypothesis C. Even at 10 kpc the distinction is not clear cut.

We conclude that globular clusters may, but need not, be a system of spheroids with an oblateness different from cluster to cluster and with equatorial planes passing through the galactic center. The indicated system becomes physically plausible if cluster equatorial planes coincide with orbital planes and the orbits are highly eccentric, so that the distortion might arise from interaction with the galactic nucleus during passages[13] of perigalacticon. To support this physical hypothesis, it must be shown that globular-cluster orbits are eccentric rather than circular, as found by Edmondson[14] sixteen years ago.

I wish to thank Dr. Thornton Page for advice in the preparation of this paper.

[13] NGC 2419 (for which $\mathfrak{E} = 9$, $r = 66$ kpc) can hardly have made more than one passage in 3×10^9 years.

[14] *A.J.*, **45**, 1, 1935.

NOTES

A STUDY OF LOW-DISPERSION SPECTRA OF M STARS IN THE RED REGION

In connection with the program of establishing spectral and luminosity characteristics of stars for objective-prism Schmidt cameras similar to that of the Warner and Swasey Observatory, it was suggested to the authors by Dr. J. J. Nassau that the red part of the spectra of M stars might be adequate for determinations of spectral types and luminosity.

For this purpose, sixteen standard M stars, consisting of a selection of both giants and dwarfs (Table 1), were photographed with the 4° objective-prism camera and Wratten

TABLE 1

STANDARD STARS

BD	m_v	Sp. Mt. W.	M_v 1935	$a-A$	$b-B$	$c-C$	$d-c$	Wt.
+57° 1359	6.5	K5	+ 0.1	0^{m}00	0^{m}20	−0^{m}11	+0^{m}10	2
+11 3008	4.9	M0	0.0	.02	.15	− .11	+ .03	2
+55 1625	4.8	M2	0.0	.11	.27	+ .02	+ .06	2
+57 1373	6.0	M3	+ 0.2	.15	.35	− .05	+ .07	2
+30 2217	7.7	M5	− 0.1	.19	.49	+ .25	− .08	1
+ 4 2729	8.8	K5	+ 6.4	.03	.10	− .09	+ .08	2
+ 1 3071	8.7	K5	+ 6.2	.02	.10	− .09	+ .10	2
− 3 3746	9.6	M0	+ 8.2	.04	.12	− .07	+ .11	1
− 4 4225	7.9	M0	+ 7.8	.07	.18	− .14	+ .06	2
+50 1725	6.8	M0	+ 8.3	.08	.19	.....	.....	1
+ 9 2636	8.8	M1	+ 8.6	.07	.19	− .05	+ .10	2
− 4 2226	10.0	M3	+ 9.9	.17	.38	− .04	+ .12	2
+43 2796	10.3	M3	+ 9.5	.20	.40	+ .06	+ .18	2
− 8 4352	9.6	M3e	+10.3	.19	.34	+ .10	+ .14	2
− 7 4003	10.6	M5	+11.0	.25	.38	+ .10	+ .16	1
−12 4523	10.0	M5	+11.0	0.24	0.32	+0.15	+0.15	1

No. 22 filter with Eastman 103-F plates. The above arrangement records the spectral range 5500–7000 A in the interval of 1.5 mm on the plates; this gives a mean dispersion of approximately 1000 A/mm.

All the M-type spectra present on the plates were registered on a recording microphotometer, and the registered curves were converted into schematic energy-curves with the aid of density scales made with the sensitometer of the Warner and Swasey Observatory. The sensitometer plates were taken from the same box, exposed through the same filter in a comparable exposure time, and developed together with the star plates. Though this method of calibration does not warrant the highest degree of photometric precision for objective-prism spectra, it was considered to be adequate for the present investigation and permits a rough quantitative test to be made of the features observed. The resulting energy-curve of each star was derived as the mean of at least two widened exposures of the same plate. The internal agreement of two exposures is very good for well-exposed spectra.

A representative energy-curve is illustrated in Figure 1. It is dominated by the bands of the Dunér II λ 6150 and Dunér III λ 5840 systems, which are probably due to the *TiO* molecule; the bands appear at M0 and increase in intensity with advancing spectral type. They are complicated by a broad depression of the sensitivity-curve of the plate in

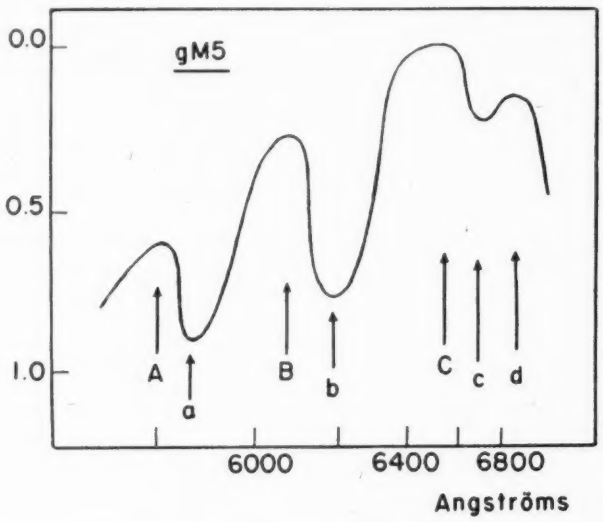

FIG. 1.—A typical schematic energy-curve, showing the points in the spectrum where density measures were made. The intensity scale is in arbitrary logarithmic units.

TABLE 2

DESIGNATIONS OF STANDARD FEATURES AND SPECTRAL REGIONS

Feature or Region	λ	Principal Contributor	Feature or Region	λ	Principal Contributor
a	5860	D lines	*A*	5780–5810	Continuous spectrum
b	6200	*TiO*	*B*	6050	Continuous spectrum
c	6700	*TiO*	*C*	6550	Continuous spectrum
d	6830	*CaH*			

the neighborhood of λ 6400; in order to separate these effects, the energy-curve of an A-type star has been used for comparison.

An inspection of the energy-curves permitted the establishment of the characteristic features which vary with spectral class and luminosity; these features are compared with adjacent regions of the spectrum. The sensitive features, together with the near-by spectral regions used as standards, are given in Table 2. The relative intensities at these points, expressed in difference in magnitude, are given in Table 1.

An interpretation of the effects thus found was attempted in terms of published in-

vestigations of the following: P. W. Merrill,[1] Y. Öhman,[2, 3] W. W. Morgan,[4] and G. P. Kuiper.[5] The results of the examination are discussed below.

Characteristics of spectral type.—The depression at *b* may serve as a criterion of spectral type, for both giants and dwarfs. If the spectral types of the Mount Wilson[6] determinations are taken as standards (the latter are based on the blue-green *TiO* bands), we obtain an increase of the *b* depression with advancing spectral type; this feature first appears at class M0. There are no distinct differences between giants and dwarfs, except at the two ends of the spectral range available for the dwarfs (K5 and M5), where a slight positive luminosity effect seems to be present. With regard to the end toward earlier types (K5–M1), this effect is in agreement with the fact that Morgan's[4] and Kuiper's[5] classifications, which are based on red *TiO* bands, are systematically earlier for K5–M2 dwarfs than those of Mount Wilson. For the latest types (>M5), they found an opposite effect. Figure 2, *a*, illustrates the correlation between the depression $b - B$ and the spectral type.

Characteristics of luminosity.—The depression $a - A$ seems to be stronger in dwarfs than in giants (Fig. 2, *b*). This is due to the negative luminosity effect for the sodium D lines. For visual inspection there is an additional luminosity effect in earlier subdivisions of the M stars, in that the shape of the depression at *a* looks different; in giants there is a broad, shallow feature degraded toward the red, while in dwarfs the absorption has a sharper appearance. Thus the two main depressions in the red may suffice to determine both spectral type and luminosity.

There is another luminosity effect which begins to be perceptible at class M2 and strengthens rapidly with advancing spectral type. It is the region λλ 6500–6850, which appears as a single, relatively sharp maximum in dwarfs; in giants this maximum becomes flattened at M2 and gradually splits into two maxima separated by a minimum near λ 6700 in later subdivisions. This very distinct luminosity effect can be accounted for by opposite effects of the adjacent regions of the *TiO* and *CaH* bands. The depression at λ 6700 due to *TiO* seems to be stronger in giants than in dwarfs; the opposite luminosity effect is displayed by the *CaH* band near λ 6700, as has been shown by Öhman.[3] This band, which is stronger in the dwarfs, cuts down the second maximum at λ 6830 (*d*). The effect is very conspicuous in late spectral subdivisions and gives an excellent means for distinguishing giants from dwarfs. Figure 2, *c*, illustrates this effect.

It therefore appears that the spectral region λλ 5500–7000, when observed with the extremely low dispersion of around 1000 A/mm, offers promising criteria for the separation of M giants and dwarfs. The practical applicability of these criteria when no photometric calibration is available and the classification is to be made by simple inspection of the spectra has been tested by the second author. The characteristics described above are sufficiently distinct to determine the spectral subdivision and to discriminate giants and dwarfs on widened spectra with the same degree of accuracy, on the average, as can be reached in the photographic region with the same instrument and prism. With an exposure time of 30 minutes, it was found that dwarf M stars could be distinguished to a limiting magnitude of 11.5 photored. This is 2 or 3 mag. fainter than the limiting magnitude for M stars on the blue-sensitive plates.

The consistency of the temperature classes assigned was tested by comparing successive estimates for a group of around two hundred stars on a pair of plates with 30-minute exposures. The resulting degree of agreement showed that a probable error of half a spectral division for a single determination could be inferred.

[1] *Spectra of Long-Period Variable Stars* (Chicago: University of Chicago Press, 1940).

[2] *Ap. J.*, **80**, 171, 1935.

[3] *Stockholms Obs. Ann.*, Vol. **12**, No. 3, 1936.

[4] *Ap. J.*, **87**, 592, 1938.

[5] *Ap. J.*, **87**, 89, 1938; **88**, 486, 1938.

[6] *Ap. J.*, **81**, 187, 1935.

It was further found possible to distinguish and classify S stars more readily than is possible with low-dispersion infrared spectra[7] taken with the same instrument. For instance, HD 177175, which is regarded as intermediate between the M and S sequences, appeared quite different, on our 103*a*-F3 plates, from a normal M star; on I-N plates with Wratten No. 89 filter it was indistinguishable from an M3 star. Although the red spectral region appears to be superior to the infrared for certain purposes of classification, the limiting magnitude is considerably less.

The authors wish to express their thanks to Dr. J. J. Nassau, director of the Warner and Swasey Observatory, for the suggestion of the subject and for advice; they also wish

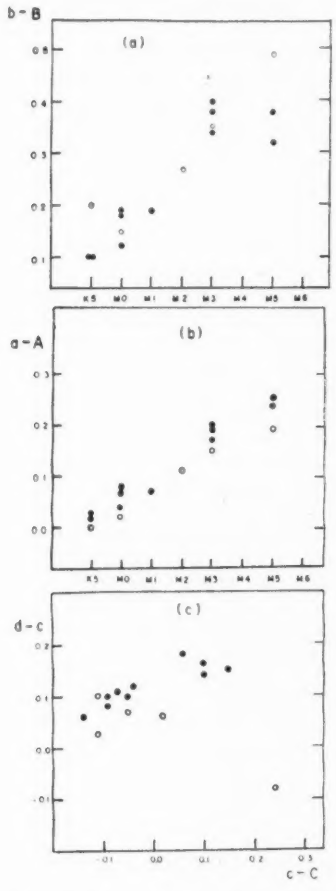

FIG. 2.—Spectral measures of standard stars. Open circles represent giant stars; filled circles, dwarf stars.

[7] J. J. Nassau and G. B. van Albada, *Ap. J.*, **109**, 391, 1949.

to acknowledge the help of Dr. A. Reiz, of the Lund Observatory, and Drs. D. A. MacRae and D. L. Harris, of the Warner and Swasey Observatory staff.

W. Iwanowska
P. A. Wayman

Warner and Swasey Observatory
July 25, 1951

SIX PECULIAR *Hα*-EMISSION STARS*

In the course of completing the *Hα* survey in the Southern Hemisphere with the Mount Wilson 10½-inch refractor and 15° objective prism, the writer has found several stars with peculiarities, in addition to a bright *Hα* line. Of these, the objects given in Table 1 have been investigated in greater detail with the Cassegrain spectrograph of the

TABLE 1

Peculiar *Hα* Emission Stars

Object	1875		m_{pg}	Type
	R.A.	Decl.		
CPD−57°2768	10^h06^m7	−57° 12′	10.0(CPD)	Mep
HD 90177	10 18.5	−59 00	9.0 var	Beq
Anon	10 49.0	−59 47*	∼10.5	Beq
SY Muscae	11 26.5	−64 44	∼11.4 var	Combination
CD−61°3575	12 37.0	−61 15	∼11.0	Combination
HD 327083	17 06.6	−40 11	10.4(CPD)	Beq

* A slightly fainter star is 28″ south and 4″ west.

74-inch Radcliffe reflector in Pretoria.

CPD−57°2768.—On objective-prism plates this star shows *TiO* bands similar to those in early M stars, together with a bright *Hα* line which is considerably stronger than that seen in long-period variable stars. Three slit spectra with a dispersion of 96 A/mm show bright lines of hydrogen and ionized calcium. The intensities of the hydrogen lines decrease slowly (*Hα* through *H*10 are visible) and do not show the anomaly that occurs in Me variables. *Ca* II is less conspicuous than hydrogen and is rather diffuse.

HD 90177.—This object was previously known as an irregular variable star[1] with a spectrum of type Be (MWC 202). Objective-prism spectra show an unusually strong bright *Hα*, a bright D3 line of helium, and the interstellar absorption line at λ 6284. Two slit spectra with dispersions of 50 A/mm reveal bright lines of *H*, *He* I, [*Fe* II], and *Fe* II. The lines *Hγ* and *Hδ* show the P Cygni effect. The presence of [*Fe* II] is unmistakable; the lines appear slightly diffuse. The absorption spectrum appears to be about that of a B2 supergiant.

Anon.—This star shows numerous P Cygni type lines, the emission components of which are unusually wide. The total widths of the emission components range up to about 11 A for *Hγ* and exceed those of DM−27°11944. Lines of *H*, *He* I, and *N* II are present, all of which display the P Cygni character. A sharp K line of *Ca* II is present in absorption only.

* This investigation has been made possible by a grant from the Horace H. Rackham School of Graduate Studies of the University of Michigan.

[1] Dorrit Hoffleit, *Harvard Bull.*, No. 913, p. 4, 1940.

SV Muscae.—This star has long been classed as a probable combination star, but slit spectra have not been available. Our objective-prism plates reveal strong bands of *TiO* and a strong bright *Hα* line. A slit spectrogram with a dispersion of 96 A/mm shows bright lines of *H*, *He* II, *He* I, *N* III, and a trace of [*O* III] λ 4363, together with an M-type absorption spectrum. Except for the weakness of [*O* III], the identity and intensity of the stronger bright lines are nearly the same as those of CI Cygni in 1942.[2]

CD−61°3575.—Objective-prism spectra show *TiO* bands and a strong bright *Hα*, while two slit spectra reveal bright lines of *H*, [*Fe* II], *Fe* II, and [*Fe* III]. The M-type spectrum is largely masked out in the blue. [*Fe* II] shows numerous lines and, with hydrogen, is the predominant feature of the spectrum. The existence of [*Fe* III] emission at λ 4655 and λ 4701 seems fairly certain, but positive identification cannot be made until wave-length determinations more accurate than those now available are made. The spectrum resembles the "1934 stage" of R Aquarii[3] in most respects.

HD 327083 (also CD−40°11253).—This star is listed in the Mount Wilson catalogue as a Be star but is classed as a G5 star in the *Henry Draper Extension*. Two Radcliffe spectra (dispersions 96 and 50 A/mm) show bright lines of hydrogen as well as *He* I λ 4922. The lines *He* I λ 4922, *Hγ*, *Hδ*, and *Hε* possess the P Cygni profile. The absorption spectrum is too faint for accurate classification, but the ratio of *He* I λ 4471 to *Mg* II λ 4481 indicates a type of about B5. It is our intention to publish more detailed descriptions of these spectra in the near future.

My deepest thanks are due to Dr. A. D. Thackeray for allowing me the use of the Radcliffe reflector and for affording me the assistance necessary to make these observations.

KARL G. HENIZE

LAMONT-HUSSEY OBSERVATORY OF THE
UNIVERSITY OF MICHIGAN
July 1951

SPECTROGRAPHIC OBSERVATIONS OF THE ECLIPSING VARIABLE X CARINAE

The eclipsing variable X Carinae[1] was spectrographically observed in 1946, 1947, and 1948 by the writer with the Wood-grating spectrograph attached to the 154-cm reflecting telescope at Bosque Alegre; the spectrograph gives a dispersion of about 42 A/mm. The 1946 observations were made on Eastman 103-O emulsion, and those of the following years on Eastman 103*a*-O emulsion, all of them with a projected slit-width of 0.038 mm. In fair seeing, the exposure times were of the order of 45 minutes.

Until Shapley's classical paper on the orbits of eclipsing binaries,[2] "the only available data concerning this star is a list of preliminary uniform elements derived by Roberts from his own unpublished observations (pp. 253, 256, of the 1905 *Report of the British Association for the Advancement of Science*)."[3] Roberts' elements, quoted in Shapley's paper[4] among the "third grade orbits," are given in the accompanying tabulation. Some

[1] Swings and Struve, *Ap. J.*, **97**, 195, 1943.

[2] P. W. Merrill, *Ap. J.*, **81**, 312, 1935.

[1] $\alpha = 8^h30^m2$; $\delta = -59°3'$ (1950.0). CD − 58°2144 = CPD − 58°1143 = HD 72698 (Sp. A0).

[2] *Contr. Princeton U. Obs.*, No. 3, 1915.

[3] *Ibid.*, p. 21.

[4] *Ibid.*, pp. 88, 89.

of the elements are also quoted in a recent paper by Plaut on "the elements of the eclipsing binaries brighter than photographic magnitude 8.50 at maximum."[5] Later on, Roberts[6] decided that the period was half the previously published one, and, ever since, the literature has indicated the period of the light-variation of X Carinae as being 0.541318 days and the light-curve as being of the Algol type.

Period	1.082636 days	$\cos i$	0.094
Depth of primary minimum	0.8+ mag.	Ratio of equatorial radii	0.878
Depth of secondary minimum	0.8 mag.	Ratio of polar axis to longest equatorial radius	0.826
Nature of primary eclipse	Partial with equal stars	Ratio of surface intensities	1.1
Light of brighter component	0.52	e	0.02
Longest equatorial radius:		ω	165°
Brighter star	0.50		
Fainter star	0.50		

New photometric observations of X Carinae have been recently made at Harvard by Mrs. Payne-Gaposchkin[7] and the published light-elements, based on photographic observations, are the following ones:

$P = 1.0826310$ days $\quad m_1 = 8.60$ mag.
$M_1 = 8.04$ mag. $\quad m_2 = 8.57$ mag.
$M_2 = 8.06$ mag.

These elements are quoted in the 1948 Kukarkin and Parenago's General Catalogue of Variable Stars, with the additional remark that the light-curve is of the β Lyrae type and that the spectrum is of composite type A0+A1. Previous references and Plaut's paper mention that the spectral type of X Carinae is A0, as the *Henry Draper Catalogue* lists.

The phases used in this work have been computed with the formula

$$\text{JD } 2415021.114 + 1.0826310E,$$

the adopted epoch of minimum being the one which is quoted in Schneller's *Katalog* for 1939 and Kukarkin and Parenago's *General Catalogue*. The available photometric elements indicate that X Carinae is a double-star system with practically equal components.

The spectrum of X Carinae at maximum light shows double lines of *H*, no lines of other elements being present. The components, of practically the same intensity, are not distinctly separated, except on some plates. At and near oppositions, the *H* lines become single and look deeper than when double. At these phases the spectrum also shows the presence of a faint and relatively sharp stellar K line of *Ca* II, which gives the impression of being sharper and fainter around secondary minimum than at around primary eclipse, according to the photometric elements. The spectral type is about A0.

The measurement of the spectrograms of X Carinae, at maximum light, was quite difficult. As has been mentioned, the separation of both components of *H* is not clearly seen on the plates, and therefore the measures are rather uncertain and the plotting of the results obtained shows a very large scatter. Because of the extreme uncertainty of the measures of many spectrograms which were not widened or sufficiently exposed, only 71 of the 115 spectrograms secured have been used in the present investigation. The wave-length interval included extends from λ 3770 to λ 4340, but it was not possible to measure all the *H* lines on all the plates in that interval.

Table 1 lists the radial velocities obtained, and Figure 1 shows the corresponding plot,

[5] *Pub. Kapteyn Astr. Lab. Groningen*, No. 54, pp. 16, 17, 1950.

[6] *V.J.S.*, **51**, 355, 1916.

[7] *Harvard Ann.*, **115**, 102, 1946.

TABLE 1

RADIAL VELOCITIES OF X CARINAE

DATE	U.T.	PHASE (DAYS)	RADIAL VELOCITIES (KM/SEC) FROM		
			Ca II	*H*	
				I	II
1948 Jan. 23	7:28	0.001	+ 9	+ 27	.....
1946 May 14	1:12	.004	+ 1	+ 15	.....
1947 Dec. 1	6:31	.010	.....	+ 7	.....
1946 June 20	22:52	.015	+15	+ 1	.....
1947 Dec. 13	4:58	.036	.....	+ 21	.....
1946 May 14	2:13	.047	.....	+ 6	.....
1947 Dec. 1	7:59	.071	.....	− 10	.....
12	3:53	.074	.....	+ 27	.....
1946 May 11	23:03	.080	.....	− 25	.....
1947 Dec. 12	4:42	.108	.....	+ 32	.....
11	3:26	.138	.....	− 5	.....
1946 May 12	0:30	.141	.....	−104	+126
1947 Dec. 12	5:30	.142	.....	− 79	+139
12	6:16	.173	.....	−107	+156
11	4:19	.175	.....	−102	+121
11	5:06	.207	.....	− 73	+137
12	7:04	.207	.....	−106	+152
1948 Jan. 30	0:52	.230	.....	−130	+144
1947 Oct. 8	8:44	.234	.....	−122	+ 94
Dec. 11	5:50	.238	.....	− 95	+ 83
1946 Dec. 23	7:54	.262	.....	− 84	+155
1948 Jan. 30	1:38	.262	.....	− 97	+141
1947 Feb. 13	7:08	.264	.....	−145	+129
Dec. 11	6:39	.272	.....	−121	+114
1948 Jan. 30	2:31	.299	.....	−126	+ 98
1947 Dec. 11	7:27	.305	.....	−102	+140
1948 Jan. 29	0:46	.308	.....	− 82	+126
30	3:20	.333	.....	− 74	+139
1947 Feb. 12	6:52	.335	.....	−126	+115
1948 Jan. 29	1:35	.342	.....	− 56	+145
1947 Mar. 8	2:51	.350	.....	−143	+133
1948 Jan. 29	3:06	.406	.....	+ 24	.....
1946 Apr. 26	1:24	.418	.....	+ 50	.....
1948 Jan. 29	3:46	.433	.....	+ 38	.....
29	4:24	.460	.....	+ 45	.....
29	5:09	.491	.....	+ 20	.....
29	6:16	.538	.....	− 20	.....
28	4:28	.545	+12	+ 32	.....
29	7:03	.570	+34	− 21	.....
1946 Apr. 22	23:21	.580	.....	+ 4	.....
1948 Jan. 28	5:24	.584	.....	0	.....
29	7:48	.602	.....	− 21	.....
1947 Feb. 9	7:48	.622	.....	+ 6	.....
1948 Jan. 28	6:18	.622	.....	− 1	.....
1947 Dec. 5	3:16	.627	.....	− 11	.....
5	4:18	.670	.....	+135	−110
5	5:14	.709	.....	+104	−113
1946 Apr. 22	0:53	.727	.....	+141	− 97
1948 Jan. 24	0:54	.727	.....	+ 85	−122
24	1:27	.750	.....	+115	−131
1947 Dec. 5	6:35	.765	.....	+122	−122
1948 Jan. 24	1:58	.772	.....	+144	− 73
1947 Dec. 5	7:23	.798	.....	+144	−118
1948 Jan. 24	2:40	.801	.....	+124	−121
24	3:24	0.831	.....	+ 92	−114

TABLE 1—*Continued*

Date	U.T.	Phase (Days)	Radial Velocities (Km/Sec) From		
			Ca II	*H*	
				I	II
1947 Dec. 4	6:12	0.832	.....	+159	− 66
3	4:50	0.857	.....	+169	− 95
1948 Jan. 23	2:15	0.866	.....	+149	− 69
24	4:14	0.866	.....	+118	−132
1947 Dec. 3	5:42	0.893	.....	+150	− 75
3	6:30	0.927	.....	+114	−133
2	4:34	0.929	.....	+148	− 50
1948 Jan. 23	4:18	0.951	.....	+ 14	.....
1947 Dec. 2	5:22	0.962	.....	− 3	.....
3	7:26	0.966	.....	+ 28	.....
Mar. 12	0:00	0.983	.....	+ 28	.....
1948 Jan. 23	5:16	0.992	.....	+ 17	.....
1946 May 13	23:22	1.011	.....	+ 53	.....
1947 Dec . 2	7:05	1.034	.....	+ 2	.....
1948 Jan. 23	6:21	1.037	.....	+ 8	.....
1947 Mar. 12	2:18	1.079	− 1	+ 5	.....

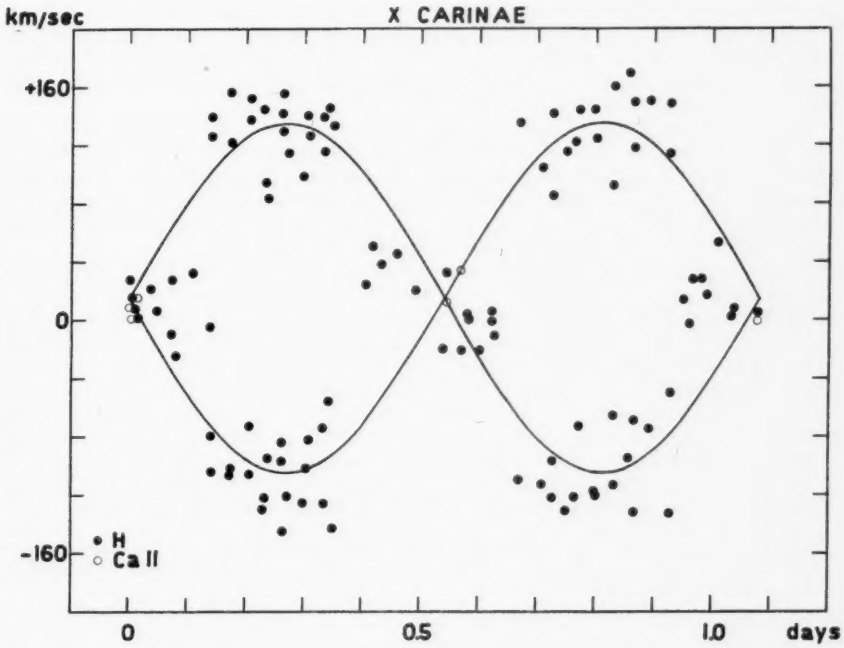

Fig. 1.—Velocity-curve of X Carinae

which suggest that

$$e \sim 0, \qquad K_1 \sim K_2 \sim 120 \text{ km/sec}, \qquad \gamma \sim +15 \text{ km/sec}.$$

The velocity-curves drawn in Figure 1 correspond to these approximate elements. Further, we obtain, from Roberts' value for i,

$$a_1 \sim a_2 \sim 1.8 \times 10^6 \text{ km} \qquad \text{and} \qquad \mathfrak{M}_1 \sim \mathfrak{M}_2 \sim 0.8 \odot.$$

In spite of the uncertainty of the radial-velocity measures, the spectrographic results of X Carinae agree with the photometric ones in suggesting that we are dealing with a system with two practically equal components. Moreover, our results indicate that the masses are smaller than normal for the spectral type of the stars involved.

I am indebted to Mr. Julio Albarracín for assisting in the reduction of the plate measurements.

JORGE SAHADE

OBSERVATORIO ASTRONÓMICO
CÓRDOBA, ARGENTINA
August 14, 1951

THE RADIAL VELOCITY OF KAPPA DRACONIS*

In a recent paper[1] G. R. Miczaika has confirmed the earlier work of S. N. Hill,[2] who had derived a period of 0.89038 day from thirty-eight spectrograms obtained at Victoria between 1923 and 1926. Miczaika slightly improved the period and found, from his velocity-curve, $K = 22.5$ km/sec; $\gamma = -11.0$ km/sec; and $f(\mathfrak{M}) = 0.00104\odot$. He concluded that the Be primary, whose mass was assumed to be $\mathfrak{M}_1 = 5\odot$, is accompanied by a dwarf of type K or M whose mass is $0.7\odot > \mathfrak{M}_2 > 0.3\odot$.

Previous investigations of spectroscopic binaries have led to the recognition of many Algol-type systems in which the fainter star is cooler, less massive, but larger than the primary. There are very few systems in which the secondary is smaller than the primary. This may be the result of observational selection, if the choice of systems is based upon their being eclipsing variables. Hence it is especially important to recognize and study those systems which resemble Miczaika's model of κ Draconis.

There is another reason why these stars are especially interesting. When the primary and secondary are nearly identical, they cannot be closer to each other than $2a_1 = 2r_1$. If the secondary is less massive than the primary ($\mathfrak{M}_2 < \mathfrak{M}_1$), the minimum separation $(r_1 + r_2)$ will be larger than in the case of two identical stars if $r_2 > r_1$, and smaller if $r_2 < r_1$. The typical Algol-type variables represent the case $r_2 > r_1$. But there are indications in the diagrams relating log P and K_1 that some systems have $r_2 < r_1$ and that in such systems the limiting value of the period that corresponds to the smallest possible separation of the components $(r_1 + r_2)$ can be much shorter than for double-lined binaries in which $r_1 = r_2$. In other words, the limiting curve on the left-hand side of Figure 1[3] is not a vertical line but slopes from the peak at the top toward the bottom at the left. This phenomenon is better shown if several uncertain stars omitted by J. H.

* This investigation was made possible by a co-operative arrangement between the Berkeley Astronomical Department of the University of California and the Mount Wilson and Palomar Observatories.

[1] *Zs. f. Ap.*, **28**, 203, 1951.

[2] *Pub. Dom. Ap. Obs. Victoria*, Vol. **3**, No. 18, 1926.

[3] See, e.g., *Stellar Evolution* (Princeton: Princeton University Press, 1950), p. 162, top of Fig. 22; and *Centennial Symposia* (Cambridge, Mass.: Harvard College Observatory, 1948), p. 213.

Moore and F. J. Neubauer from their last catalogue of spectroscopic binaries[4] are retained.

In order to ascertain whether κ Draconis is one of these interesting systems, I obtained 107 spectrograms, on Eastman O-III plates, with the single-prism spectrograph of the Mount Wilson 60-inch telescope. Because of the shortness of the period, all but the last four spectrograms were secured on four successive nights (March 24, 25, 26, and

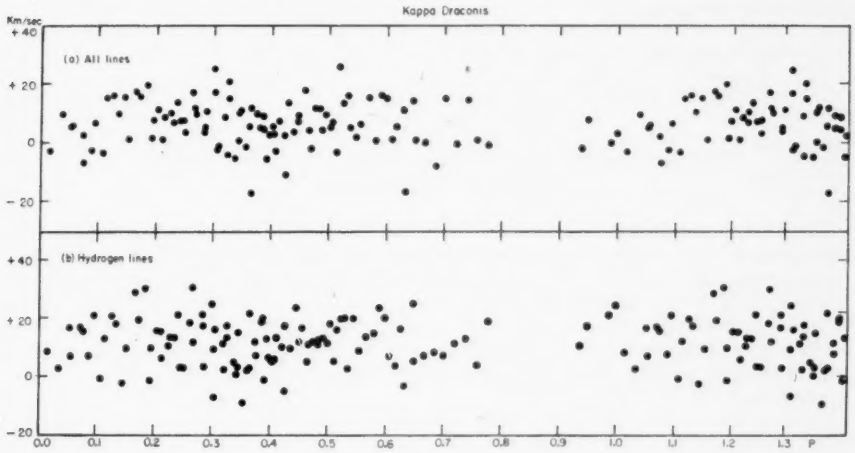

FIG. 1

TABLE 1

SUMMARY OF RADIAL VELOCITIES OF KAPPA DRACONIS

DATE 1951 (U.T.)	RADIAL VELOCITY (KM/SEC)		DATE 1951 (U.T.)	RADIAL VELOCITY (KM/SEC)	
	All Lines	*H* Lines		All Lines	*H* Lines
Mar. 24	+ 5.2	+11.5	Mar. 27	+ 3.8	+ 7.8
25	+10.0	+14.5	Aug. 12	−11.2	− 4.1
26	+10.7	+12.3	13	−10.5	−10.9

27, 1951 U.T.), and by working on the same star throughout each of these nights it was possible to cover nearly the entire cycle with a large number of uniform exposures.

The results were entirely negative. No variation in excess of the probable error was apparent in the radial velocities. The mean velocities for the four nights in March and the two in August are shown in Table 1. Figure 1 shows the velocities obtained from all lines (*a*) and from the *H* lines alone (*b*). The observations in August, 1951, differ systematically from those obtained in March.

At my request, Dr. Miczaika has re-examined his results but has found no substantial difference from those he had previously published. We must conclude that the short-

[4] *Lick Obs. Bull.*, No. 521, 1948.

period variation in velocity is not always present and that the star is not, at present, to be regarded as a bona fide binary. Perhaps the variation recorded by Hill and by Miczaika represents some effect of rotation. Miczaika correctly remarks that the period of 0.9 day is consistent with the period derived from the widths of the *He* I absorption lines.

This result does not invalidate previous conclusions regarding the existence of very close systems in which $r_2 < r_1$. We know that a few such systems exist, and we must try to find more of them.

O. STRUVE

BERKELEY ASTRONOMICAL DEPARTMENT
UNIVERSITY OF CALIFORNIA
September 4, 1951

THE MILKY WAY FROM SAGITTARIUS TO CEPHEUS IN THE INFRARED

A plate of the Milky Way in the photographic infrared has been taken with the Greenstein-Henyey wide-angle camera[1] and is reproduced by Figure 1 (*left*). This exposure, obtained on a hypersensitized Eastman I-N plate behind Corning 5850 and Corning 2403 filters, includes the spectral range λλ 7200–8800 and extends from Sagittarius to Cepheus. It was taken on July 7, 1951, with an exposure time of 1½ hours. A comparison exposure, taken without filter on a 103*a*-F3 plate, including the spectral region λλ 3800–6800, is shown in Figure 2. This plate was taken on July 6, 1951, with an exposure time of 20 minutes.

As has been emphasized many times, especially by Stebbins and Whitford,[2,3] the decrease in absorption of interstellar matter toward longer wave lengths makes infrared radiation much more effective for space penetration than ordinary photographic or visual light. If we take the effective wave lengths for the I-N and 103*a*-F3 plates as approximately λ 8000 and λ 4800, respectively, we find from Whitford's interstellar absorption-curve[4] that the total absorption, A, at these wave lengths, expressed in terms of the color excess E_1, is about $A_{\lambda\,8000} = 3.2E_1$ and $A_{\lambda\,4800} = 7.2E_1$, respectively. In addition, the N plate is more sensitive to the light of the population II red stars, which are strongly concentrated toward the galactic center,[5] while the F3 plate is more sensitive to the light of the nearer blue stars and emission nebulosities of the Milky Way. For both these reasons the infrared plate gives a better picture of the over-all structure of the more distant regions of our galaxy.

In the infrared plate the dark rift in the Milky Way runs all the way through the galactic bulge, with approximately the same width everywhere. It should be noted that the galactic bulge mentioned here refers to the large bright area, about 18° × 30° in size, near the southern limit of the illustration, corresponding to the central bulge seen in edge-on spirals. The galactic bulge investigated by Stebbins and Whitford[3] at λ 10,300 is a much smaller, more highly concentrated area, about 3°.5 × 8° in size, lying in the middle of the rift at $l = 326°.5$. On the infrared plate the two sides of the Milky Way have more nearly equal surface brightnesses than on the panchromatic plate, not only at the galactic bulge but also farther north, where the west side is filled in with radiation. The structure of the rift is much more regular and sharply defined in the infrared ex-

[1] O. Struve, *Sky and Telescope*, **10**, 215, 1951.

[2] J. Stebbins, *Centennial Symposia* (Cambridge, Mass.: Harvard College Observatory, 1948), p. 3; A. E. Whitford, *Centennial Symposia*, p. 155.

[3] J. Stebbins and A. E. Whitford, *Ap. J.*, **106**, 235, 1947.

[4] *Ap. J.*, **107**, 102, 1948.

[5] W. Baade, *Ap. J.*, **100**, 137, 1944.

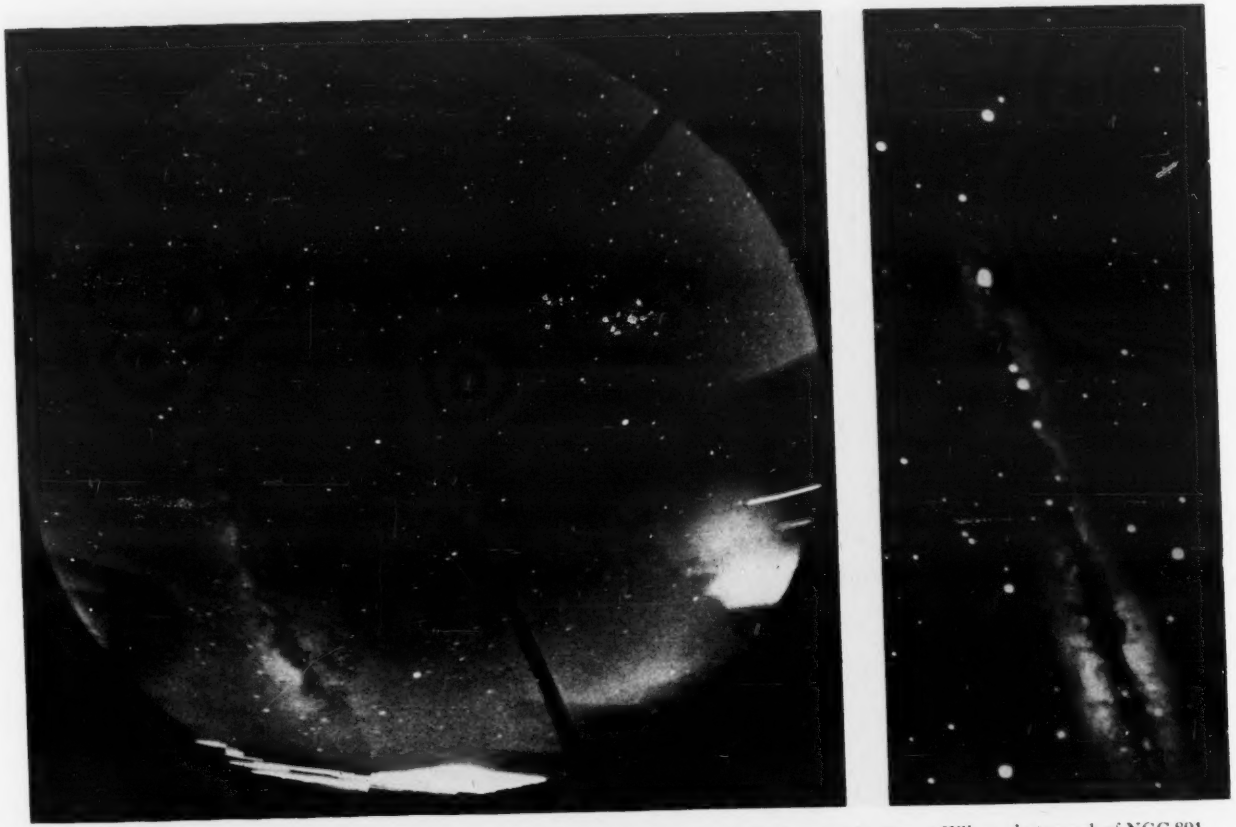

FIG. 1.—*Left*, infrared wide-angle photograph of the Milky Way from Sagittarius to Cepheus; *right*, Mount Wilson photograph of NGC 891

FIG. 2.—Panchromatic wide-angle photograph of the Milky Way from Sagittarius to Cepheus

posure, especially in the region of the galactic bulge. All the differences between the infrared and the panchromatic plates are those associated with, on the one hand, great space penetration and averaging of absorption over large distances and, on the other hand, lower space penetration and more pronounced effects of the near-by dark clouds.

In addition, there is a very rapid decrease in surface brightness of the Milky Way from the galactic bulge northward on the infrared plate; this effect, though present, is much less marked on the panchromatic exposure.

Attention should be called to the strong diffuse illumination near the southern horizon in the infrared photograph, which does not appear on the panchromatic exposure. As Dr. A. B. Meinel has pointed out to us, this shows the great strength of the infrared airglow emission spectrum.

For purposes of comparison, Figure 1 (*right*) shows a reproduction of a plate taken at Mount Wilson[6] of the edge-on extragalactic nebula NGC 891. This illustration has been cut to show a little more than half the nebula, corresponding to the part of our galaxy that is shown by the wide-angle plate. The similarity between the two photographs is striking; in the two cases the galactic bulge and the dark rift of constant thickness appear quite analogous. Also, the steep gradient of light from the center of the galaxy out to the edge shows well in both plates, even though part of this effect is lost in NGC 891 because of the fact that the central bulge is burned out. As the position of the sun is well outside the bright central regions of our galaxy, the analogy between the two illustrations is valid.

We wish to express our sincere thanks to W. W. Morgan, who has helped us in all stages of this work.

DONALD OSTERBROCK*
STEWART SHARPLESS

YERKES OBSERVATORY
August 15, 1951

ON AN INTEGRAL EQUATION OF CHANDRASEKHAR AND MÜNCH

Recently Chandrasekhar and Münch[1] derived an integrodifferential equation for dealing with the problem of the fluctuations in brightness in the Milky Way. In this note we shall obtain their equation more directly by a simple reformulation of their problem, which at the same time relates it to the general theory of continuous stochastic processes.[2]

Chandrasekhar and Münch considered the following problem: Given (1) that there is a deterministic contribution of amount $\beta d\tau$ from the element of length $d\tau$, at $t = \tau$ (this is due to the stars occurring with a uniform distribution along t) to the intensity measured at $t = 0$; (2) that clouds occur with a Poisson distribution $e^{-\alpha t}(\alpha t)^n/n!$ in any element of length t, where α is the probability per unit t that a cloud occurs in any interval; (3) that a cloud has a transparency factor q (i.e., it reduces the intensity of radiation of the light of the stars immediately behind it by this factor), with a probability density $\psi(q)$ so that $\alpha\psi(q)dq$ is the probability per unit t that radiation of a given intensity u "jumps" to an interval between uq and $u(q + dq)$. Given all this, what is the frequency function, $g(u, \xi)$, governing the probability with which an observer at the origin will

[6] Taken with the 60-inch telescope at Mount Wilson, November 23/24, 1916; exposure time 7 hours 15 minutes. We are greatly indebted to Dr. I. S. Bowen, director of the Mount Wilson and Palomar Observatories, for permission to use this photograph.

* Atomic Energy Commission Pre-doctoral Fellow in Astrophysics.

[1] *Ap. J.*, **112**, 380, 1950.

[2] Cf. A. Ramakrishnan, *Proc. Cambridge Phil. Soc.*, **46**, 598, 1950, and the references given there.

measure an intensity u when the system extends to a distance $t = \xi$ along the line of sight?

We shall now show that, by reformulating the foregoing problem in the following manner, we can derive the integral equation of Chandrasekhar and Münch quite simply and without recourse to the rather long procedure they have adopted.

Given (1) that there is a deterministic contribution of amount $\beta d\tau$ from $d\tau$ at $t = \tau$ to the intensity u when the system extends to a distance $t = \xi$; (2) that the probability per unit t that an intensity of magnitude u drops to an interval lying between uq and $u(q + dq)$ is $\alpha\psi(q)dq$ (in the physical problem this is due to the interception of clouds, but for mathematical purposes we need not specify this); given these, what is the frequency function $g(u, \xi)$ governing the intensity u? We shall presently show that the two formulations are entirely equivalent. But the second formulation yields the integral equation of Chandrasekhar and Münch immediately if we use the Markovian property of the stochastic process defined by $g(u, \xi)$.

Following the standard procedure of solving continuous stochastic problems,[2] we shall consider the effect on $g(u, \xi)$ of an increase in ξ of $d\xi$. We have: (1) A contribution to the probability $g(u, \xi + d\xi)du$ if the state (u', ξ) existing with probability $g(u', \xi)du'$ jumps to the state u; the measure of this contribution is

$$\alpha g(u', \xi)\psi\left(\frac{u}{u'}\right)\frac{du}{u'}du'd\xi \qquad \left(\frac{u}{u'} = q\right);$$

the measure of the total contribution, therefore, is[3]

$$\alpha du d\xi \int_{u'} \psi\left(\frac{u}{u'}\right) g(u', \xi)\frac{du'}{u'}.$$

(2) A depletion in the probability of the state (u, ξ) if the radiation of intensity u drops to u' when we increase ξ by $d\xi$; the measure of this depletion is

$$\alpha g(u, \xi)\, d\xi du \int_0^u \psi\left(\frac{u'}{u}\right)\frac{du'}{u} = \alpha g(u, \xi)\, du d\xi ,$$

since

$$\int_0^1 \psi(q)\, dq = 1 .$$

At the same time, on account of the deterministic contribution of amount $\beta d\xi$, the state $(u - \beta d\xi, \xi)$ "moves" to the state $(u, \xi + d\xi)$. Combining all this, we have

$$g(u, \xi + d\xi)\, du = g(u - \beta d\xi, \xi)\, du - \alpha g(u, \xi)\, du d\xi + du d\xi \alpha \int_u^{\beta\xi} g(u', \xi)\psi\left(\frac{u}{u'}\right)\frac{du'}{u'}.$$

[3] Here and in the sequel, $\int_x$ means integration over the whole range of the variable x. In the case on hand the limits of u' are obviously u and $\beta\xi$, since $g(u, \xi)$ vanishes for $u > \beta\xi$. However, as Chandrasekhar and Münch have observed in their paper, at $u = \beta\xi$ the function $g(u, \xi)$ has a delta-function singularity. This is due to the fact that there is a finite probability of magnitude $e^{-\alpha\xi}$ that no cloud intercepts the radiation in the interval 0 to ξ. This is also the probability that the observer measures an intensity of magnitude exactly equal to $\beta\xi$. But this circumstance does not affect the arguments leading to the derivation of the fundamental equation. In a private communication Dr. Chandrasekhar has informed me that the singularity at $u = \beta\xi$ must be taken into account in the solution of the equation (see S. Chandrasekhar and G. Münch, *Ap. J.*, **114**, 110, 1951).

Letting $d\xi \to 0$, we obtain

$$\frac{\partial g(u, \xi)}{\partial \xi} = -\alpha g(u, \xi) - \beta \frac{\partial g(u, \xi)}{\partial u} + \alpha \int_u^{\beta\xi} g(u', \xi) \psi\left(\frac{u}{u'}\right) \frac{du'}{u'}.$$

When $\alpha = \beta = 1$, the foregoing reduces to the integrodifferential equation of Chandrasekhar and Münch.

It may be noticed that, when $\beta = 1$,

$$\int_u^{\xi} g(u', \xi) \psi\left(\frac{u}{u'}\right) \frac{du'}{u'} = \int_{u/\xi}^{1} g\left(\frac{u}{q}, \xi\right) \psi(q) \frac{dq}{q},$$

and the transition probability $(u' \to u)$ is homogeneous in u' and u. In view of this, the integral equation is reducible by using Mellin's transformation:

$$p(s, \xi) = \int_0^{\infty} u^{s-1} g(u, \xi)\, du; \qquad g(u, \xi) = \frac{1}{2\pi i} \int_{\sigma - i\infty}^{\sigma + i\infty} p(s, \xi)\, e^{-s} ds,$$

where s is a complex variable. This transformation reduces the equation to

$$\frac{\partial p(s, \xi)}{\partial \xi} = -\alpha p(s, \xi) + \alpha \eta(s)\, p(s, \xi) + \beta(s-1)\, p(s-1, \xi),$$

where

$$\eta(s) = \int_0^{\infty} q^{s-1} \psi(q)\, dq.$$

When $s = n + 1$ and n is a nonnegative integer, $p(n, \xi)$ gives the $(n-1)$th moment of u. In such a case the difference-differential equation for $p(n, \xi)$ can be solved by iteration, as shown by Chandrasekhar and Münch.

We shall now examine in detail the duality between the two formulations. The duality consists in the realization that the probability that a transition from u will occur in an interval dt is equal to the probability that a change in u follows the interception of a cloud in dt. If $R(u, u', t)du'$ is the probability per unit t that a transition $(u' \to u)$ takes place, then the total probability per unit t of a transition from u is

$$\int_{u'} R(u, u', t)\, du' = \alpha(u, t).$$

If the probability that an interception will occur is independent of u, then α will be independent of u. The conditional probability that, given that a transition from u has occurred, the transition is of the $(u \to u')$ type is

$$\psi(u, u', t) = \frac{R(u, u', t)}{\alpha(u, t)}.$$

(Note that $\int_{u'} \psi(u, u', t)du' = 1$ for all u and t.) Of course, the total probability per unit t that any transition takes place is given by

$$\int_u g(u, t)\, \alpha(u, t)\, du.$$

If α is independent of u, the foregoing reduces to α, since $\int_u g(u, t)du = 1$. In this latter

case $R(u, u')du'$ is expressible as a function of q where $q = u'/u$; thus, writing it as $R(q)dq$, we have

$$R(q, t) = \alpha(t)\psi(q, t).$$

Further,

$$R(q, t) = \alpha(t)\psi(q)$$

if ψ is independent of t. If α is independent of t, it can be normalized to 1 without loss of generality by suitably choosing a unit of t. It is to be noted that, even if α is a function of t, the number of transitions (which is equal to the number of interceptions) obeys a Poisson distribution with a mean $\bar{n} = \int_0^t \alpha dt$. The distribution $\bar{\omega}(n, t)$ is Poisson if the probability that an interception occurs in an interval dt is *independent* of the occurrence of an interception in any other interval. If this were not so (this is a purely hypothetical assumption and has no physical meaning in the astrophysical problem under consideration), $\bar{\omega}(n, t)$ would not be Poissonian, and, for example, we may have to define $\alpha(n, t)dt$ as the total probability that an interception occurs at t, given that n interceptions have occurred previously. Then we must write $R(n, q, t) = \alpha(n, q, t)\psi(n, q, t)$ where $R(n, q, t)dt$ is the probability that a q-transition will take place in dt, given that n transitions have already taken place. In such a case the stochastic process defined by $g(u, t)$ is no longer Markovian, but the Markovian property can be restored by defining a new function $g(n, u, t)$, where $g(n, u, t)dt$ is the *joint* probability that the intensity measured by the observer lies between u and $u + du$ *and* that n "collisions" have occurred previously. The function then satisfies the equation

$$\frac{\partial g(n, u, t)}{\partial t} = -\alpha(n, t)\, g(n, u, t) - \beta \frac{\partial g(n, u, t)}{\partial u} + \int_{u/\beta t}^{1} g\left(n-1, \frac{u}{q}, t\right) R(n-1, q, t) \frac{dq}{q}.$$

ALLADI RAMAKRISHNAN

MADRAS, INDIA
September 14, 1951